VRIJE UNIVERSITEIT

Silent witnesses
Freshwater bivalves as archives of environmental variability in the Rhine-Meuse delta

ACADEMISCH PROEFSCHRIFT

ter verkrijging van de graad Doctor aan
de Vrije Universiteit Amsterdam,
op gezag van de rector magnificus
prof.dr. L.M. Bouter,
in het openbaar te verdedigen
ten overstaan van de promotiecommissie
van de faculteit der Aard- en Levenswetenschappen
op woensdag 2 december 2009 om 15.45 uur
in de aula van de universiteit,
De Boelelaan 1105

door

Emma Adriana Agnes Versteegh

geboren te 's-Hertogenbosch

Silent witnesses - Freshwater bivalves as archives of environmental variability in the Rhine-Meuse delta

In Dutch: Stille getuigen - Zoetwaterbivalven als archief van omgevingsvariabiliteit in de Rijn-Maasdelta

Author: Emma A. A. Versteegh

Cover design: Juliëtte Verberk (http://www.metjuliette.nl/)

Cover photos: shell sections: Saskia Kars; shells: Emma Versteegh; water: Juliëtte Verberk.

Photos inside:
p. 12: Taking water samples at Hagestein (photo by Sarah Tynan)
p. 26: Collecting unionids at Zetten (photo by Ane Wiersma)
p. 46: Preparing unionids for photography (photo by Ane Wiersma)
p. 62: Collecting unionids at Zetten (photo by Ane Wiersma)
p. 90: Measuring pH at Hagestein (photo by Ane Wiersma)
p. 112: Measuring pH at Hagestein (photo by Renee Hoekzema)
p. 132: Measuring an tagging unionids (photo by Ane Wiersma)
p. 144: Fish ladder at Hagestein (photo by Renee Hoekzema)
p. 164: Putting on waders at Hagestein (photo by Renee Hoekzema)
p. 172: Taking water samples at Lith (photo by Renee Hoezema)

Bittervoorns leggen hun eitjes in een zoetwatermossel. Dat kan lukken of mislukken, maar in ieder geval is het een hele plechtigheid. Er is vrij wat voor nodig.

Het wijfje dat de eieren legt natuurlijk in de eerste plaats. Dan de van niets wetende mossel, die een weinig openstaat, zodat het eigeleidertje in zijn ademspleet gebracht kan worden en tenslotte het mannetje, dat de eieren bevrucht als ze goed en wel in de mossel terecht zijn gekomen. Ieder doet dus zijn deel en doorgaans heel wat bewuster, dan bij andere voortplantingen wel het geval is. [...]

Bruiloften onder het oog van de dood hebben iets verstolens. Zo was het ook met de bruiloft van het bittervoorntje Blaude en het mannetje Passy. Hij geleidde haar naar een lichte mossel, driftig en zijn felle kleuren sproeiend in het water. Er waren nog twee mannetjes, Roumy en Torquy, die deelnamen aan het ceremonieel. Want die vonden het een zalige liefhebberij om de mossel te bedotten. Iedere keer als zij ertegenaan stieten en zo veel mogelijk water tegen de spleet spoten, sloot de mossel zich.

Zo'n dier weet niet veel, maar wel wat open is en wat dicht. Iedere keer als men hem bestookte, sloot hij zich. Even later ging hij dan weer open en dan bleek het sluiten voor niets gedaan te zijn. Passy, Roumy en Torquy kwamen er dan opnieuw aan, hervatten tierig het aanstoten en spuwen en de mossel ging weer dicht. Dicht, dacht hij dan en hij bezat inderdaad het gelukkig vermogen om die gedachte waar te maken. Als hij dan toch weer open moest en bemerkte dat er in die tussentijd volstrekt niets met hem was gebeurd, aarzelde hij wel even met dichtgaan als de drie mannetjes hun charge herhaalden, maar hij deed het toch maar, al kwam er ergens in zijn vage reageren wel iets opzetten van een indruk dat hij al die moeite voor niets deed. Later ging hij weer open. Bij een herhaling van de aanval sloot hij zich nu wel heel wat langzamer, wel wetende dat hij slachtoffer was van de eenzijdigheid van zijn mogelijkheden en zijn onbetekenende schrikachtigheid. En dus niet zonder gemelijkheid. Toen hij daarna opnieuw open was gaan staan en er bleek niets gebeurd te zijn, blééf hij open, want hij was nu gewend aan de zachte stootjes van de voornneuzen en hun onbeduidende spuwstroompjes, ook al verdubbelden de drie voorns hun pogingen en botsten Passy, Torquy en Roumy tegen de mossel, op wat zij aannamen dan de kitteligste plekjes waren. Jawel! dacht de mossel dan. Meer niet. Maar dan toch in ieder geval heel duidelijk. Jawel! en hij bleef open. Dat was het ogenblik voor Blaude om haar eitjes te leggen.

A. Koolhaas, Het grote stikken. Uit: Dekkers, M. Midas Dekkers leest A. Koolhaas. Uitgeverij Maarten Muntinga bv, Amsterdam. 2005. Oorspronkelijk uit: Koolhaas, A. Gekke Witte. Uitgeverij G. A. van Oorschot, Amsterdam 1959.

Contents

Dankwoord / Acknowledgements

te nemen en metingen te doen, en mijn moeder, Marie-Louise Friedrichs, die mij daarbij vele malen vervangen heeft als ik op een conferentie of vakantie was.

Dank aan Rijkswaterstaat, en vooral Gerard Wittenberg, dat ik mijn kooien in de vistrappen mocht zetten. Bedankt ook Wim Kuijper (Universiteit Leiden), Rob Molenbeek (Universiteit van Amsterdam), Anthonie van Peursen, Jelle Reumer (Natuurhistorisch Museum Rotterdam), Frank Wesselingh (Naturalis) en de Rijksdienst voor het Cultureel Erfgoed, voor jullie vrijgevigheid wat betreft de schelpen. Thank you Gerhard Bauer and Rüdiger Bless for being so generous to send me some of your shells. Bedankt, Wim Mook voor het achterhalen van een dataset die cruciaal is gebleken voor dit proefschrift.

Thanks to the Australian colleagues, Patrick De Deckker, Steve Eggins, Les Kinsley, Malcolm McCulloch and Sarah Tynan, for the warm welcome and good cooperation at the Australian National University in Canberra. Thank you Jens Zinke, Craig Grove and Miriam Pfeiffer for letting me join you on your coral drilling fieldwork to Zanzibar. This was not only a useful experience, but it was also very special to be back in Zanzibar after 5 years.

De collega's op de VU stonden garant voor veel gezelligheid tijdens pauzes of borrels, met onderwerpen variërend van harde wetenschap tot hilarische nonsens. Dank voor de geweldige tijd: Lia Auliaherliaty, Ronald van Balen, Kay Beets, Bert Boekschoten, Sjoerd Bohncke, Aafke Brader, Martin van Breukelen, Jop Brijker, Hanneke Bos, Maarten Corver, Jan van Dam, Mascha Dedert, Stefan Engels, Gerald Ganssen, Dorothée Hippler, Jochem Jongma, José Joordens, Kees Kasse, Bram van der Kooij, Dick Kroon, Anco Lanckreijer, Edith van Loon-van den Berg, Cedric van Meerbeeck, Sandra Merten, Jos de Moor, Andreas Paul, Frank Peeters, Orson van de Plassche († 04-05-2009), Maarten Prins, Hans Renssen, Didier Roche, Margot Saher, Jan Smit, Simon Troelstra, Els Ufkes, Jef Vandenberghe, Suzan Verdegaal, Geert-Jan Vis, Mirjam Vriend († 13-05-2008), Hubert Vonhof, Bas van der Wagt, Philip Ward, Tjeerd van Weering, Ane Wiersma, Alex Wright en Jens Zinke.

De twee mensen met wie ik misschien wel het meeste promotiegerelateerd lief en leed heb gedeeld zijn mijn VU kamergenoten en tevens paranimfen, Aafke Brader en José Joordens. Bedankt voor de fijne gesprekken, de inspiratie en vooral jullie enorme steun.

Een groot deel van mijn vrije tijd heb ik besteed aan mijn voorzitterschap van de Jongerenwerkgroep voor Sterrenkunde, en aan het organiseren van kampen voor deze vereniging. Dank aan mijn medebestuursleden en

Samenvatting

Achtergrond

Hoewel het geologisch verleden toont dat het klimaat van nature kan veranderen, concludeert het Intergovernmental Panel on Climate Change (IPCC) dat het grootste deel van de opwarming van de afgelopen 50 jaar veroorzaakt is door menselijke activiteiten, zoals grootschalige ontbossing en het verbruik van fossiele brandstoffen. Het IPCC verwacht ook dat het effect van de klimaatopwarming de komende eeuw regionaal zal verschillen, met in West-Europa nattere zomers en drogere winters.

Nederland heeft een kwetsbare positie in de Rijn-Maasdelta, en het is dan ook van groot belang om onze kennis over extreme neerslag en gerelateerde overstromingen en droogtes te verbeteren. In het recente verleden, in 1993 en 1995, hebben er in ons land omvangrijke overstromingen plaatsgevonden (Figuur 1.1). Deze veroorzaakten grote schade, en leidden in 1995 zelfs tot de evacuatie van meer dan 200.000 mensen uit het Nederlandse rivierengebied. Ernstige droogtes kwamen bijvoorbeeld voor in 1976 en 2003 (Figuur 1.2). Als gevolg van die droogtes ontstond er een watertekort in de landbouw, en hadden elektriciteitscentrales een gebrek aan koelwater. Droogte kan ook zorgen voor verslechterde waterkwaliteit, hetgeen een directe impact heeft op de drinkwatervoorziening, en ook de rivierecologie in gevaar brengt. Men verwacht dat als gevolg van klimaatverandering, de ernst en frequentie van overstromingen en droogtes zullen toenemen in de loop van de 21$^{\text{ste}}$ eeuw.

Voorspellingen over het toekomstige klimaat worden gedaan door middel van modellen. Om natuurlijke fluctuaties en de invloed van menselijk handelen te kunnen kwantificeren en vervolgens betrouwbare extrapolaties naar de toekomst te doen zijn realistische data, gemeten op verschillende tijdschalen, onontbeerlijk. Instrumentele datareeksen zijn op zijn best enkele honderden jaren oud. Voor kennis over het klimaat vóór die tijd zijn we afhankelijk van zogenaamde proxy's. Een proxy is een meetbare grootheid die gebruikt kan worden om andere, niet direct meetbare, grootheden uit het geologische verleden te reconstrueren. Voorbeelden van proxy's zijn zuurstofisotopen in ijskernen (proxy voor temperatuur en ijsvolume gedurende ijstijden en interglacialen) of de breedte van jaarringen in bomen (proxy voor temperatuur of neerslag gedurende de laatste millennia).

Dit project onderzoekt het gebruik van de scheikundige samenstelling van groeilijnen in de schelpen van zoetwatermossels als proxy voor veranderingen in rivieromstandigheden gedurende de laatste 5000 jaar. Daarbij ligt de nadruk op veranderingen in waterafvoer (debiet) tijdens overstromingen en droogtes.

Sclerochronologie

Veel aquatische organismen, zoals koralen, slakken en bivalven (tweekleppigen), vormen periodieke groeilijnen in hun skelet, analoog aan de jaarringen in bomen. Omgevingskenmerken van het betreffende organisme worden vastgelegd in deze groeilijnen. Zo dienen deze skeletten als archief voor veranderingen in het groeimilieu. De studie van periodieke groeikenmerken in skeletonderdelen van aquatische organismen wordt sclerochronologie genoemd.

Veel sclerochronologisch onderzoek is gedaan aan mariene bivalven, waarbij de zuurstofisotopensamenstelling (δ^{18}O) gebruikt wordt als proxy voor temperatuur of zoutgehalte van het water. In zoetwatermossels kan δ^{18}O dienen als proxy voor paleohydrologie, dus veranderingen in waterbron, debiet of neerslagpatronen. Deze studie onderzoekt de toepasbaarheid van zowel de stabiele zuurstof- als koolstofisotopensamenstelling (δ^{13}C) van zoetwatermossels als omgevingsproxy en paleohydrologische proxy in de rivieren Maas en Rijn.

Nederlandse zoetwatermossels

Zoetwaterweekdieren komen veel voor in de Nederlandse rivieren en meren. De meerderheid behoort tot de gastropoden (slakken), maar er komen ook verschillende soorten tweekleppigen voor. De zoetwaterweekdieren die in deze studie gebruikt worden behoren tot de familie Unionidae (rivierparelmossels of Najaden). Unionidae kunnen slecht tegen zout water (max. ~ 3 ‰ zoutgehalte) en komen dus alleen voor in zoet water. Wereldwijd zijn ruim 900 soorten beschreven. De grootste diversiteit komt voor in Noord-Amerika. Veel soorten zijn bedreigd door overbevissing, vervuiling, verlies van habitat en invasieve exoten. In Nederland wordt deze de familie van Unionidae vertegenwoordigd door zes soorten. Ze vormen grote schelpen, leven half begraven in het sediment en kunnen een leeftijd tot 15 jaar bereiken.

In deze studie worden vier soorten Unionidae gebruikt (Figuur 1.7):

- *Unio crassus nanus* Lamarck, 1819 (Bataafse stroommossel). De schelp is elliptisch tot ovaal, bereikt maximale afmetingen van 40 x 70 mm en wordt gevonden in stromend water, meestal in rivieren. In vergelijking met de andere Nederlandse unioniden geeft deze soort de voorkeur aan het grofste, zandige sediment en is het meest gevoelig voor vervuiling en lage zuurstofgehaltes. *U. crassus* is door vervuiling in Nederland uitgestorven sinds 1968.
- *Unio pictorum* (Linnaeus, 1758) (Schildersmossel). Deze soort heeft

15

een dikke schelp en een langwerpige elliptische vorm met een maximale afmeting van 44 x 110 mm, komt voor in zowel stilstaand als stromend water en verdraagt enige vervuiling.

- *Unio tumidus* Philipsson, 1788 (Bolle stroommossel). De schelp heeft een eivorm met een gebogen rand. De maximale grootte bedraagt 62 x 125 mm. Deze soort prefereert stromend water, maar komt ook voor in stilstaand water. Van de Nederlandse unioniden heeft *U. tumidus* de hoogste tolerantie voor vervuiling.

- *Anodonta anatina* (Linnaeus, 1758) (Vijvermossel). *Anodonta*soorten hebben dunnere schelpen dan de bovengenoemde *Unio*soorten. *A. anatina* heeft een ovale vorm met een prominente hoekige vleugel aan de bovenkant, bereikt een maximale grootte van 80 x 132 mm, en komt voor in zowel stromend als stilstaand water.

Zoetwatermossels worden vaak gevonden in archeologische opgravingen, omdat ze door prehistorische mensen gebruikt werden als voedsel, gereedschap en versiering. Zogenaamde schelpenmiddens (afvalhopen van consumptie van schelpen) zijn gevonden in Australië, Indonesië, Noord-Amerika en Afrika. In Noord-Amerika vormden zoetwatermossels ooit een belangrijke bron voor de commerciële visserij, waarbij de schelpen werden gebruikt voor het maken van knopen. Tegenwoordig worden zoetwatermossels bevist voor de productie van parelmoerkorreltjes die worden gebruikt in de parelkweek. De Europese soorten worden beschouwd als oneetbaar en werden alleen gegeten ten tijde van ernstige hongersnood. Ze werden gebruikt als veevoeder, voor prehistorisch gereedschap en voor sieraden. *U. pictorum* (de schildersmossel) dankt zijn naam aan het feit dat de schelpen door schilders werden gebruikt als verfbakjes.

De Rijn-Maasdelta

De rivieren Maas en Rijn vertegenwoordigen twee verschillende riviertypes, respectievelijk een regenrivier en een gecombineerde smeltwater/regenrivier. Het stroomgebied van de Maas ligt in het noordoosten van Frankrijk, Oost-België en Zuid-Nederland. Het gemiddelde debiet in Borgharen is 274 m^3/s. Na zware regenval in het afvoerbekken kan het debiet oplopen tot meer dan 3000 m^3/s. De Rijn is met een stroomgebied van 185.300 km^2 een van de grootste riviersystemen in West-Europa, en voert smeltwater af uit de Alpen en neerslag uit Zuid-Duitsland. Het gemiddelde debiet bij Lobith is 2200 m^3/s, maar piekafvoeren kunnen wel 13.000 m^3/s bedragen.

Zuurstofisotopen in de hydrologische cyclus

De chemische eigenschappen van de schelpen die in dit onderzoek gebruikt worden zijn ratio's van stabiele isotopen van zuurstof (O) en koolstof (C). Van beide elementen komen van nature atomen voor met een verschillende massa (stabiele isotopen). Zuurstof komt voor als drie verschillende stabiele isotopen: ^{16}O (99.76 %), ^{17}O (0.035 %) en ^{18}O (0.20 %). Het meten van ^{17}O levert weinig meer informatie op dan gehaald kan worden uit de hoeveelheid ^{18}O, die nauwkeuriger gemeten kan worden doordat dit isotoop in hogere concentraties voorkomt. In verschillende stadia in de hydrologische cyclus vindt zogenaamde fractionering plaats tussen de verschillende isotopen. Zeewater heeft een min of meer constante zuurstofisotopenverhouding (δ^{18}O) die gedefinieerd is als 0 ‰. Als door verdamping wolken vormen boven de oceaan, zullen de watermoleculen die lichtere isotopen bevatten makkelijker verdampen. Wolken bevatten dus minder ^{18}O en hebben een negatieve δ^{18}O waarde. Als de wolken vervolgens landinwaarts bewegen zullen watermoleculen met ^{18}O ook nog eens eerder uitregenen (Figuur 1.8). Door deze processen is de δ^{18}O waarde van het regenwater steeds negatiever naarmate men verder landinwaarts komt. Neerslag die valt op grote hoogte of in een koud klimaat bevat extra weinig ^{18}O. Voor Europa resulteert dit in een karakteristieke water δ^{18}O kaart met lagere waarden landinwaarts en richting hogere breedtegraden en hoogten (Figuur 1.9).

De Maas is een regenrivier met het stroomgebied in Noordoost-Frankrijk, Oost-België en Zuid-Nederland. De gemiddelde δ^{18}O waarde bedraagt daarom ~ -7.1 ‰. Het Rijnstroomgebied ligt verder landinwaarts in de Zwitserse Alpen en Zuid-Duitsland. Deze rivier wordt niet alleen gevoed door regen, maar ook door smeltwater uit de Alpen. Dit resulteert in veel lagere gemiddelde δ^{18}O waarden van ~ -9.2 ‰. Naast deze gemiddelden vertonen beide rivieren seizoensmatige δ^{18}O patronen. In de Maas reflecteert δ^{18}O die van het grondwater tijdens de winter, wanneer de invloed van verdamping klein is. Tijdens de zomer zijn de δ^{18}O waarden hoger door verdamping en neerslag met hogere δ^{18}O waarden. Deze processen resulteren in zomermaxima van -6.0 tot -6.5 ‰ en minimale waarden van -7.7 tot -8.4 ‰ gedurende de winter. In de Rijn zorgt de extra input van smeltwater met hele lage δ^{18}O waarden gedurende de zomer voor een karakteristiek patroon met maximale waarden tijdens de winter van ~ -8.2 ‰ en zomerminima van ~ -10.0 ‰ (Figuur 1.10).

17

Stabiele koolstofisotopen

Het chemisch element koolstof heeft twee stabiele isotopen: ^{12}C (98.9 %) and ^{13}C (1.1 %) (en een radioactieve: ^{14}C, die hier verder buiten beschouwing gelaten wordt). De relatieve samenstelling van verschillende materialen kan sterk verschillen door fractioneringprocessen. Fractionering van stabiele koolstofisotopen vindt bijvoorbeeld plaats als koolstofdioxide (CO_2) oplost in water tot de verschillende componenten van opgelost anorganisch koolstof: waterstofcarbonaat (H_2CO_3), bicarbonaat (HCO_3^-) en carbonaat (CO_3^{2-}). Ook tijdens allerlei biologische processen vindt fractionering plaats. Fotosynthese bijvoorbeeld, selecteert sterk tegen ^{13}C. Dit resulteert in lage koolstofisotopenratio's ($\delta^{13}C$ waarden) voor plantenmateriaal.

Stabiele koolstofisotopenratio's van opgelost anorganisch koolstof in rivieren vertonen meestal een seizoensmatige cycliciteit. Achtergrondwaarden reflecteren normaal gesproken die van grondwater. In de winter zijn de waarden lager door de bijdrage van CO_2 afkomstig van de afbraak van landplanten die weinig ^{13}C bevatten. Tijdens de zomer zijn de waarden hoog, omdat de bijdrage van organisch materiaal van het land beperkt is, door isotopenuitwisseling met CO_2 in de atmosfeer en doordat fotosynthese van algen en waterplanten ^{12}C uit het opgelost anorganisch koolstof verwijdert. In de Maas en de Rijn liggen de waarden normaal gesproken tussen -8 ‰ in de zomer en -15 ‰ in de winter.

Doel en onderzoeksvragen

Het doel van deze studie is de mogelijkheden te onderzoeken de scheikundige samenstelling van zoetwatermossels toe te passen als proxy voor rivieromstandigheden in het verleden, om uiteindelijk laat Holocene rivieromstandigheden te kunnen reconstrueren. Binnen deze context worden de volgende onderzoeksvragen gesteld:

1. Worden seizoensmatig veranderende stabiele zuurstof- en koolstofisotopenratio's van het water vastgelegd in de groeibanden van zoetwatermossels? Welke ecologische parameters beïnvloeden de nauwkeurigheid van $\delta^{18}O$ en $\delta^{13}C$ waarden van de schelp als proxysysteem in de Maas en de Rijn? Worden verschillen in rivieromstandigheden tussen de Maas en de Rijn, zoals zichtbaar in zuurstofisotopenratio's van het water, vastgelegd in de schelpen?

2. Kunnen we modellen construeren voor groei binnen een seizoen en tussen meerdere jaren, gebaseerd op stabiele zuurstof- en koolstofisotopenchemie van rivierwater en gelijktijdige sclerochronologische

schelpendatareeksen?

3. Wat is de empirische relatie tussen gemeten water $\delta^{18}O$ waarden en debiet van de rivieren? Kunnen we water $\delta^{18}O$ waarden uit het verleden reconstrueren en vervolgens in verband brengen met gemeten debietwaarden? Kunnen seizoenen met extreem hoge en lage debieten herkend worden in gereconstrueerde water $\delta^{18}O$ waarden en debiet datareeksen?

4. Wat kunnen $\delta^{18}O$ datareeksen van zoetwatermossels ons vertellen over rivierontwikkelingen en klimaat gedurende het laat Holoceen? Kunnen we de effecten van laat Holocene klimaatschommelingen op honderd- tot duizendjaarlijkse schaal herkennen in de seizoensmatige signalen in zoetwatermossels? Wat waren de effecten van laat Holocene klimaatveranderingen op seizoensmatige water $\delta^{18}O$ waarden en gerelateerde rivieromstandigheden (de bijdrage van smeltwater uit de Alpen en zomerdroogtes in de Maas)?

Benadering

Voor het beantwoorden van deze vragen hebben we voor de volgende benadering gekozen:

1. De installatie van monitorstations in zowel de Rijn als de Maas. Locaties werden geselecteerd in vistrappen bij stuwen in de rivieren; een in Lith (Maas) en een in Hagestein (Lek, aftakking van de Rijn). Een vistrap is een klein kanaal dat vismigratie stroomopwaarts mogelijk maakt. Vistrappen zijn ideaal voor ons experiment, omdat het waterniveau hier relatief constant is en ze door hekken beschermd zijn tegen vandalisme. Er is een kooi ontworpen die sediment kan bevatten, zodat de mossels zichzelf in kunnen graven, maar zó, dat er ook water over de mossels kan stromen. Levende zoetwatermossels werden verzameld in het riviertje de Linge (een kleine aftakking van de Rijn), dat bekend staat om zijn hoge populatiedichtheid van deze dieren. De verzamelde mossels werden gemeten, gemerkt en in de kooien gezet. Gedurende 1,5 jaar werden iedere twee weken watermonsters genomen bij de monitorplaatsen en de watertemperatuur werd continu gemeten. Een gedetailleerde beschrijving van het monitorexperiment en de resultaten wordt gegeven in de hoofdstukken 2 en 3 van dit proefschrift.

2. De vergelijking van zuurstof- en koolstofisotopendatareeksen van schelpen uit geselecteerde twintigste-eeuwse tijdsintervallen met gemeten tijdseries van fysische en chemische rivierwaterdata. Deze data-

reeksen geven de mogelijkheid om de monitorresultaten te vergelijken met meerjarige schelpendatareeksen. Resultaten van de 20$^{\text{ste}}$ eeuwse schelpen worden gepresenteerd in hoofdstuk 4, 5 en 6.

3. Toepassing van de ontwikkelde proxy op laat Holocene mollusken uit archeologische vondsten en paleogeografische boringen. Resultaten staan in hoofdstuk 7 van dit proefschrift en gaan voornamelijk over de Rijn, omdat archeologisch Maasmateriaal erg zeldzaam bleek te zijn.

Techieken

Om veranderingen in stabiele isotopenratio's in schelpen in de tijd waar te nemen, moeten interne groeibanden op hoge resolutie bemonsterd worden. Hiertoe werden de schelpen eerst ingegoten in epoxyhars, zodat ze niet zouden breken wanneer doorsneden van 300 μm dikte werden gemaakt. Deze doorsneden werden vervolgens op een glasplaatje gelijmd. Het glasplaatje werd vastgemaakt op een Micromill. Een Micromill is een tandartsboor verbonden aan een microscoop en een computer. De boor en de schelpsectie kunnen langs X, Y en Z-assen nauwkeurig ten opzichte van elkaar bewegen. Met de Micromill kunnen met grote precisie monsters genomen worden langs de groeilijnen in de parelmoerlaag van de schelp tot op een ruimtelijke resolutie van 30 μm (Figuur 1.12, 1.13 en 1.14). Hierna werden de δ^{18}O en δ^{13}C waarden van schelpmonsters op een van twee isotopenratio massaspectrometers gemeten (Figuur 1.15).

Vastlegging van water δ^{18}O en δ^{13}C waarden door zoetwatermossels

Zoetwatermossels in de Maas en de Rijn bouwen hun schelp op in zuurstofisotopisch evenwicht met het water. Seizoensmatige patronen in schelp δ^{18}O waarden zijn het resultaat van variatie in zowel water δ^{18}O waarden als temperatuur. Zoetwatermossel δ^{18}O datareeksen kunnen daardoor dienen als proxy voor δ^{18}O waarden van rivierwater in het verleden, waarvan dan vervolgens seizoensmatige variatie in debiet en rivierdynamiek kan worden afgeleid.

Schelpen uit de rivieren Maas en Rijn verschillen aanzienlijk van elkaar in gemiddelde δ^{18}O waarden. Dit verschil reflecteert het verschil in water δ^{18}O waarden tussen de twee rivieren (regenrivier en smeltwater-/regenrivier). Deze gemiddelde δ^{18}O waarden kunnen gebruikt worden om via fossiele mosselen uit een oud rivierkanaal te bepalen of die stroom werd gevoed door de Maas, de Rijn of beide rivieren.

De δ^{13}C waarde van opgelost anorganisch koolstof in de rivier heeft een

seizoensmatige cyclus met lage waarden in de winter en lente. Aan het begin van de zomer nemen de waarden abrupt toe als gevolg van verwijdering van ^{12}C door fotosynthese van fytoplankton. Deze seizoensmatige δ^{13}C cyclus wordt nauwkeurig vastgelegd in de δ^{13}C waarden van groeibanden van zoetwatermossels. δ^{13}C datareeksen van zoetwatermossels kunnen potentieel dienen als proxy voor primaire productiviteit in het verleden, hoewel andere parameters (bijvoorbeeld de bijdrage van metabolisch koolstof of CO_2-uitwisseling met de atmosfeer) waarschijnlijk ook invloed hebben op δ^{13}C waarden van de schelp.

Groei van de schelpen

Nu bekend is dat zoetwatermossels zowel water δ^{18}O als δ^{13}C getrouw vastleggen in de schelp, kunnen we groei reconstrueren, zowel binnen een seizoen als over meerdere jaren. De seizoensmatige schelp δ^{18}O datareeksen hebben het patroon van een afgeknotte sinusoïde met smalle pieken en brede dalen. Dit patroon wordt veroorzaakt door een combinatie van de invloed van temperatuur op δ^{18}O en groeionderbrekingen tijdens de wintermaanden. Deze datareeksen kunnen gebruikt worden voor de nauwkeurige reconstructie van groei over meerdere jaren. In de eerste 2 tot 3 jaar van hun leven groeien zowel *Unio pictorum* als *U. tumidus* relatief snel. Daarna vertraagt de groei aanzienlijk. Een dergelijke afname van groeisnelheid gedurende het leven komt veel voor bij zoetwatermossels.

Inzicht in de groei binnen een seizoen, wordt verkregen door de constructie van een niet-lineair model, gebaseerd op de correlatie van δ^{18}O en δ^{13}C variatie in water en schelpen. De start van de groei in de lente en groeistop in de herfst worden geïnduceerd door watertemperatuur, terwijl groeisnelheid binnen het seizoen het resultaat is van primaire productiviteit (voedselbeschikbaarheid).

Het verband tussen water δ^{18}O waarden en debiet

Voor de beoogde toepassing van schelp δ^{18}O waarden als proxy voor debiet moeten we eerst de relatie tussen debiet en schelp δ^{18}O waarden karakteriseren. Voor de Maas is die relatie logaritmisch. Dit biedt de mogelijkheid debiet uit het verleden te reconstrueren via gereconstrueerde water δ^{18}O waarden.

Periodes van laag debiet ($\leq$ 6 m^3/s) tijdens de zomer worden meestal vastgelegd in de schelpen. Uit deze studie blijkt dat periodes van hoog debiet niet kunnen worden gereconstrueerd uit schelpen δ^{18}O datareeksen. Dit komt doordat de voorspellende kracht van water δ^{18}O waarden voor debiet

beperkt is in de normaal tot hoog debiet situatie, vanwege de logaritmische relatie tussen deze twee variabelen.

Voor de Rijn werd geen significante relatie gevonden tussen debiet en water $\delta^{18}O$ waarden, omdat het een gecombineerde regen-/smeltwaterrivier is en de relatie tussen $\delta^{18}O$ waarden en debiet daardoor complexer dan in de Maas. Kwantitatieve reconstructie van water $\delta^{18}O$ waarden en debiet uit het verleden door middel van zoetwatermossel $\delta^{18}O$ waarden is daarom niet mogelijk. Extreem grote smeltwaterbijdrages uit de Alpen kunnen waarschijnlijk wel worden gedetecteerd door hun zeer lage water $\delta^{18}O$ waarden.

Het Holoceen

De laatste stap naar reconstructie van rivierdynamiek in het verleden, is de analyse van laat Holocene schelpen.

Er is al veel onderzoek gedaan naar de variaties in het klimaat van Europa gedurende het laat Holoceen. Hoewel in deze recente geologische periode de fluctuaties in temperatuur en neerslaghoeveelheden meestal klein zijn in vergelijking met de grote glaciaal-interglaciaal oscillaties van het Pleistoceen, zijn er ook enkele grotere klimaattrends en oscillaties beschreven. Rond 5000 jaar geleden had West-Europa een warm en droog klimaat. Dit duurde tot ongeveer 2800 jaar geleden. Toen veranderde het klimaat vrij abrupt naar koelere en nattere omstandigheden. In de Romeinse tijd beschrijven enkele auteurs een warmere periode, gevolgd door een koudere periode tussen 400 en 700 n. Chr. De Middeleeuwse Warme Periode duurde ongeveer van 950 tot 1200 en wordt gekarakteriseerd door opvallend warme, droge zomers en natte winters. De temperatuur was vergelijkbaar met die van de eerste helft van de twintigste eeuw. De koudste fase van het laat Holoceen, de periode tussen 1550 en 1700, wordt de Kleine IJstijd genoemd. De Kleine IJstijd wordt gekenmerkt door zeer strenge winters en natte zomers, die maar weinig kouder waren dan tegenwoordig.

Alle bestudeerde schelpen uit het verleden hebben gemiddelde, minimale en maximale $\delta^{18}O$ waarden die vallen binnen de bandbreedte van de recente exemplaren. Dat wijst erop dat de smeltwaterhoeveelheden en de ernst van droogtes toen hetzelfde waren als tegenwoordig. Waarschijnlijk zijn de klimaatvariaties op de schaal van honderden tot duizenden jaren te subtiel om makkelijk herkend te worden in deze datareeksen. De grote variatie in milieuomstandigheden tussen de jaren en binnen een groeiseizoen zorgt voor een aanzienlijke hoeveelheid ruis in de schelp $\delta^{18}O$ datareeksen. Hieruit kunnen we concluderen dat deze schelpen beter geschikt zijn voor

het bestuderen van omgevingsvariabiliteit op een schaal van seizoenen tot maximaal tientallen jaren.

Twee middeleeuwse schelpen vertonen variatie in gereconstrueerde water $\delta^{18}O$ waarden, met een periode van ~ 7 tot 10 jaar. Mogelijk is dit het gevolg van variabiliteit in de Noord-Atlantische Oscillatie (NAO), die sterk gerelateerd is aan weerspatronen in Europa gedurende de lente en de zomer, en bijbehorende rivierafvoer.

Om sterkere conclusies te kunnen trekken over variabiliteit in rivierdynamiek tijdens het laat Holoceen, zou een grotere hoeveelheid schelpen, met daarin een veelvoud aan groeiseizoenen, geanalyseerd moeten worden. De schijnbare detectie van NAO-variabiliteit prikkelt de nieuwsgierigheid en roept om meer onderzoek aan zoetwatermossels uit de Middeleeuwen, vooral aan langlevende soorten.

Conclusies

Deze studie onderzoekt schelpchemie van zoetwatermossels als proxy voor rivierdynamiek in het verleden. Het is een van de eerste studies waarbij een monitorexperiment gecombineerd wordt met de analyse van een verzameling recente monsters uit het wild, en met de toepassing van de proxy op laat Holoceen materiaal. We hebben laten zien dat drie soorten *Unio* hun omgeving getrouw vastleggen met betrekking tot zowel stabiele isotopen van zuurstof als van koolstof. Dit maakt *Unio*'s nuttig voor toepassing in paleoklimatologisch onderzoek.

Door verschillende hoge-resolutie chemische datareeksen te combineren, konden we modellen construeren voor groei van de schelp, zowel tussen de jaren als binnen één seizoen.

De grote variatie in omstandigheden tussen verschillende plaatsen in de rivier en tussen verschillende tijdstippen zorgt voor een aanzienlijke hoeveelheid ruis in het klimaatsignaal. Dit betekent dat zowel lokale omstandigheden als omgevingsvariatie tussen de seizoenen het laag-frequente klimaatgerelateerde signaal in deze schelpen kunnen verhullen. In vergelijking met de meeste zoetwatersystemen zijn de omstandigheden in zeeën en oceanen meestal stabieler met betrekking tot temperatuur en water $\delta^{18}O$. Daarom zijn de datareeksen van zoetwaterschelpen moeilijker te interpreteren dan hun mariene equivalenten.

Deze problemen kunnen geminimaliseerd worden door voldoende schelpen per tijdsinterval te analyseren, en zo het volle bereik aan variabiliteit te meten. Ook zijn nauwkeurige groeimodellen nodig om inzicht te krijgen in de groei tussen tussen de jaren en binnen één seizoen. Zo kunnen

beschikbare klimaatdata nauwkeuriger gekoppeld worden aan schelpmonsters. Verder is het wenselijk meerdere proxy's binnen een organisme te gebruiken, zoals bijvoorbeeld de combinatie van stabiele isotopenratio's met diverse sporenelementen. Daarmee worden de foutmarges op klimaatreconstructies kleiner. Rivierdebiet kan ook op een andere manier gereconstrueerd worden, namelijk door het zoutgehalte in de monding van een rivier te bepalen op basis van $\delta^{18}O$, $\delta^{13}C$ en bariumdatareeksen in zoutwaterschelpen. De combinatie van deze methodes met zoetwatermossel $\delta^{18}O$ datareeksen kan de reconstructie van het debiet betrouwbaarder maken.

Als aan bovenstaande suggesties voldoende tegemoetgekomen wordt, kunnen stabiele isotopenratio's in archeologische schelpen dienen als proxy voor het reconstrueren van rivierdynamiek, eventuele droogtes en smeltwaterbijdrage. Zulke reconstructies zijn belangrijk voor het valideren van modellen die de invloed van toekomstige klimaatveranderingen in de Rijn-Maasdelta voorspellen.

About the author

Emma Versteegh was born in 's-Hertogenbosch on 12 December 1978. For the first 19 years of her life she lived in Kerkdriel in the Dutch *rivierengebied* (the area between the rivers Rhine and Meuse). She finished grammar school at the Stedelijk Gymnasium 's-Hertogenbosch in 1997, and afterwards took part in the International Biology Olympiad in Turkmenistan. After obtaining a preparatory degree in medicine at Utrecht University, she switched to biology at that same university. In August 2003 she obtained her MSc degree in animal behaviour and marine ecology with the theses "Foraging behaviour and coping strategies in wild Great Tits" and "Migration behaviour and habitat choice in coral reef fish". For the latter project she lived on Zanzibar for 5 months, learned SCUBA diving, and became enthusiastic about marine biological research. From 2003 to 2005 she worked at the Pax Christi College in Druten as a teacher in biology and science, while she obtained a teaching degree from Utrecht University. In September 2005 she started her PhD research at the VU University Amsterdam, which she completes with this thesis. Since March 2009 she has been working as a postdoctoral researcher at the Vrije Universiteit Brussel. There she continues working on bivalve biogeochemistry, including marine shells from the Scheldt estuary (Belgium) and Disko Bay (Greenland). In her spare time Emma loves to sing in the Capella Sanctorum Michaelis et Gudulae, go for a run in the Brussels park, or read novels or books on popular science.

Chapter 1

Introduction

1.1 Background

Ongoing climate change is of major concern for the 21st century and beyond. Although the geological past shows the importance of natural climate variability, the Intergovernmental Panel on Climate Change (IPCC) concludes that most of the global warming in the past 50 years has very likely been caused by human activities such as the burning of fossil fuels and massive deforestation. The effects of global warming are predicted to vary regionally in the coming century; for Western Europe an increase in precipitation is predicted in winter, whilst droughts are expected to occur more frequently in the summer at the end of this century (IPCC, 2007). Considering the vulnerable position of the Netherlands in the Rhine-Meuse delta (Kabat et al., 2003), it is therefore vital to improve our understanding of extreme precipitation events and related river floods and droughts. In the recent past, severe flooding events took place in 1993 and 1995. The flood of 1995 led to extensive damage and the precautionary evacuation of more than 200,000 inhabitants of the Dutch river area (TAW, 1995; Figure 1.1). Droughts such as those in 1976 and 2003 (Figure 1.2), on the other hand, limit water availability for agriculture and the cooling water of power plants (Rutten et al., 2008), and can cause the deterioration of water

Figure 1.1: Flooding of the river Meuse in 1995 (http://www.wldelft.nl/).

Figure 1.2: Extensive exposure of the riverbed during extremely low water levels in the river Waal (Rhine) at Gameren in 2003 (http://www.ru.nl/).

quality, threatening drinking water supplies and impacting on river ecology (Van Vliet and Zwolsman, 2008).

The project Climate Scenarios-9 (CS-09) "Modelling and reconstructing precipitation and flood frequency in the Meuse catchment during the late Holocene" is part of the national BSIK 'Climate changes Spatial Planning' programme. Project CS-09 aims to compare climate scenarios with past fluctuations in climate, with the main focus on precipitation. It also examines the role played by changing land use and land cover in the climate system, and the effects on the hydrological cycle and water management. This subproject of CS-09 investigates the use of freshwater mollusc shells as archives for changes in river conditions during the past 5000 years, in particular changes in discharge during flooding and drought events.

1.2   The Rhine-Meuse delta

The Rhine-Meuse delta comprises a large part of the Netherlands. The rivers represent two different types: the Meuse is a rain-fed river and the
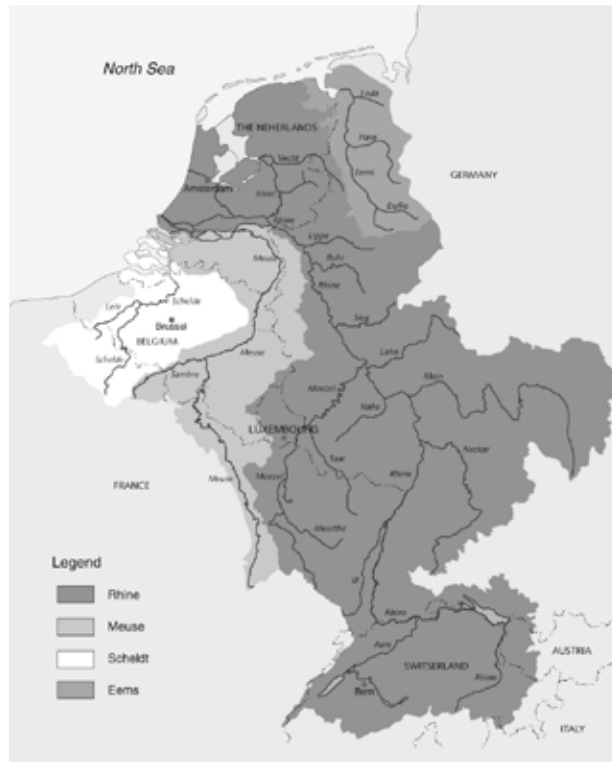
Figure 1.3: The Rhine and Meuse drainage basins (adapted after Ten Brinke, 2006).

Rhine is a meltwater/rain-fed river. The Meuse basin, with an area of ca. of 33,000 km², lies in the northeast of France, eastern Belgium and the south of the Netherlands (Figure 1.3). Average discharge at Borgharen is 274 m³/s and the highest peak discharges exceed 3000 m³/s. The Rhine is one of Western Europe's largest river systems with a basin of 185,300 km². It drains meltwater from the Alps and precipitation from southern Germany (Figure 1.3). Average discharge of the Rhine at Lobith is 2200 m³/s, but peak discharges can be as high as 13,000 m³/s (Berendsen and Stouthamer, 2001).

1.3   European late Holocene climate

The late Holocene variation of the European climate has been well studied. Although fluctuations in temperature and precipitation regimes are small compared to the large glacial-interglacial oscillations of the Pleistocene, several major climatic trends and oscillations can be recognised (Figure 1.4). At around 5000 BP, Western Europe experienced a continental cli-

C14 years BP	Years BP/AD	Archaeological period	Geological time	Glacier extension	Lake level	Temperature
	1500 AD		LIA			
		Middle Ages	MWP			
	500 AD		Late Holocene			
		Roman time	RWP			
2000	12 AD	Late Iron Age (Iron Age)	Subatlantic			−0.4°C 1856-1980 mean +0.4°C
2250	2250 BP	Middle Iron Age				
2450	2500 BP	Early Iron Age				
2600	2800 BP	Late Bronze Age (Bronze Age)				
2900	3100 BP	Middle Bronze Age B				
3300	3500 BP	Middle Bronze Age A / Early Bronze Age	Middle Holocene	Subboreal		
3450	3800 BP	Late Neolithic B (Neolithic)		glacier retreat / lower lake level	glacier advance / higher lake level	
3650	4000 BP	Late Neolithic A				
3950	4500 BP	Middle Neolithic B				
4300	4900 BP	Middle Neolithic A				

Figure 1.4: Archaeological and geological time periods during the middle to late Holocene in the Netherlands (Louwe Kooijmans et al., 2005), records of extension of the Great Aletsch glacier (Switzerland), west-central European lake-level records (Holzhauser et al., 2005) and Northern Hemisphere temperature reconstruction (Mann et al., 2003). LIA = Little Ice Age; MWP = Medieval Warm Period; RWP = Roman Warm Period.

mate (warm and dry), during a time interval known as the Subboreal. This lasted until about 2800 BP, when the climate changed rather abruptly to more oceanic (cooler and wetter) conditions. This time interval is known as the Subatlantic (Van Geel et al., 1996).

During Roman times some authors document a warmer interval (Roman Warm Period, RWP), followed by a colder period between 400 and 700 AD, the Dark Ages (Hass, 1996).

The Medieval Warm Period (MWP) lasted from about 950 until 1200 AD (Brázdil et al., 2005) and was accompanied by a maximum in solar activity (Jirikowic and Damon, 1994; Bard et al., 2000). The MWP is characterised by markedly warm, dry summers and wet winters (Lamb, 1965; Mann et al., 1999; Cook et al., 2004; Goosse et al., 2005; Goosse et al., 2006). The temperatures were similar to those of the first half of the twentieth century, with an anomaly of -0.03 to +0.20 °C (Crowley and Lowery, 2000; Bradley et al., 2003). The coldest phase of the late Holocene was the Little Ice Age (LIA). It consisted of several cold intervals between 1400 and 1900 AD (Mann et al., 1998) and was accompanied by several solar activity minima (Bard et al., 2000, Luterbacher et al., 2001). The coldest period was between 1550 and 1700 AD (Lamb, 1965; Shabalova and Van Engelen, 2003;

Brázdil et al., 2005). The LIA is characterised by severely cold and dry winters and wetter summers, which were only slightly cooler (~ -0.2 °C) than today (Luterbacher et al., 2001; Cook et al., 2004; Luterbacher et al., 2004; Guiot et al., 2005; Figure 1.4).

1.4   Palaeogeography of the Rhine-Meuse delta

During the late Holocene both climate and human activities had their influence on morphology and discharge rates of the Rhine and Meuse. Low sea levels during the early Holocene caused river-channels to be incising-meandering. From approximately 8000 BP until 4000 BP rapid sea level rise changed the fluvial style from incising meandering via aggrading meandering to straight anastomosing in the western and middle part of the delta. After 4000 BP the fluvial style changed back to aggrading meandering (Berendsen and Stouthamer, 2001). At this time Western Europe experienced a continental climate (warm and dry), during a time interval known as the Subboreal. Around 2800 BP the climate changed from relatively warm and dry, to cooler and wetter conditions; this is know as the Subboreal-Subatlantic transition (Van Geel et al., 1996). As a result, dis-

Figure 1.5: Palaeogeographical map of the Rhine and Meuse in the Netherlands (after Berendsen and Stouthamer, 2001).
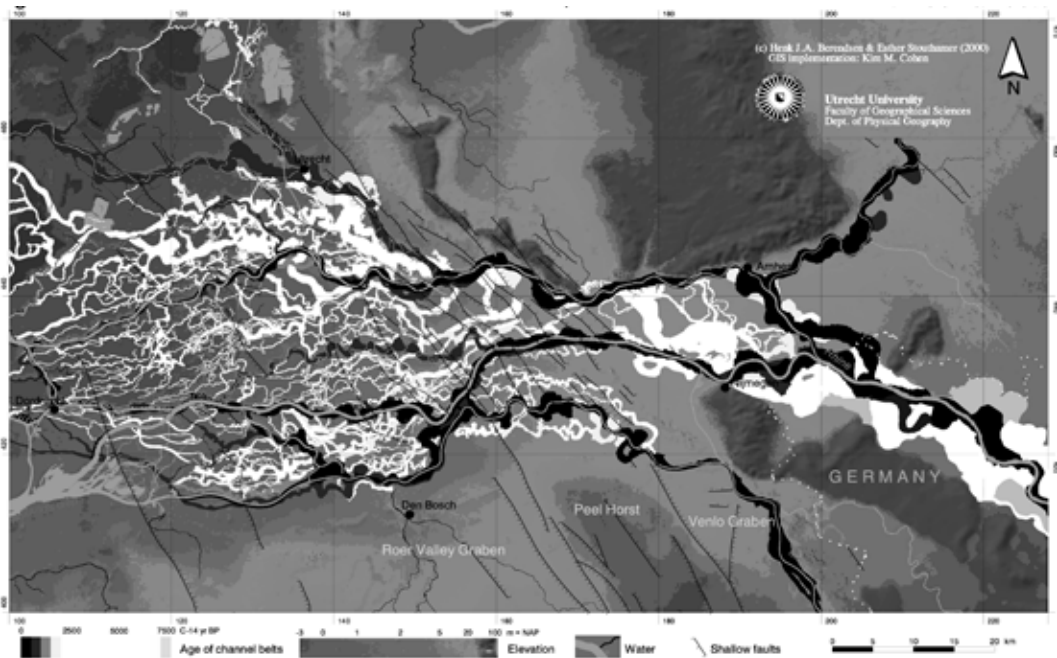
charge in the rivers increased. Since that time, both the wavelength of meanders and the number of channels increased towards a maximum around 2000 BP (Roman Period). Until this time the Oude Rijn (Old Rhine) was the main distributary of the Rhine and flowed into the North Sea at Katwijk. After that time the main drainage of the Rhine shifted to the southwest and drained into the Meuse estuary near Rotterdam (Berendsen and Stouthamer, 2001). An overview of the Holocene channel belts in the Rhine-Meuse delta is given in figure 1.5.

Human influence in the Rhine-Meuse delta started with the beginning of agriculture and related clearing of forests during the Neolithic (6400-3650 BP). During the Roman occupation the Old Rhine was the northernmost border of the Roman Empire. Many villages were founded along the rivers and even small canals were dug, locally changing the course of the rivers. Human influence strongly increased from 1100 AD with the embankment of the rivers, which was complete around 1300 AD. The Old Rhine was dammed near Wijk bij Duurstede in 1122 AD, the Hollandse IJssel in 1285 and the Linge in 1307 AD, reducing the number of Rhine distributaries to the current three: Lower Rhine-Lek, Waal and IJssel (Berendsen and Stouthamer, 2001).

Freshwater mollusc shells are potential archives of climatic and environmental change. As they are often encountered in archaeological contexts, it is of interest to examine whether the variability described above can be detected in shells from several Holocene time intervals.

1.5   Sclerochronology

Many aquatic organisms, such as corals, gastropods and bivalves form periodic growth increments in their skeletons, similar to the growth rings of trees. As environmental characteristics are recorded in these growth increments (e.g. Figure 1.6), these skeletons can serve as archives of environmental change. The study of periodic features in the skeletal portions of aquatic organisms has been termed sclerochronology (Hudson et al., 1976; Jones, 1983). Much sclerochronological research has been done on marine bivalves using the stable oxygen isotope composition ($\delta^{18}O$) as a proxy for temperature or salinity (Carré et al., 2005; Chauvaud et al., 2005; Schöne et al., 2005a; Thébault et al., 2007; Dunca et al., 2009). In freshwater bivalves, $\delta^{18}O$ has been demonstrated to be a proxy for palaeohydrology, such as changes in water source, discharge or rainfall patterns (Dettman et al., 1999; Rodrigues et al., 2000; Davis and Muehlenbachs, 2001; Kaandorp et al., 2003; Ricken et al., 2003; Verdegaal et al., 2005; Gajurel et al., 2006;
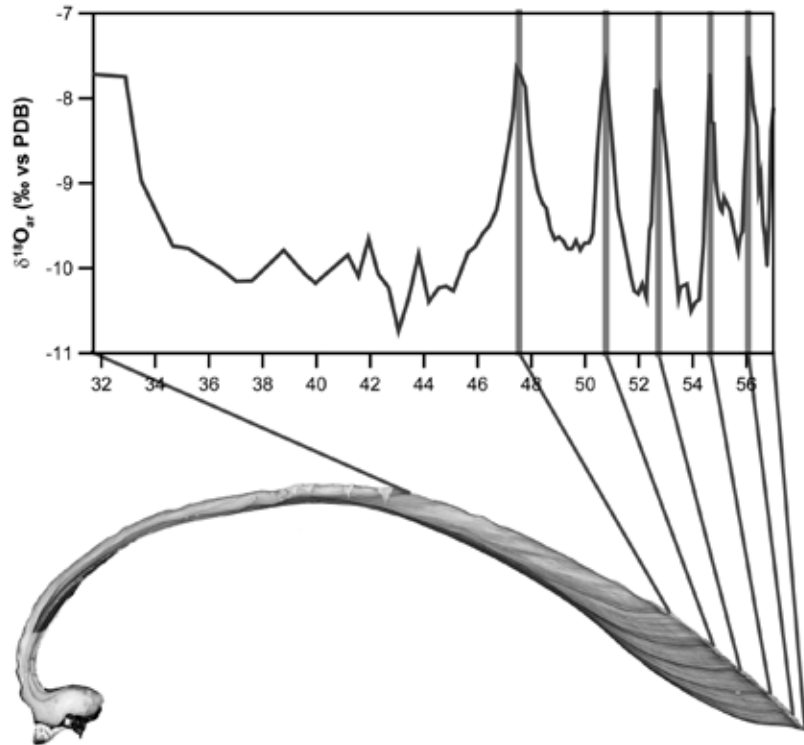
Figure 1.6: A transverse section through a *Unio tumidus* shell and the shell aragonite $\delta^{18}O$ ($\delta^{18}O_{ar}$) record of the same specimen. Growth cessations, usually occurring in winter, are visible as dark internal growth lines in the shell and as narrow positive peaks in the shell $\delta^{18}O_{ar}$ record.

Goewert et al., 2007). The current study applies both oxygen and carbon stable isotope compositions ($\delta^{13}C$) of unionid freshwater bivalves as environmental and palaeohydrological proxies in the rivers Meuse and Rhine.

1.6   Freshwater molluscs in the Netherlands

Freshwater molluscs are common in Dutch rivers, streams and lakes. The majority belong to the gastropods (snails), but several bivalve species are also encountered. The freshwater mussels used in this study are members of the bivalve family Unionidae within the order Unionoida (pearly mussels or naiads). Unionoida have only slight tolerance to increased salinities (up to ~ 3 ‰) and are thus restricted to freshwater.

Worldwide over 900 species have been described, the greatest diversity of which occurs in North America. Many species are endangered due to over-exploitation, environmental pollution, habitat destruction and the in-

troduction of invasive exotic species (Bauer, 1988; Williams et al., 1993; Ricciardi et al., 1998; Schloesser and Masteller, 1999; Burlakova et al., 2000; Gillies et al., 2003; Klocker and Strayer, 2004). In the Netherlands, six members of the family Unionidae represent this order. They form large shells, live half buried in the sediment (semi-infaunal) and can reach an age of up to 15 years (Gittenberger et al., 1998).

In this project four species of Unionidae are used:

- *Unio crassus nanus* Lamarck, 1819 (Thick shelled river mussel). The shell is elliptical to oval and reaches a maximum size of 40 x 70 mm. This species is found in flowing water, usually in rivers. In comparison with the other Dutch unionids it prefers the coarsest sandy sediments and is most sensitive to pollution and low oxygen levels. *U. crassus* has been extinct in the Netherlands since 1968 due to environmental pollution (Figure 1.7a) (Gittenberger et al., 1998).

- *Unio pictorum* (Linnaeus, 1758) (Painter's mussel). This species is thick-shelled and has an elongated elliptical shape with a maximum size of 44 x 110 mm. It is found in both stagnant and flowing waters and tolerates some pollution (Figure 1.7b) (Gittenberger et al., 1998).

- *Unio tumidus* Philipsson, 1788 (Swollen river mussel). The shell has an egg-like shape with a prominently curved edge. Its maximum size is 62

Figure 1.7: a. *Unio crassus*; b. *U. pictorum*; c. *U. tumidus*; d. *Anodonta anatina*. Scale bars represent 1 cm.
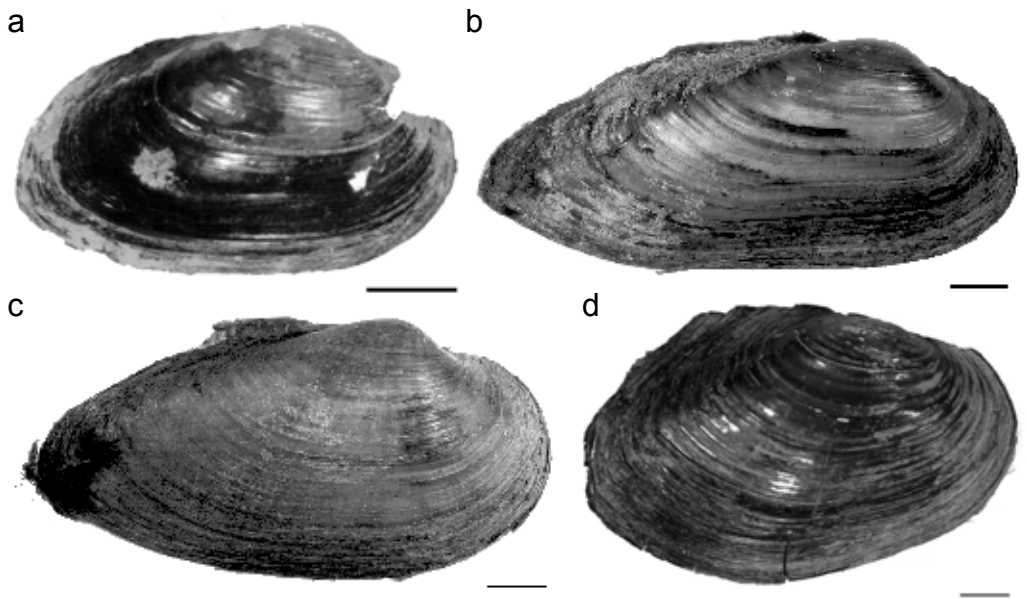
x 125 mm. This species prefers flowing water but also occurs in stagnant waters. Among the Dutch unionids it has the highest tolerance for pollution (Figure 1.7c) (Gittenberger et al., 1998).

- *Anodonta anatina* (Linnaeus, 1758) (Duck mussel). *Anodonta* species have much thinner shells than the above *Unio* species. *A. anatina* has an oval shape with a prominent hooked wing on top and reaches a maximum size of 80 x 132 mm. It occurs in both stagnant and flowing waters (Figure 1.7d) (Gittenberger et al., 1998).

Unionid shells are readily found in archaeological finds, as prehistoric humans used unionid shells for food, tools and ornamental objects. Shell middens are known from Australia (Russell-Smith et al., 1997), Indonesia (Joordens et al., 2009), North America (Parmalee and Klippel, 1974; Peacock and James, 2002) and Africa (Plug and Pistorius, 1999). In North America, freshwater mussels used to represent an important commercial fishery in which shells were used in the manufacture of buttons (Howard, 1922). Today, freshwater mussel shells are used for the production of seed pearls in the cultured pearl industry (Williams et al., 1993). The European species are considered inedible and were only eaten in times of severe famine, but were sometimes used as cattle food (Tudorancea, 1972) or in prehistoric tools and jewellery (Gittenberger et al., 1998). *U. pictorum* (Painter's mussel) owes its name to the fact that the shells were once used by painters to hold paint (Gittenberger et al., 1998).

1.7   Oxygen isotopes in the hydrological cycle

Chemical records that are extracted from unionid shells and applied as environmental proxies in this project encompass stable isotope values of oxygen and carbon.

The chemical element oxygen has three stable isotopes: ^{16}O, ^{17}O and ^{18}O. Natural abundances of these isotopes are 99.76 %, 0.035 % and 0.20 %, respectively. Fractionation between these isotopes takes place during several processes in the hydrological cycle. Measuring ^{17}O gives little more information than can be gained from observing ^{18}O, which is more accurately measurable due to its higher abundance (Mook, 2000).

When clouds form, ^{16}O evaporates more easily than ^{18}O. Therefore clouds and the resulting precipitation are depleted in ^{18}O and have negative δ^{18}O values. ^{18}O is preferentially removed by precipitation, so the further land inwards clouds are transported, the lower the δ^{18}O of water (δ^{18}O$_w$) values (Figure 1.8). High altitude and cold climate precipitation is especially low in ^{18}O (Dansgaard, 1964). For Europe this results in a characteristic δ^{18}O$_w$
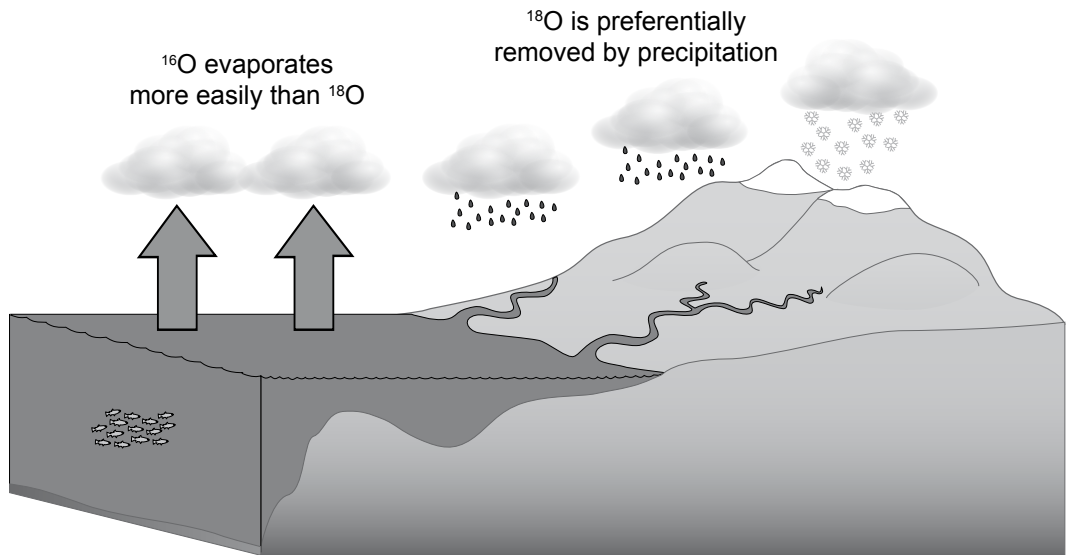
Figure 1.8: Oxygen isotopes in the hydrological cycle.

Figure 1.9: Weighted annual $\delta^{18}O_w$ in precipitation over Europe. Note the more depleted $\delta^{18}O_w$ values land inwards and towards higher latitudes (Source: Global Network for Isotopes in Precipitation (GNIP) of the IAEA/WMO: http://www-naweb.iaea.org/).
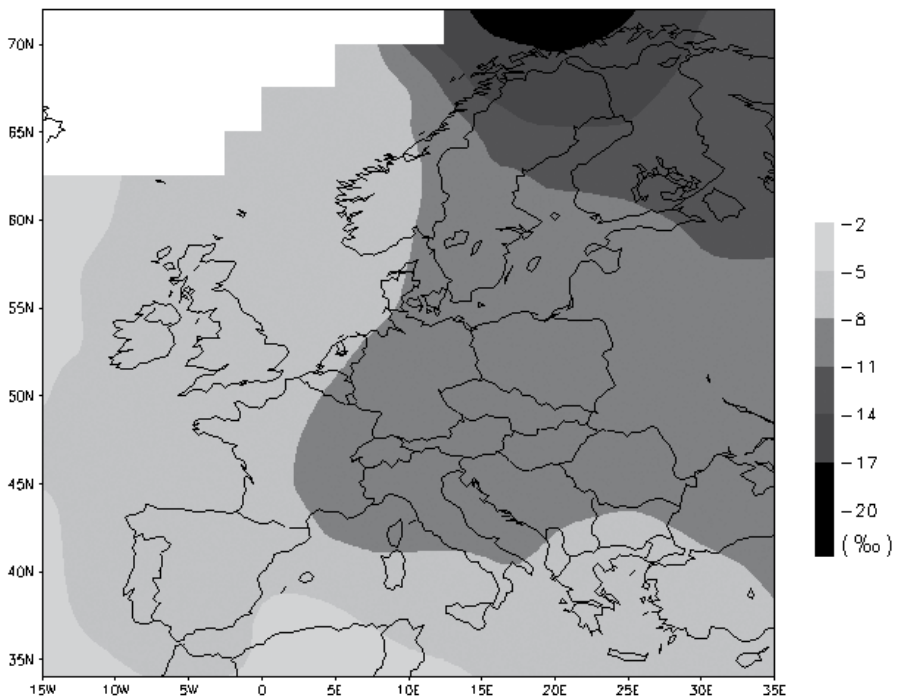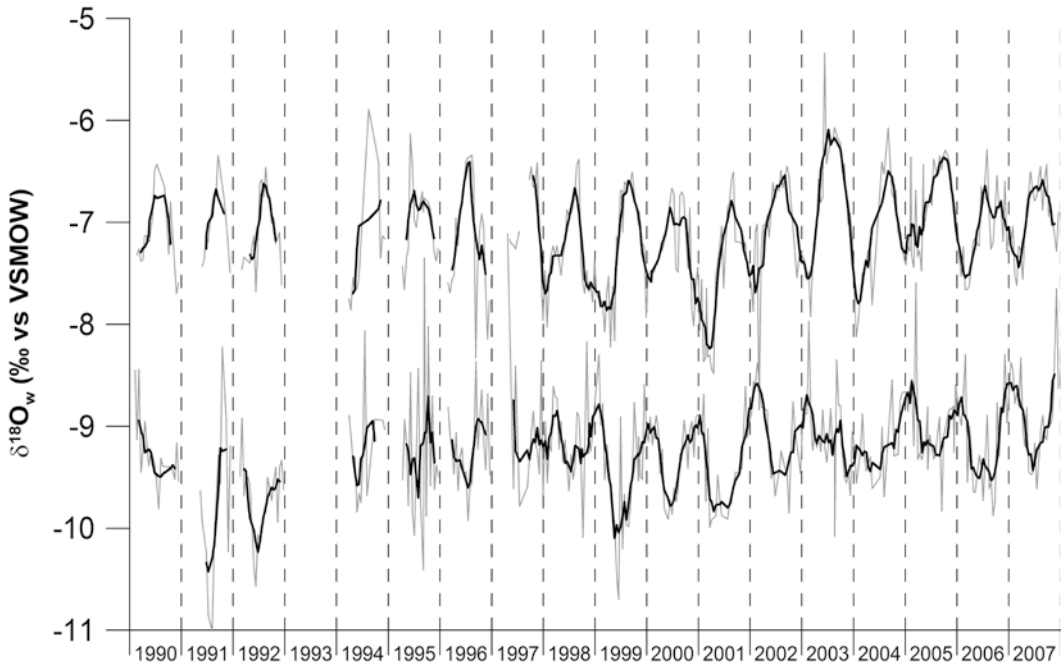
Figure 1.10: Opposing $\delta^{18}O_w$ seasonality in the rivers Meuse (top) and Rhine (bottom) during the years 1990-2007 (Data: Centre for Isotope Research, University of Groningen).

map with lower values land inwards, and towards higher latitudes and altitudes (Figure 1.9).

The Meuse is a rain-fed river with its basin located in north-eastern France and east Belgium and hence has an average $\delta^{18}O_w$ of ~ -7.1 ‰. The Rhine basin is located further land inwards in the Swiss Alps and southern Germany. As a result this river is not only fed by rain, but also by meltwater from the Alps resulting in much lower average $\delta^{18}O_w$ values of ~ -9.2 ‰. On top of these average values, both rivers exhibit seasonal $\delta^{18}O_w$ patterns. For the Meuse, in winter, when evaporation is low, $\delta^{18}O_w$ reflects the composition of groundwater, whereas in summer $\delta^{18}O_w$ values are higher due to evaporation and enriched summer rainfall. These processes result in summer maximal values of -6.0 to -6.5 ‰ and winter minimal values of -7.7 to -8.4 ‰. In the Rhine, the additional input of isotopically depleted meltwater during summer (Mook, 1968) results in a characteristic pattern with winter maximal values of ~ -8.2 ‰ and summer minimal values of ~ -10.0 ‰ (Figure 1.10).

1.8   Stable carbon isotopes

The chemical element carbon has two stable isotopes: ^{12}C and ^{13}C. Their natural abundances are 98.9 % and 1.1 %, respectively (Mook, 2000). The relative compositions of different materials may differ greatly due to several fractionation processes. Equilibrium fractionation of stable carbon isotopes occurs in dissolved inorganic carbon (DIC) in water, resulting in different stable carbon isotope ratios ($\delta^{13}C$) for the DIC compounds (CO_2(aq); H_2CO_3; HCO_3^- and CO_3^{2-}). In addition, many biological processes cause kinetic fractionations. Photosynthesis, for example, strongly discriminates against ^{13}C (Farquhar et al., 1989; McConnaughey et al., 1997), resulting in depleted $\delta^{13}C$ values for plant material.

Stable carbon isotope ratios of dissolved inorganic carbon ($\delta^{13}C_{DIC}$) in rivers tend to have a seasonal cyclicity. Background $\delta^{13}C_{DIC}$ values of river water normally reflect those of groundwater, but are lowered during winter due to input of CO_2 from the decomposition of terrestrial plant material depleted in ^{13}C (Hellings et al., 1999; Mook, 2000). $\delta^{13}C_{DIC}$ values are higher in summer, because the input of terrestrial organic material is limited, and due to isotopic exchange with atmospheric CO_2 and preferential removal of ^{12}C from the DIC pool by photosynthetic activity (Mook, 1968; Hellings et al., 1999; Mook, 2000). In the rivers Meuse and Rhine, $\delta^{13}C_{DIC}$ values normally lie between -8 ‰ (VPDB) in summer and -15 ‰ (VPDB) in winter.

1.9   Aim and research questions

In this study we aim to examine the possibilities and limitations of using freshwater mussel chemistry as a proxy for past river conditions, and to make a first attempt towards the reconstruction of late Holocene river conditions. In this context the following research questions are posed:

- Are seasonally changing stable oxygen and carbon isotope ratios of the ambient water recorded in growth bands in unionid freshwater mussels? Which ecological parameters influence the accuracy of shell aragonite $\delta^{18}O$ and $\delta^{13}C$ ($\delta^{18}O_{ar}$ and $\delta^{13}C_{ar}$) values as proxy systems in the Meuse and Rhine rivers? Are differences between the Meuse and Rhine river conditions, as reflected in oxygen isotopic values of the water, recorded in unionid shells?
- Can we establish models for interannual and intraseasonal growth rates from stable oxygen and carbon isotope chemistry of river water and equivalent sclerochronological shell records?
- What is the empirical relation between measured water $\delta^{18}O_w$ values

and river discharge? Can we reconstruct past $\delta^{18}O_w$ values and subsequently link these to measured river discharge values? Can extreme low and high discharge events be recognised in the reconstructed $\delta^{18}O_w$ and discharge records?

- What can unionid $\delta^{18}O_{ar}$ records tell us about past river conditions and climate during the late Holocene? Can we recognise effects of late Holocene centennial scale climatic trends on seasonal signals in unionid shells?

1.10   Approach

In order to address these questions we decided on the following approach:

1.   Installation of monitoring stations in both the Rhine and the Meuse. Locations were selected in fish ladders near weirs in the rivers: one in Lith (the Meuse) and one in Hagestein (the Lek, a Rhine distributary). Fish ladders are small streams that enable migratory fish to move up-river (Figure 1.11a). These are ideal for our experiment due to their relatively constant water levels, and their protected position from vandalism. Cages were designed that could contain sediment for the mussels to bury themselves in, but still allowed water to flow freely over the mussels (Figure 1.11b). Living freshwater mussels were collected in the river Linge (a small distributary of the Rhine), which is known for its high abundances of these animals (Gittenberger et al., 1998; Figure 1.11c). The collected mussels were measured, tagged and put in the cages (Figure 1.11d). For a 1.5-year period, water samples were collected at the monitoring sites every two weeks and water temperature was measured continuously. A detailed description of the monitoring experiment and the results is given in chapters 2 and 3 of this thesis.

Figure 1.11: a) Fish ladder at Lith (Meuse); b) Cage overgrown with algae at Lith; c) Collecting freshwater mussels in the river Linge; d) Placing the mussels in the cage at Hagestein (Lek).
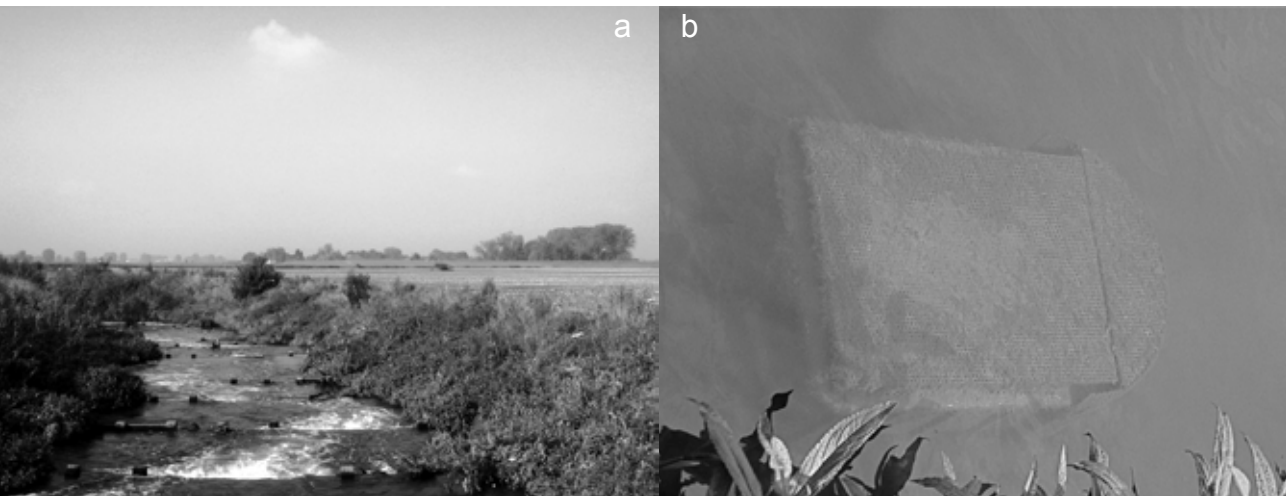
2. Comparison of shell archives from selected 20th century time intervals with known time series of physical and chemical river water data. These records enable us to verify the monitoring results with multi-annual shell records. Material for this part of the research was selected from collections at Naturalis (Netherlands National Museum of Natural History), the zoological museum of Amsterdam (University of Amsterdam) and from private collections. Water $\delta^{18}O_w$ data came from the Centre for Isotope Research (University of Groningen) and water temperature and discharge data were obtained from Rijkswaterstaat (Dutch Directorate for Public Works and Water Management; http://www.waterbase.nl/). Results of the 20th century shells are presented in chapters 4 (Versteegh et al., 2009), 5 and 6.

3. Application of the developed proxy to late Holocene molluscs from archaeological finds and palaeogeographic cores. Shell material was supplied by W. Kuijper (Leiden University) and the State Service for Cultural Heritage. Results can be found in chapter 7 of this thesis and mainly concern the Rhine river system, as Meuse material proved to be very rare.

1.11   Techniques

To observe changes in shell stable isotope ratios over time, internal growth increments must be sampled at a very high resolution. Shells were first embedded in epoxy resin to prevent them from breaking when sections of 300 μm thickness were cut along the dorso-ventral axis of the shell. These sections were then glued to a glass slide. The resulting slide was mounted on a Merchantek Micromill, which consists of an XYZ stage connected to a microscope, a fixed dental drill, and a computer (Figures 1.12a-b). With

Figure 1.12a-b: The Merchantek Micromill drilling a shell sample. Samples are mounted on a computer-controlled XYZ-stage under a fixed dental drill. Software allows complex drill patterns to be drawn.

the micromill, samples can be taken from the nacreous layer of the shell, along the growth lines, with a very high accuracy and a spatial resolution up to 30 µm (Figures 1.13a-b and 1.14). Drill bit diameter was ~ 800 µm with a drilling depth of ~ 250 µm (Figure 1.15b).

Shell samples were analysed for $\delta^{18}O_{ar}$ and $\delta^{13}C_{ar}$ on either of two isotope ratio mass spectrometers (IRMS): a Thermo Finnigan MAT 252 equipped with a Kiel-II device (Figure 1.15a) or a Thermo Finnigan Delta+ mass spectrometer equipped with a GasBench-II preparation device (Figure 1.15b). On both systems the long-term standard deviation of a routinely analysed in-house $CaCO_3$ standard was < 0.1 ‰. This $CaCO_3$ standard is regularly calibrated to NBS 18, 19 and 20. Typical sample size for the MAT 252 system lies at 10-20 µg. For the Delta+ system samples of 20-50 µg

Figure 1.13: a) Thin section of a shell of which 14 samples were taken. b) In spite of the ~ 800 µm thickness of the dental drill a much smaller sample can be drilled.
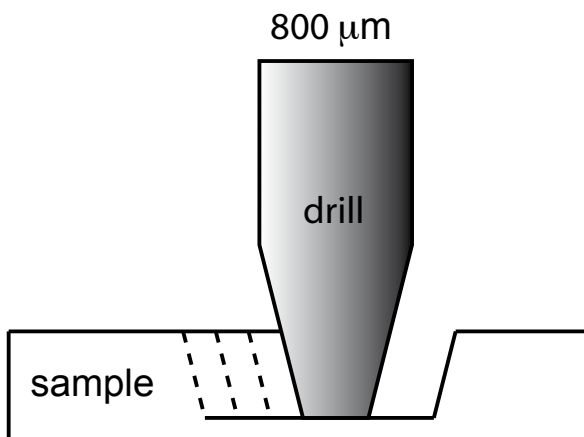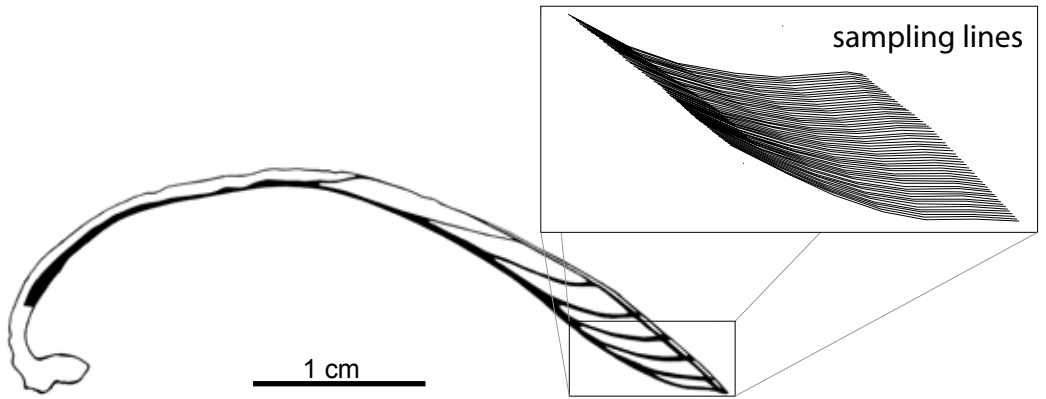
Figure 1.14: Schematic representation of Micromill sample lines in a transverse section of a unionid shell

are required. Both $\delta^{18}O_{ar}$ and $\delta^{13}C_{ar}$ are reported in ‰ vs. Vienna PeeDee Belemnite (VPDB).

Water samples were analysed for $\delta^{18}O_w$ and $\delta^{13}C_{DIC}$ on the Thermo Finnigan Delta+ mass spectrometer with the GasBench-II, $\delta^{18}O_w$ is reported in ‰ vs. Vienna Standard Mean Ocean Water (VSMOW) and $\delta^{13}C_{DIC}$ in (VPDB). The long-term standard deviation of a routinely analysed in-house water standard is < 0.1 ‰ for $\delta^{18}O_w$ values and is < 0.15 ‰ for $\delta^{13}C_{DIC}$ values, respectively.

Figure 1.15: a) Thermo Finnigan MAT 252 with Kiel-II device. b) Thermo Finnigan Delta+ with Gas-Bench-II.

1.12   Structure of the thesis

This PhD thesis comprises six chapters describing different parts of the research within the project "The geochemistry of freshwater molluscs as a proxy for palaeo-floods of rivers Rhine and Meuse", accompanied by an introduction and a synthesis. Five chapters (Chapter 2-5, 7) are also papers (to be) published in peer-reviewed journals. For this reason there is some overlap between the chapters, mainly in the introduction and material and methods sections.

Chapter 2

A new cage design for monitoring semi-infaunal freshwater mussels (Unionidae)

Abstract

Semi-infaunal freshwater mussels are often kept in cages for biomonitoring studies. Several different cage designs have been used. We introduce a new design consisting of a PVC box with a perforated stainless steel lid. The cages contained sediment and were placed in fish ladders in two Dutch rivers. Three species of Unionidae grew in the cages for a period of up to 20 months. Mussels were very mobile in the cage and sometimes clumped together. Growth rates were low, but similar to those of specimens collected in the wild. Survival rates were high until 12 months after the start of the experiment. After that time many individuals died in one cage. Apart from this mortality event, survival rates in *Unio pictorum* and *U. tumidus* were 100 %. *Anodonta anatina* had much lower survival rates and is thus less suitable for keeping in cages.

2.1 Introduction

Many different cage designs have been used for monitoring adult Unionidae. Most cage types are either suspended in the water column (Hickey et al., 1995; Englund and Heino, 1996; Malley et al., 1996; Martel et al., 2003; Friedman and Mower, 2004) or are in contact with sediment (Kauss and Hamdy, 1985; Muncaster et al., 1990; Kauss and Hamdy, 1991; Hyötyläinen et al., 2002; Martel et al., 2003). None of these cages, however, enable the mussels to bury themselves into the sediment. These conditions are known to increase stress levels in unionids (Englund and Heino, 1996) and cause lethal deformities in *Corbicula* (Bij de Vaate, pers. comm.). The current monitoring sites are in a riverbed without soft substrate, so cages cannot be partly buried. In this situation we need a cage design, which actually contains sediment.

Flexible material cage designs are either pillow cages, made of folded wire (Kauss and Hamdy, 1985; Muncaster et al., 1990; Kauss and Hamdy, 1991), or an oval design (Hyötyläinen et al., 2002). Rigid cages are often suspended on a floating device (Hickey et al., 1995; Malley et al., 1996; Martel et al., 2003). A third method is to attach mesh bags to a frame. Mussels can be placed in these bags either individually (Martel et al., 2003) or in a small group (Friedman and Mower, 2004). All of these designs yield good survival rates for periods up to 12 months.

For this experiment a cage design is favoured in which the molluscs stay healthy for a period of up to 20 months, and shells can be removed for observation and returned without damage. We prefer a cage of rigid material so that it cannot be easily damaged. The cage material also needs to be resistant to corrosion, and the construction of the cage should prevent the surprisingly mobile mussels from escaping (Kaandorp et al., 2003), damage by vandalism, or predation by rats (*Rattus norvegicus*) and muskrats (*Ondatra zibethicus*; Hanson et al., 1989; Diggins and Stewart, 2000). We aim to reproduce the natural situation as accurately as possible in order to provide optimal growing conditions. For an overview of caging methods see table 2.1.

2.2 Materials and Procedures

2.2.1 Cage design

The cage design consists of a PVC box (height 22 cm, area 40 x 60 cm) with a 5 cm high top cage of stainless steel plate with 5 mm round perforations. A lid and a curved front are made of the same material. The PVC box is

Table 2.1: Overview of caging methods for freshwater mussels

Author	Type	Material	Size	# mussels / cage	Sediment	Duration	Species	Survival
Muncaster et al., 1990	pillow cages	1.5 cm open-mesh galvanised wire	45 x 45 cm		in contact with sediment	40 days	*Elliptio complanata & Lampsilis radiata*	98 %
Kauss & Hamdy,1985; Kauss & Hamdy, 1991	pillow cages	1.5 cm open-mesh galvanised wire	30 x 36 x 10 cm	5	in contact with sediment	3 weeks	*Elliptio complanata*	98 %
Hickey et al., 1995	cylindrical	stainless steel 10 mm mesh	40 cm long x 15 cm diam.	100	no	6 - 12 months	*Hyridella menziesi*	high
Malley et al., 1996	cubic	wood frame, plastic 4 mm mesh	36 x 36 x 36 cm	10	no	40 - 90 days	*Pyganodon grandis*	75 - 100 %
Hyötyläinen et al., 2002	oval	steel wire and polyester net	50 x 70 cm		in contact with sediment	10 months	*Anodonta anatina*	97 - 100 %
Martel et al., 2003.	individually tied off bags on frame	plastic mesh		ca. 50	no	60 days	*Elliptio complanata*	97 - 100 %
	rigid cages	stainless steel	80 x 80 x 20 cm	ca. 50	in contact with sediment	60 - 110 days	*Elliptio complanata*	97 - 100 %
Friedman & Mower, 2004	bags attached to frame	0.25" mesh size plastic netting	4" diam. 5' long	8	no	66 - 67 days	*Elliptio complanata*	99 %
Current study	box with lid	PVC box, perforated stainless steel top	22 x 40 x 60 cm	21 - 23	contains sediment	12 – 20 months	*Unio pictorum*	43 - 100 %
							Unio tumidus	0 - 100 %
							Anodonta anatina	22 - 25 %
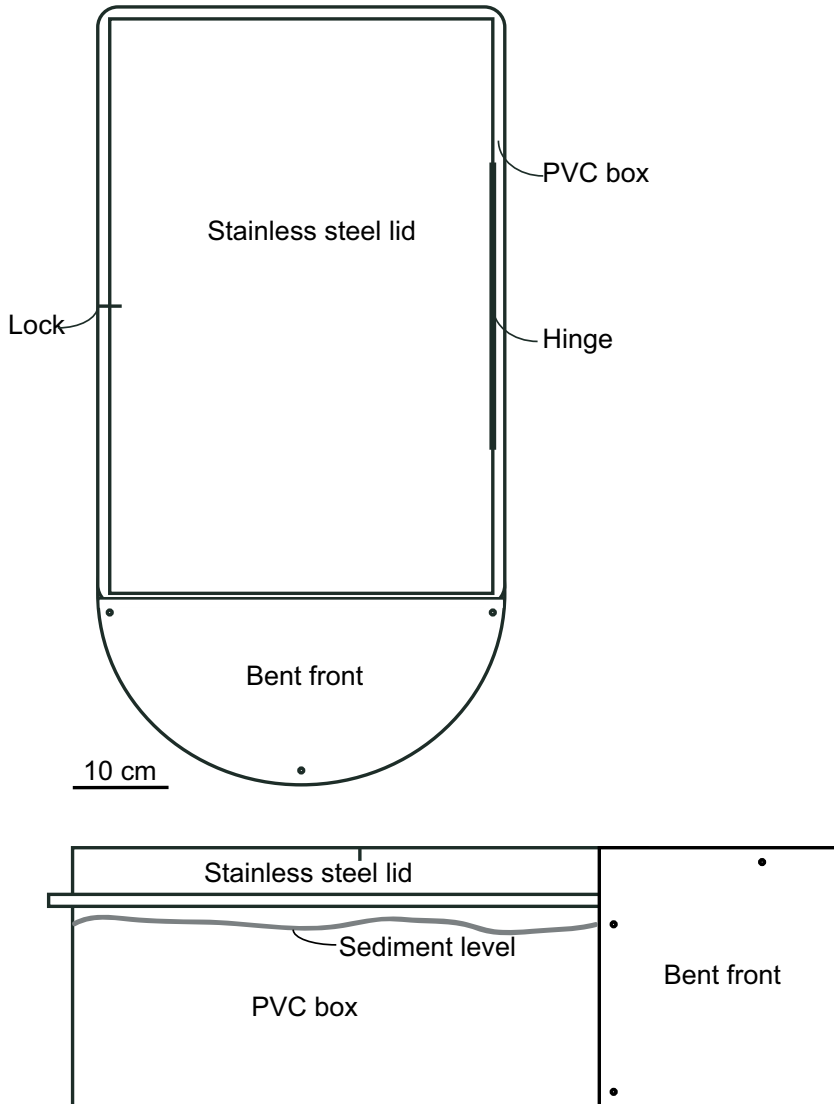
Figure 2.1: Technical drawings of the freshwater mussel cage.

filled with sand collected close to the monitoring site, and deep enough for the mussels to bury themselves into the sediment. The 5 cm top gives the mussels some breathing space above the sediment. The lid prevents the mussels from escaping and predators from entering. The bent front is made for extra streamline and to prevent branches and other litter from clogging the cage (Figures 2.1 and 2.2).
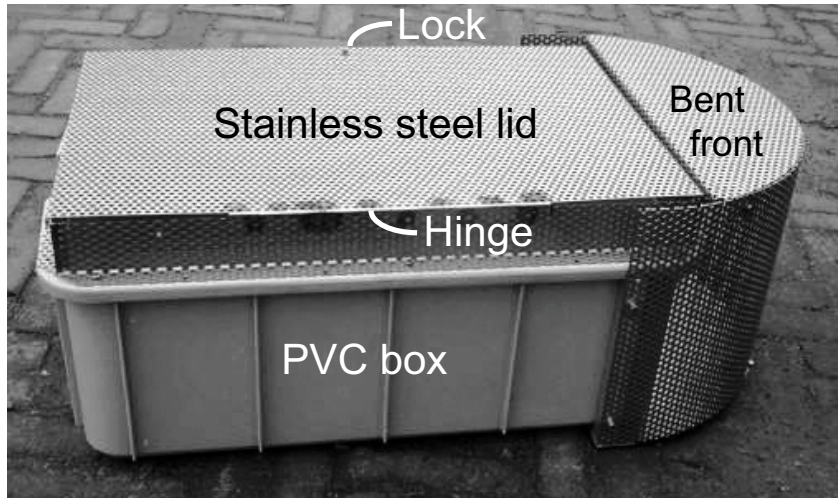
Figure 2.2: Cage before placement in the fish ladder.

2.2.2 Studied species

Freshwater mussels of the family Unionidae are large bivalves that are common in rivers of the Netherlands. In the 1960s and 1970s environmental pollution caused unionid populations to severely decline in the Meuse and Rhine. Large mussels were not observed at all in the Rhine (Peeters and Wolff, 1973). Since that time water chemistry has improved and the Rhine has been recolonised by several unionid species, including the species studied (Admiraal et al., 1993).

The Dutch unionids reach an age of approximately 15 years. All full-grown Unionidae have a semi-infaunal lifestyle, whilst as a juvenile they are infaunal. (Negus, 1966; Gittenberger et al., 1998) Three species are used in this research:

- *Anodonta anatina* (Figure 2.3a) has a rounded oval shape and a thin shell. Its maximum length is 132 mm and it can be found in stagnant as well as flowing waters (Gittenberger et al., 1998).

- *Unio pictorum* (Figure 2.3b) has an elongated shape and reaches a length of maximum 110 mm. It is found in stagnant as well as in flowing waters and can tolerate some pollution (Gittenberger et al., 1998).

- *Unio tumidus* (Figure 2.3c) has an egg-like shape with a prominently curved edge. Its length is maximum 125 mm. This species prefers flowing water but also occurs in stagnant waters. Of these three species it has the highest tolerance for pollution (Gittenberger et al., 1998).
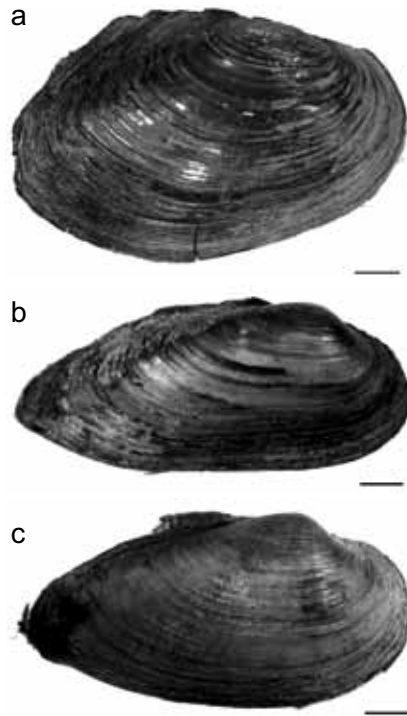
Figure 2.3: Species used in this study: a: *Anodonta anatina*, b. *Unio pictorum*, c. *Unio tumidus*. Scale bars are 1 cm.

2.2.3 Monitoring sites

For this monitoring experiment, cages were placed in fish ladders. A fish ladder is a small flowing canal with "stairs" of different water levels. These are constructed near weirs or dams, enabling migratory fish to migrate up- and downriver (Figure 2.4). For our experiment we selected two fish ladders located in two weir-and-lock complexes in the rivers Meuse and Lek (a Rhine distributary) in the Netherlands. The Meuse weir is situated near Lith, and the Lek weir at Hagestein (Figures 2.4 and 2.5). These fish ladders were chosen for their protected position from vandalism and relatively constant water levels and flow speeds. One cage was placed at each site. The studied species occur naturally in both the Meuse and Rhine river systems, including the fish ladders (own observations).

2.2.4 Collection, tagging and staining of shells

In January 2006 living freshwater mussels of the three species were collected and tagged using 8 x 4 mm Hallprint type FPN glue-on shellfish tags

Figure 2.4: Fish ladder at Lith (photo: Sarah Tynan).

Figure 2.5: Map of part of the Dutch Rhine-Meuse delta showing the shell collection site at Zetten, and monitoring sites at Hagestein and Lith. (Made with Online Map Creation http://www.aquarius.geomar.de/.)
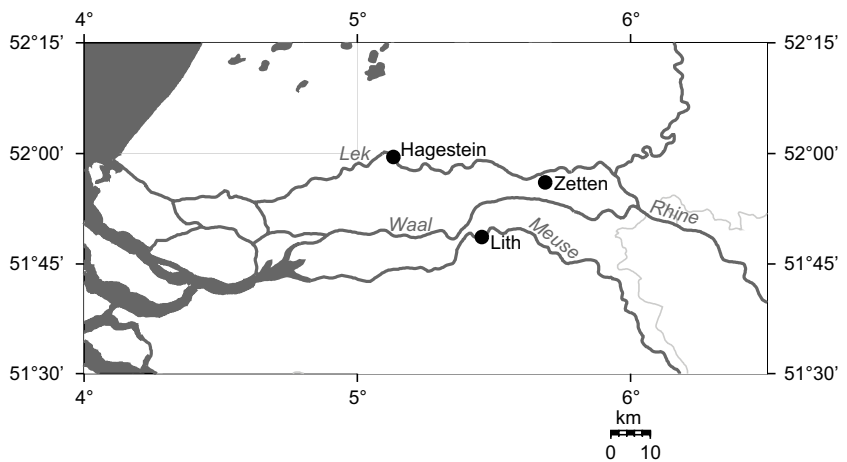
with cyanoacrylate adhesive (Lemarié et al., 2000; Ross et al., 2001; Figure 2.6). The monitoring station at Hagestein was installed on the same day, whilst the station at Lith was set up in July 2006. Temperature was monitored every hour with an ATAL ATX-01E temperature data recorder in a waterproof container. In June 2006 one third of the mussels were stained by a 24 h immersion in a 250 mg/l solution of calcein in river water (Eads and Layzer, 2002). Another third were stained by a 24 h immersion in a 60 mg/l solution of calcein in river water (Day et al., 1995). The last third of the mussels were not stained. In July another 10 additional mussels for the Lith site were stained with a 250 mg/l solution of calcein in river water (Table 2.2). Both calcein staining methods resulted in a fluorescent growth line visible in a transverse section of the shell (Figure 2.7).

2.3   Assessment

2.3.1   Behaviour of the mussels

During the fortnightly visits to the monitoring sites several observations were made. The mussels were very mobile within their cage, which could clearly be seen from the traces they left in the sand. This supports the necessity of a closed cage design. Sometimes a small group clumped together in one corner of the cage. In winter the mussels had a tendency to bury themselves completely in the sand, which is in support of the necessity of sediment in the cage. During summer they were at the sand surface with their siphons exposed to the water.

Figure 2.6: Five of the *Unio pictorum* shells just after collection and tagging. Scale in centimetres.

Table 2.2: Number of individuals per monitoring station with species, collection site and staining method.

Monitoring site	Species	Staining (mg/l)	# of individuals
Hagestein (Lek)	*Anodonta anatina*	0	3
		60	3
		250	3
	Unio pictorum	0	3
		60	2
		250	2
	Unio tumidus	0	2
		60	2
		250	3
Total Hagestein			23
Lith (Meuse)	*Anodonta anatina*	0	1
		250	3
	Unio pictorum	0	2
		60	3
		250	9
	Unio tumidus	0	1
		60	1
		250	1
Total Lith			21

2.3.2 Survival

Though the number of specimens was too low to perform any statistical analyses, several observations on survival rates could be made. In Hagestein survival rates were very high (89 - 100 %) for up to 14 months after the start of the experiment. Between April 5th and July 12th 2007 almost all mussels died, resulting in survival rates of 0 - 43 % (Figure 2.8). This sudden high death rate may have been caused by an anoxic event, a bloom of poisonous algae, parasites, or disease. When the experiment ended we noticed that the sand in the cages had a thread-like structure and looked and smelled foul. This was probably because the sand was processed too much by the mussels, due to the high population density. In Lith the mussels were monitored for only 12 months and no such mortality event occurred. Here, the two *Unio* species (100 % survival) appeared to be more tolerant to the transplant and caging conditions than the *Anodonta* (25% survival; Figure 2.9). There was no effect of the staining method on survival.
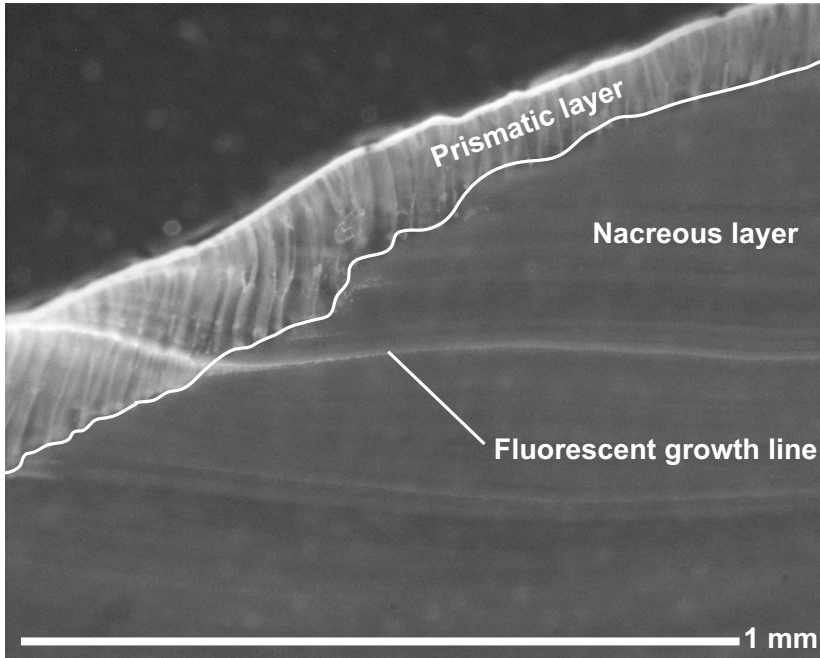
Figure 2.7: Fluorescent growth line in a shell stained with 60 mg/l calcein.

2.3.3 Growth

Shells were measured with a digital calliper. Length was measured along the longest axis of the shell; height was measured along the dorso-ventral axis perpendicular to the growth lines (Figure 2.10). Length and height growth were divided by the number of days the shell was in the cage during the growing season (water temperature $\geq$ 12 °C; Howard, 1922; Negus, 1966; Dettman et al., 1999). Length growth per month varied between 0 - 1.26 mm for *Anodonta anatina*, 0 - 0.70 mm for *Unio pictorum*, and 0 - 0.64 mm for *U. tumidus* (Figure 2.11). Height growth per month varied between 0 - 0.83 mm for *A. anatina*, 0 - 0.27 mm for *U. pictorum*, and 0 - 0.34 mm for *U. tumidus* (Figure 2.12). This apparently low growth rate is not exceptional, since free-living shells of comparable sizes had a height growth 0.13 - 3.5 mm/month (*U. pictorum*) and 0.08 - 0.15 mm/month (*U. tumidus*) in their last season of growth (Versteegh et al., 2009; Chapter 4). Dettman et al. (1999) also report similarly low growth rates (0.7 - 1.6 mm/y) in three North American species. Thus, considering our own data, keeping the mussels in cages does not seem to affect their growth negatively.
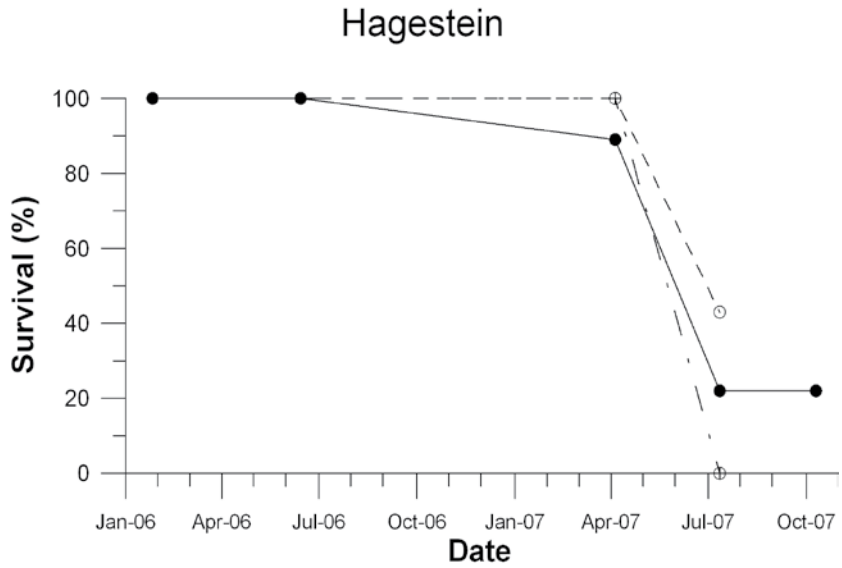
Hagestein

Figure 2.8: Survival of mussels at Hagestein from January 26th 2006 to October 10th 2007. Solid line is *Anodonta anatina* (n = 9), dashed line is *Unio pictorum* (n = 7), and dash-and-dot line is *U. tumidus* (n = 7). A sudden mortality event is evident between April 5th and July 12th 2007.

Figure 2.9: Survival of mussels at Lith from July 6th 2006 to October 10th 2007. Solid line is *Anodonta anatina* (n = 4), dashed line is *Unio pictorum* (n = 14) and *U. tumidus* (n = 3) (both had 100% survival rates).

Lith
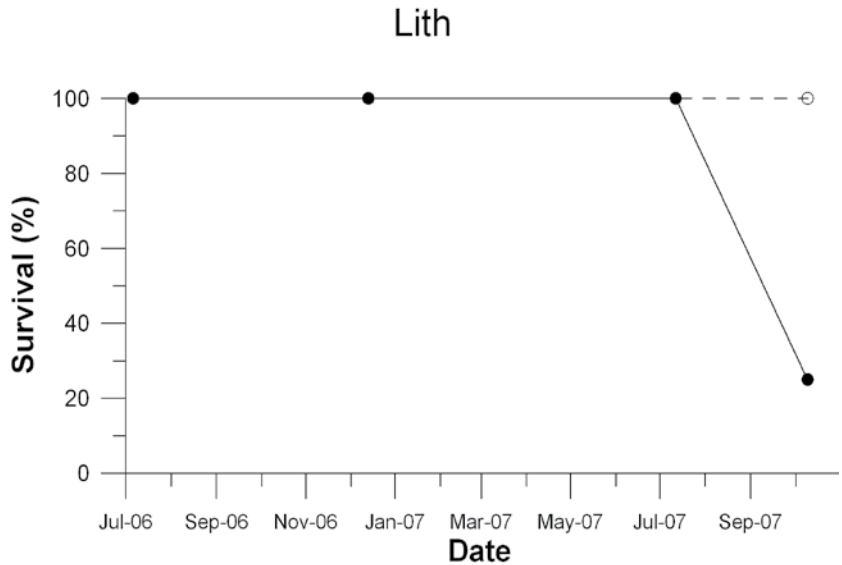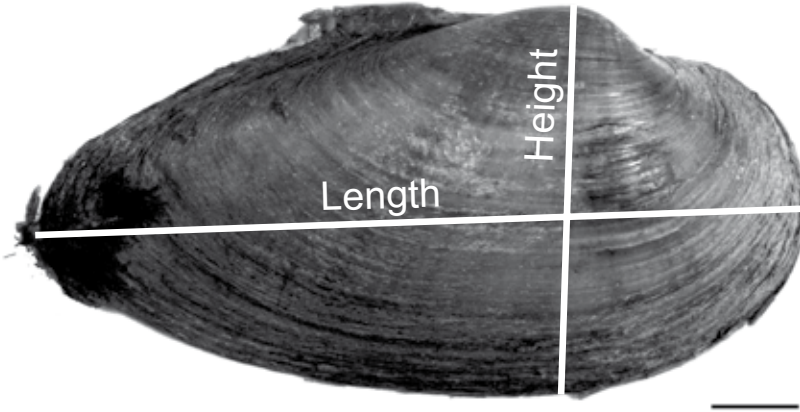
Figure 2.10: Measurement of shell length and height.

2.4   Discussion

We aimed to develop a cage design in which unionids could be kept for a prolonged period (up to 20 months) under optimal growth and survival conditions.

The current experiment is compared with other freshwater caging experiments in table 2.1. The apparent low survival rates in the current experiment can be fully ascribed to a single mortality event in one of the cages. This event happened after more than 14 months. No other project listed in table 2.1 had been running that long. The caging experiment that lasted the longest is described by Hickey et al. (1995), and lasted 12 months. After the current experiment had been running for 12 months, just one specimen had died. If the mortality event at Hagestein is not taken into account, survival rates are 100% for both *Unio* species, and 25 - 89 % for *Anodonta anatina*. This latter species is thus less suitable for keeping in cages.

Another factor, which might have influenced survival rates, is the transplantation of the animals and related changes in water chemistry. These three species occur naturally in both the Meuse and the Lek, so chemistry of these rivers is suitable for sustaining them. Transplantation from the Linge to the Lek, both Rhine distributaries, probably involved only minor differences in water composition. To a lesser extent this holds true for the Meuse as well. The shells bought in the pet shop were of unknown origin and might have experienced larger changes in water chemistry. In addition these individuals might have been in a worse condition from the start of the experiment due to starvation during their stay in the pet shop aquarium.
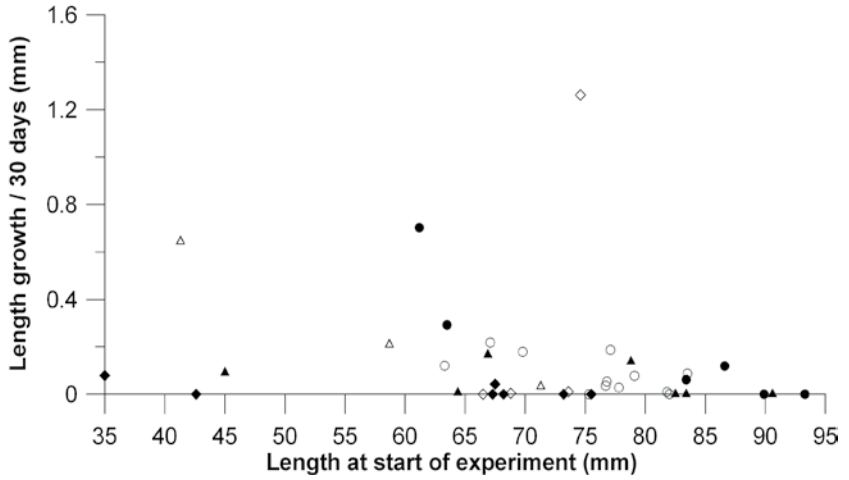
Figure 2.11: Average length growth per 30 days in the growing season. Diamonds represent *Anodonta anatina*, circles are *Unio pictorum*, and triangles are *U. tumidus*. Solid symbols represent the Hagestein (Lek) location, open symbols are Lith (Meuse). Many specimens do not show any measurable growth.

Figure 2.12: Average height growth per 30 days in the growing season. Diamonds represent *Anodonta anatina*, circles are *Unio pictorum*, and triangles are *U. tumidus*. Solid symbols represent the Hagestein (Lek) location, open symbols are Lith (Meuse). Many specimens do not show any measurable growth.
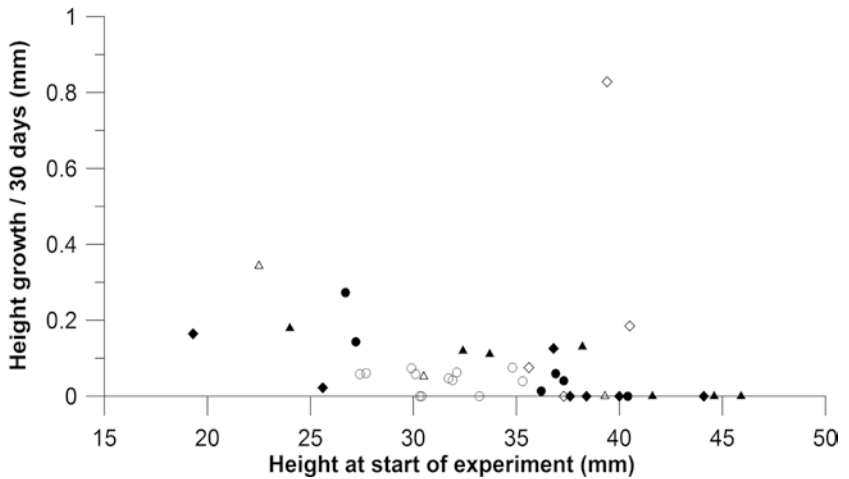
2.5   Comments and recommendations

The cages became overgrown by algae and zebra mussels (*Dreissena polymorpha*) within a few weeks and needed to be cleaned regularly. Negative effects of overgrowth might be partially avoided by using mesh or stainless steel plates with larger holes.

Because flow velocity is higher outside the cages than inside the cages, up to 10 cm of fine sediment was deposited in the cages. This happened especially during high discharge events when the rivers carried a high sediment load. When water levels were low enough to be able to approach the cages again we removed this clay to leave some space to the mussels and prevent them from suffocating. A future cage design would have a top made of mesh instead of stainless steel to create a higher flow of water over the mussels and to prevent high sedimentation rates of clay in the cages. In addition it is desirable to make the top somewhat higher to create more space for the mussels to move when additional sediment is deposited in the cages.

In this experiment the curved front of the cage was perhaps not necessary, because of the low flow velocity at the sites. The line with buoys at the entrance to the fish ladder also prevented branches and other large items from floating in. In other locations this could still be a useful aspect of the cage design.

Water levels fluctuated due to river discharge variability and tidal influence (only Hagestein). Water levels above the cages fluctuated therefore and cages were sometimes 2 m deep, whilst at other times they were only 10 cm under water. In January 2007, the cage top in Lith was exposed by a few centimetres, but the mussels still had space, and at that moment were not active because of the low water temperatures in winter.

However not unusual in adult unionids, it appears that most shells grew very little. This can be problematic for the application of this method in comparison of shell and water chemistry. Higher growth rates can probably be achieved by using juvenile specimens instead of adults and by putting fewer individuals in the cages (lower population density; less competition). Intensive competition by clumping can be avoided by compartmenting the cage.

In addition, it appears that unionids are highly sensitive to handling and transplantation. It is therefore desirable to perform future experiments in the same river as where the mussels were collected, and minimise the frequency and duration of handling for measuring, tagging and staining.

Chapter 3

Intraseasonal growth rate variation in unionid freshwater mussels as determined by oxygen and carbon isotope shell chemistry

Abstract

By means of a monitoring experiment in the rivers Meuse and Lek (Rhine basin) in the Netherlands, we have established the relation between oxygen and carbon isotope compositions ($\delta^{18}O$ and $\delta^{13}C$) in shells of unionid freshwater bivalves, and river water conditions. Our aim was to use this relation to construct an intraseasonal growth rate model for these shells. The results of the monitoring experiment show that shell $\delta^{18}O$ values of the ventral margins exactly matched the predicted $\delta^{18}O$ values based on coupled water $\delta^{18}O$ and water temperature values on the day the experiment concluded. The seasonal range of measured $\delta^{18}O$ variability in shells, matched the range of the predicted $\delta^{18}O$ values, with the exception of the winter season when these unionids do not grow. Sharp rises in river water bicarbonate $\delta^{13}C$ values were reflected accurately in the $\delta^{13}C$ of shell aragonite. These isotope connections were explored in several tuning exercises for the reconstruction of growth rates of the shells. Methods based on peak matching and time-axis shifting of either: 1) the measured shell $\delta^{18}O$ record relative to the predicted shell $\delta^{18}O$ record, or: 2) the shell $\delta^{13}C$ record relative to the bicarbonate $\delta^{13}C$ values, yielded similar growth models with an apparent ~ 2 month mismatch between $\delta^{18}O$ and $\delta^{13}C$ records. The best growth rate model for the shells resulted from fine-tuning a combination of $\delta^{18}O$ and $\delta^{13}C$ results with shells exhibiting fast growth during June, the month with highest food availability. Furthermore, the variability in growth rate shows that onset and cessation of growth is mainly influenced by water temperature.

3.1 Introduction

The Meuse and the Rhine, and its distributaries, are the largest river systems in the Netherlands. Both rivers have caused damaging floods (e.g. 1993 and 1995) and experienced droughts (e.g. 1976 and 2003; Tol and Langen, 2000; De Wit et al., 2007). Large flood events generally occur during the winter season, a period when freshwater shells do not record the chemical composition of ambient water due to growth cessation. Droughts however, occurring during summer and autumn, can be recorded in growth increments. These droughts limit water availability for agriculture and cooling water for power plants. In addition, water quality deteriorates, threatening drinking water supplies and impacting river ecology (Van Vliet and Zwolsman, 2008). Both floods and droughts are expected to occur more frequently due to an increase in precipitation extremes caused by climate change (Parmet and Burgdorffer, 1995; Gregory et al., 1997; Arnell, 1999; Booij, 2002; Bürger, 2002; Pfister et al., 2004; Tu, 2006; IPCC, 2007; Ward et al., 2008). Insight in past river dynamics is crucial for predicting the impact of future climate change.

Freshwater mussels of the family Unionidae record characteristics of ambient water chemistry in their aragonitic growth increments (e.g. oxygen and carbon isotope ratios; $\delta^{18}O_{ar}$ and $\delta^{13}C_{ar}$) at high temporal resolution (Rodrigues et al., 2000; Ricken et al., 2003; Verdegaal et al., 2005). Usually, seasonal patterns are found in both $\delta^{18}O_{ar}$ and $\delta^{13}C_{ar}$ values. $\delta^{18}O_{ar}$ values are generally in equilibrium with ambient water (Dettman et al., 1999; Kaandorp et al., 2003; Gajurel et al., 2006; Goewert et al., 2007). $\delta^{13}C_{ar}$ values of mollusc shells have yielded useful environmental information, but many questions concerning the processes behind seasonal $\delta^{13}C_{ar}$ records remain unanswered. Several authors reported covariation between carbon isotopes in shell aragonite and those of dissolved inorganic carbon (DIC) (Fritz and Poplawski, 1974; Buhl et al., 1991; Aucour et al., 2003; Kaandorp et al., 2003). Others did not find a detectable relation between $\delta^{13}C_{ar}$ and $\delta^{13}C_{DIC}$, which is usually ascribed to the incorporation of metabolic carbon into the shell (Fastovsky et al., 1993; Veinott and Cornett, 1998; Ricken et al., 2003; Geist et al., 2005; Verdegaal et al., 2005; Gajurel et al., 2006). However, Gillikin et al. (2009) suggest that an ontogenetic increase in metabolic carbon does not exclude $\delta^{13}C$ data of unionid freshwater mussels from being a useful environmental proxy. Detection of a relation between $\delta^{13}C_{ar}$ and $\delta^{13}C_{DIC}$ in previous studies may have been hampered by uncertainties in time correlation of isotope records in water with those in shells (Dettman et al., 1999).

65

The temporal matching of water isotope data with shell isotope records is essential to reconstruct detailed intraseasonal growth rate changes. Although ontogenetic growth rate patterns have been well described in unionids (Morris and Corkum, 1999; Anthony et al., 2001), information on intraseasonal growth is sparse and not very detailed (Howard, 1922; Negus, 1966). It has been demonstrated that ontogenetic growth rates are influenced by factors like temperature (Dettman et al., 1999; Goodwin et al., 2003), turbidity, nutrient availability and primary productivity (Arter, 1989; Kesler et al., 2007; Valdovinos and Pedreros, 2007). Now, in order to understand the environmental signals recorded in the chemistry of the shells, it is essential to document the influence of these factors on intraseasonal growth rates of shells. In this study, we present a monitoring experiment investigating three unionid species that naturally occur in the Meuse and Rhine: *Anodonta anatina*, *Unio pictorum*, and *U. tumidus*. Our aims are:

1. To investigate whether isotope chemistry of shell growth increments can be used as a proxy of past seasonal changes in river water composition;

   a. Are $\delta^{18}O_{ar}$ values in shells in equilibrium with $\delta^{18}O_w$ values of ambient water during the period of the monitoring experiment?

   b. Are seasonal $\delta^{13}C_{HCO3^-}$ patterns in river water recorded in the range of $\delta^{13}C$ values within shell aragonite during the monitoring experiment?

2. To establish a method to calculate intraseasonal growth rates by matching temporal changes in oxygen and carbon isotope chemistry of river water and equivalent sclerochronological shell records;

3. To understand the environmental factors driving seasonal growth rate changes.

3.2   Materials & methods

3.2.1   Monitoring

Aragonitic Unionidae are abundant in the Dutch part of the Rhine-Meuse delta. They can reach an age of approximately 15 years and sizes up to 13 cm. (Gittenberger et al., 1998). In this study, adult specimens of *Unio pictorum*, *U. tumidus* and one juvenile *Anodonta anatina* were used.

Monitoring sites were established in fish ladders near weirs in the rivers Meuse and Lek (a Rhine distributary) in the Netherlands. These sites were selected for the relatively constant water levels and flow velocities. The Meuse weir is situated near Lith, the Lek weir at Hagestein (Figure 3.1).
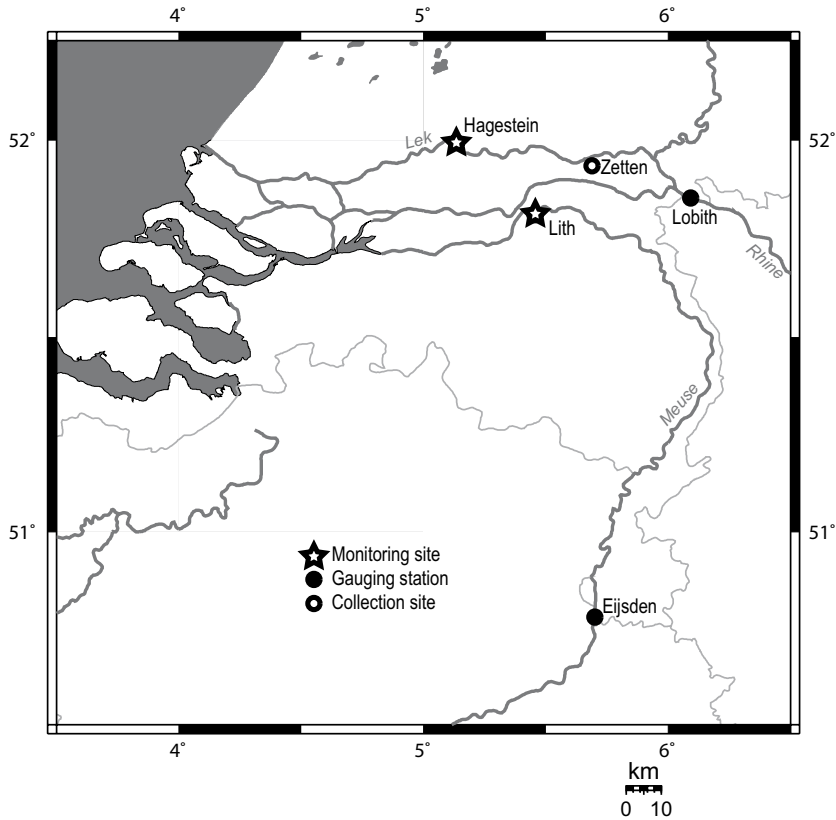
Figure 3.1: Map of part of the Dutch Rhine-Meuse delta with shell collection site at Zetten, monitoring sites at Hagestein and Lith and Rijkswaterstaat gauging stations at Eijsden and Lobith (Made with Online Map Creation http://www.aquarius.geomar.de/).

A cage was constructed to contain the mussels during the experiment. An elaborate description and evaluation of this cage design is described in chapter 2.

On the 26th of January 2006, living specimens of the three species were collected from the river Linge at Zetten (Figure 3.1). This small distributary of the Rhine is known for its high densities of unionids (Gittenberger et al., 1998). The mussels were tagged using 8 x 4 mm Hallprint type FPN glue-on shellfish tags with cyanoacrylate adhesive standard 'Superglue' (Lemarié et al., 2000; Ross et al., 2001; Figure 3.2). The monitoring station at Hagestein was installed that same day. The monitoring station at Lith was occupied on the 6th of July 2006, when living mussels, purchased at a pet shop, were added into the cage. The 12th of July 2007, the experi-

67

Figure 3.2: Four of the *Unio tumidus* shells just after collection and tagging. Scale in centimetres.

ment was concluded at both sites by killing the mussels through freezing. Specifications of the specimens are given in table 3.1.

Water samples for isotope analysis were taken biweekly for a period of 18 months at Hagestein and a period of 12 months at Lith. The 100 ml samples were poisoned with two drops of a solution of 15 mg of I_2 and 30 mg of KI per ml of milliQ water (Mook, 2000). Water temperature was logged with an ATAL ATX-01E temperature data recorder in a waterproof container at 1-hour resolution.

Data on pH and chlorophyll *a* content of the water (a measure of primary productivity), measured biweekly, were obtained from Rijkswaterstaat (Dutch Directorate for Public Works and Water Management) at Eijsden (Meuse) and Lobith (Rhine; Figure 3.1).

3.2.2 Analyses

Eleven shells were embedded in epoxy resin. Sections of 300 μm thickness were cut perpendicular to the growth lines, along the dorso-ventral axis (Figure 4.1). The nacreous layer of the shells was sampled with a Merchantek Micromill micro sampler. The drill bit diameter was ~ 800 μm. Considering the minimal amount of carbonate required for mass spectrometry, the highest possible sampling resolution was chosen. The distance between samples was usually 30 μm, but in very thin shells, this sometimes went up to 200 μm. Drilling depth was ~ 250 μm.

Table 3.1: Specifications of shell samples.

#	Species	Length (mm)	Height (mm)	Height along curve of shell (mm)	Collection site	Monitoring site	Staining (mg/l)	Start date	End date
3110	*Unio tumidus*	78.8	38.2	54	Linge; Zetten	Hagestein	60	26-Jan-06	5-Apr-07
3114	*Unio pictorum*	63.5	27.2	39	Linge; Zetten	Hagestein	60	26-Jan-06	12-Jul-07
3115	*Unio pictorum*	86.6	36.9	50	Linge; Zetten	Hagestein	0	26-Jan-06	12-Jul-07
3117	*Unio pictorum*	61.2	26.7	39	Linge; Zetten	Hagestein	0	26-Jan-06	5-Apr-07
3119	*Unio tumidus*	45.0	24.0	34	Linge; Zetten	Hagestein	250	26-Jan-06	12-Jul-07
3129	*Unio tumidus*	64.4	32.4	43	Linge; Zetten	Hagestein	0	26-Jan-06	12-Jul-07
3135	*Anodonta anatina*	35.0	19.3	25	Linge; Zetten	Hagestein	250	26-Jan-06	12-Jul-07
3149	*Unio pictorum*	75.3	30.4	43	Pet shop	Lith	60	6-Jul-06	14-Dec-06
3153	*Unio pictorum*	81.8	33.2	47	Pet shop	Lith	60	6-Jul-06	14-Dec-06
3170	*Unio pictorum*	77.1	31.9	44	Pet shop	Lith	250	6-Jul-06	12-Jul-07
3172	*Unio pictorum*	69.8	29.9	44	Pet shop	Lith	250	6-Jul-06	12-Jul-07

Both carbonate and water samples were analysed for $\delta^{18}O$ and $\delta^{13}C$ values on a Thermo Finnigan Delta+ mass spectrometer equipped with a GasBench-II preparation device. For carbonate ~ 10-50 μg of sample was required. The long-term standard deviation of a routinely analysed in-house $CaCO_3$ standard is < 0.1 ‰. This $CaCO_3$ standard is regularly calibrated to NBS 18, 19 and 20. The long-term standard deviation of a routinely analysed in-house water standard is < 0.1 ‰ for $\delta^{18}O_w$ values and is < 0.15 ‰ for $\delta^{13}C_{DIC}$ values, respectively.

3.2.3   Calculation of predicted $\delta^{18}O_{ar}$ values

Measured temperature and $\delta^{18}O_w$ values of ambient river water were used to calculate predicted $\delta^{18}O_{ar}$ values, using the equation of Grossman and Ku (1986) in the form suggested by Dettman et al. (1999):

$$1000 \ln\alpha = 2.559\left(10^6 T^{-2}\right) + 0.715 \tag{3.1}$$

where T is the water temperature in degrees Kelvin and α is the fractionation between water and aragonite described by:

$$\alpha_{water}^{aragonite} = \frac{\left(1000 + \delta^{18}O_{ar}\left(VSMOW\right)\right)}{\left(1000 + \delta^{18}O_w\left(VSMOW\right)\right)} \tag{3.2}$$

Where *ar* is shell aragonite and *w* is water. All oxygen isotope values are calculated relative to Vienna Standard Mean Ocean Water (VSMOW). $\delta^{18}O_{ar}$ values are, however, usually expressed relative to Vienna Pee Dee Belemnite (VPDB). To convert $\delta^{18}O_{ar}$ (VSMOW) values to $\delta^{18}O_{ar}$ (VPDB) values, the following equation has been used (Gonfiantini et al., 1995):

$$\delta^{18}O_{ar}\left(VSMOW\right) = 1.03091\left(1000 + \delta^{18}O_{ar}\left(VPDB\right)\right) - 1000 \tag{3.3}$$

3.2.4   Calculation of bicarbonate $\delta^{13}C$ values and the fractionation with aragonite

DIC consists of three carbonic species: H_2CO_3, HCO_3^- and CO_3^{2-}. Their proportions depend on temperature and pH (Figure 3.3). Environmental carbon used for calcification is incorporated by the mussel in the form of HCO_3^- (Mook and Vogel, 1968; Kaandorp et al., 2003). The species of DIC in water are described by the following net reaction:
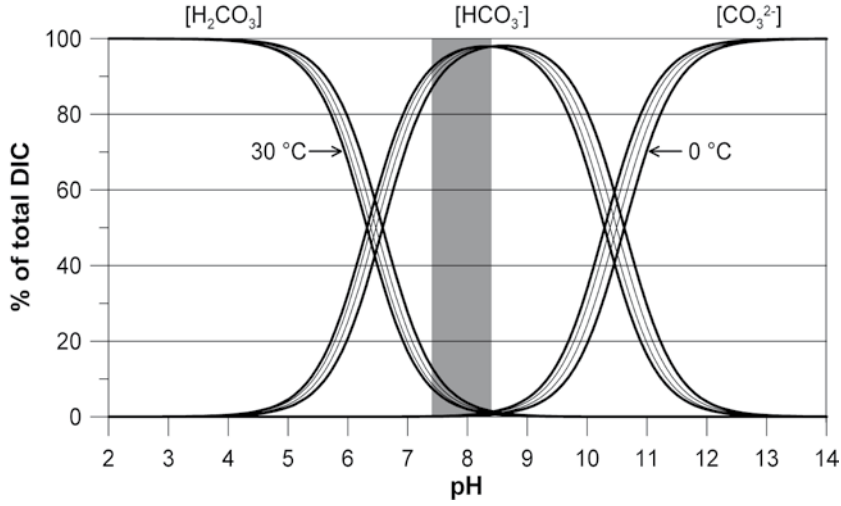
Figure 3.3: Bjerrum plot for the three carbonic species at different pH plotted for temperatures 0, 10, 20 and 30 °C. The grey bar indicates pH range of the rivers Meuse and Rhine.

$$CO_2(g) + H_2O \xleftrightarrow{K_{CO_2}} H_2CO_3 \xleftrightarrow{K_1} H^+ + HCO_3^- \xleftrightarrow{K_2} 2H^+ + CO_3^{2-} \quad (3.4)$$
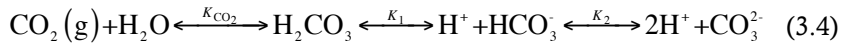
Because the river water pH values ranged between 7.4 and 8.4, DIC consisted mainly of HCO_3^- and low concentrations of H_2CO_3 and CO_3^{2-} (Figure 3.3). The relative concentrations of H_2CO_3, HCO_3^- and CO_3^{2-} are obtained using the following equations (Clark and Fritz, 1997; Zeebe and Wolf-Gladrow, 2001):

$$K_1 = \frac{[H^+][HCO_3^-]}{[H_2CO_3]} \quad (3.5)$$

$$K_2 = \frac{[H^+][CO_3^{2-}]}{[HCO_3^-]} \quad (3.6)$$

$$pK_1 = 1.1 \cdot 10^{-4} T_C^2 - 0.012 T_C + 6.58 \quad (3.7)$$

$$pK_2 = 9 \cdot 10^{-5} T_C^2 - 0.0137 T_C + 10.62 \quad (3.8)$$

$$[H_2CO_3] = DIC \Big/ \left(1 + \frac{K_1}{[H^+]} + \frac{K_1 K_2}{[H^+]}\right) \tag{3.9}$$

$$[HCO_3^-] = DIC \Big/ \left(1 + \frac{[H^+]}{K_1} + \frac{K_2}{[H^+]}\right) \tag{3.10}$$

$$[CO_3^{2-}] = DIC \Big/ \left(1 + \frac{[H^+]}{K_2} + \frac{[H^+]}{K_1 K_2}\right) \tag{3.11}$$

where T_c is the temperature in °C. Because of the first and second dissociations of CO_2 in water, the following applies:

$$[H^+] = [HCO_3^-] + [CO_3^{2-}] \tag{3.12}$$

Combined with the relative concentrations, the above relation yields absolute concentrations of all three carbonic species and total DIC. The isotopic fractionation of dissolved CO_2 relative to HCO_3^- is given by the following equation (Mook, 2000):

$$\varepsilon_{H_2CO_3/HCO_3^-} = \frac{-9866}{T_K} + 24.12\text{‰} \tag{3.13}$$

Subsequently, bicarbonate $\delta^{13}C$ values ($\delta^{13}C_{HCO3}$) are calculated using the ratio H_2CO_3/HCO_3^- and the fractionation between them.
Isotopic enrichment factors between shell aragonite and HCO_3^- are calculated using the relation (Romanek et al., 1992):

$$\alpha_{bicarbonate}^{aragonite} = \frac{\left(1000 + \delta^{13}C_{ar}(VPDB)\right)}{\left(1000 + \delta^{13}C_{HCO_3^-}(VPDB)\right)} \tag{3.14}$$

For inorganic precipitation of aragonite $\alpha_{ar/HCO3-}$ is 2.7 ± 0.6 ‰ (Romanek et al., 1992). In the biogenic aragonite of Peruvian unionids however, a de-

pletion of 4.0 ± 0.7 ‰ has been found, resulting in the equation (Kaandorp et al., 2003):

$$\delta^{13}C_{ar} = \delta^{13}C_{HCO_3^-} - 4\text{‰}$$
(3.15)

3.3   Results

3.3.1   River water

Water temperatures in both locations varied seasonally with summer temperatures rising to about 25 °C and winter values as low as 2 °C (Figures 3.4 and 3.5). The sharp trough to 0 °C in the Meuse water temperatures (Figure 3.5) must have been due to accidental exposure of the top of the cage, containing the temperature logger, caused by low water level in the fish ladder. However, since the mussels do not grow in winter, this is of no consequence for this study (Anthony et al., 2001; Goewert et al., 2007; Kesler et al., 2007; Versteegh et al., 2009; Chapter 4).

pH values of the Lek varied between 7.5 and 8.4 and those of the Meuse between 7.4 and 8.2, with no obvious seasonal patterns. In this pH range most of the DIC is present as HCO_3^- (Figure 3.3).

During the period July 2006-July 2007, the Lek $\delta^{18}O_w$ values varied between -9.8 ‰ and -7.9 ‰ (VSMOW) with an average of -8.9 ± 0.5 ‰ (VSMOW) (Figure 3.4). During that same period the Meuse $\delta^{18}O_w$ values varied between -8.1 ‰ and -6.4 ‰ (VSMOW) with an average of -7.1 ± 0.5 ‰ (VSMOW) (Figure 3.5). In addition to our data, we obtained access to a $\delta^{18}O_w$ dataset of both rivers, covering the years 2006 and 2007 from the Centre for Isotope Research (University of Groningen), measured at Eijsden and Lobith (Figure 3.1). Both datasets have been plotted in figures 3.4 and 3.5. The $\delta^{18}O_w$ records generally correspond, with the notable exception that in both rivers our measurements yield significantly lower $\delta^{18}O_w$ values around December 2006/January 2007, due to unknown factors. Since the shells did not grow during those months, this is of no consequence for matching of measured and predicted $\delta^{18}O_{ar}$ records.

The $\delta^{13}C_{HCO3-}$ values measured in this study range between -13.6 ‰ (VPDB) and -7.9 ‰ (VPDB) in the Lek and -15.3 ‰ (VPDB) and -8.6 ‰ (VPDB) in the Meuse (Figures 3.6 and 3.7; due to the pH range of these rivers, the difference between $\delta^{13}C_{HCO3-}$ and $\delta^{13}C_{DIC}$ is negligible). Chlorophyll *a* concentrations exhibit seasonal patterns with 'background' values of 2 μg/l in both rivers and peaks, occurring in late spring / early summer, up to 39
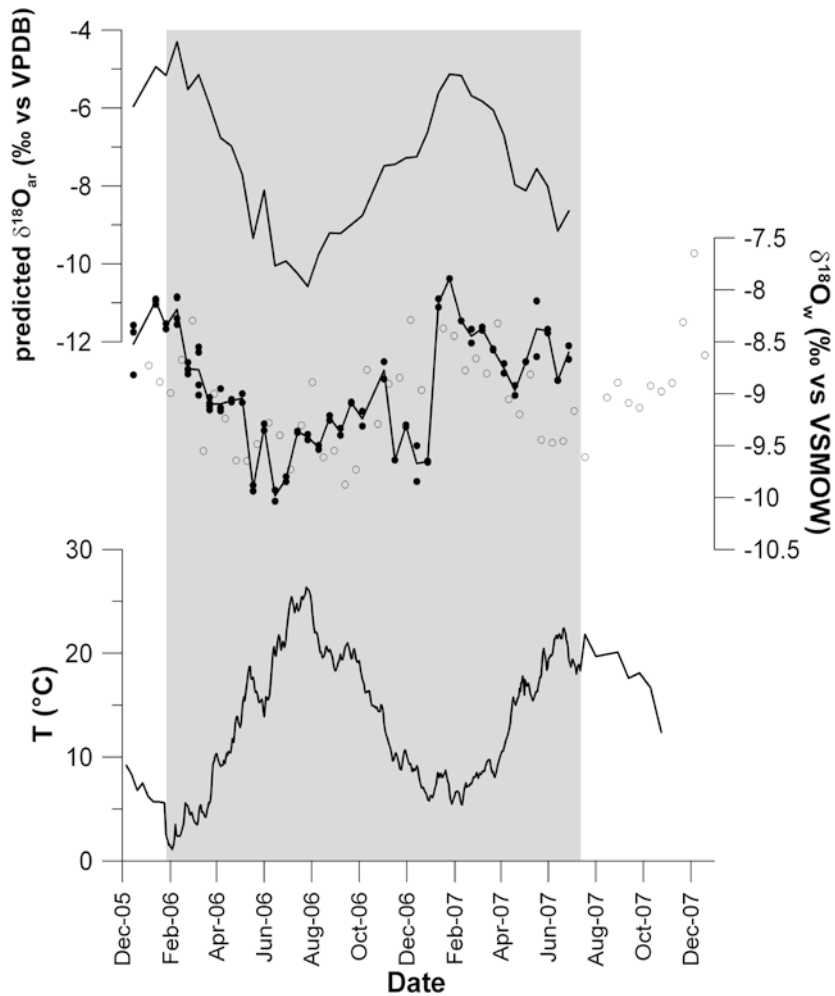
Figure 3.4: Water temperature (bottom), $\delta^{18}O_w$ values (middle) and resulting predicted $\delta^{18}O_{ar}$ values (top) in the Lek in 2006 and 2007. For $\delta^{18}O_w$ values both our own dataset (black dots and solid line) and a dataset from the Centre for Isotope Research, University of Groningen (open circles) are shown. Only our own dataset is used for calculation of predicted $\delta^{18}O_{ar}$ values. Shaded in grey is the duration of the monitoring experiment.

µg/l in the Lek and 56 µg/l in the Meuse (Figures 3.6 and 3.7).

3.3.2   Isotopic composition of shells

During the monitoring period $\delta^{18}O_{ar}$ values of the shells varied between -5.2 and -10.8 ‰ (VPDB) in the Lek (Figures 3.8a-g) and between -6.1 and -6.8 ‰ (VPDB) for the Meuse (Figures 3.9a-c). These $\delta^{18}O_{ar}$ values corroborate
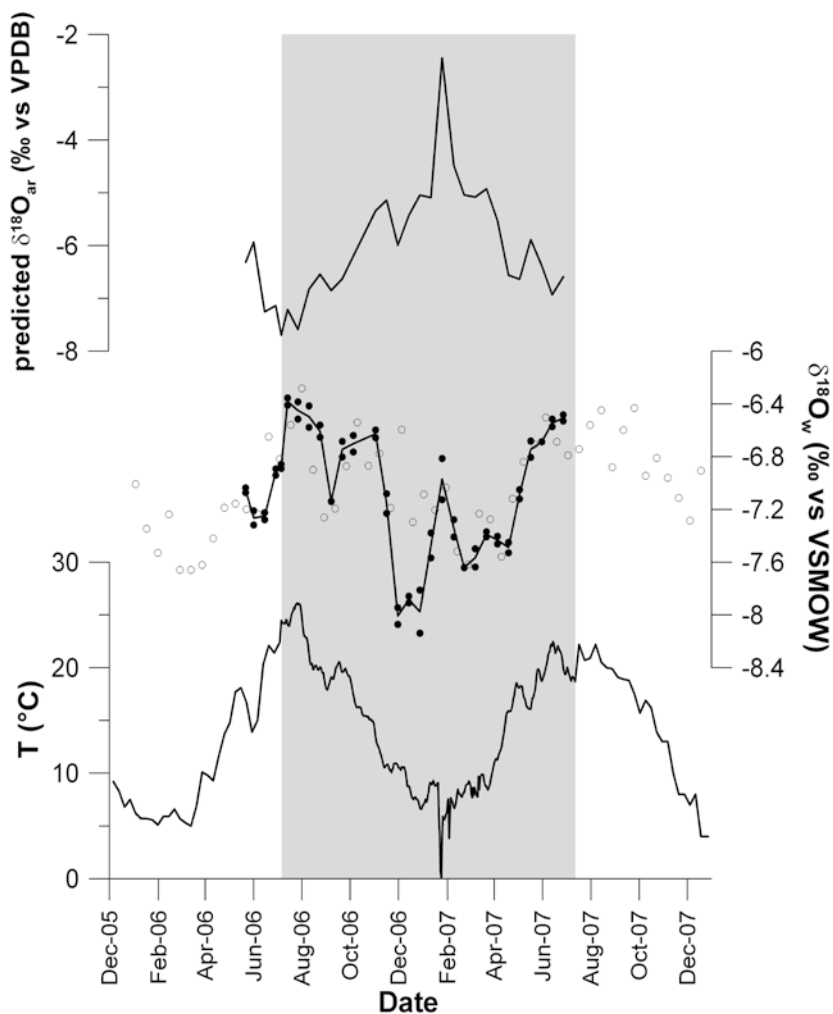
Figure 3.5: Water temperature (bottom), $\delta^{18}O_w$ values (middle) and resulting predicted $\delta^{18}O_{ar}$ values (top) in the Meuse in 2006 and 2007. For $\delta^{18}O_w$ values both our own dataset (black dots and solid line) and a dataset from the Centre for Isotope Research, University of Groningen (open circles) are shown. Only our own dataset is used for calculation of predicted $\delta^{18}O_{ar}$ values. Shaded in grey is the duration of the monitoring experiment.

our previous observations for shells from these rivers, which were on average ~ -9.1 ‰ (VPDB) for the Rhine river system and ~ -6.3 ‰ (VPDB) for the Meuse (Versteegh et al., 2009; Chapter 4). The shells from Lith grew too slowly to resolve any seasonal variations during the monitoring experiment, and these shells are therefore excluded from further analysis. With one (single) exception, the Hagestein shells did show seasonal patterns: a
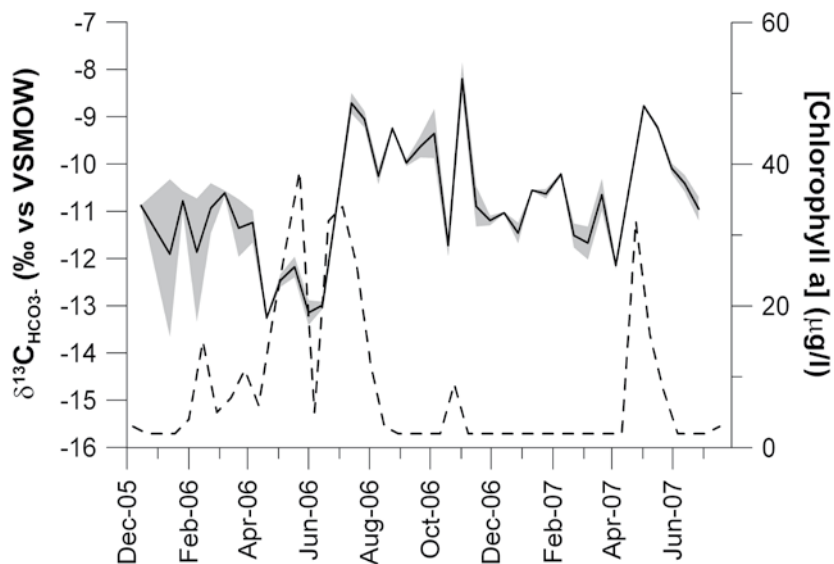
Figure 3.6: $\delta^{13}C_{HCO3-}$ values for the Lek at Hagestein (solid line) and chlorophyll *a* concentration (dashed line) during the monitoring experiment.

Figure 3.7: $\delta^{13}C_{HCO3-}$ values for the Meuse at Lith (solid line) and chlorophyll *a* concentration (dashed line) during the monitoring experiment. The grey area indicates the range of samples measured in duplicate. Chlorophyll *a* is an indicator of phytoplankton abundance. $\delta^{13}C_{HCO3-}$ values clearly rise during each phytoplankton bloom. This is caused by preferential removal of ^{12}C by photosynthesis (McConnaughey et al., 1997; Al-Aasm et al., 1998)
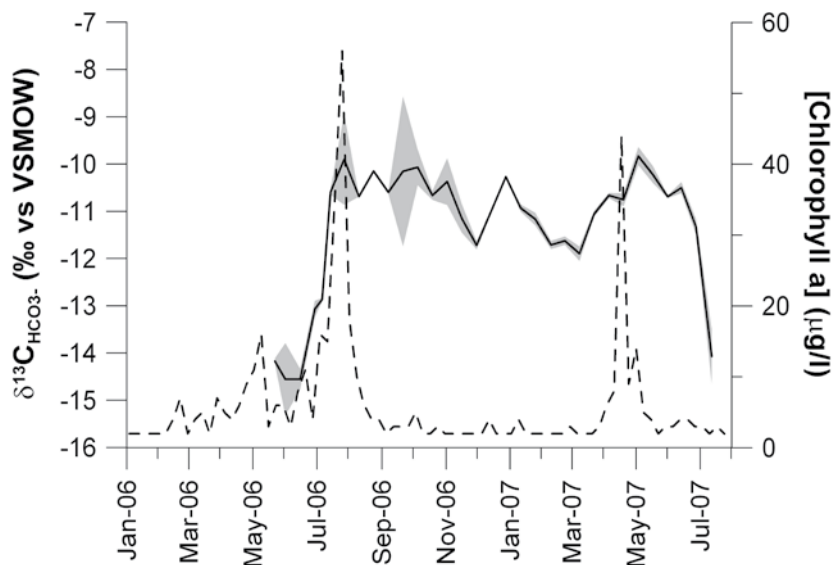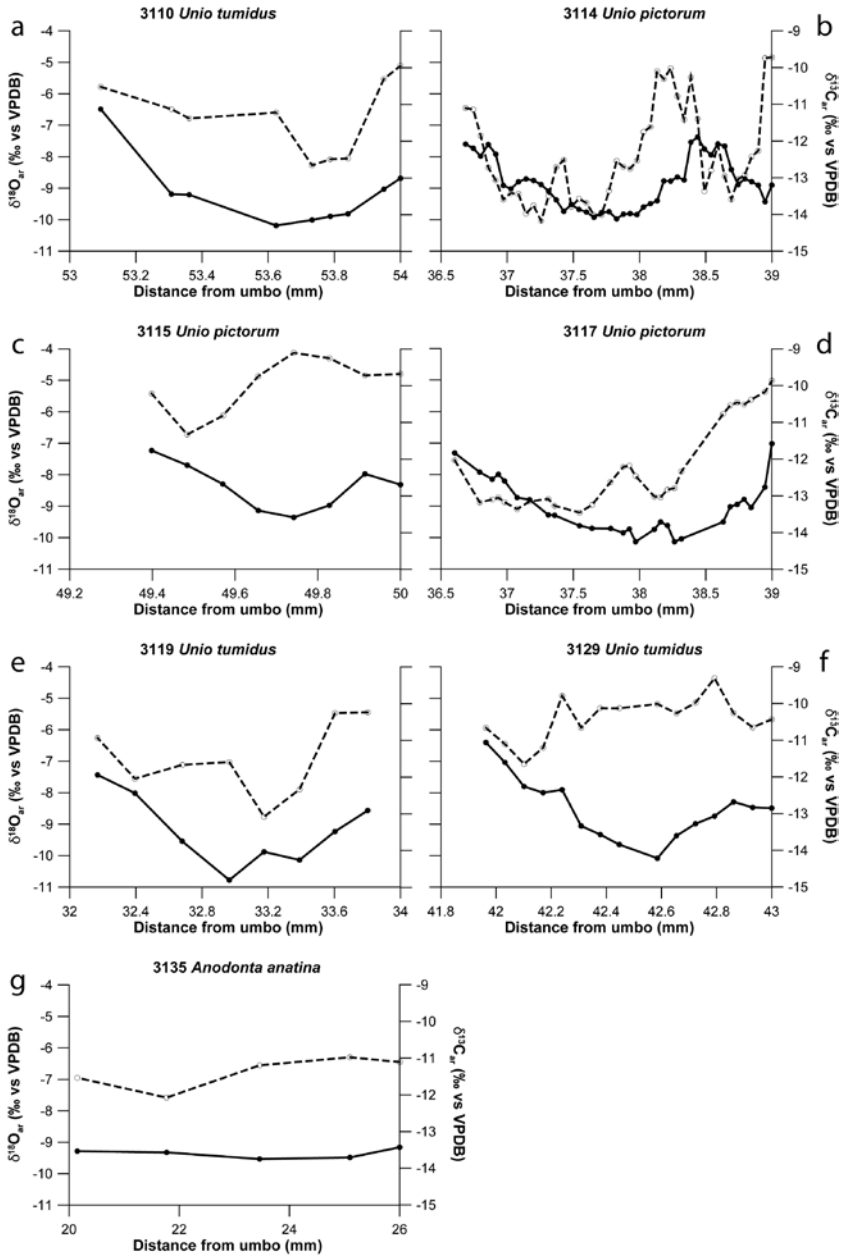
Figure 3.8a-g: $\delta^{18}O_{ar}$ values (solid lines and symbols) and $\delta^{13}C_{ar}$ values (dashed lines and open symbols) of the seven shells grown in Hagestein. Both the $\delta^{18}O_{ar}$ and $\delta^{13}C_{ar}$ records show a seasonal pattern, sometimes correlating and sometimes anti-correlating. The experiment covered the time interval January 2006-April 2007 in shells 3110 (a) and 3117 (d) and January 2006-July 2007 in the other shells.

broad trough in summer and a narrow peak in winter together representing one year of growth (See also Versteegh et al., 2009; Chapter 4).

The range of $\delta^{13}C_{ar}$ values during the monitoring experiment is -9.1 to -14.2 ‰ (VPDB) in the Lek (Figures 3.8a-g) and -11.2 to -13.3 ‰ (VPDB) in the Meuse (Figures 3.9a-c). The smaller range in values for the Meuse is possibly due to slow shell growth during the experiment, which resulted in a lower temporal resolution for the samples. In the Lek, where sampling

Figure 3.9a-c: $\delta^{18}O_{ar}$ values (solid lines and symbols) and $\delta^{13}C_{ar}$ values (dashed lines and open symbols) of the four shells grown in Lith. Due to the small amount of shell precipitated during the experiment, sampling resolution was too low to record any seasonality in either the $\delta^{18}O_{ar}$ or the $\delta^{13}C_{ar}$ record. The experiment covered the time interval July 2006-December 2006 in shells 3149 (a) and 3153 (b) and July 2006-July 2007 in shell 3172 (c).
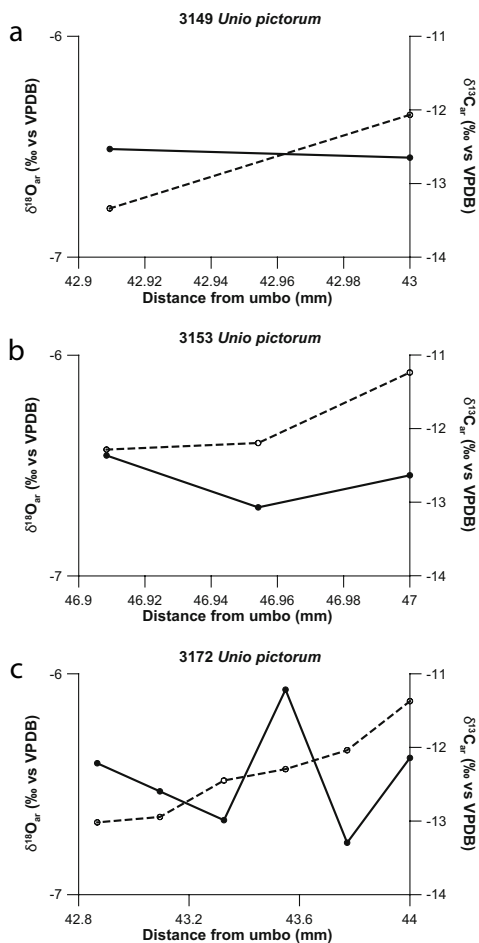
resolution was higher, we observe a seasonal pattern in $\delta^{13}C_{ar}$ values in all shells (except for the 3135 shell, which has a low sampling resolution).

3.4 Discussion

3.4.1 Seasonal isotope variation of river water

$\delta^{18}O_w$ values of the Meuse and Rhine are known to display a seasonal cycle (Data: Centre for Isotope Research, University of Groningen; Figure 1.10). Seasonal variation in amount and composition of different source waters causes this cyclicity. The $\delta^{18}O_w$ value of the Meuse is determined by the relative contributions of groundwater and surface runoff. In winter, when evaporation is limited, $\delta^{18}O_w$ values reflect those of groundwater, whereas in summer $\delta^{18}O_w$ values are higher due to evaporation and enriched summer precipitation (Mook, 1968).

In spring and early summer, the Rhine river system $\delta^{18}O_w$ values become isotopically depleted by meltwater from the Alps released into the river. This meltwater, and the location of the Rhine basin land inwards on the European continent, result in overall lower $\delta^{18}O_w$ ratios than those of the Meuse with lowest values in summer and highest values in winter (Mook, 1968; Ricken et al., 2003). Thus, the Rhine and Meuse exhibit opposing seasonal $\delta^{18}O_w$ cycles as previously described by Mook (1968; Figures 3.4 and 3.5).

Figure 3.10: $\delta^{13}C_{HCO3-}$ values for the Rhine and Meuse during the years 1967-1969 (data: W. G. Mook).
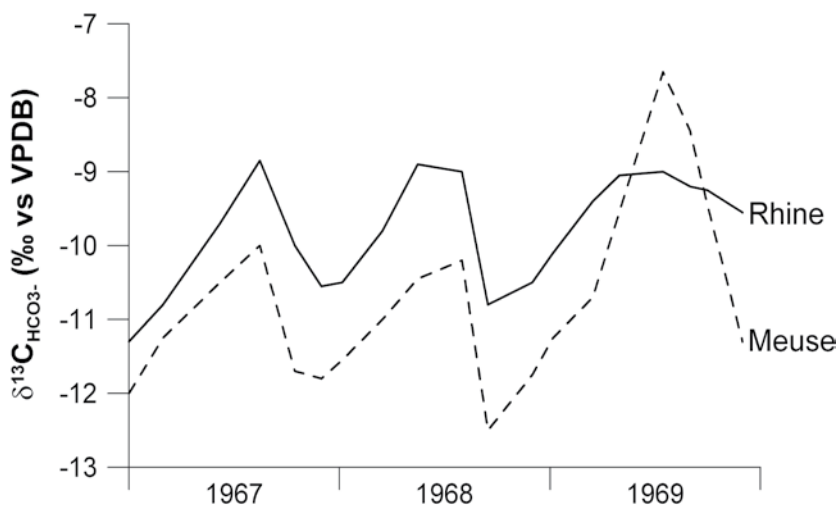
With respect to $\delta^{13}C_{HCO_3^-}$ values, an earlier record exhibited seasonal patterns in both rivers, with values ranging from -12.5 to -7.7 ‰ (VPDB) (Figure 3.10) with low values in winter and high values in summer (Mook,1968; Mook, 2000). Higher values in summer were ascribed to isotopic exchange with atmospheric CO_2 (Mook and Vogel, 1968). We found seasonal patterns in $\delta^{13}C_{HCO_3^-}$ values in both rivers as well. Generally low $\delta^{13}C_{HCO_3^-}$ values occurred in winter and spring and high $\delta^{13}C_{HCO_3^-}$ values occurred in summer. The shifts towards positive values occurred rather abruptly, which suggests that other mechanisms for seasonality of $\delta^{13}C_{HCO_3^-}$ values may play a role in addition to the proposition by Mook and Vogel (1968) that high $\delta^{13}C_{HCO_3^-}$ values in summer are due to carbon isotopic exchange with atmospheric CO_2. For instance, metabolic effects, like those of photosynthesis and respiration, are expected to have a profound influence on both ambient water $\delta^{13}C_{HCO_3^-}$ values and shell $\delta^{13}C_{ar}$ values (McConnaughey et al., 1997; McConnaughey and Gillikin, 2008); photosynthesis by phytoplankton preferentially removes ^{12}C from the DIC pool (Fritz and Poplawski, 1974; Al-Aasm et al., 1998;), increasing $\delta^{13}C_{ar}$ values of shell aragonite. At the same time, phytoplankton, having very low $\delta^{13}C$ values, forms an important component of the unionid diet (Nichols and Garling, 2000; Raikow and Hamilton, 2001). Algal and microbial carbon possibly lowers shell $\delta^{13}C_{ar}$ values, depending on the level of metabolic carbon that has been incorporated (McConnaughey and Gillikin, 2008). We therefore investigate a possible relation between $\delta^{13}C_{HCO_3^-}$ values and primary productivity by using chlorophyll *a* concentrations as a proxy for the latter. Chlorophyll *a* datasets (representing phytoplankton abundance and thus primary productivity) are compared with measured $\delta^{13}C_{HCO_3^-}$ values in figures 3.6 and 3.7. Sharp rises in $\delta^{13}C_{HCO_3^-}$ values can be seen to follow chlorophyll *a* peaks in both rivers, albeit with a less abrupt rise in the Meuse than in the Lek in 2007. We therefore ascribe these rises in $\delta^{13}C_{HCO_3^-}$ values to preferential removal of ^{12}C by phytoplankton photosynthesis (Figures 3.6 and 3.7).

3.4.2 Equilibrium precipitation of shell aragonite: oxygen isotopes

We investigated whether the two *Unio* species precipitated their shell in oxygen isotopic equilibrium with ambient water during the monitoring experiments, using $\delta^{18}O_w$ values and water temperature to predict $\delta^{18}O_{ar}$ values (Equations 3.1-3.3; Figures 3.4 and 3.5). The measured $\delta^{18}O_{ar}$ values at the ventral margin of the three shells that remained in the experiment until the end (3114, 3115 and 3129; Figures 3.11b, c and f) match the

predicted values on that date (Table 3.2). The mussels were harvested on the 12th of July 2007. Water isotope measurements from that date unfortunately failed so instead samples taken the 27th of June 2007 were used. This is no problem for our analysis since the amount of time averaged in one ventral margin sample is about on week in shell 3114, but many weeks in 3115 and 3129. This latter fact is also the most likely cause for the deviations of up to 0.32 ‰ from the predicted value. These deviations are, however, small and not in a specific direction, confirming that aragonite was precipitated in oxygen isotopic equilibrium with ambient water.

Table 3.2: Predicted and measured $\delta^{18}O_{ar}$ values for ventral margin samples

#	$\delta^{18}O_w$	T (°C)	predicted $\delta^{18}O_{ar}$	measured $\delta^{18}O_{ar}$
3114	-8,60	20,5	-8,64	-8,90
3115	-8,60	20,5	-8,64	-8,32
3129	-8,60	20,5	-8,64	-8,49

3.4.3 Seasonal shell oxygen isotope records

The measured $\delta^{18}O_{ar}$ records typically show a truncated sinusoidal pattern (e.g. Figure 3.8b), caused by a combination of temperature fractionation and seasonal growth cessation (Grossman and Ku, 1986; Dettman et al., 1999; Goodwin et al., 2003). Since the shells did not grow in winter, $\delta^{18}O_{ar}$ records contain (invisible) gaps resulting in juxtaposed increments of (summer) shell growth.

The fact that aragonite is precipitated in oxygen isotopic equilibrium with ambient water enables us to compare predicted and measured $\delta^{18}O_{ar}$ records and subsequently determine the temperature of seasonal growth initiation and cessation. For this comparison, measured $\delta^{18}O_{ar}$ summer segments were aligned (matched) separately with relevant parts of the predicted $\delta^{18}O_{ar}$ record based on $\delta^{18}O_w$ and temperature of the river water. The first sample of each summer segment was dated according to the specific calendar date of the relevant sample in the predicted $\delta^{18}O_{ar}$ record: the first day of spring when measured values matched our predictions. The same approach was used for anchoring the last measured sample of the shell segment to the predicted value in autumn. This method documented that shell growth initiated at 13.5 ± 2.8 °C and ceased at 13.5 ± 4.2 °C. This corresponds to values previously found (Howard ,1922; Negus, 1966; Dettman et al., 1999).

3.4.4   Shell carbon isotope records

The shifts in the $\delta^{13}C_{HCO3-}$ records are sufficiently large (> 2 ‰) to be recorded in bivalve shells (Gillikin et al., 2006a). This indeed appears to be the case: although the sampling resolution in shell 3135 from Hagestein and the three shells from Lith was too low to reveal seasonal patterns in $\delta^{13}C_{ar}$ (Figures 3.8g and 3.9a-c), both amplitude and values of $\delta^{13}C_{ar}$ for the other Hagestein shells correspond well with measured $\delta^{13}C_{HCO3-}$ (Figures 3.8a-f).

3.4.5   Intraseasonal growth models

Given the results of the monitoring experiment both the $\delta^{18}O_{ar}$ and $\delta^{13}C_{ar}$ records appear to record seasonal variation in ambient water. These datasets, combined with the river water $\delta^{18}O_w$ and $\delta^{13}C_{HCO3-}$ records, will now be applied to document variability in intraseasonal growth rates. We present four intraseasonal growth models: (1) a linear model; (2) a model based on measured and predicted seasonal $\delta^{18}O_{ar}$ records; (3) a model based on the comparison of seasonal $\delta^{13}C_{HCO3-}$ and $\delta^{13}C_{ar}$ records, and (4) a model combining measured and predicted $\delta^{18}O_{ar}$ records as well as $\delta^{13}C_{HCO3-}$ and $\delta^{13}C_{ar}$ records. For the reconstruction of these growth models, shells 3114 and 3117, exhibiting the highest growth rates, were used.

1. Linear growth model

Although it is unlikely that intraseasonal summer growth is linear, no robust non-linear growth model is available yet for unionids. Thus, as a first step towards comparison of the measured and predicted $\delta^{18}O_{ar}$ records and subsequent construction of an intraseasonal growth model, we started by assuming linear growth between the previously determined spring and autumn dates of onset and cessation of growth (Figures 3.11a-g). A relatively close correspondence between the predicted and measured $\delta^{18}O_{ar}$ records is observed in most shells. However, some shell records are somewhat offset in time compared to predicted values, suggesting growth rate variation with higher growth rate in spring and lower growth rate later in the season (e.g. shells 3114, 3117 and 3129; Figures 3.11b, d, f).

Subsequently, $\delta^{13}C_{HCO3-}$ and shell $\delta^{13}C_{ar}$ values of all Hagestein shells have been plotted using growth rates on the same linear scale as those from the previously discussed $\delta^{18}O_{ar}$ records (Figures 3.12a-g). The shapes of the $\delta^{13}C_{HCO3-}$ and $\delta^{13}C_{ar}$ records, plotted using the linear growth rate method, are very similar for five of the Hagestein shells (i.e. 3110, 3114, 3117, 3119 and 3115 only in the 2007 season; Figures 3.12a-e). However, there appears a mismatch between the peaks and troughs of the $\delta^{13}C_{HCO3-}$ and $\delta^{13}C_{ar}$

records with a duration of about 3 months. There is no obvious physiological mechanism in these organisms to explain this apparent time-shift, thus the mismatch is likely an artefact of the use of a linear intraseasonal growth rate model.

2. Oxygen isotopes: peak matching and time-axis shifting

To understand the environmental factors driving seasonal growth rate changes and to reduce the mismatch of shell and water data in the linear growth model, we next attempted to construct an improved intraseasonal growth rate model based on peak matching. Since $\delta^{18}O_{ar}$ values are in equilibrium with the ambient water we cannot only match the first and last samples of the measured $\delta^{18}O_{ar}$ summer segments with the predicted $\delta^{18}O_{ar}$ profiles, but all samples of each complete summer segment. First the peaks and troughs in the records are matched and then the remaining measured $\delta^{18}O_{ar}$ values between the peaks and troughs are shifted along the time axis to the closest values on the predicted $\delta^{18}O_{ar}$ graph (Figure 3.13a; Freitas et al., 2006). This results in a growth model with fast growth in early summer and slower growth during the rest of the season. To validate this model we plot $\delta^{13}C_{HCO3-}$ and $\delta^{13}C_{ar}$ values together on the same time-scale (Figure 3.13b). After this procedure the apparent time lag between $\delta^{13}C_{HCO3-}$ and $\delta^{13}C_{ar}$ values is reduced by a third in comparison to the linear model.

3. Carbon isotopes: peak matching and time-axis shifting

Unlike the predicted $\delta^{18}O_{ar}$ record, the $\delta^{13}C_{HCO3-}$ record exhibits several sudden leaps in values. These may serve as anchor points. In this approach, first $\delta^{13}C_{ar}$ records were fitted to the $\delta^{13}C_{HCO3-}$ record using the above-described method of peak matching and time-axis shifting (Figures 3.14a-b). Then, predicted and measured $\delta^{18}O_{ar}$ were plotted on the same timescale. In model 3, the time lag between predicted and measured $\delta^{18}O_{ar}$ is in the order of two months, which is similar to the $\delta^{13}C$ time lag in model 2. Hence there does not appear to be a significant improvement of the age model when using model 3 as opposed to model 2; what is gained in the better match of $\delta^{13}C$ data is lost in the poorer match of $\delta^{18}O$ data.

4. Combined $\delta^{18}O$ and $\delta^{13}C$ records: peak matching and time-axis shifting

Both the $\delta^{18}O_{ar}$ records and the shell $\delta^{13}C_{ar}$ records appear to record seasonal variation in ambient water of $\delta^{18}O_w$ and $\delta^{13}C_{HCO3-}$, respectively. Therefore, we next attempt to construct a fourth intraseasonal growth model by simultaneously matching peaks in the $\delta^{13}C$ and $\delta^{18}O$ records. This leads to a good match between the predicted and measured $\delta^{18}O_{ar}$ records, as well
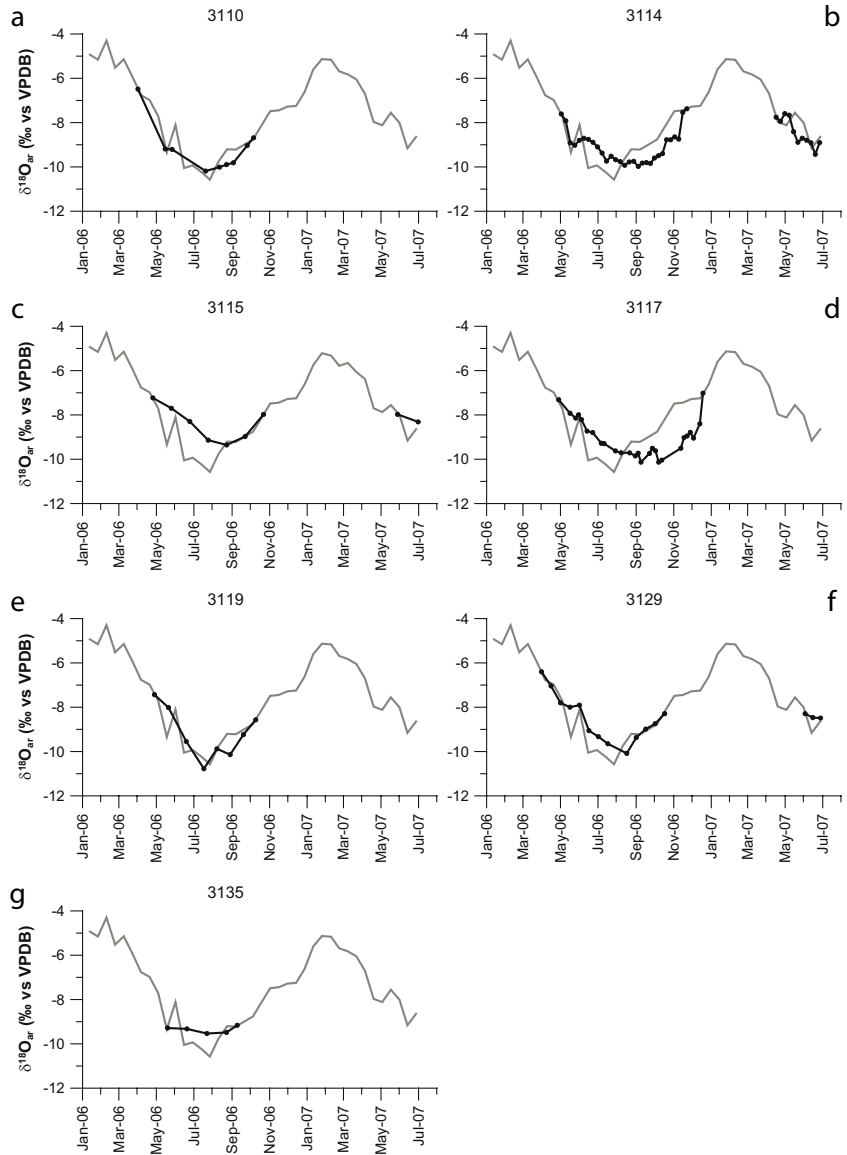
Figure 3.11a-g: Predicted $\delta^{18}O_{ar}$ values (grey lines) plotted with individual shell $\delta^{18}O_{ar}$ values (solid black lines and symbols) for Hagestein, using a linear growth model. A close correspondence between these records is observed in most shells. Some shells clearly show differential intraseasonal growth resulting in a time-shift of the measured $\delta^{18}O_{ar}$ record relative to the predicted $\delta^{18}O_{ar}$ record (shells 3114, 3117 and 3129). Shells 3110, 3119 and 3129 are *Unio tumidus*, shells 3114, 3115 and 3117 are *U. pictorum* and shell 3135 is *Anodonta anatina*.
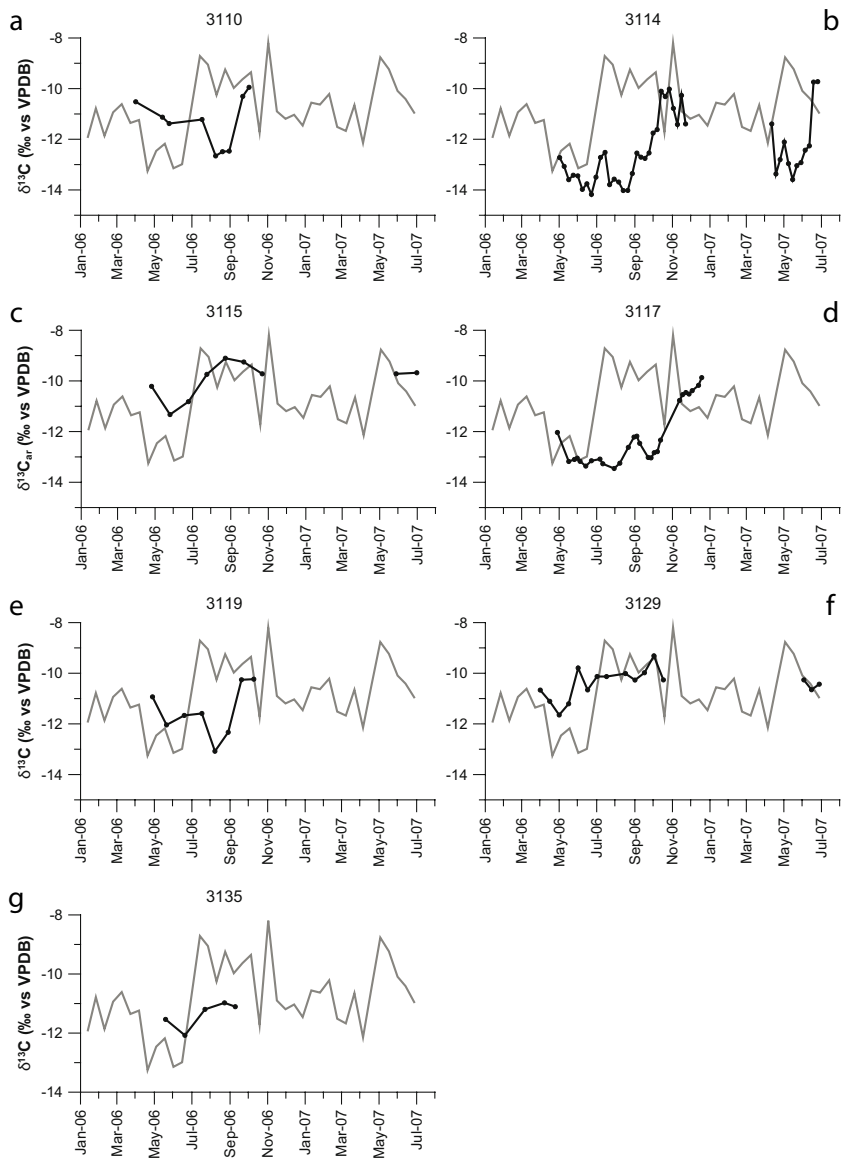
Figure 3.12a-g: $\delta^{13}C_{HCO3-}$ values of the Lek river water (grey lines) and $\delta^{13}C_{ar}$ values of each individual shell (solid black lines and symbols). $\delta^{13}C_{ar}$ values appear to correlate with $\delta^{13}C_{HCO3-}$ values, although there is an apparent time-shift. This is probably an artefact caused by the linear intraseasonal growth model used here. Shells 3110, 3119 and 3129 are *Unio tumidus*, shells 3114, 3115 and 3117 are *U. pictorum* and shell 3135 is *Anodonta anatina*.
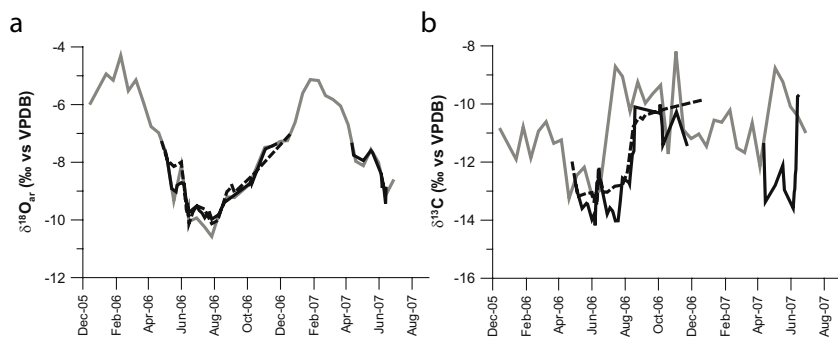
Figure 3.13: Construction of an age model using $\delta^{18}O$ values: a) Shell $\delta^{18}O_{ar}$ records of *Unio pictorum* shells from Hagestein, 3114 (solid black line) and 3117 (dashed black line), fitted over the predicted $\delta^{18}O_{ar}$ record (solid grey line) by means of first matching of peaks and troughs and subsequent horizontal shifting of the predicted $\delta^{18}O_{ar}$ record; b) Shell $\delta^{13}C_{ar}$ records of the same shells plotted with the $\delta^{13}C_{HCO3-}$ record (solid grey line) on the same timescale as figure 3.13a. There is a mismatch of ~ 2 months between these records.

as the $\delta^{13}C_{ar}$ and $\delta^{13}C_{HCO3-}$ records, if faster growth in early summer is allowed for (Figures 3.15a-b and 3.16a-b). As such, growth model 4 appears to solve time lag problems observed in models 2 and 3 in a satisfactory way.

Comparison of the growth functions

Growth functions resulting from the four different models are shown in figures 16a-b. The linear model obviously has constant growth rates through-

Figure 3.14: Construction of an age model using $\delta^{13}C$ values: a) shell $\delta^{13}C_{ar}$ records of *Unio pictorum* shells from Hagestein, 3114 (solid black line) and 3117 (dashed black line), are fitted over the $\delta^{13}C_{HCO3-}$ record (solid grey line) by means of first matching of peaks and troughs and subsequent horizontal shifting of the $\delta^{13}C_{HCO3-}$ record; b) Shell $\delta^{18}O_{ar}$ records of the same shells plotted over the predicted $\delta^{18}O_{ar}$ record on the same timescale as in figure 3.14a. Again, there is an apparent ~ 2 month mismatch.
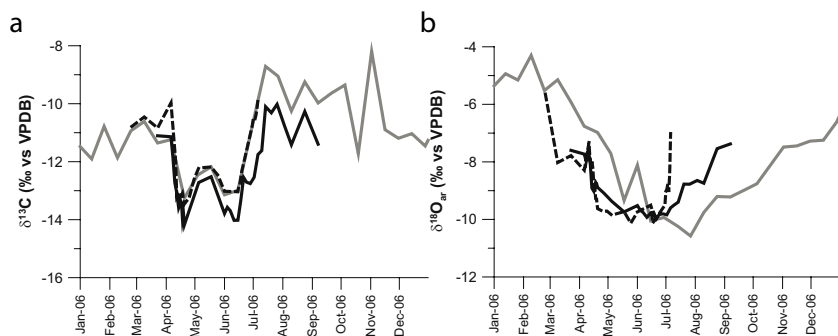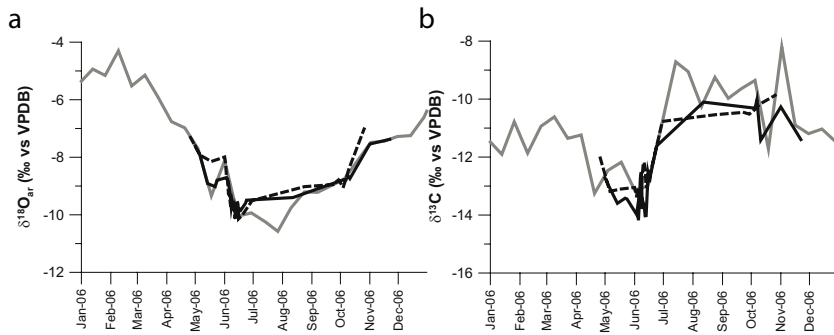
Figure 3.15: Construction of an age model using both the $\delta^{18}O$ and the $\delta^{13}C$ records: a) Shell $\delta^{18}O_{ar}$ records of *Unio pictorum* shells from Hagestein, 3114 (solid black line) and 3117 (dashed black line), plotted with the predicted $\delta^{18}O_{ar}$ record (solid grey line); b) Shell $\delta^{13}C_{ar}$ records of the same shells plotted with the $\delta^{13}C_{HCO3-}$ record (solid grey line) on the same timescale as figure 3.15a. When a very high growth rate in June is assumed followed by a much slower growth rate for the rest of the season, it is possible to achieve a reasonably good fit in both records simultaneously.

out the season. The $\delta^{18}O$-based model shows differential growth with three (shell 3114) or two (shell 3117) peaks and low-growth intervals in between. The above-described two-month time shift is evident again when the $\delta^{13}C$-based model is compared to the $\delta^{18}O$-based model. The combined $\delta^{18}O/\delta^{13}C$ model shows a large growth peak at the same time as the $\delta^{18}O$ model, followed by a time interval of low growth and then a smaller peak before growth ceases during winter (Figures 3.16a-b). This fourth model provides the best fit, because it aligns shifts in both $\delta^{18}O$ and $\delta^{13}C$ records. As such,

Figure 3.16: Growth rates of *Unio pictorum* at Hagestein during the growing season. a) shell 3114; b) shell 3117. For each shell all four growth models are shown. Dashed grey line is the linear model; dashed black line is the $\delta^{18}O$-based model; solid grey line is the $\delta^{13}C$-based model; solid black line is the combined $\delta^{18}O$ and $\delta^{13}C$ model.
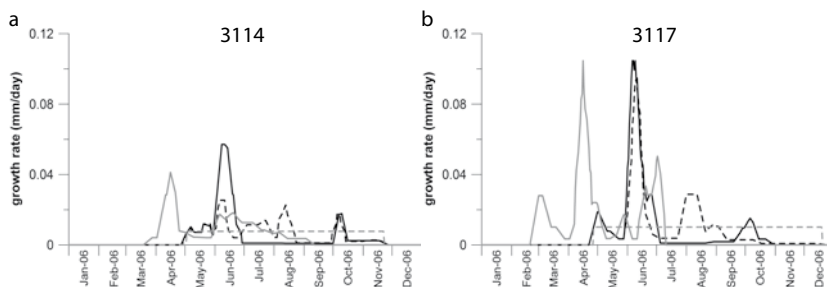
model 4 supposedly yields the most accurate representation of intraseasonal growth (Figure 3.16).

In summary, *Unio pictorum* starts growing when water temperatures reach 13.5 °C in spring. They continue to grow at a moderate rate during spring, before accelerating to up to five times the previous growth rate during early summer (June), when there is plenty of food available. As time progresses growth slows down considerably, until it comes to a complete halt when temperatures fall below 13.5 °C again.

The growth peak in June coincides with the Chlorophyll *a* peak in the river, suggesting that intraseasonal growth is mainly influenced by phytoplankton abundance (Figure 3.6; chlorophyll *a*). This factor was already known to have a positive effect on the ontogenetic growth of North-American Unionidae (Kesler et al., 2007) and European *Anodonta* (Jokela and Mutikainen, 1995), although unionids feed on bacteria and fine particulate organic matter as well (Nichols and Garling, 2000; Vaughn and Hakenkamp, 2001; Christian et al., 2004). It has to be noted that other factors influencing growth cannot be entirely ruled out. These might include pollution with heavy metals, low oxygen content of the water and elevated salinities, especially in dry time intervals (Admiraal et al., 1993; Hartmann et al., 2007).

The water $\delta^{13}C_{HCO3-}$ record exhibits significant differences between samples taken every fortnight and clearly has not enough time-resolution to reveal all high frequency variation. Higher time-resolution sampling could possibly have enabled a more precise fit of both the $\delta^{18}O_{ar}$ and $\delta^{13}C_{ar}$ records to the predicted $\delta^{18}O_{ar}$ and ambient water $\delta^{13}C_{HCO3-}$ record.

3.5   Conclusions

We have demonstrated that unionid species, living in the Rhine and Meuse rivers, precipitate skeletal aragonite in oxygen isotopic equilibrium with ambient water. Shell $\delta^{18}O_{ar}$ values are a result of ambient water $\delta^{18}O_{w}$ values and temperature. River $\delta^{13}C_{HCO3-}$ values exhibit a seasonal cycle with low values in winter and spring. Suddenly rising values in early summer are due to preferential removal of ^{12}C from the DIC pool by phytoplankton photosynthesis. This seasonal $\delta^{13}C_{HCO3-}$ cycle is accurately recorded in $\delta^{13}C_{ar}$ values of growth increments in unionid shells.

Based on a correlation of intraseasonal $\delta^{18}O$ and $\delta^{13}C$ variation in ambient water and shells, a growth model is constructed which indicates non-linear growth of these unionids. Onset and cessation of growth of unionid freshwater mussels are induced by water temperature, whereas intraseasonal

growth rates are a result of primary productivity (food availability).

This study demonstrates the potential of unionid shell chemistry for palaeoclimate studies. Freshwater bivalve $\delta^{18}O_{ar}$ records can serve as a proxy for past river $\delta^{18}O_w$ values, in relation to discharge seasonality and river dynamics. Freshwater bivalve records can potentially serve as a proxy for past primary productivity, although other parameters (e.g. CO_2 exchange with atmosphere) will likely affect $\delta^{13}C_{ar}$ as well.

Oxygen isotope composition of bivalve seasonal growth increments and ambient water in the rivers Rhine and Meuse

Abstract

The application of oxygen isotope ratios ($\delta^{18}O$) from freshwater bivalves as a proxy for river discharge conditions in the Rhine and Meuse rivers is investigated. We compared a dataset of water temperature and water $\delta^{18}O$ values with a selection of recent shell $\delta^{18}O$ records for two species of the genus *Unio* in order to establish: (1) whether differences between the rivers in water $\delta^{18}O$ values, reflecting river discharge conditions, are recorded in unionid shells; and (2) to what extent ecological parameters influence the accuracy of bivalve shell $\delta^{18}O$ values as proxies of seasonal water oxygen isotope conditions in these rivers. The results show that shells from the two rivers differ significantly in $\delta^{18}O$ values, reflecting different source waters for these two rivers. The seasonal shell $\delta^{18}O$ records show truncated sinusoidal patterns with narrow peaks and wide troughs, caused by temperature fractionation and winter growth cessation. Interannual growth rate reconstructions show an ontogenetic growth rate decrease. Growth lines in the shell often, but not always, coincide with winter growth cessations in the $\delta^{18}O$ record, suggesting that growth cessations in the shell $\delta^{18}O$ records are a better age estimator than counting internal growth lines. Seasonal predicted and measured $\delta^{18}O$ values correspond well, supporting the hypothesis that these unionids precipitate their shells in oxygen isotopic equilibrium. This means that (sub-) fossil unionids can be used to reconstruct spring-summer river discharge conditions, such as Meuse low discharge events caused by droughts and Rhine meltwater influx events caused by melting of snow in the Alps.

4.1 Introduction

The Meuse and the Rhine are the major rivers in the Netherlands. Interannual discharge variation has a profound effect on the often densely populated riparian areas. Both river systems have caused damaging floods (e.g., 1993, 1995) and droughts (e.g., 1976, 2003) with significant economic damage. In the context of the ongoing discussion on anthropogenic climate change, there is growing concern about the frequency of future floods. For a better prediction of future river dynamics, accurate reconstructions of pre-industrial river dynamics, including discharge seasonality and frequencies of floods and droughts, are a prerequisite. Since the instrumental record only goes back to the early twentieth century, the development of accurate proxy records at high temporal resolution is of great relevance.

The Meuse and Rhine are rivers of a different type: the Meuse is rain-fed, while the Rhine is mixed, fed by both rain and meltwater. The different origin of source waters for both rivers leads to distinct differences in the seasonal oxygen isotopic variation of water ($\delta^{18}O_w$) (Mook, 1968). The Meuse shows lowest $\delta^{18}O_w$ values in winter when precipitation is highest and high $\delta^{18}O_w$ values in summer when precipitation is low. As a typical meltwater river, the Rhine has lowest $\delta^{18}O_w$ values in spring and summer when the input of isotopically depleted meltwater from the Alps is high. Ricken et al. (2003) and Verdegaal et al. (2005) suggested that oxygen isotope ratios of aragonite from unionid bivalve shells ($\delta^{18}O_{ar}$) can be used as proxies for seasonal variation of water composition and meltwater fluxes, thus potentially providing high-resolution archives for the reconstruction of pre-industrial river dynamics.

Significant sclerochronological research has been done on marine bivalves using stable oxygen isotope composition as a proxy for temperature or salinity (Witbaard et al., 1994; Bice et al., 1996; Dutton et al., 2002; Schöne et al., 2003; Schöne et al., 2004; Carré et al., 2005; Chauvaud et al., 2005), and more recently the scope has broadened to freshwater bivalves. In several studies, shell $\delta^{18}O_{ar}$ values were confirmed to be a reliable proxy for river conditions in different climate zones (Dettman et al., 1999; Rodrigues et al., 2000; Kaandorp et al., 2003; Ricken et al., 2003; Kaandorp et al., 2005; Gajurel et al., 2006; Goewert et al., 2007).

In this paper we further explore the applicability of this proxy for the Rhine and Meuse rivers by comparing a dataset of water temperature and $\delta^{18}O_w$ values with a selection of $\delta^{18}O_{ar}$ records from shells of *Unio pictorum* and *U. tumidus*. Both instrumental data and shells span the time interval between 1990-2005. We address the following questions: (1) Are differences

93

between the Meuse and Rhine river conditions, as reflected in oxygen isotopic values of the water, recorded in unionid shells and, if so, are these recorded in bulk shell and in seasonal shell $\delta^{18}O_{ar}$ records? (2) To what extent do ecological parameters (ontogenetic growth variation, winter growth cessation, and habitat preference) influence the accuracy of $\delta^{18}O_{ar}$ values and the reliability of reconstructions of past river conditions based on these records? (3) Can we detect inter-specific fractionation of $\delta^{18}O_{ar}$ values between the two species of *Unio*?

4.2 Materials and methods

4.2.1 Species and Collection

Freshwater mussels of the genus *Unio* are large bivalves that have a worldwide distribution and are common in freshwater sites in the Netherlands. They can reach an age of ~ 15 years. During the adult phase of growth all Unionidae live half-buried in the sediment with their siphons exposed

Figure 4.1: *Unio* shells. Scale bars = 1 cm. a) *U. pictorum*; b) *U. tumidus*.
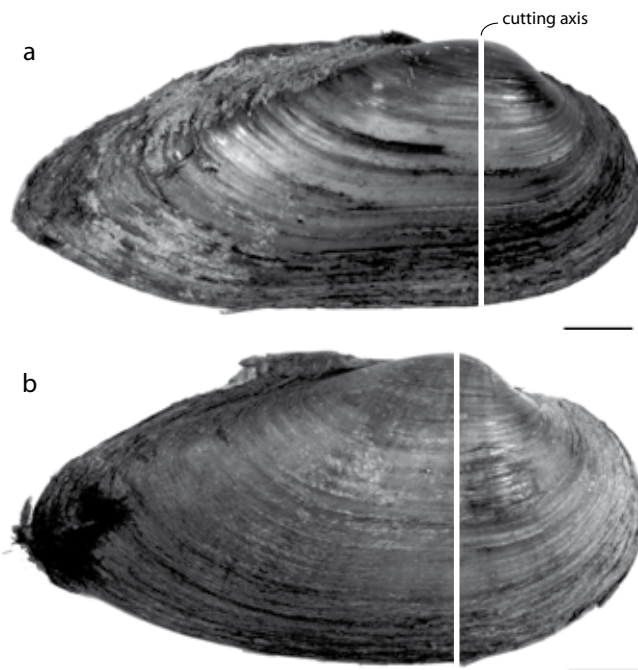
(semi-infaunal); as juveniles, however, they are completely buried in the sediment (infaunal lifestyle; Negus, 1966; Gittenberger et al., 1998). The two species of *Unio* studied include *U. pictorum* (Figure 4.1a) and *U. tumidus* (Figure 4.1b). *Unio pictorum* has an elongate shape, a maximum length of ~ 110 mm, and is found in both stagnant and flowing waters; it can tolerate some pollution. *Unio tumidus* (Figure 4.1b) is ovoid in shape with a prominently curved edge and a maximum length of ~ 125 mm. This species prefers flowing water but also occurs in stagnant waters. Of the two species, *U. tumidus* has the higher pollution tolerance (Gittenberger et al., 1998).

Seven shells from the Meuse, Rhine, or one of its distributaries were collected alive or fresh (a shell is fresh when there are still remnants of the adductor muscles present). Three shells were collected from the Meuse, one in 1998, near the village of Grevenbicht, and the other two in 2005, one near Kerkdriel and one near Lith, The Netherlands. Another three shells were collected from the Waal (a Rhine distributary), one in 1998 near Tuil

Figure 4.2: Map of the Dutch river system showing collection sites of shells (black dots) and locations of Rijkswaterstaat gauging stations (open circles). Map made with Online Map creation: http://www.aquarius.geomar.de/
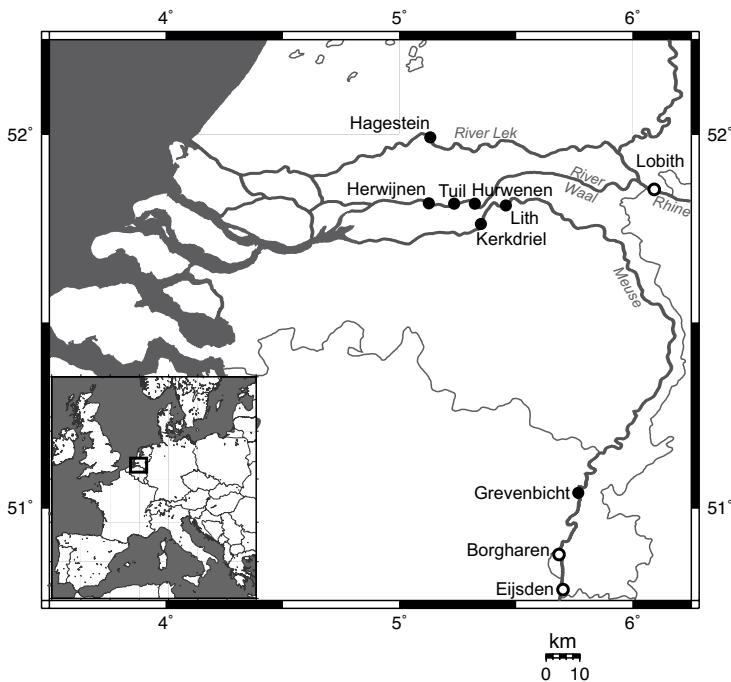
and two in 2003, from Herwijnen and Hurwenen. One shell was collected near Hagestein from the Lek, another Rhine distributary, in 2005 (Figure 4.2).

4.2.2 Collection of River Data

Data on water temperature and discharge were obtained from Rijkswaterstaat (Dutch Directorate for Public Works and Water Management; http://www.waterbase.nl/). More specifically, data from their gauging stations at Lobith (Rhine) and Eijsden (Meuse; Figure 4.2) provided the longest and most complete records. Data on the discharge of the Alpine Rhine at Rekingen (Germany) up to the year 2001 were obtained from the Bundesanstalt für Gewässerkunde (Federal Institute of Hydrology). The temperature datasets have a sampling resolution of 14 days up to 1993 and after that a sampling resolution of 7 days. The discharge data have a sampling resolution of 1 day.

4.2.3 Sampling and Analysis of Shells

Shells were embedded in epoxy resin and thin sections of 300 μm were cut perpendicular to the growth lines, from the umbo along the maximum height of the shell (Figures 4.1a-b). Thin sections were photographed with reflected light. The nacreous layer (Figure 4.3) of the shell was sampled with a Merchantek Micromill microsampler. Not all shells could be sampled up to the umbo; therefore most of the growth curves do not span the first few years of growth. For shells in which the first growth cessation sampled was < 20 mm from the umbo, this was assumed to be the second year of growth. When the first growth cessation sampled was > 20 mm from

Figure 4.3: Schematic cross section of a *Unio* shell. Note the light (opaque) growth increments and the dark (transparent) growth lines. Each season the animal adds a growth increment in summer and a growth line in winter. A thin periostracum, prismatic layer, and a thick nacreous layer grow at the ventral margin. A thin portion of the nacreous layer is added on the inside of the shell.
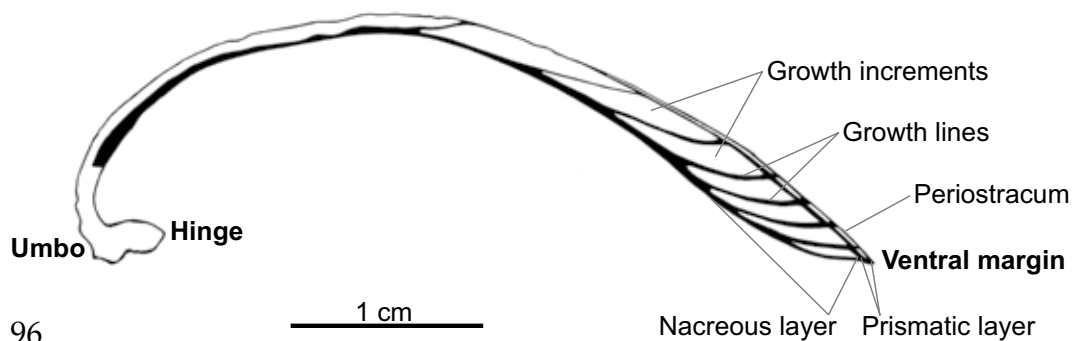
the umbo, we assumed this was the third year of growth. This assumption was based on the distances in the shell from the Herwijnen site, which was sampled completely up to the umbo. Drill bit diameter was ~ 800 μm and sampling resolution was 100-500 μm corresponding to a time span of 3 days to 2 months, depending on growth rate. Drilling depth was ~ 250 μm. Samples were analysed for $\delta^{18}O_{ar}$ values either on a Thermo Finnigan MAT 252 mass spectrometer equipped with a Kiel-II device or a Thermo Finnigan Delta+ mass spectrometer with a GasBench-II. On both systems the long-term standard deviation of a routinely analysed in-house $CaCO_3$ standard was < 0.1 ‰. This $CaCO_3$ standard is regularly calibrated to NBS 18, 19, and 20 (National Institute of Standards and Technology). Typical sample size for the MAT 252 system lies at 10-20 μg. For the Delta+ system samples of 20-50 μg are required. Occasional duplicate analyses confirmed that these two systems gave comparable results.

4.2.4   Calculation of Predicted $\delta^{18}O_{ar}$ Values

To establish whether the two *Unio* species precipitate the $\delta^{18}O_{ar}$ of their shell in equilibrium with the ambient water we used $\delta^{18}O_w$ values and temperature of ambient river water to calculate predicted $\delta^{18}O_{ar}$ values ($\delta^{18}O_{pred}$). A dataset of $\delta^{18}O_w$ values, taken from gauging stations Lobith and Eijsden (Figure 4.2) and spanning the time interval 1990-2005, was obtained from the Centre for Isotope Research, University of Groningen. The temperature record was linearly interpolated in order to obtain a measure of temperature on every date that $\delta^{18}O_w$ values were known. Values of $\delta^{18}O_{pred}$ were calculated using the equation for biogenic aragonite by Grossman and Ku (1986) and Dettman et al. (1999):

$$1000 \ln \alpha = 2.559 \left(10^6 T^{-2}\right) + 0.715 \tag{4.1}$$

where T is the water temperature in degrees Kelvin and α is the fractionation between water and aragonite described by:

$$\alpha^{aragonite}_{water} = \frac{\left(1000 + \delta^{18}O_{ar}\left(VSMOW\right)\right)}{\left(1000 + \delta^{18}O_{w}\left(VSMOW\right)\right)} \tag{4.2}$$

Kim et al. (2007) recently demonstrated that this relation is the same in synthetic aragonite.
All water oxygen isotope values are reported relative to VSMOW (Vienna
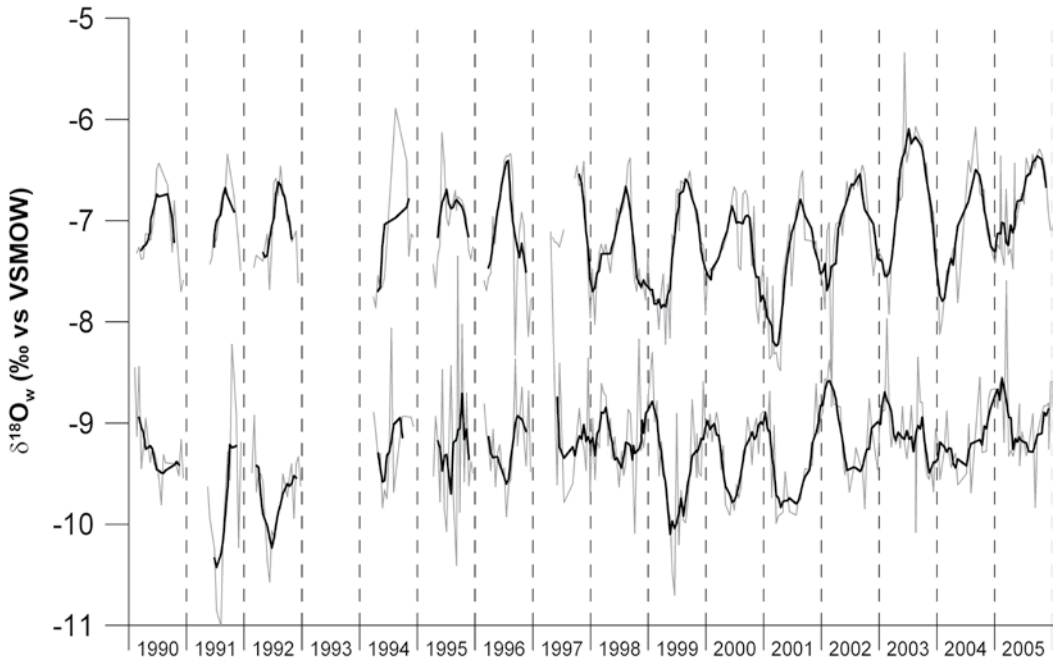
Figure 4.4: Seasonal $\delta^{18}O_w$ values of the Meuse (upper grey line) and Rhine (lower grey line) for 1990–2005. Running average is plotted as a solid black line (Data from Centre for Isotope Research, University of Groningen). VSMOW = Vienna Standard Mean Ocean Water.

Standard Mean Ocean Water). $\delta^{18}O_{ar}$ values are reported relative to VPDB (Coplen, 1996). To convert $\delta^{18}O_{ar}$ (VSMOW) to $\delta^{18}O_{ar}$ (VPDB), the equation of Gonfiantini et al. (1995) is used.

4.3   Results

4.3.1   River Data

The $\delta^{18}O_w$ dataset generally has a sampling resolution of 14 days, though especially in the early years of the record, large hiatuses are present. When a gap in the record is > 30 days, it is shown as a gap in figure 4.4. Absolute $\delta^{18}O_w$ values confirm the general isotopic difference between the Meuse and Rhine, as already suggested by Mook (1968). The two $\delta^{18}O_w$ records show distinct seasonal anti-phase cyclicity. Generally, Rhine $\delta^{18}O_w$ values are lowest in summer, whereas the Meuse has lowest $\delta^{18}O_w$ values in winter. Seasonal $\delta^{18}O_w$ variation is of similar amplitude in both rivers.

4.3.2   Measured $\delta^{18}O_{ar}$ Values in Shells

Growth incremental $\delta^{18}O_{ar}$ analysis of the shells studied yielded between
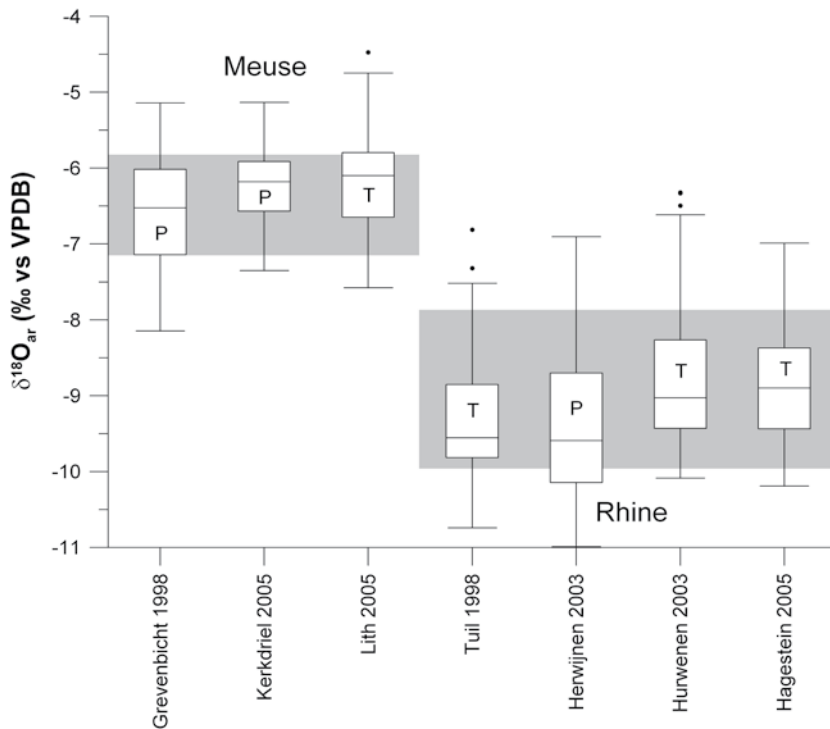
Figure 4.5: Box plots of $\delta^{18}O_{ar}$ values of all specimens. Boxes include median and first two quartiles; last two quartiles are represented by lines and outliers by dots. Gray bands show values (± 1 σ) of $\delta^{18}O_{pred}$ (prediction of $\delta^{18}O_{ar}$ values; see text for further discussion) for both rivers during the growing season (April-October). P = *Unio pictorum*; T = *U. tumidus*; VPDB = Vienna Pee Dee Belemnite.

62-174 $\delta^{18}O_{ar}$ values per specimen. To visualise this amount of data at the level of bulk shell composition, the data range of each specimen is presented in a box plot (Figure 4.5). Meuse shells have an average $\delta^{18}O_{ar}$ value of ~ -6.3 ‰ (versus VPDB) and those from the Rhine, an average of ~ -9.1 ‰ (versus VPDB). Thus, shells from the two rivers appear to differ considerably in $\delta^{18}O_{ar}$ values by ~ 2.8 ‰. Furthermore, the total range of $\delta^{18}O_{ar}$ values for the Rhine shells is somewhat higher than for Meuse shells.

The $\delta^{18}O_{ar}$ values measured along the shell growth axis can also be plotted as a function of distance from the umbo (Figures 4.6 and 4.7). The $\delta^{18}O_{ar}$ records of all shells show a distinct cyclic pattern with relatively narrow peaks and wide troughs. In the Meuse shells, $\delta^{18}O_{ar}$ values vary between -4.5 ‰ and -8.1 ‰ (Figures 4.6a-c). Shells from the Rhine and its distributaries have $\delta^{18}O_{ar}$ values ranging from -6.3 ‰ to -11.0 ‰ (Figures 4.7a-d). Dark growth lines, as observed under reflected light, are indicated by grey
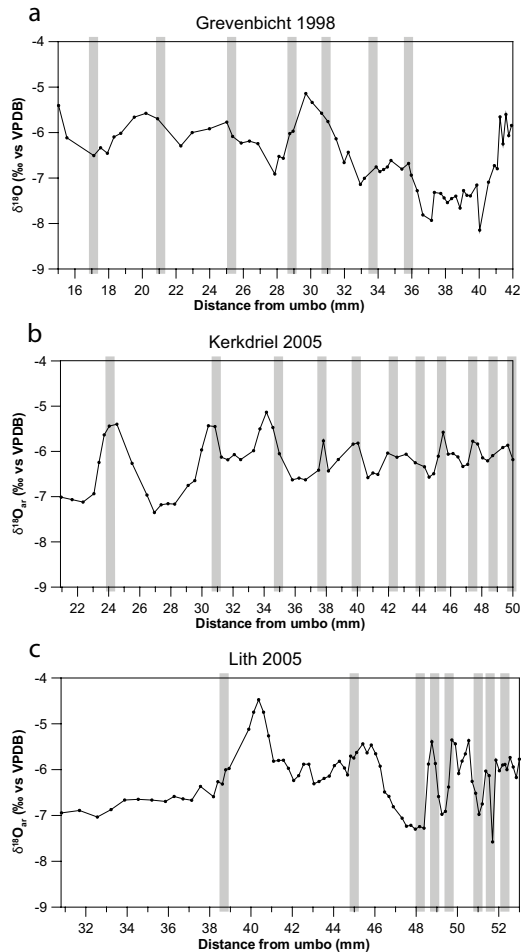
Figure 4.6: $\delta^{18}O_{ar}$ records of the shells from the Meuse. All shells show a clear seasonal pattern. Sharp upward peaks reflect winter growth cessation and low values, the summer growth season. Locations of dark growth lines are indicated by grey bars. a and b are *Unio tumidus*, c is *U. pictorum*.

bands in figures 4.6 and 4.7. They consist of a different aragonite structure from the light increments (Jones, 1983) and are interpreted to correspond to a slowing down of growth prior to growth cessation. In our material, growth lines often, but not always, coincide with peaks in the $\delta^{18}O_{ar}$ record. In our samples, for example, this appears to be the case in the shells from Kerkdriel (Figure 4.6b, grey bars), Tuil (Figure 4.7a), and Herwijnen (Figure 4.7b). In the shell from Grevenbicht (Figure 4.6a), however, the dark lines do not match a peak in the oxygen isotope signal.
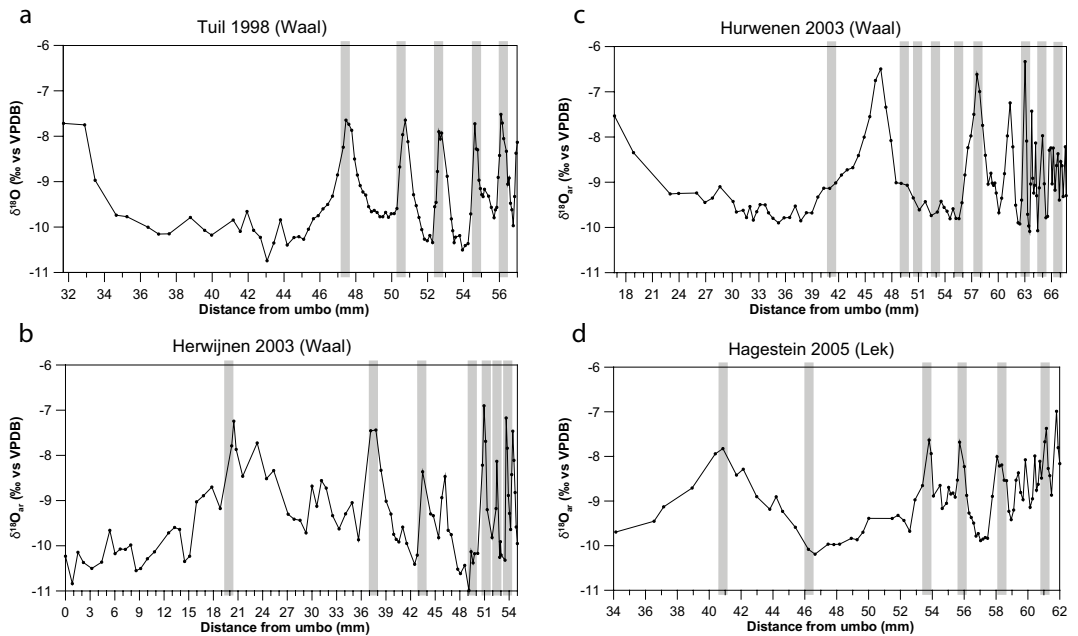
Figure 4.7: $\delta^{18}O_{ar}$ records of the shells from the Rhine distributaries Waal and Lek. All shells show a clear seasonal pattern. Sharp upward peaks reflect winter growth cessation and low values, the summer growth season. Locations of dark growth lines are indicated by grey bars. a, c and d are *Unio tumidus*, b is *U. pictorum*.

4.4   Discussion

4.4.1 $\delta^{18}O_w$ variation of the Meuse and Rhine rivers

The seasonal isotopic variation of the Meuse (Figure 4.4) is determined by the relative contributions of groundwater and surface runoff. In winter, when evaporation is limited, low $\delta^{18}O_w$ values reflect the composition of groundwater, whereas in summer, $\delta^{18}O_w$ values are higher due to evaporation and enriched summer rainfall (Mook, 1968). These processes result in an average $\delta^{18}O_w$ value of ~ -7.1 ‰ (VSMOW) with summer maximum values of ~ -6.4 ‰ (VSMOW) and winter minima of ~ -8.0 ‰ (VSMOW). The Rhine river catchment, however, has an important source area in the Alps. Since snow in the Alps has comparatively low $\delta^{18}O_w$ values (due to the altitude effect; Dansgaard, (1964)), alpine meltwater causes Rhine $\delta^{18}O_w$ values to be lower in summer than in winter (Mook, 1968). This results in a characteristic pattern with an average $\delta^{18}O_w$ value of ~ -9.2 ‰, winter maximum values of ~ -8.4 ‰ and summer minimum values of ~ -9.8 ‰ (Figure 4.4).

101
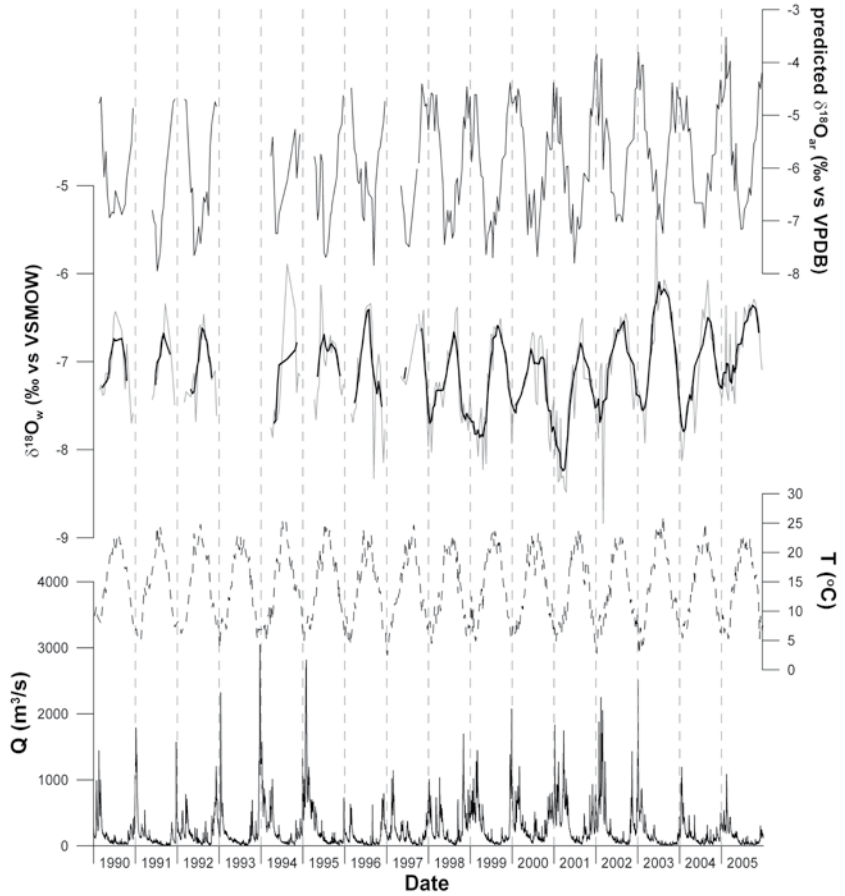
Figure 4.8: Discharge (Q) plotted with $\delta^{18}O_w$ values (and running average), water temperature (T), and $\delta^{18}O_{pred}$ values for the Meuse. The Meuse has high discharge and low $\delta^{18}O_w$ values in winter. The $\delta^{18}O_{pred}$ values, however, are highest in winter, because of the temperature effect.

4.4.2   Calculation of seasonal $\delta^{18}O_{pred}$ patterns

In the time interval for which we have shell isotope data, significant seasonal, but only limited interannual differences are evident in the $\delta^{18}O_{pred}$ values (Figures 4.8 and 4.9). The Rhine exhibits a larger annual range of values than the Meuse. This is the result of the opposing effects of the seasonal variation of $\delta^{18}O_w$ values and temperature on the $\delta^{18}O_{pred}$ values for the Meuse river. In the Rhine, on the other hand, the seasonal $\delta^{18}O_w$ signal is amplified in the $\delta^{18}O_{ar}$ records by temperature seasonality, resulting in a larger range of $\delta^{18}O_{pred}$ values. Summer $\delta^{18}O_{pred}$ minima for 1992-2005 range between -7.95 ‰ (VPDB) and -6.94 ‰ for the Meuse, and -11.68
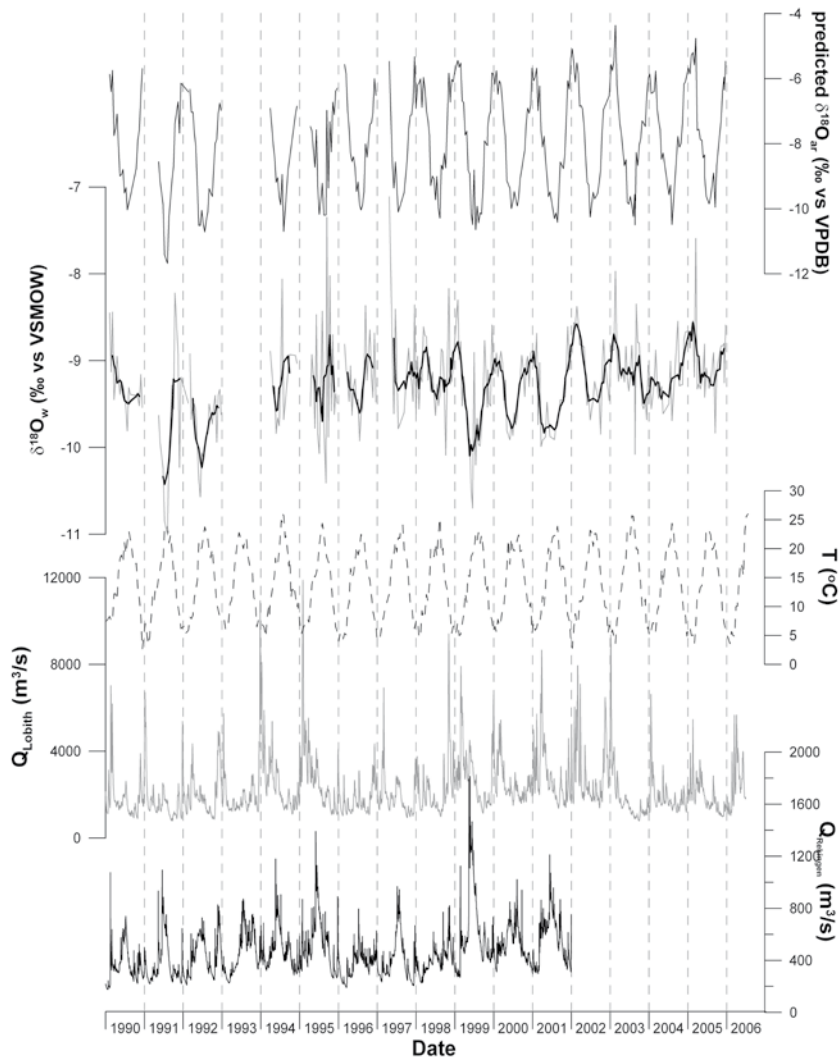
Figure 4.9: Discharge (Q) plotted with $\delta^{18}O_w$ values (and running average), water temperature (T), and $\delta^{18}O_{pred}$ values for the Rhine. This river has its highest discharge in winter, but smaller discharge peaks can be seen in spring and summer. These may be the results of snow melting in the Alps. Generally $\delta^{18}O_w$ values are high in winter and low in summer; however, the pattern is more irregular than in the Meuse. For the $\delta^{18}O_{pred}$ record, the seasonal pattern is enhanced by the temperature effect.

103

‰ and -9.95 ‰ for the Rhine shells. Some differences can be observed between low- (e.g. 2003) and high-discharge summers (e.g. 2000) in the Meuse (Figure 4.8), and some summer meltwater pulses can be recognised in the Rhine (e.g. 1999; Figure 4.9). The recognition of other high-discharge summers (e.g. 1992; Figure 4.8) or meltwater pulses (e.g. 1994 and 1995; Figure 4.9) in the $\delta^{18}O_{ar}$ record, however, is not always straightforward.

4.4.3   Unionid Growth Patterns

The seasonal $\delta^{18}O_{ar}$ records of the unionids studied show a truncated sinusoidal pattern with narrow peaks and wide troughs (Figures 4.6a-c, 4.7a-d). This cyclicity is caused by a combination of temperature fractionation and winter growth cessation (Grossman and Ku, 1986; Dettman et al., 1999; Goodwin et al., 2003). In summer the shells grow relatively fast due to high water temperatures, resulting in wide troughs in the $\delta^{18}O_{ar}$ record. In spring and autumn, at intermediate water temperatures, shells grow more slowly (Howard, 1922; Negus, 1966). This causes the steep slope of the $\delta^{18}O_{ar}$ record during these seasons (Goodwin et al., 2003). Shell growth stops when water temperature falls below ~ 12 °C and thus no environmental data are recorded in the shell in winter (Howard, 1922; Negus, 1966; Dettman et al., 1999; Anthony et al., 2001; Goewert et al., 2007; Kesler et al., 2007). These growth cessations cause the narrow positive peaks in the isotopic record. Cycle counting shows that the total number of growing seasons recorded in the shells varies between two in the shell from Grevenbicht (Figure 4.6a) and 10 in the shell from Kerkdriel (Figure 4.6b), both from the Meuse.

The winter growth cessations, as identified by positive peaks in the $\delta^{18}O_{ar}$ record, often occur at or near macroscopically identifiable dark (transparent) internal growth lines (Negus, 1966; Jones, 1980; Brey and Mackensen, 1997; Schöne et al., 2007), but the two signals do not always match (Kesler and Downing, 1997; Surge et al., 2001). Thus, it appears that growth lines may be caused by factors other than temperature, such as water levels (causing temporary exposure), food availability, spawning (Jones, 1983; Schöne et al., 2005a), turbidity or flow rates (causing detachment of the mussel from its position in the sediment), or predation (Ravera and Sprocati, 1997; Zahner-Meike and Hanson, 2001).

Applying the time control provided by the $\delta^{18}O_{ar}$ record, it is possible to plot annual ontogenetic growth rates for both unionid species studied (Figure 4.10). In the first two to three years of life both species grew very fast, up to 30 mm/year. Subsequently, growth slows considerably to ~ 1.0 mm/year.
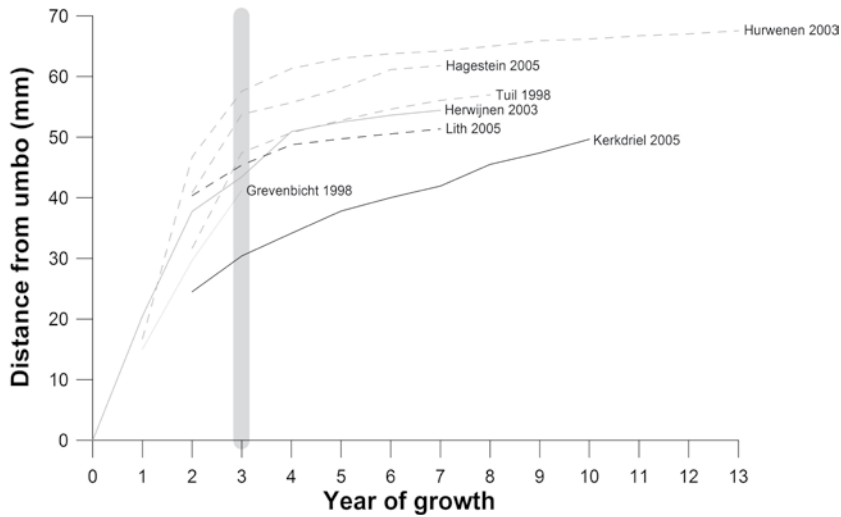
Figure 4.10: Growth of the shells studied. Meuse shells are shown in black; Rhine shells in grey. Solid lines = *Unio pictorum*; dashed lines = *U. tumidus*. Grey bar = point where growth appear to suddenly slow. Because most shells could not be sampled up to the umbo, these plots are floating (see text for further explanation).

Growth rate differences between specimens are significant, but cannot be clearly attributed to river- or species-specific growth patterns.

The general ontogenetic growth-rate decrease that is evident in all shells corresponds well with previously published unionid growth records (e.g. Ravera and Sprocati, 1997; Aldridge, 1999; Christian et al., 2000; Anthony et al., 2001). Furthermore, calculated annual growth rates along the dorso-ventral axis of the adult shells in our study (0.5-2.3 mm/y) are similar to those in the North American unionids *Alasmidonta viridis*, *Lampsilis ovata ventricosa* and *L. radiata siliquoidea* (0.7-1.6 mm/y; Dettman et al., 1999).

4.4.4 Intraseasonal growth rates: establishing seasonal $\delta^{18}O_{ar}$ age models

While the gradually decreasing interannual growth rates can be reconstruct-ed relatively well (Figure 4.10), growth rate changes within each grow-ing season are not well understood. This is potentially problematic for the coupling of $\delta^{18}O_{ar}$ records with instrumental data, because intraseasonal age models are, as a consequence, relatively poorly constrained. Previously published studies have generally adopted one of two possible approaches: (1) Peaks in the $\delta^{18}O_{ar}$ record are aligned with the $\delta^{18}O_{pred}$ record calcu-lated from the instrumental data, which usually involves calculation of winter growth cessation hiatuses. In between such hiatuses, growth rate is

105

assumed to be linear (Dettman et al., 1999; Kaandorp et al., 2003; Ricken et al., 2003); (2) Starting from a crude age model of shell growth, point-by-point time-axis shifting of $\delta^{18}O_{ar}$ values towards $\delta^{18}O_{pred}$ values is performed under the assumption that the shell was precipitated in perfect isotopic equilibrium (Freitas et al., 2006; Goewert et al., 2007). When isotopic equilibrium is sufficiently demonstrated, the latter approach is the most realistic. Its proper application, however, relies on instrumental records of sufficiently high temporal resolution collected at the same location as the shells. In the present study, instrumental records (temperature and $\delta^{18}O_{w}$ values) were taken from gauging stations at Eijsden and Lobith, which are relatively far away from shell collection sites (Figure 4.2). Furthermore, limited temporal resolution of $\delta^{18}O_{w}$ values is likely not to cover all details of riverine $\delta^{18}O_{w}$ variation. For this reason we adopted method (1) for the construction of intraseasonal bivalve age models.

4.4.5   Comparing $\delta^{18}O_{pred}$ and $\delta^{18}O_{ar}$ values

A comparison between $\delta^{18}O_{pred}$ and $\delta^{18}O_{ar}$ values is shown in figure 4.5, with $\delta^{18}O_{pred}$ values during the growing season (April-October, 1990-2005) shown as grey bars. Generally, $\delta^{18}O_{ar}$ values compare well to $\delta^{18}O_{pred}$ values, and show that the difference between the Rhine and Meuse can be identified based on bulk shell $\delta^{18}O_{ar}$ data only. The two species *Unio pictorum* and *U. tumidus* (Figure 4.5, P and T) show indistinguishable average $\delta^{18}O_{ar}$ values and ranges for both rivers. This leads us to conclude that no obvious inter-specific fractionation of $\delta^{18}O_{ar}$ values is present.

4.4.6 $\delta^{18}O_{ar}$ records and their fit with $\delta^{18}O_{pred}$ values

Since collection dates of specimens studied are known, we next assigned calendar years to seasonal growth increments of each specimen based on counting the $\delta^{18}O_{ar}$ cycles from the ventral margin towards the umbo. This worked for all but two specimens studied. These two had growth rates in the adult phase that were too low to resolve annual cyclicity. As a consequence, for shells from Lith (Figure 4.6c) and Hurwenen (Figure 4.7c) calendar years could not be assigned, and these shells were not used for the comparison of $\delta^{18}O_{pred}$ values with $\delta^{18}O_{ar}$ values.

$\delta^{18}O_{ar}$ records of shell growth increments were then compared with $\delta^{18}O_{pred}$ values for the years 1992-2005 years (Figures 4.11a-b, 4.12a-c). There generally is a good correspondence between the $\delta^{18}O_{pred}$ and $\delta^{18}O_{ar}$ records. Seasonal cyclicity in $\delta^{18}O_{pred}$ values is easily identified in shell $\delta^{18}O_{ar}$ records. The fit between $\delta^{18}O_{pred}$ and $\delta^{18}O_{ar}$ values can be quantified by calculating a linear regression between these records, the results of which are shown
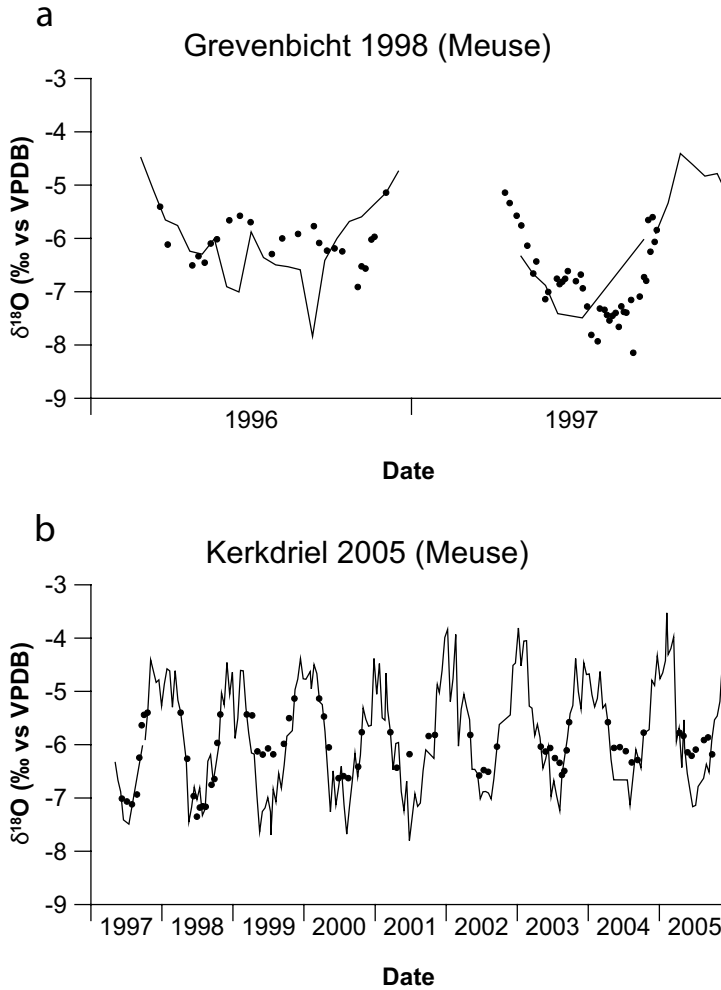
Figure 4.11: $\delta^{18}O_{pred}$ record (solid lines) for the Meuse with shells (both *Unio pictorum*; black dots) plotted over the summer season.

in table 4.1. Although all regressions are significant, it is evident that the scatter of the data is significant and the equations describing the regression lie far from the expected Y = X. This can in principle be caused by isotopic disequilibrium, age-model uncertainties (i.e. no linear growth), or spatial heterogeneity of river-water temperature and $\delta^{18}O_w$ values.

Isotopic equilibrium of unionids growing in the Meuse and Rhine river cannot be tested with the datasets available in this study, because the required conditions of precise temporal and spatial correlation between $\delta^{18}O_{pred}$ values and $\delta^{18}O_{ar}$ values cannot be met. In a recent monitoring ex-
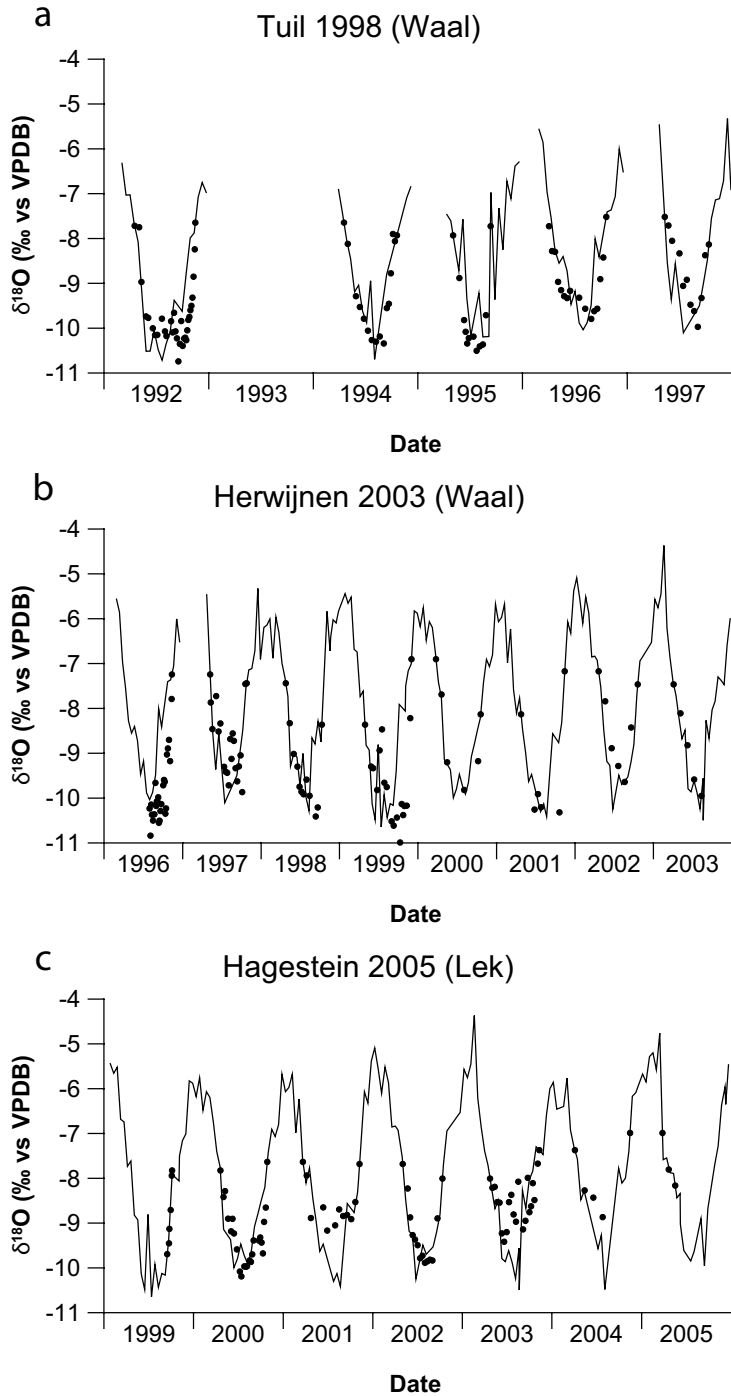
Figure 4.12: $\delta^{18}O_{pred}$ record (solid lines) for the Rhine distributaries plotted with shells (black dots). a and c are *Unio tumidus*, b is *U. pictorum*.

periment in the Meuse and Rhine rivers, however, isotopic equilibrium has been demonstrated for both species used in this study. This is in line with other studies on unionids, which generally point towards shell growth in isotopic equilibrium (Dettman et al., 1999; Kaandorp et al., 2003; Goewert et al., 2007). For this reason we do not believe that isotopic disequilibrium contributes significantly to the uncertainties in the linear regression presented in table 4.1.

Table 4.1: Statistics of linear regression between $\delta^{18}O_{pred}$ and $\delta^{18}O_{ar}$ values.

Shell	Equation	R^2	p
Grevenbicht 1998 (Meuse)	Y = 0.301X - 4.335	0.195	0.002
Kerkdriel 2005 (Meuse)	Y = 0.619X - 2.174	0.578	0.000
Tuil 1998 (Waal)	Y = 0.708X - 2.941	0.487	0.000
Herwijnen 2003 (Waal)	Y = 0.500X - 4.817	0.235	0.000
Hagestein 2005 (Waal)	Y = 0.663X - 2.902	0.564	0.000

A more important source of uncertainty lies in the construction of a detailed seasonal growth model. As discussed above, we have applied a linear growth model, although it is likely that shells do not grow linearly. Indications for this growth pattern are phase lags between $\delta^{18}O_{pred}$ and $\delta^{18}O_{ar}$ records, which can be observed in several specimens (e.g. Grevenbicht, season 1997; Tuil, season 1992; Herwijnen, season 1996; Hagestein, season 2000; Figures 4.11 and 4.12). It is difficult to correct for these phase lags because they do not occur consistently in the dataset. Such age-model uncertainties are less conspicuous in the summer $\delta^{18}O_{ar}$ minima because in that interval the slope of the $\delta^{18}O_{ar}$ record is close to zero, so comparison between the $\delta^{18}O_{pred}$ and $\delta^{18}O_{ar}$ records is relatively reliable in the summer period.

Out of four shells that span > 5 years of growth (Figures 4.11 and 4.12), two show rather inconsistent correspondence between $\delta^{18}O_{pred}$ and $\delta^{18}O_{ar}$ summer minima. Shells from Kerkdriel and Hagestein show some years in which $\delta^{18}O_{pred}$ and $\delta^{18}O_{ar}$ summer minima correspond well, and some years in which $\delta^{18}O_{ar}$ values are higher by a maximum of ~ 1.5 ‰. The most likely explanation for the lack of correspondence in these shells is that they were collected in waters with only a restricted connection to the river, where summer evaporation can cause significant shifts to higher $\delta^{18}O_{w}$ values. In the shells from Tuil and Herwijnen the correspondence between $\delta^{18}O_{pred}$ and $\delta^{18}O_{ar}$ summer mimima is relatively good. Particularly for the shell from Tuil the interannual differences in $\delta^{18}O_{pred}$ summer minima ap-

109

pear to be recorded accurately in $\delta^{18}O_{ar}$ values. Thus it seems that shells collected from the river itself are more likely to accurately record differences in interannual summer conditions, and subfossil and fossil unionids are potentially applicable to reconstruct past climate and associated river conditions in the Rhine and Meuse rivers.

4.5   Conclusions

Shells from the rivers Rhine and Meuse differ significantly in bulk $\delta^{18}O_{ar}$ values and accurately reflect the difference of $\delta^{18}O_{w}$ values between the two rivers. This indicates that the palaeogeography of the Dutch river systems can potentially be reconstructed on the basis of bulk $\delta^{18}O_{ar}$ data of fossil shells. Furthermore, our data show that the two species analysed (*Unio pictorum* and *U. tumidus*) have indistinguishable average $\delta^{18}O_{ar}$ values and ranges, suggesting that inter-specific fractionation of $\delta^{18}O_{ar}$ values does not influence such reconstructions.

The seasonal $\delta^{18}O_{ar}$ records of the unionids studied show a truncated sinusoidal pattern with narrow peaks and wide troughs, caused by a combination of temperature fractionation and winter growth cessation. This record can be used to reconstruct accurate interannual growth rate variation.

Macroscopically identifiable growth lines in transverse sections of the shell often, but not always, coincide with peaks in the $\delta^{18}O_{ar}$ record. Some growth lines are not caused by winter growth cessation, but possibly relate to environmental factors such as predation damage, spawning, or summer droughts. Therefore growth-line counting to obtain an interannual growth model is inherently unreliable in these shells.

There is generally good correspondence between the $\delta^{18}O_{pred}$ and $\delta^{18}O_{ar}$ records. Seasonal cyclicity in $\delta^{18}O_{pred}$ values is easily identified in shell $\delta^{18}O_{ar}$ records, supporting the hypothesis that these unionids precipitate their shell in oxygen isotopic equilibrium. Shells studied thus record riverine summer conditions at high temporal resolution and (sub-) fossil unionids are potentially applicable to reconstruct summer river dynamics in the Rhine and Meuse systems. In particular, Meuse summer drought and Alpine meltwater discharge in the Rhine may be reconstructed based on shell $\delta^{18}O_{ar}$ records.

Chapter 5

Is 20ᵗʰ century summer discharge in the river Meuse recorded in the shell chemistry of freshwater mussels (Unionidae)?

Abstract

In this chapter we use unionid shell aragonite oxygen isotope ratios ($\delta^{18}O_{ar}$) as a proxy for past discharge in the river Meuse. We developed the proxy from a modern dataset for the reference time interval 1997-2007, which showed a logarithmic relation between measured water oxygen isotope ratios ($\delta^{18}O_w$) of Meuse water and discharge values. To test this relation in the past, $\delta^{18}O_{ar}$ records from shells from two time windows (1910-1918 and 1969-1977) were converted into $\delta^{18}O_w$ values using existing water temperature records. These $\delta^{18}O_w$ values were then applied to calculate discharge values. The logarithmic relation provides a comparison of calculated discharge values with measured discharge values for the same two time windows to verify the proxy. Growth incremental $\delta^{18}O_{ar}$ records were extracted from the aragonite of four *Unio* shells. We found that summer reconstructed $\delta^{18}O_w$ ($\delta^{18}O_{wr}$) values in the shells from 1910-1918 show a similar range as the summer $\delta^{18}O_w$ values for the reference time interval 1997-2007, whilst summer $\delta^{18}O_{wr}$ values for the time interval 1969-1977 are anomalously high. These high $\delta^{18}O_w$ values suggest that the river Meuse experienced severe summer droughts during the latter time interval. We attempted to quantify discharge values from the $\delta^{18}O_{wr}$ values using the logarithmic relation between $\delta^{18}O_w$ and discharge values. Comparison of the calculated summer discharge results with the available instrumental discharge data shows that Meuse low discharge events below a threshold value of 6 m^3/s can be detected in the $\delta^{18}O_w$ record, but true quantification remains problematic.

5.1 Introduction

The Meuse is one of the large river systems in the Netherlands. It is a rain-fed river characterised by a pronounced rainfall-evaporation regime causing low discharge in summer and high discharge in winter (De Wit et al., 2007). Its 33,000 km^2 basin drains the northeast of France and eastern Belgium. Average discharge at Borgharen (Figure 5.1) is 274 m^3/s; highest peak discharges exceed 3000 m^3/s and low-flow events can be less than 2 m^3/s. Floods (e.g. 1993 and 1995) and droughts (e.g. 1976 and 2003) do occur, and both are expected to become more frequent due to an increase in precipitation extremes caused by climate change (Parmet and Burgdorffer, 1995; Gregory et al., 1997; Arnell, 1999; Bürger, 2002; Pfister et al., 2004; Tu, 2006; Ward et al., 2008). Large flood events mainly happen during the winter season when freshwater mussels do not grow. Severe drought in the Meuse hinterland generally occurs during the summer-autumn time interval, which results in low Meuse river discharge. These droughts limit water availability for agriculture and cooling water for power plants. In addition,

Figure 5.1: Map the river Meuse in the Netherlands. Shell collection sites are black dots; Rijkswaterstaat gauging stations are circles. (Made with Online Map Creation: http://www.aquarius.geomar.de/)
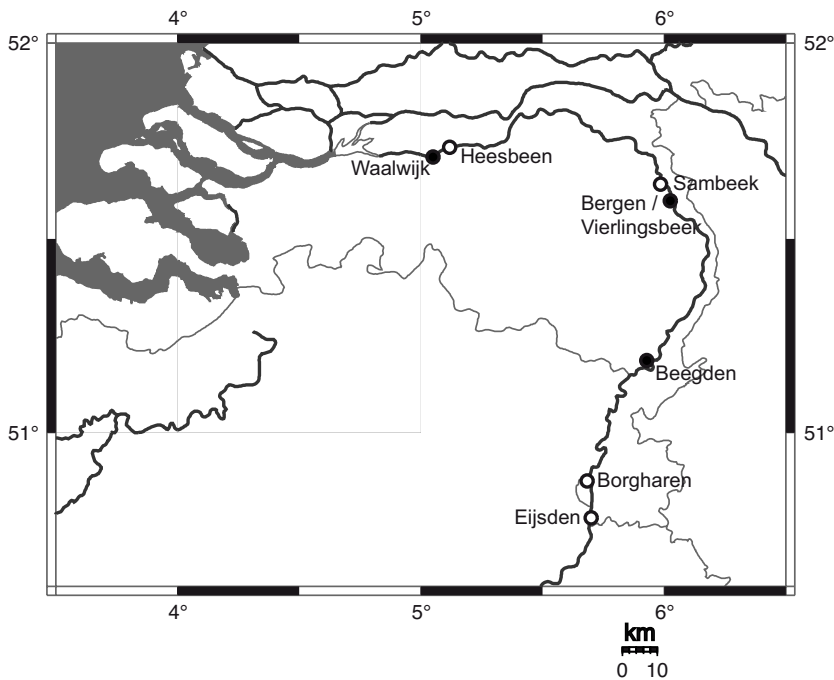
water quality deteriorates during episodes of droughts, threatening drinking water supplies and impacting river ecology (Van Vliet and Zwolsman, 2008). Reduced discharge and associated water chemistry can potentially be recorded freshwater bivalve shells.

In order to improve our understanding of river dynamics and to predict impacts of future climate change, it is important to gain insight in past discharge seasonality and frequencies of floods and droughts. The instrumental Meuse discharge record only goes back to the early 20th century. Therefore it is crucial to develop proxies for river discharge prior to instrumental recordings.

A likely candidate for such a proxy is stable oxygen isotope ratios from the shells of unionid freshwater bivalves growing in this river. Previously these records have been demonstrated to be a useful proxy for past rainfall patterns, water source or river discharge (Ricken et al., 2003; Kaandorp et al., 2005; Verdegaal et al., 2005; Gajurel et al., 2006; Goewert et al., 2007). In this study we investigate the possibilities and limitations of unionid aragonite oxygen isotope ratios ($\delta^{18}O_{ar}$ values) as a proxy for past river discharge in the river Meuse. Shell aragonite is precipitated in annual growth increments, clearly visible in dorso-ventral sections of the shell. $\delta^{18}O_{ar}$ values of these growth increments are generally in equilibrium with ambient water oxygen isotope ratios ($\delta^{18}O_{w}$ values) (Dettman et al., 1999; Kaandorp et al., 2003; Ricken et al., 2003; Gajurel et al., 2006; Goewert et al., 2007). Analysing growth increments at high spatial resolution can thus reveal seasonal patterns in $\delta^{18}O_{ar}$. Unionids cease growing below a certain temperature threshold (Howard, 1922; Dettman et al., 1999; Dunca and Mutvei, 2001; Goewert et al., 2007), which is ~ 12-13.5 °C for the species used here (Negus, 1966; Chapter 3). Therefore, only summer conditions can be recorded in the shell and winters are represented by hiatuses.

We previously established that freshwater bivalve $\delta^{18}O_{ar}$ values can be used as a proxy for past water compositions during summer by showing that aragonite in modern shells is precipitated in isotopic equilibrium with the ambient water (Chapter 3). However, no attempt has yet been made to calculate $\delta^{18}O_{w}$ values from $\delta^{18}O_{ar}$ values with the aim of reconstructing river discharges.

In this chapter we aim to: 1) investigate whether $\delta^{18}O_{w}$ values can be used as a proxy for discharge by using a dataset of measured $\delta^{18}O_{w}$ values and discharge values from the time interval 1997-2007; 2) reconstruct $\delta^{18}O_{w}$ values for two twentieth century time intervals (1910-1918; 1969-1977) on the basis of molluscan $\delta^{18}O_{ar}$ records; 3) use reconstructed $\delta^{18}O_{w}$ ($\delta^{18}O_{wr}$) val-

ues to reconstructed river discharge values and compare these with measured river discharge during the same two selected time intervals; 4) identify extreme high and low summer discharges in the $\delta^{18}O_{wr}$ record.

5.2   Materials and methods

5.2.1   Freshwater mussels

Freshwater mussels of the genus *Unio* are abundant in freshwater bodies in the Netherlands. They form shells up to 12.5 cm in length and can live for up to 15 years (Gittenberger et al., 1998). Three species are studied here: *U. crassus*, which has been extinct in the Netherlands since 1968 (Gittenberger et al., 1998), *U. pictorum* and *U. tumidus*.

5.2.2   Shell collection

Four twentieth century shells from the river Meuse were taken from museum and private collections. All were collected alive, and thus the $\delta^{18}O_{ar}$ records of these shells can be exactly matched with the available instrumental records of water temperature and discharge of the river Meuse of the corresponding time interval. Two sets of shells were collected in different locations: two specimens collected in 1918, from Beegden and Bergen, respectively; and two specimens collected in 1977 from Vierlingsbeek and Waalwijk. For specifications of all specimens and collection sites the reader is referred to figure 5.1 and table 5.1.

Table 5.1: Specimens collected.

Year	River	Location	Species	Length (mm)	Height (mm)	Height along curve of shell (mm)
1918	Meuse	Beegden	*Unio tumidus*	80.5	42.5	68
1918	Meuse	Bergen*	*Unio crassus*		32.6	34
1977	Meuse	Vierlingsbeek	*Unio pictorum*	88.0	39.0	52
1977	Meuse	Waalwijk	*Unio pictorum*	79.5	33.5	44

* Previously analysed by Verdegaal et al. (2005)

5.2.3   Collection of river-data

Water temperature and discharge variability (river discharge: Figure 5.2) have been measured since the beginning of the twentieth century by Rijkswaterstaat (Dutch Directorate for Public Works and Water
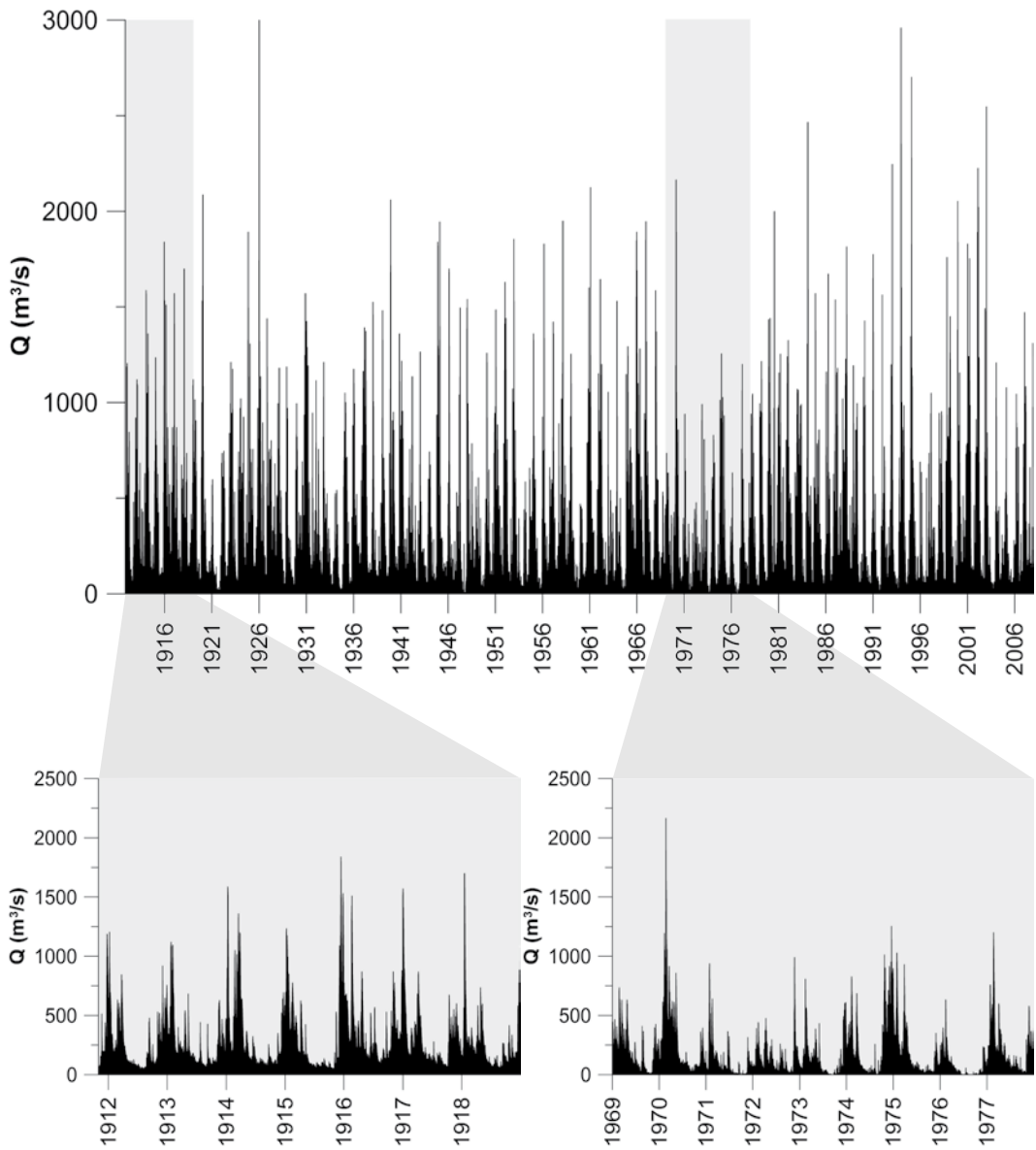
Figure 5.2: Discharge (Q) of the Meuse for the time interval November 1911 to December 2007. Considerable long-term variation in both maxima and minima is visible. Blown-up figures show discharges for the time intervals in which the shells grew. The time interval 1912-1918 has several high-discharge summers (e.g. 1916 and 1917), whereas the time interval 1969-1977 generally has very dry summers and exhibits several severe summer droughts (e.g. 1971 and 1976).
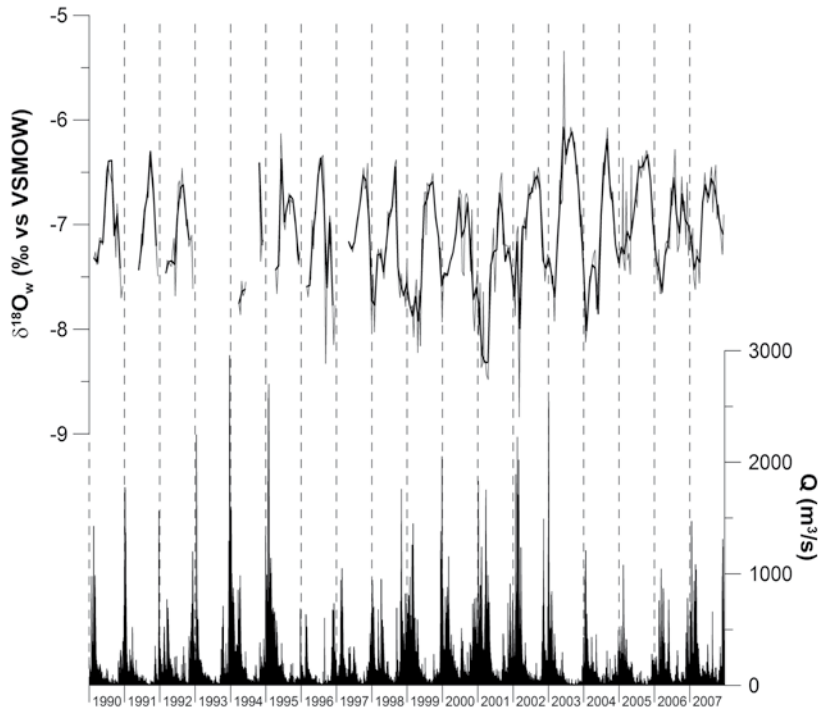
Figure 5.3: Discharge (Q) measured at Borgharen and seasonal $\delta^{18}O_w$ values sampled at Eijsden (raw data in grey and re-sampled data (simple cubic spline, 30 day resolution) in black) for the river Meuse during the time interval 1997-2007.

Management; http://www.waterbase.nl/). Temperature data for the $\delta^{18}O_w$ reconstruction were taken from the gauging station closest to the collection site. For the Bergen 1918 shell, the closest gauging station was Borgharen; for the Vierlingsbeek 1977 shell this was Sambeek; and for the Waalwijk 1977 shell temperature data from Heesbeen were used (Figure 5.1). Discharge data were used from the gauging station at Borgharen.

The only continuous multi-year $\delta^{18}O_w$ record for the river Meuse has been measured at Eijsden during the time interval 1990-2007 (Figure 5.1). We obtained this dataset from the Centre for Isotope Research, University of Groningen (Figure 5.3). We do have measurements of Meuse $\delta^{18}O_w$ values measured at Lith during one year (June 2006-July 2007). Using this dataset we established that $\delta^{18}O_w$ values measured at Eijsden and Lith during the same time period correspond well (Chapter 3, Figure 3.4).

5.2.4   Sampling and analysis of shells

Shells were embedded in epoxy resin and thin sections of 300 μm were cut perpendicular to the growth lines, along the dorso-ventral axis of the shell (Figures 4.1a-b). The nacreous layer of the shell was sampled with a Merchantek Micromill microsampler. Drill bit diameter was ~ 800 μm and sampling resolution was 100-500 μm corresponding to a time span of 6 days to > 2 months, depending on growth rate. Drilling depth was ~ 250 μm. Samples were analysed for $\delta^{18}O_{ar}$ values either on a Finnigan MAT 252 mass spectrometer equipped with a Kiel-II device or a Finnigan Delta+ mass spectrometer with a GasBench-II. On both systems the long-term standard deviation of a routinely analysed in-house $CaCO_3$ standard was < 0.1‰. This $CaCO_3$ standard is regularly calibrated to NBS 18, 19, and 20 (National Institute of Standards and Technology). Typical sample size for the MAT 252 system lies at 10-20 μg. For the Delta+ system samples of 20-50 μg are required. Occasional duplicate analyses confirmed that these two systems gave comparable results.

5.2.5   Calculation of $\delta^{18}O_{wr}$ values

For the calculations of $\delta^{18}O_{wr}$, the equation of Grossman and Ku (1986) as modified by Dettman et al. (1999) was used:

$$1000 \ln \alpha = 2.559 \left(10^6 T^{-2} \right) + 0.715 \tag{5.1}$$

where T is the water temperature in degrees Kelvin and α is the fractionation between water and aragonite described by:

$$\alpha_{\text{water}}^{\text{aragonite}} = \frac{\left(1000 + \delta^{18}O_{ar} \left(\text{VSMOW} \right) \right)}{\left(1000 + \delta^{18}O_{w} \left(\text{VSMOW} \right) \right)} \tag{5.2}$$

Where *ar* is shell aragonite and *w* is water.

$\delta^{18}O_{w}$ values are reported relative to VSMOW, whereas $\delta^{18}O_{ar}$ values are reported relative to VPDB (Coplen, 1996). $\delta^{18}O_{ar}$ (VSMOW) values were converted to $\delta^{18}O_{ar}$ (VPDB) using the equation of Gonfiantini et al. (1995):

$$\delta^{18}O_{ar} \left(\text{VSMOW} \right) = 1.03091 \left(1000 + \delta^{18}O_{ar} \left(\text{VPDB} \right) \right) - 1000 \tag{5.3}$$

5.3 Results

5.3.1 River data

The complete discharge record from Borgharen, covering the time interval November 1911-2007, is shown in figure 5.2. Both the maximum discharge values and the minimum discharge values show marked seasonal dry and wet intervals. The shells studied here grew in either an interval with relatively normal to high summer discharges (1910-1918), or a time interval with exceptionally low discharge values (1969-1977). These two time intervals are shown in the blown-up figures of figure 5.2.

To facilitate qualitative comparison with the $\delta^{18}O_{wr}$ output, we calculated the mean, minimum and maximum discharges for the shell growing season (April-October) of each year. We subsequently classified the years into five discharge classes by applying k-means cluster analysis on the natural logarithm of these values. We labelled these classes "very high", "high", "normal", "low" and "very low" (Figure 5.4). The two lowest minimum discharge classes ("low" and "very low") represent summers in which the minimum discharge was ≤ 6 m^3/s. Since the shells presented here grew in the time intervals 1910-1918 and 1969-1977, only the relevant summers are shown in figure 5.4.

From the discharge record, it appears that the time interval 1910-1918 had

Figure 5.4: Discharges categorised in five classes with respect to mean, minimum and maximum discharges during the season April-October 1912-1918 and 1969-1977 at Borgharen. For 1910 and 1911 no discharge data were available.
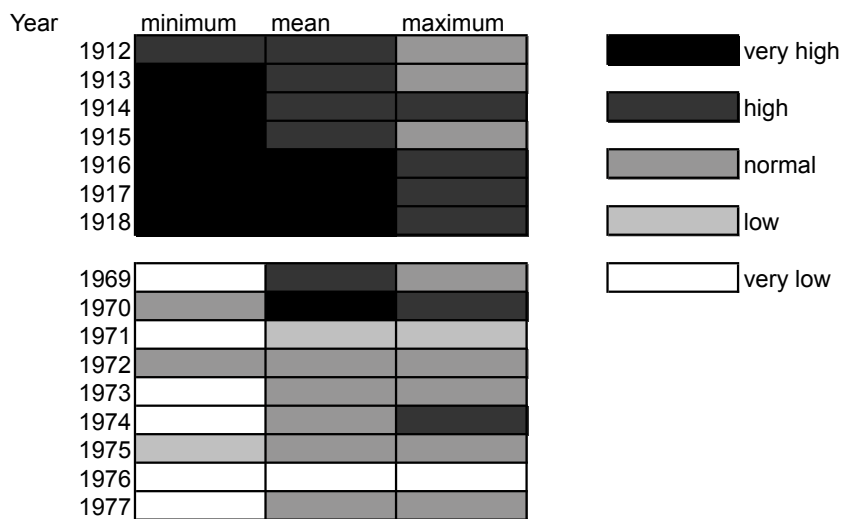
high discharges, whereby in the years 1916, 1917 and 1918 the Meuse experienced very high mean discharges and very high minimum discharges; the latter was also the case for the years 1913, 1914 and 1915 (Figure 5.4). In contrast, during the time interval 1969-1977 the Meuse experienced several extremely dry summers with minima ≤ 2 m^3/s: 1969, 1971, 1973, 1974, 1976 and 1977, whereby during the year 1976 the seasonal mean and maximum was also very low. The year 1976 was exceptionally dry and hot (Können and Fransen, 1996) and had the longest time interval with extremely low discharges of the entire 1912-2007 record (Figure 5.4). The reference time interval for which $\delta^{18}O_w$ values are available (1997-2007) is mainly characterised by low mean summer discharges, with average minimum discharges. The summer of 2003 was the one-but-driest in the 1912-2007 record. This resulted in low discharge of the Meuse. Despite the above, both discharge and $\delta^{18}O_w$ values have a sufficient range to calculate their relation from this record (see discussion).

Figure 5.5a-d: $\delta^{18}O_{ar}$ records of the four shells: a. Beegden 1918 (*Unio tumidus*); b. Bergen 1918 (*U. crassus*); c. Vierlingsbeek 1977 (*U. pictorum*); d. Waalwijk 1977 (*U. pictorum*). All shells show a truncated seasonal pattern with sharp upward pointing peaks reflecting winter growth stops and low values reflecting summer growth seasons. $\delta^{18}O_{ar}$ data of the Bergen 1918 shell have previously been published by Verdegaal et al. (2005).
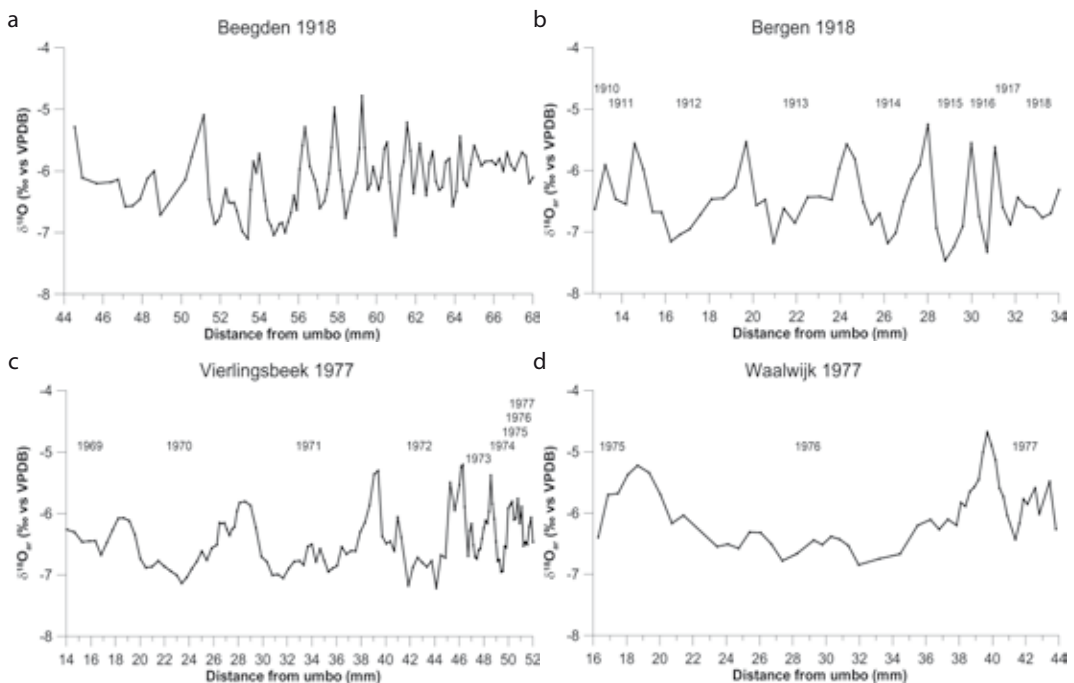
5.3.2   Measured $\delta^{18}O_{ar}$ values in shells

The $\delta^{18}O_{ar}$ records of the shells show the truncated sinusoidal pattern typical for seasonal growth (Figures 5.5a-d). One year of growth is represented by a wide summer trough and a narrow positive peak. This narrow peak corresponds to $\delta^{18}O_{ar}$ values precipitated during slow growth just prior to and shortly after the winter growth cessation (Grossman and Ku, 1986; Dettman et al., 1999; Goodwin et al., 2003; Versteegh et al., 2009; Chapter 4). In these shells $\delta^{18}O_{ar}$ values vary between -4.7 and -7.5 ‰ (VPDB), which is representative for the river Meuse (Versteegh et al., 2009; Chapter 4). The total number of growing seasons recorded in the shell varies between two in Waalwijk 1977 (Figure 5.5d) and over 14 in Beegden 1918 (Figure 5.5a).

5.4   Discussion

In order to test the applicability of unionid $\delta^{18}O_{ar}$ values as proxy for river $\delta^{18}O_{w}$ values and, ultimately, discharge, we first need to determine if there is a detectable relation between these two. Subsequently, we reconstruct river $\delta^{18}O_{w}$ values during the lifetime of the shell and finally attempt to reconstruct river discharge.

5.4.1   Empirical relation between $\delta^{18}O_{w}$ values and discharge

The measured $\delta^{18}O_{w}$ record of 1990-2007 contains several hiatuses during the years 1990-1997, which inhibit a comprehensive comparison of the relation between $\delta^{18}O_{w}$ and discharge. However, the time interval 1997-2007 is suitable for such an exercise. We therefore focus on the interval 1997-2007, for which the data are complete, to model the relation between $\delta^{18}O_{w}$ and discharge values. The 1997-2007 record shows that the Meuse has an average $\delta^{18}O_{w}$ value of -7.1 ‰ (VSMOW) with summer maxima of -6.0 to -6.5 ‰ (VSMOW) and winter minima of -7.7 to -8.4 ‰ (VSMOW; Figure 5.3). Some extreme high and low summer discharge events can be recognised in the $\delta^{18}O_{w}$ record: the relatively high discharge time intervals during the summers of 2000 and 2001 coincide with the two lowest summer $\delta^{18}O_{w}$ peaks, and the very dry summer of 2003 resulted in extremely high peak $\delta^{18}O_{w}$ values (Figure 5.3).

To evaluate whether a quantifiable relation between $\delta^{18}O_{w}$ and discharge exists, these variables were used for constructing a correlation diagram (Figure 5.6). The relation between $\delta^{18}O_{w}$ and discharge (Q) is a logarithmic, because the differences between mean and minimum and mean and maximum discharge within one year are both about an order of magni-
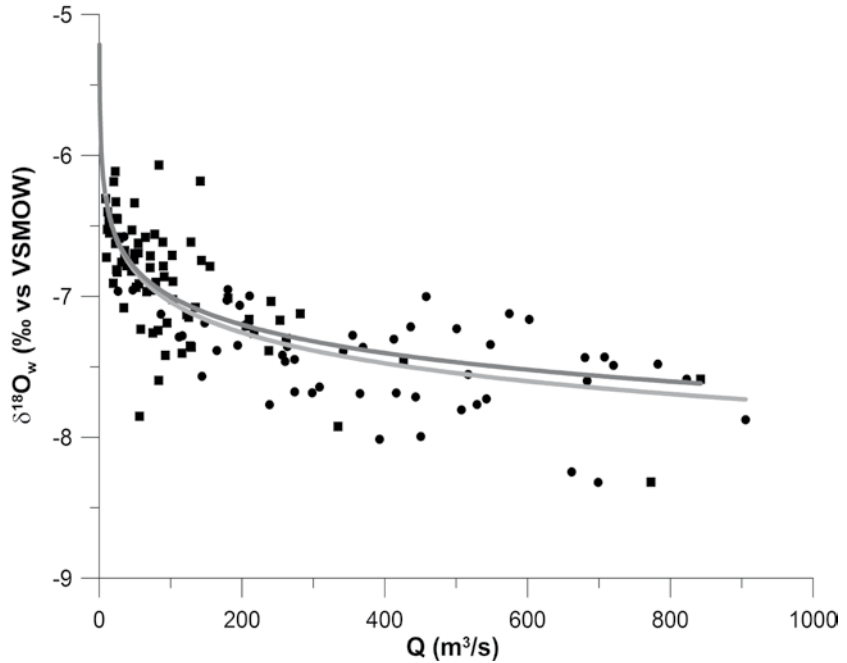
Figure 5.6a: Correlation of discharge (Q) and $\delta^{18}O_w$ values for the Meuse during the years 1997 to 2007 for all months (circles) with a logarithmic fit (light grey line) with equation: $\delta^{18}O_w$ = -0.315 * ln Q - 5.592 (R^2 = 0.604; p = 0.000) and for the growing season of the shells (squares) with a logarithmic fit (dark grey line) with equation: $\delta^{18}O_w$ = -0.291 * ln Q - 5.659 (R^2 = 0.439; p = 0.000).

tude. In addition discharge cannot have a negative value. The logarithmic relation has the following equation (full data set):

$$\delta^{18}O_w = -0.315 * \ln Q - 5.592 \tag{5.4}$$

We were particularly interested in this relation for the summer time interval, since these mussels precipitate their shells only during summer (April-October; Negus, 1966; Chapter 3). For the summer data this relation has the following equation:

$$\delta^{18}O_w = -0.291 * \ln Q - 5.659 \tag{5.5}$$

The logarithmic regressions approximate the data points well, using the full dataset (R^2 = 0.604; p = 0.000) or only the summer data (R^2 = 0.439; p = 0.000; for statistics of linear and quadratic regressions see table 5.2). However, the variance of data points is ~ 1 ‰ for a given discharge value.

The data used to construct figure 5.6 have a minimum discharge value of 9 m³/s and a maximum of 842 m³/s (during this time interval lower discharges ($\geq$ 5.7 m³/s) occurred, but not on the dates $\delta^{18}O_w$ measurements were taken), whereas the total discharge variation during the summers from November 1911 to 2007 ranged from < 2 to 2000 m³/s. Because the relation between discharge and $\delta^{18}O_w$ is logarithmic, $\delta^{18}O_w$ values will only differ slightly between the normal to extremely high summer discharge situations. Therefore it is not possible to detect and reconstruct high summer discharges reliably. In the low to extremely low discharge situations, however, $\delta^{18}O_w$ values will show a significant shift towards higher values, enabling detection of summer droughts in the river Meuse (Figure 5.6).

Table 5.2: Equations and statistics for different fits between $\delta^{18}O_w$ values and discharge in the Meuse.

	Equation	R^2	p
Full data set	Y = -0.002 * X - 6.772	0.502	0.000
	Y = -0.315 * ln X - 5.592	0.604	0.000
	Y = -6.608 - 0.003 * X + 0.00000266 * X²	0.583	0.000
Only summer	Y = -0.002 * X - 6.629	0.446	0.000
	Y = -0.291 * ln X - 5.659	0.439	0.000
	Y = -6.575 - 0.003 * X + 0.00000153 * X²	0.460	0.000

5.4.2 Reconstructed $\delta^{18}O_w$ records

We aimed to reconstruct $\delta^{18}O_w$ values and subsequently link the $\delta^{18}O_{wr}$ patterns to known river discharge variation. Firstly, to each individual growing season in the shell $\delta^{18}O_{ar}$ records, a calendar year needs to be assigned. Due to the ontogenetic decrease of growth rate, growth increments are narrower in the adult shell and in some cases cannot be resolved with the Micromill sampling technique used here. This is the case for the Beegden 1918 shell (Figure 5.5a). In this shell, the growth seasons could not be identified up to the ventral margin and thus calendar years could not be assigned to the seasons. Therefore we excluded this shell from the $\delta^{18}O_w$ reconstructions. The other three shells exhibited high growth rates throughout their lives, which made them useful for the $\delta^{18}O_w$ reconstructions presented here.

We calculated $\delta^{18}O_w$ values from measured $\delta^{18}O_{ar}$ values and water temperatures, using equations 5.1-5.3. We previously established that growth starts when water temperature rises above 13.5 °C and ceases when water temperature falls below that temperature (Chapter 3). These temperatures

125
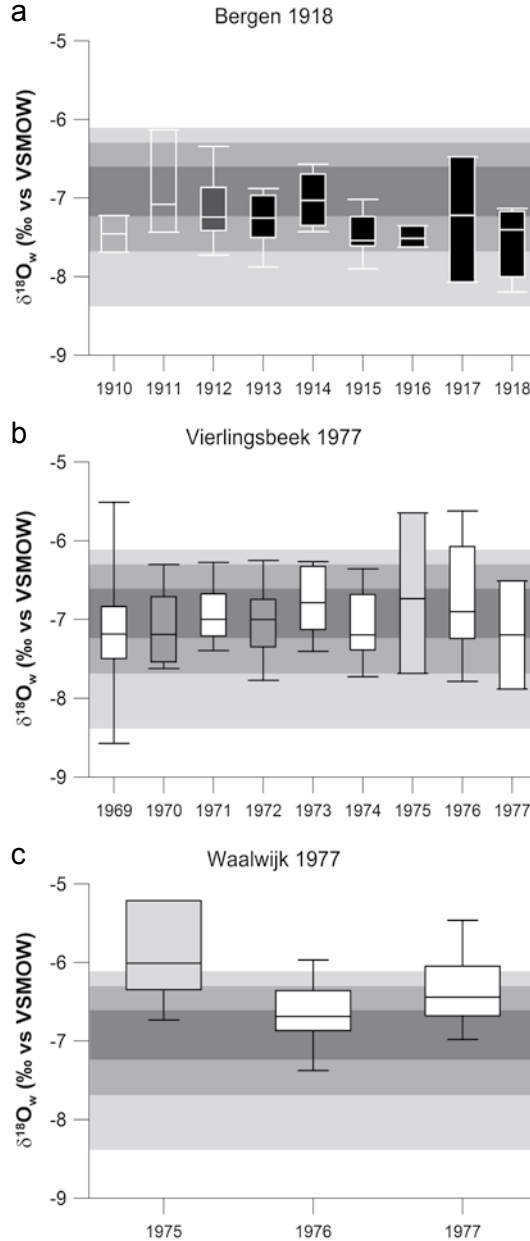
Figure 5.7a-c: Box-whisker diagrams showing reconstructed δ¹⁸Oₓ records per season for three shells from the Meuse. Colours of the boxes indicate if discharge was very high (black), high (dark grey), normal (medium grey), low (light grey) or very low (white; see figure 5.4). In the background dark to light grey areas indicate 2 %, 5 %, 25 %, 75 %, 95 % and 98 % percentiles of δ¹⁸Oₓ values during the growing season (April-October) of the 1997-2007 record. a: Bergen 1918 (*Unio crassus*), b: Vierlingsbeek 1977 (*U. pictorum*), c: Waalwijk 1977 (*U. pictorum*).

126

were used to determine the dates of onset and cessation of growth for each year. It is likely that intraseasonal growth is non-linear. However, since no robust growth model is available yet for these species, intraseasonal growth was assumed to be linear. In order to clearly visualise the range of $\delta^{18}O_{wr}$ values we chose to plot these data per season by means of a box-whisker diagram. From the 1997-2007 $\delta^{18}O_w$ dataset, measurements of the months April to October (the growth season of the shells) were selected. The 2 %, 5 %, 25 %, 75 %, 95 % and 98 % percentiles of these data were calculated (Figure 5.7a-c), in order to compare instrumental $\delta^{18}O_w$ data with the $\delta^{18}O_{wr}$ values.

5.4.3 Molluscan $\delta^{18}O_{ar}$ as a recorder of low summer discharge

As described above, low but not high summer discharges can be recognised in river $\delta^{18}O_w$ values and are potentially recorded by unionids. We therefore focus on the low to extremely low discharge events that occurred during the lifetime of the 1977 shells (the 2 lowest classes in the minimum discharge record).

In both the Vierlingsbeek 1977 and the Waalwijk 1977 the majority of $\delta^{18}O_{wr}$ values range above the 95 % percentile of 1997-2007 data (representing 5 % highest values) and in 1975, 1976 and 1977 $\delta^{18}O_{wr}$ values even range above the 98 % percentile of 1997-2007 (representing 2 % highest values) (Figures 5.7b-c). This suggests that $\delta^{18}O_{wr}$ values from unionid shells are a useful proxy for summer low discharge events. However, the proxy does not appear to work in all years: during 1972, $\delta^{18}O_{wr}$ values range above the 95 % percentile, whereas minimum discharge was normal during that year; the year 1974 did have a very low minimum discharge, but $\delta^{18}O_{wr}$ values do not range above the 95 % percentile (Figure 5.7b). Possible causes for the failure to detect low discharge events can be: (1) this low-discharge summer was not accompanied by high $\delta^{18}O_w$ values in the river; or (2) the shell experienced a temporary growth shutdown due to an environmental disturbance. If this type of temporary growth shutdown is indeed the case, and occurs often, this poses a serious problem for the reliability of the proxy. Erroneous recording of a low discharge season might happen when a shell grew in an environment relatively isolated from the riverbed, experiencing a large influence of local evaporation. The use of a larger set of shells would enable us to distinguish between these possibilities.

5.4.4 Quantitative reconstruction of summer discharge

To investigate if past Meuse discharges can be quantified we calculated reconstructed discharges using equation 5.5. Because we focus on the low
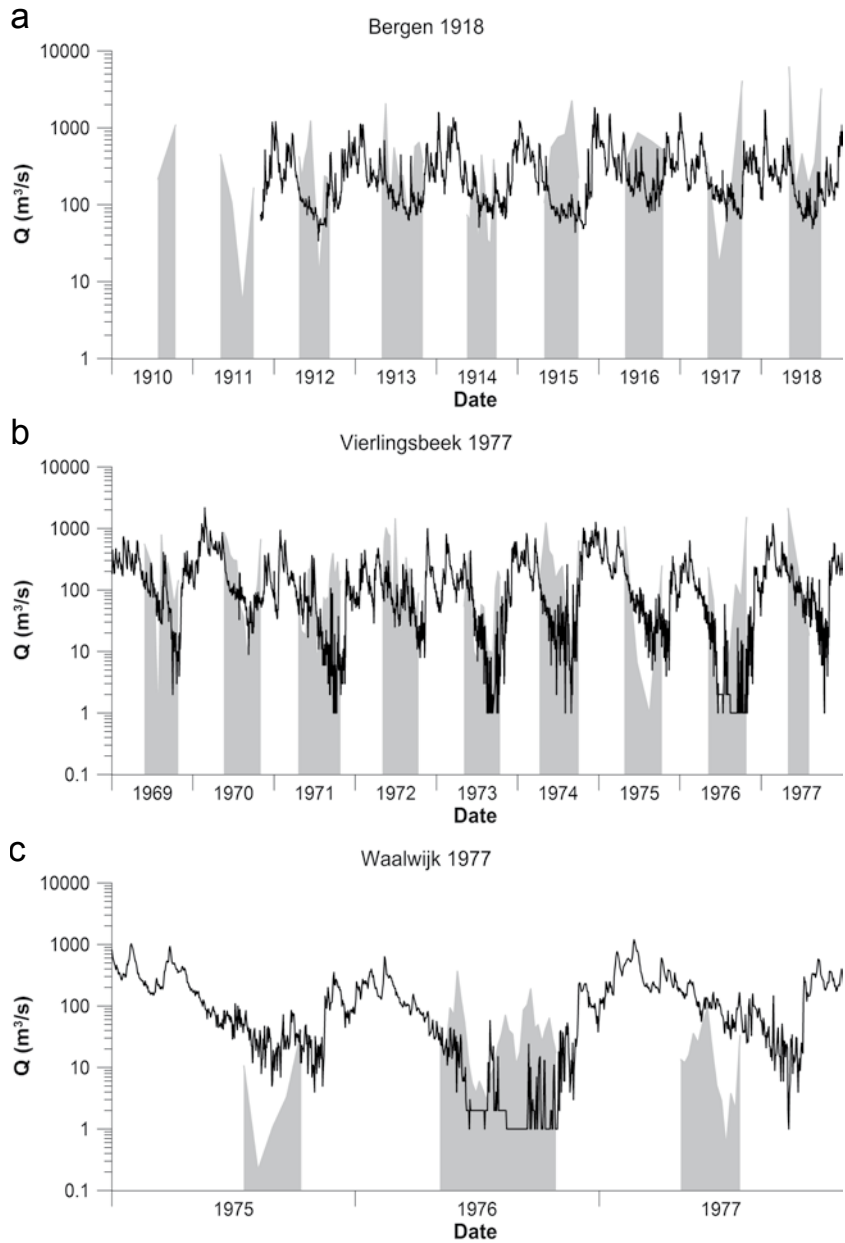
Figure 5.8a-c: Reconstructed (grey) and actual measured discharges (black line) per season. High discharge summers cannot accurately be reconstructed and result in large errors (e.g. 1917 and 1918 in the Bergen shell). All low discharge events in the 1969 to 1977 time interval can be reconstructed from shell $\delta^{18}O_{ar}$ values. The timing of these events is not always accurate; this is due to the linear intraseasonal age model used here.

discharge situation, reconstructed and measured discharges are plotted on a logarithmic scale (Figures 5.8a-c). Correlations between measured and reconstructed discharge are poor in all three shells (Table 5.3). Visual comparison in figure 5.8 confirms that high-discharge events cannot be reconstructed. In the cases of the years 1917 and 1918 reconstructed discharge values are even much higher than ever recorded in the Meuse. The quantitative reconstruction of low discharge appears accurate in the years 1970, 1972 and 1973 in the Vierlingsbeek shell. The other dry summers appear to show the right lower boundary of discharge values, but not with the right timing (e.g. 1969 and 1976 in the Vierlingsbeek shell and 1976 and 1977 in the Waalwijk shell). This timing discrepancy probably occurs because we assumed linear intraseasonal growth, which is not likely for Unionidae (Howard, 1922; Negus, 1966; Chapter 3). Another complicating factor is that we cannot be absolutely certain about the assignment of calendar years to parts of the shell $\delta^{18}O_{ar}$ records. Factors which might cause mistakes in the assignment of calendar years are: 1) small amounts of growth during the adult phase of the shell, with resulting low temporal resolution; 2) little or no growth during one summer, due to unfavourable environmental conditions, and resulting in an invisible gap in the record; 3) recording of an additional $\delta^{18}O_{ar}$ peak during another time of the year than winter. This could happen when, due to a low discharge interval, a shell temporarily lives in a pool, which has high $\delta^{18}O_{w}$ values. Reconstruction and true quantification of low discharge events in the Meuse remains problematic for two main reasons: the variance of the discharge-$\delta^{18}O_{w}$ relation is considerable, because multiple factors (like source area of the precipitation or local evaporation) may play a role; $\delta^{18}O_{ar}$ values might not always reflect $\delta^{18}O_{w}$ values in the main river channel, because local habitats may differ in for example their connection to the river of the influence of evaporation. Sampling a larger number of shells would probably clarify this latter issue.

Table 5.3: Statistics of correlations between measured and reconstructed discharge.

Shell	Equation	R^2	p
Bergen 1918	Y = 3.92 X + 76.0	0.082	0.036
Vierlingsbeek 1977	Y = 5.85 X + 46.1	0.046	0.022
Waalwijk 1977	Y = -0.085 X + 43.7	0.007	0.565
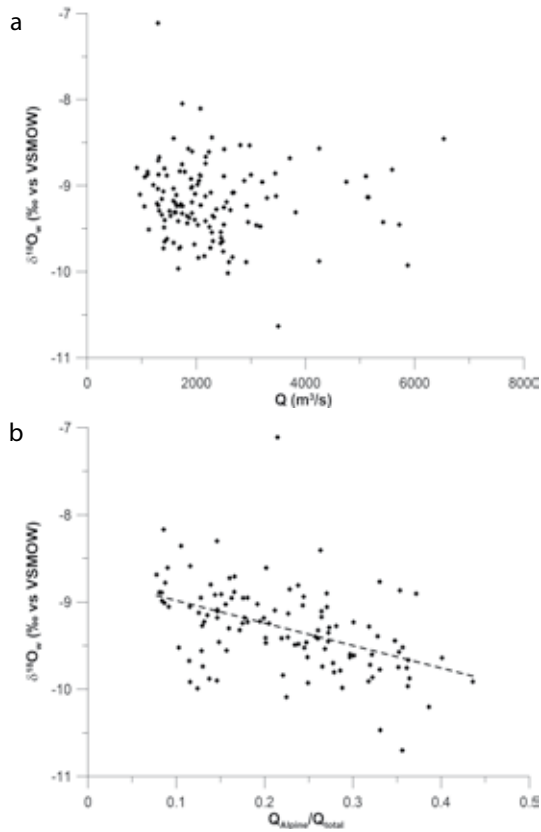
Figure 5.9a-b: Correlations between discharge and $\delta^{18}O_w$ values in the Rhine over the time interval 1997-2007; a. total discharge at Lobith; b. relative amount of Alpine discharge compared to total discharge at Lobith. No significant relation can be detected.

5.4.5 Implications for the Rhine

The Rhine, like the Meuse, has a seasonal pattern in $\delta^{18}O_w$ values. This seasonal pattern, however, has a very different appearance. Seasonally, the Rhine $\delta^{18}O_w$ values become isotopically depleted by meltwater from the Alps released into the river in spring and early summer. This meltwater and the location of the Rhine basin on the European continent, result in overall lower $\delta^{18}O_w$ ratios than those of the Meuse with lowest values in summer and highest values in winter (Mook, 1968; Ricken et al., 2003; Versteegh et al., 2009; Chapter 4).

Because different source waters play a role in the Rhine, there is no straightforward relation between discharge and $\delta^{18}O_w$ values in this river (Figure 5.9a). In an attempt to unravel the effects of the two main source waters

(i.e. Alpine snow melt and southern Germany precipitation), the relative contribution of Alpine discharge is plotted with $\delta^{18}O_w$ values in figure 5.9b. Although there appears to be a trend between these variables, this relation is not significant. Therefore, reconstructing past $\delta^{18}O_w$ values and discharges from unionid $\delta^{18}O_{ar}$ values is not possible in the Rhine. However, extremely high Alpine meltwater pulses, represented by excursions towards very negative $\delta^{18}O_w$ values (Figure 4.9), might still be detected in these shells.

5.5   Conclusions

Due to global warming, extreme precipitation events are expected to become more frequent in the Meuse basin, probably leading to extremely low and high discharges of this river. In order to better predict impacts of future climate change, knowledge of the past is essential. Therefore we investigated the utility of freshwater mussel $\delta^{18}O_{ar}$ values as a proxy for past $\delta^{18}O_w$ and extreme discharges of the river Meuse.

We found that in the Meuse there is a logarithmic relation between discharge and $\delta^{18}O_w$ values. Furthermore, unionid freshwater mussels record ambient $\delta^{18}O_w$ values in the $\delta^{18}O_{ar}$ values of growth increments in their shells, suggesting that past $\delta^{18}O_w$ values and Meuse discharge can be reconstructed.

However, due to the logarithmic relation between discharge and $\delta^{18}O_w$ values, only low-discharge summers can be detected qualitatively. Meuse low discharge events below a threshold value of 6 m^3/s can be detected in the $\delta^{18}O_{wr}$ records. True quantification of summer discharges is complicated by noise in both the relation between discharge and $\delta^{18}O_w$ values and between unionid $\delta^{18}O_{ar}$ values and those of the river water. Quantitative reconstructions of past $\delta^{18}O_w$ values and Meuse discharge might be realised by analysing many more samples (e.g. 30) from the same time interval, than the three specimens presented here.

Due to the absence of a straightforward relation between discharge and $\delta^{18}O_w$ values in the Rhine, reconstructing past $\delta^{18}O_w$ values and discharges from unionid $\delta^{18}O_{ar}$ values is not possible in this river. However, extremely high Alpine meltwater pulses might still be detected.

Chapter 6

Can unionid stable carbon isotope records serve as an environmental proxy?

Abstract

In the construction of unionid bivalve shells, two carbon sources are used: environmental dissolved inorganic carbon (DIC) and metabolic carbon (C_m). These two sources have different stable carbon isotope ($\delta^{13}C$) values and together result in a seasonal record of shell aragonite $\delta^{13}C$ ($\delta^{13}C_{ar}$) values. If these are to be used as a proxy for past water $\delta^{13}C_{DIC}$ values, it is important to know the relative contribution of C_m to freshwater bivalve $\delta^{13}C_{ar}$ values, possibly obscuring an environmental signal. In this study 11 multi-annual shell aragonite stable oxygen isotope ($\delta^{18}O_{ar}$) and $\delta^{13}C_{ar}$ records of three different unionid species from the rivers Rhine and Meuse are investigated. We aim to determine if there are general patterns in $\delta^{13}C_{ar}$ seasonality that are similar between individuals and to discern any ontogenetic trends in $\delta^{13}C_{ar}$ values, possibly indicating ontogenetic trends in relative C_m contribution. Comparison of seasonal $\delta^{18}O_{ar}$ and $\delta^{13}C_{ar}$ records shows that in some years, $\delta^{13}C_{ar}$ values are highest during summer, whereas in other years they peak during spring/autumn. Comparison with the seasonal pattern of $\delta^{13}C_{DIC}$ in the river water implies that if a shell exhibits high $\delta^{13}C_{ar}$ values during summer and low $\delta^{13}C_{ar}$ values during winter, it likely recorded $\delta^{13}C_{DIC}$ values. However, if a shell has high $\delta^{13}C_{ar}$ values during winter and low $\delta^{13}C_{ar}$ values in summer, input of C_m probably influenced $\delta^{13}C_{ar}$ values. It appears that about half of the individuals make a switch to increased contribution of C_m in their shell during ontogeny, whereas others do not. We hypothesise that the individuals showing this switch are the females, contributing more energy to reproduction than the males by brooding. Linear ontogenetic trends in $\delta^{13}C_{ar}$ values show a negative value in about half of the individuals. The other shells show a positive trend or not trend at all. The individuals exhibiting a negative trend are not always the same individuals that show the "metabolic switch" mentioned above. Therefore this result does not yield conclusive evidence supporting either sex differences or ontogenetic trends in relative C_m contribution. Application of $\delta^{13}C_{ar}$ records of these unionids as a proxy for past $\delta^{13}C_{DIC}$ values is still possible when a minimal contribution of C_m in the seasons examined is assured by checking the absence of correlation between $\delta^{13}C_{ar}$ and $\delta^{18}O_{ar}$ values and strong negative trends in $\delta^{13}C_{ar}$ values.

6.1   Introduction

Seasonal $\delta^{13}C_{ar}$ values of freshwater mollusc shells may yield useful environmental information, for example on phytoplankton productivity (Chapter 3) or changes in landscape vegetation (Kaandorp et al., 2003; Goewert et al., 2007). $\delta^{13}C_{ar}$ values are the result of two carbon sources used for shell construction: environmental dissolved inorganic carbon (DIC) and metabolic carbon (C_m), ultimately derived from food (McConnaughey et al., 1997).

Background $\delta^{13}C_{DIC}$ values of river water generally reflect those of groundwater (-12 to -15 ‰ (VPDB)). $\delta^{13}C_{DIC}$ values are usually lowest during winter due to input of CO_2 from decomposition of terrestrial plant material depleted in ^{13}C ($\delta^{13}C \approx$ -26 to -29 ‰ (VPDB); Hellings et al., 1999; Mook, 2000). During summer $\delta^{13}C_{DIC}$ values are higher because the input of terrestrial organic material is lower and due to isotopic exchange with atmospheric CO_2 ($\delta^{13}C \approx$ -7.5 ‰ (VPDB)) and preferential removal of ^{12}C from the DIC pool by phytoplankton photosynthetic activity (Mook, 1968; Hellings et al., 1999; Mook, 2000; Chapter 3). In the rivers Meuse and Rhine $\delta^{13}C_{DIC}$ values normally lie between -8 ‰ (VPDB) in summer and -15 ‰ (VPDB) during winter (Chapter 3).

If $\delta^{13}C_{ar}$ values of unionid freshwater mussels are to be used as a proxy for past water $\delta^{13}C_{DIC}$ values and related primary productivity, it is important to know the relative contribution of C_m to freshwater bivalve $\delta^{13}C_{ar}$ values, possibly obscuring an environmental signal. $\delta^{13}C$ values of C_m lie around -25 to -27 ‰ (VPDB) (Veinott and Cornett, 1998; Dettman et al., 1999), and estimates of the proportion of C_m in shell aragonite range from 5 to 80 % (Veinott and Cornett, 1998; Aucour et al., 2003; Gajurel et al., 2006; McConnaughey and Gillikin, 2008). However, $\delta^{13}C_{ar}$ values can often still be applied as an environmental proxy. This is the case if the offset of $\delta^{13}C_{ar}$ values relative to $\delta^{13}C_{DIC}$ values is constant (Kaandorp et al., 2003), if certain parts of the shell are still in equilibrium (Veinott and Cornett, 1998), or when environmental effects on $\delta^{13}C_{ar}$ values are so large, they overwhelm the effect of C_m contribution (Goewert et al., 2007; Gillikin et al., 2009). Several authors reported covariation between carbon isotopes in shell aragonite and those of DIC (Fritz and Poplawski, 1974; Buhl et al., 1991; Aucour et al., 2003; Kaandorp et al., 2003), whilst others did not. The absence of covariation between $\delta^{13}C_{ar}$ and $\delta^{13}C_{DIC}$ values has been ascribed to the incorporation of C_m into the shell (Fastovsky et al., 1993; Veinott and Cornett, 1998; Ricken et al., 2003; Geist et al., 2005; Verdegaal et al., 2005; Gajurel et al., 2006).

We previously demonstrated that unionid $\delta^{13}C_{ar}$ values reflect those of bicarbonate (HCO_3^-) in ambient water in a 1.5-year monitoring experiment (Chapter 3, Figures 3.6, 3.7 and 3.10). In our experiment $\delta^{13}C_{ar}$ values were very similar to $\delta^{13}C_{DIC}$ values (bicarbonate $\delta^{13}C$ values being similar to $\delta^{13}C_{DIC}$ values for the pH range studied). The experiment ran for 1.5 years and it appeared that $\delta^{13}C_{ar}$ directly reflected $\delta^{13}C_{DIC}$. However, it cannot be excluded that the constant offset of -2.7 ‰ with respect to inorganic aragonite (Romanek et al., 1992) was caused by the input of C_m. Also, under different circumstances than in our experiment (e.g. less competition/ higher food availability, higher turbidity, juvenile specimens), an observable amount of C_m might be incorporated in the shell.

Recently Gillikin et al. (2009) found that unionid freshwater mussels increase the amount of metabolic carbon incorporated in the shell ontogenetically, as shown by depletion of ^{13}C in the adult part of the $\delta^{13}C_{ar}$ records. These results suggest that unionids use different carbon pools during their life cycle. Although the (adult) shells in our experiment do not appear to show any input of C_m, possible ontogenetic trends could not be detected due to the limited duration of the experiment.

In this study 11 multi-annual $\delta^{18}O_{ar}$ and $\delta^{13}C_{ar}$ records of three different unionid species from the rivers Rhine and Meuse are investigated. These specimens were collected between 1918 and 2005 and their $\delta^{18}O_{ar}$ records have been discussed before in chapters 4 (Versteegh et al., 2009) and 5. We pose the following research questions:

1. Do these multi-annual records show similar $\delta^{13}C_{ar}$ seasonality as the (shorter) monitoring records?
2. Are there general patterns in $\delta^{13}C_{ar}$ seasonality that are similar between shells?
3. Can we discern any ontogenetic trends in $\delta^{13}C_{ar}$ values, possibly indicating ontogenetic trends in relative C_m contribution?
4. Can unionid $\delta^{13}C_{ar}$ records serve as a palaeo-environmental proxy?

6.2   Material and methods

In the Netherlands, freshwater mussels of the genus *Unio* are represented by three species: *U. crassus nanus* Lamarck, 1819 (extirpated since 1968), *U. pictorum* (Linnaeus, 1758) and *U. tumidus* Philipsson, 1788 (Gittenberger et al., 1998). In this study all three species are investigated.

The shells presented here were collected from the rivers Meuse, Waal and Lek (both Rhine distributaries) during the 20th century. $\delta^{18}O_{ar}$ records of these shells have already been presented in chapters 4 (Versteegh et al.,

2009) and 5.

Thin sections of the shells were sampled with a Merchantek Micromill microsampler. Resulting powder samples were analysed for $\delta^{13}C_{ar}$ values either on a Thermo Finnigan MAT 252 mass spectrometer equipped with a Kiel-II device or a Thermo Finnigan Delta+ mass spectrometer with a GasBench-II.

An elaborate description of the species, collection sites and methods for sampling and analysis can be found in chapters 4 (Versteegh et al., 2009) and 5.

6.3   Results

Seasonal $\delta^{18}O_{ar}$ and $\delta^{13}C_{ar}$ records of the shells are presented in figures 6.1a-k. The $\delta^{18}O_{ar}$ records have been presented before in chapter 4 (Versteegh et al., 2009; Figures 4.6 and 4.7) and chapter 5 (Figure 5.5) and exhibit truncated sinusoidal patterns caused by a combination of temperature fractionation and winter growth cessation (Grossman and Ku, 1986; Dettman et al., 1999; Goodwin et al., 2003). Narrow peaks represent growth cessations and wide troughs represent rapid summer growth. In chapter 3 we demonstrated that growth rates vary considerably throughout the growing season, and are highest during the summer month with the highest food availability (June).

The $\delta^{13}C_{ar}$ records display seasonal patterns. A striking feature of these records is that in some seasons the $\delta^{18}O_{ar}$ and $\delta^{13}C_{ar}$ records appear to co-vary, whereas in other seasons these are out of phase. Since the $\delta^{18}O_{ar}$ record is mainly a reflection of temperature, this means that in some years, $\delta^{13}C_{ar}$ values are highest during summer, whereas in other years they peak during spring/autumn. Of these 11 shells, 4 individuals exhibit seasonal $\delta^{13}C_{ar}$ patterns that are out of phase with the $\delta^{18}O_{ar}$ record throughout the life of the shell (Figures 6.1c, d, i and j; Table 6.1). In 6 individuals the $\delta^{18}O_{ar}$ and $\delta^{13}C_{ar}$ records are out of phase in the juvenile shell and co-vary in the adult shell (Figures 6.1a, b, f, g, h and k; Table 6.1). One individual has a mixed pattern in which some seasons correlate whereas some others are out of phase without an apparent ontogenetic trend in this phase behaviour (Figure 6.1e; Table 6.1).

In order to recognise possible ontogenetic patterns in $\delta^{13}C_{ar}$ values, we plotted a linear trend line through the multi-annual $\delta^{13}C_{ar}$ records (Figures 6.1a-k). The equations of these trend lines are given in table 6.1. Six of these 11 shells show an ontogenetic decrease in annually $\delta^{13}C_{ar}$ values (Figures 6.1b,
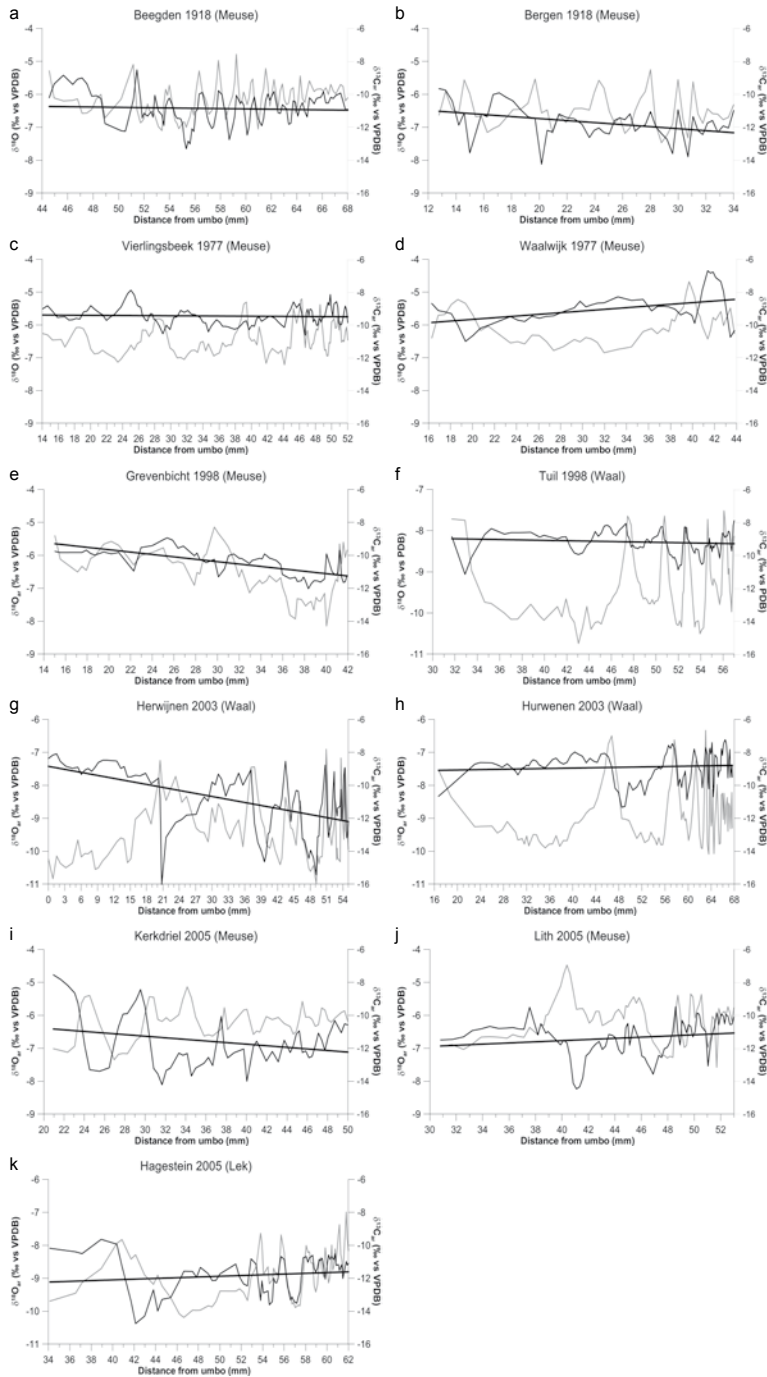
Figure 6.1a-k: $\delta^{18}O_{ar}$ (grey lines) and $\delta^{13}C_{ar}$ (thin black lines) records of 11 twentieth century unionids. A linear fit is drawn through each $\delta^{13}C_{ar}$ record. a, f, h, j and k are *Unio tumidus*, b is *U. crassus*, c, d, e, g and i are *U. pictorum*.

c, e, f, g and I; Table 6.1), whereas 3 individuals show an increase (Figures 6.1d, j and k; Table 6.1) and 2 individuals exhibit no ontogenetic trend in $\delta^{13}C_{ar}$ values (Figures 6.1a and h; Table 6.1).

6.4   Discussion

We aimed to understand multi-annual $\delta^{13}C_{ar}$ records of unionid shells, and examine possible general patterns and ontogenetic trends in $\delta^{13}C_{ar}$ values for 11 *Unio* shells. First we need to understand the background conditions that determine DIC values by identifying the sources of carbon to riverine DIC, and characterise the seasonal variability of these sources. As discussed above $\delta^{13}C_{DIC}$ values of river water are lowest during winter due to input of CO_2 from decomposition of terrestrial plant material, and highest during summer because the input of terrestrial organic material is low and due to isotopic exchange with atmospheric CO_2 and photosynthetic activity (Mook, 1968; Hellings et al., 1999; Mook, 2000; Chapter 3). In the rivers Meuse and Rhine $\delta^{13}C_{DIC}$ values vary between -8 ‰ (VPDB) in summer and -15 ‰ (VPDB) during winter (Chapter 3, Figures 3.6, 3.7 and 3.10).

The described seasonality in $\delta^{13}C_{DIC}$ (or similar $\delta^{13}C_{HCO3}$) values in the Rhine and Meuse has been observed during three years by Mook (2000) and at higher resolution in this study (Chapter 3). It appears reasonable to assume that this general pattern is true for all years. This implies that if a shell exhibits high $\delta^{13}C_{ar}$ values during summer and low $\delta^{13}C_{ar}$ values during winter (out of phase with the $\delta^{18}O_{ar}$ record), it is likely that it recorded $\delta^{13}C_{DIC}$ values. However, if a shell has high $\delta^{13}C_{ar}$ values during winter and low $\delta^{13}C_{ar}$ values in summer (covariation with $\delta^{18}O_{ar}$), it appears that some other factor must have influenced $\delta^{13}C_{ar}$ values.

A likely factor to influence $\delta^{13}C_{ar}$ values, is the input of C_m into the shell. The relative contribution of C_m is larger when metabolic activity of the animal is higher. Factors enhancing metabolic activity can be high temperatures, high food availability, gametogenesis, hatching and brooding of glochidia (unionid larvae) in the marsupial of females (Dettman et al., 1999), or recovery after a predator attack.

Most of these mechanisms (except recovery after a predation attempt) would result in low $\delta^{13}C_{ar}$ values during summer months and high $\delta^{13}C_{ar}$ values during spring/autumn. However, it cannot be excluded that $\delta^{13}C_{DIC}$ values follow a different seasonal pattern in some years with minima in summer and maxima in winter and that unionids still faithfully record these $\delta^{13}C_{DIC}$ values. Alternatively, temperature might have a direct effect on fractionation of carbon into the unionid shell (Grossman and Ku, 1986).

Table 6.1: Specifications of shell samples.

Sample	Year	River	Species	Length (mm)	Height (mm)	Height along curve of shell (mm)	Correlation with $\delta^{18}O_{ar}$	Equation linear fit
Beegden	1918	Meuse	*Unio tumidus*	80.5	42.5	68	- → +	Y = -0.00948 * X - 10.32
Bergen	1918	Meuse	*Unio crassus*		32.6	34	- → +	Y = -0.0614 * X - 10.24
Vierlingsbeek	1977	Meuse	*Unio pictorum*	88.0	39.0	52	-	Y = -0.00278 * X - 9.34
Waalwijk	1977	Meuse	*Unio pictorum*	79.5	33.5	44	-	Y = 0.0510 * X - 10.68
Grevenbicht	1998	Meuse			31.4	42	+/-	Y = -0.0727 * X - 8.20
Tuil	1998	Waal	*Unio tumidus*		41.2	57	- → +	Y = -0.0120 * X - 8.59
Herwijnen	2003	Waal	*Unio pictorum*	89.0	39.5	55	- → +	Y = -0.0610 * X - 8.85
Hurwenen	2003	Waal	*Unio tumidus*	99.5	52.0	68	- → +	Y = 0.00584 * X - 9.19
Kerkdriel	2005	Meuse	*Unio pictorum*	91.5	38.5	50	-	Y = -0.0483 * X - 9.82
Lith	2005	Meuse	*Unio tumidus*	76.5	39.5	53		Y = 0.0353 * X - 12.94
Hagestein	2005	Lek	*Unio tumidus*	94.0	47.0	62	- → +	Y = 0.0221 * X - 12,98

Approximately half (6 out of 11) of the shells presented here exhibit the pattern described above with out of phase behaviour in the juvenile shell and covariation in the adult. It has been suggested that this is a switch to "metabolic mode", induced by the onset of sexual reproduction (Verdegaal et al., 2005). Another common pattern is anticorrelation throughout the life of the shell (4 out of 11 specimens). These unionids appear to record $\delta^{13}C_{DIC}$ values throughout their lives.

All shells examined were of adult size (though some shells appear to be only 2-3 years old, based on their $\delta^{18}O_{ar}$ records; Figures 6.1d-e) and both patterns of ontogenetic correlation between $\delta^{18}O_{ar}$ and $\delta^{13}C_{ar}$ values appear to be common in the population. We suggest that these two categories represent male and female individuals. In unionids females make the largest energetic investment in reproduction, hatching and brooding the glochidia in their marsupia for several months (Jokela, 1996). This might well cause the switch to metabolic mode, observed in 6 of the shells. The shells in which this switch is absent are the males, which do not make this large investment in reproduction. The one shell showing anticorrelation in some seasons and covariation in others, might be a female that did not reproduce during all years, as is common among unionids (Jokela and Mutikainen, 1995; Haag and Staton, 2003).

In order to detect any ontogenetic trends in relative C_m contribution we plotted linear fits through the $\delta^{13}C_{ar}$ records. Ontogenetic trends in $\delta^{13}C_{ar}$ values show a decrease in 6 out of 11 shells, a positive trend in 3 shells and no linear trend in 2 individuals. The direction of a possible linear trend in $\delta^{13}C_{ar}$ values does not appear to be related to the phase behaviour mentioned above. From these results it appears that ontogenetic increases in C_m contribution do occur, but are generally small and are certainly not present in all individuals.

6.5   Conclusions

We aimed to determine if multi-annual $\delta^{13}C_{ar}$ records show similar seasonality as the (shorter) monitoring records and if there are general patterns in $\delta^{13}C_{ar}$ seasonality that are similar between shells. During some seasons $\delta^{13}C_{ar}$ records indeed show similar seasonality as in the monitoring experiment ($\delta^{13}C_{ar}$ values peak in summer). However these multi-annual records also reveal many seasons in which $\delta^{13}C_{ar}$ values peak around the winter growth cessation. $\delta^{13}C_{DIC}$ values of river water are lowest during winter and highest during summer. This means that if a shell exhibits high $\delta^{13}C_{ar}$ values during summer and low $\delta^{13}C_{ar}$ values during winter, it is likely that

it recorded $\delta^{13}C_{DIC}$ values. However, if a shell has high $\delta^{13}C_{ar}$ values during winter and low $\delta^{13}C_{ar}$ values in summer, it appears that contribution of C_m has influenced $\delta^{13}C_{ar}$ values.

With respect to the phase-behaviour between $\delta^{18}O_{ar}$ and $\delta^{13}C_{ar}$ values, two general patterns can be discerned: some *Unio* individuals make a switch to increased contribution of C_m in their shell during ontogeny, whereas others do not. The individuals showing this switch are likely the females, contributing more energy to reproduction than the males by brooding. This hypothesis calls for more research in individuals of which the sex is known, but is beyond this thesis.

We also aimed to discern any ontogenetic trends in $\delta^{13}C_{ar}$ values, possibly indicating ontogenetic trends in relative C_m contribution. Direct observation of linear ontogenetic trends in $\delta^{13}C_{ar}$ values shows a negative trend in about half of the individuals. The other shells show a positive trend or not trend at all. The individuals exhibiting a negative trend are not always the same individuals that show the "metabolic switch" mentioned above. Therefore this result does not yield conclusive evidence supporting either sex differences or ontogenetic trends in relative C_m contribution.

Ultimately, we aimed to find if unionid $\delta^{13}C_{ar}$ records can serve as a palaeo-environmental proxy. However complex, the above findings do not exclude $\delta^{13}C_{ar}$ records of these *Unio* species from application as a proxy for past $\delta^{13}C_{DIC}$ values. For this application, seasons need to be selected in which C_m contribution to the shell was minimal. This can be assured by verifying the absence of both correlation between $\delta^{13}C_{ar}$ and $\delta^{18}O_{ar}$ values and strong negative trends in $\delta^{13}C_{ar}$ values.

Freshwater bivalves record NAO-related river water $\delta^{18}O$ variability during the Medieval Warm Period

Abstract

The previously developed tool, shell aragonite $\delta^{18}O$ of unionid freshwater mussels as a proxy for past river conditions in the Rhine and Meuse, is applied to a set of 9 shells from several climatic intervals in the late Holocene. The single Meuse shell lived during the Subboreal and its aragonite $\delta^{18}O$ values are similar to recent specimens. The Rhine shells presented come from the Subboreal, Roman Warm Period and Medieval Warm Period (MWP). These shells show averages and ranges of aragonite $\delta^{18}O$ values similar to present day Rhine specimens. This indicates that environmental conditions, Rhine river dynamics, Alpine meltwater input and drought severity, during these time intervals, were similar to the 20th century. We found, however, that these shells cannot be used for recording subtle centennial to millennial time scale climatic variation due to their relatively short lifespan and the large interannual and intraseasonal variation in environmental conditions in the rivers, but they are very suitable for studying seasonal to decadal scale climate variability. The two shells with the longest lifespan appear to show decadal scale variability in reconstructed water $\delta^{18}O$ values during the MWP, probably forced by the North Atlantic Oscillation, which is an important mode of variability influencing precipitation regimes over Europe.

7.1   Introduction

In previous work, we established that unionid freshwater bivalves record ambient water $\delta^{18}O$ ($\delta^{18}O_w$) values faithfully, that droughts in the Meuse can be reconstructed by means of seasonal shell aragonite $\delta^{18}O$ ($\delta^{18}O_{ar}$) records and that these records can serve as a proxy for past river conditions (Versteegh et al., 2009; Chapters 3, 4 and 5). In this chapter we apply this tool to a collection of archaeological shells from different time intervals in the late Holocene.

In the Rhine and Meuse drainage basins, the forthcoming climate change for the 21st century includes an increase in precipitation magnitude and frequency in winter, and decreased amounts of precipitation and longer droughts in summer (IPCC, 2007). As a result winter floods will become more frequent and more intense in both the Meuse (Parmet and Burgdorffer, 1995; Bürger, 2002; Tu, 2006; Ward, 2009) and the Rhine (Aerts et al., 2006). In addition, the Rhine would progressively change from a rain-fed/meltwater river into mainly a meltwater river (Pfister et al., 2004; Ricken et al., 2004). Summer droughts would increase in intensity across Western Europe, causing increase in frequency of summer low flows (Arnell, 1999; De Wit et al., 2007).

For a better prediction of future river dynamics, accurate reconstructions of pre-industrial river conditions, including discharge seasonality and frequencies of floods and droughts, are essential. Questions arise such as: (1) what were the natural dynamics of the rivers Rhine and Meuse during the late Holocene; (2) are the recent changes in Rhine and Meuse river dynamics unique, or have these changes occurred previously during the late Holocene?

In order to find answers to these questions, palaeo-river records are needed, with sufficient resolution at the seasonal time-scale. Since the instrumental record only goes back to the early twentieth century, the development of accurate proxy records at high temporal resolution is necessary. A useful proxy record is provided by stable isotope profiles of growth increments in freshwater bivalves.

Sclerochronology of unionid freshwater bivalves has proven to be a powerful tool in palaeoclimate research. $\delta^{18}O_w$ values are incorporated in seasonal growth increments of shell aragonite in isotopic equilibrium with ambient water (Mook and Vogel, 1968; Fritz and Poplawski, 1974; Dettman and Lohmann, 1993; Dettman et al., 1999; Chapter 3). Shell $\delta^{18}O_{ar}$ values have successfully been applied as a proxy for rainfall patterns, water source or river discharge (Rodrigues et al., 2000; Kaandorp et al., 2005; Verdegaal

et al., 2005; Gajurel et al., 2006; Goewert et al., 2007). Seasonal variability in $\delta^{18}O_w$ values is faithfully recorded in $\delta^{18}O_{ar}$ records of Unionidae in Northwest European rivers, with the exception of the winter season, when the shells do not grow. We previously demonstrated that through the relation between discharge and $\delta^{18}O_w$ values in the Meuse, unionid $\delta^{18}O_{ar}$ records reveal the occurrence of past low-discharge summers (Chapter 5). Ricken et al. (2003) have suggested that in the Rhine, Alpine snowmelt events can be recognised in unionid $\delta^{18}O_{ar}$ records as excursions towards low $\delta^{18}O_{ar}$ values.

In this chapter, we present $\delta^{18}O_{ar}$ records of several late Holocene unionid shells. These organisms have lived under different climate regimes and associated river conditions (see next paragraph). From the $\delta^{18}O_{ar}$ records, we reconstruct $\delta^{18}O_w$ profiles. These $\delta^{18}O_w$ profiles give us insight into past river dynamics, such as extreme seasonal droughts and meltwater pulses or their frequencies (for methodology see chapter 5). The $\delta^{18}O_{ar}$ records in unionid bivalves, which are mostly derived from archaeological sites, would thus provide insight in seasonal aspects of changing river conditions with a temporal resolution of about two weeks, particularly during summer, because the bivalves do not grow during winter (Versteegh et al., 2009; Chapters 3 and 4). We selected 9 late Holocene shells from various time horizons within the time interval 4800 BP-1700 AD. Unfortunately the river Meuse is represented by only 1 shell; there were no other Meuse shells available within the archaeological archives. As a result the Meuse will only be discussed briefly and the outcomes of this chapter will be mainly focused on variability in Rhine conditions.

7.2   Climatic and palaeogeographic background

7.2.1   Late Holocene climate in Western Europe

In comparison to the large oscillations between glacial and interglacial climate during the Pleistocene, the Holocene is a climatically relatively stable time interval in Western Europe. Still, on a smaller scale, several Holocene climatic trends and oscillations have been recognised. For the late Holocene (5000-0 BP) these are summarised in figure 7.1.

From about 5000 to 2800 BP western European climate was dominated by continental (warm and dry) conditions. This time interval is known as the Subboreal. Around 2850-2760 BP this abruptly changed to more oceanic (cooler and wetter) conditions, known as the Subatlantic. In terms of precipitation this shift was significant, raising groundwater levels and forc-

C14 years BP	Years BP/AD	Archaeological period		Geological time		Glacier extension	Lake level	Temperature
	1500 AD				LIA			
		Middle Ages		Late Holocene	MWP			
	500 AD							
		Roman time			RWP			−0.4°C 1856-1980 mean +0.4°C
2000	12 AD	Late Iron Age	Iron Age		Subatlantic			
2250	2250 BP	Middle Iron Age						
2450	2500 BP	Early Iron Age						
2600	2800 BP	Late Bronze Age	Bronze Age					
2900	3100 BP	Middle Bronze Age B						
3300	3500 BP	Middle Bronze Age A / Early Bronze Age		Middle Holocene	Subboreal			
3450	3800 BP	Late Neolithic B	Neolithic			glacier retreat / lower lake level ← → glacier advance / higher lake level		
3650	4000 BP	Late Neolithic A						
3950	4500 BP	Middle Neolithic B						
4300	4900 BP	Middle Neolithic A						

Figure 7.1: Archaeological and geological time periods during the middle to late Holocene in the Netherlands (Louwe Kooijmans et al., 2005), records of extension of the Great Aletsch glacier (Switzerland), west-central European lake-level records (Holzhauser et al., 2005) and Northern Hemisphere temperature reconstruction (Mann et al., 2003). Approximate ages and age-uncertainties of shell samples are indicated by grey bars.

ing the abandonment of populated areas in the northern Netherlands (Van Geel et al., 1996). During Roman times some authors have documented a warmer interval (Roman Warm Period, RWP; Hass, 1996; Holzhauser et al., 2005). Climate reconstructions of the RWP are sparse but indicate temperatures similar to or slightly warmer than today (Frisia et al., 2005). The RWP was followed by a colder phase between 400 and 700 AD (Hass, 1996). The Medieval Warm Period (MWP) lasted from about 950 until 1200 AD (Brázdil et al., 2005) and is characterised by warm, dry summers and wet winters (Lamb, 1965; Mann et al., 1999; Esper et al., 2002; Cook et al., 2004; Goosse et al., 2005; Goosse et al., 2006). It consisted of several warm spells (Crowley and Lowery, 2000) of which the 10th century had warm summers and cold winters and the 13th century had the highest summer temperatures (Shabalova and Van Engelen, 2003). The actual temperatures during the MWP were similar to those of the first half of the twentieth century (-0.03 to +0.20 °C; Crowley and Lowery, 2000; Bradley et al., 2003).

The coldest phase of the late Holocene was the Little Ice Age (LIA). It consisted of several cold intervals between 1400 and 1900 AD (Mann et al., 1998) and coincided with a period of low solar irradiance values (Bard

149

et al., 2000). The coldest time interval was between 1550 and 1700 AD (Lamb, 1965; Shabalova and Van Engelen, 2003; Brázdil et al., 2005). The LIA is characterised by severely cold and dry winters. However, due to winter growth cessation, the freshwater bivalves studied here cannot record this. LIA summers were wetter and probably only slightly cooler (~ -0.2 °C) than today (Luterbacher et al., 2001; Cook et al., 2004; Luterbacher et al., 2004; Guiot et al., 2005).

In summary, the long-term summer temperature changes between different late Holocene climatic intervals probably did not exceed ~ 0.4 °C. This is a small difference in comparison to the Late Glacial Maximum, when summer temperatures were 6-12 °C below those of the present day (Wu et al., 2007). With respect to late Holocene precipitation regimes, true quantification is often problematic, but significant shifts are suggested by peat bog records (Van Geel et al., 1996), glacier extension records and lake level changes (Holzhauser et al., 2005).

7.2.2   Palaeogeography of the Rhine-Meuse delta

The palaeogeographic evolution of the Rhine-Meuse delta has also been of importance for river dynamics. Late Holocene morphology and discharge of the rivers Rhine and Meuse have been modified by both climate variability and human activity.

During the early Holocene, river channels were incising meandering due to low sea level. From approximately 8000 BP until 4000 BP rapid sea level rise changed the fluvial style from incising meandering via aggrading meandering to straight anastomosing in the western and middle part of the delta. After 4000 BP the fluvial style changed back to aggrading meandering (Berendsen and Stouthamer, 2001). During the Subboreal-Subatlantic transition discharge of the rivers increased (Van Geel et al., 1996) and since that time, both the wavelength of meanders and the number of channels increased towards a maximum around 2000 BP (Roman Period; Berendsen and Stouthamer, 2001). Before 500-700 AD the Oude Rijn (Old Rhine) was the main distributary of the Rhine and flowed into the North Sea at Katwijk. After that time the main drainage of the Rhine shifted to the southwest and drained into the Meuse estuary near Rotterdam. This was due to several factors like coastal erosion, increasing tidal influence, continuing aggradation of the channel belts of the Utrecht system and tectonic movements (Berendsen and Stouthamer, 2001).

Human influence started with clearing of forests and the beginning of agriculture during the Neolithic (6400-3650 BP; Berendsen and Stouthamer, 2001). During the Roman occupation the Old Rhine was the northernmost

border of the Roman Empire. Many villages were founded along the rivers and even small canals were dug, locally changing the course of the rivers. Human activity (deforestation) increased after the Roman Period, increasing the frequency of extreme discharge events (Berendsen and Stouthamer, 2001). Human influence strongly proceeded from 1100 AD onwards with embankment of the rivers, which was completed around 1300 AD. The Old Rhine was dammed near Wijk bij Duurstede in 1122 AD, the Hollandse IJssel in 1285 and the Linge in 1307 AD, reducing the number of Rhine distributaries to the current three: Lower Rhine-Lek, Waal and IJssel (Berendsen and Stouthamer, 2001). During the twentieth century several weirs were built to regulate water levels for shipping.

In general the palaeogeographic evolution with respect to the wavelength of meanders and the number of channels of the Meuse-Rhine delta is not expected to have had a major influence on $\delta^{18}O_w$ values during the late Holocene, because the drainage basins of the rivers stayed the same. In smaller channels, however, the influence of local evapotranspiration and runoff on shell composition might be more noticeable than in large channels. During the time interval from the Subatlantic until 1100 AD there were many small river channels. When examining shells from this time interval, it has to be kept in mind that these are more likely to have originated from small channels and thus may have experienced a large influence of local runoff and/or evapotranspiration. These local factors would both result in higher reconstructed $\delta^{18}O_w$ values than if the shells lived in a large river channel.

On the other hand, embankment of the rivers and deforestation in the drainage basin may have caused increased peak discharge values and the frequency of floods. For the river Meuse this has been demonstrated by Ward et al. (2008). Through the decreased influence of evapotranspiration in the drainage basin, this will be accompanied by lower $\delta^{18}O_w$ values of river water.

7.3   Aim and research questions

Within the above context we aim to examine what the $\delta^{18}O_{ar}$ records of a selection of freshwater bivalves from different late Holocene time intervals can tell us about past climate and river conditions. Research questions are:

1. Can centennial to millennial scale late Holocene climatic variations be recognised in unionid $\delta^{18}O_{ar}$ records and corresponding reconstructed $\delta^{18}O_w$ records?
2. What were the effects of late Holocene climate change on seasonal

Table 7.1: Overview of the shell samples.

Place	Location	Estimated shell age	Age based on	Channel belt (Berendsen & Stouthamer, 2001: their App. 1)	Species	Length (mm)	Height (mm)	Height along curve of shell (mm)	References
Spijkenisse	Hekelingen	4839-4437 BP	associated archaeology		*Unio crassus nanus*	42.0	22.5	30	(Kuijper, 1990)
Montfoort	Tiendweg 'DAG 7'	4080-3915 BP	calibrated age of abandonment	Zuid-Stuivenberg crevasse (#205)	*Unio crassus nanus*			32	(Verdegaal et al., 2005)
Houten	Tiellandt	2950-2736 BP	calibrated age of abandonment	Houten (#74)	*Unio crassus nanus*	n.a.*	35.5	47	
Utrecht	Roman watchtower	40-70 AD	associated archaeology	Oude Rijn (#133)	*Unio crassus nanus*		28.5	37	(Van der Kamp, 2007)
Vleuten-De Meern	Roman road	50-270 AD	associated archaeology	Oude Rijn (#133)	*Unio sp.*		34.8	50	
Kerk-Avezaath 1	Huis Malburg	1050-1250 AD	associated archaeology	Linge #97 (Daver crevasse)	*Unio tumidus*	54.5	31.5	41	(Oudhof et al., 2000)
Kerk-Avezaath 2	Huis Malburg	1050-1250 AD	associated archaeology	Linge #97 (Daver crevasse)	*Unio crassus nanus*	69.5	36.0	50	(Oudhof et al., 2000)
Wijk bij Duurstede		~ 1200 AD	associated archaeology	Nederrijn (#116)	*Unio crassus nanus*			43	(Verdegaal et al., 2005)
Gorinchem	Kazerneplein	1500-1700 AD	associated archaeology	Waal / Merwede (#175)	*Unio crassus nanus*	50.5	31.0	41	

* This shell was broken, so the original length could not be measured.

(summer) $\delta^{18}O_w$ values and related river conditions (i.e. Alpine melt-water input, Meuse summer droughts)?

3. Can we distinguish any influence of palaeogeography, embankment of the rivers or land-use changes in these records?

7.4   Materials and methods

7.4.1   Shells

Unionid freshwater bivalves are common in both the Meuse and Rhine river systems. Historically three species of the genus *Unio* were present: *U. pictorum*, *U. tumidus* and *U. crassus nanus*. The latter has been extirpated since 1968 (Gittenberger et al., 1998), but is the most common species in archaeological finds. It is not entirely clear why these shells are found in archaeological context in the Netherlands. Although human consumption of unionid freshwater mussels is widely known from aboriginal sites in Australia (Russell-Smith et al., 1997), Indonesia (Joordens et al., 2009), North America (Parmalee and Klippel, 1974; Peacock and James, 2002) and Africa (Plug and Pistorius, 1999), in Europe unionids were rarely eaten by humans. However they were sometimes used as cattle food (Tudorancea, 1972), in (pre-) historic tools and jewellery, or as a receptacle for paint (*U. pictorum*; Gittenberger et al., 1998). This is presumably how the valves ended up in archaeological finds.

Nine shells ranging from ~ 300 to ~ 4900 years old were collected from different archaeological finds and palaeogeographical cores in the Dutch Rhine-Meuse delta. These comprise two specimens from the Subboreal time interval, one from around the transition between the Subboreal and the Subatlantic, two from the Roman time interval, three shells of medieval age, and one from the LIA (Figure 7.1; Table 7.1). By comparing collection locations with palaeogeographic maps (Berendsen and Stouthamer, 2001), it has been determined that the Spijkenisse (4839-4437 BP) shell likely originated from the Meuse, whereas the others lived in distributaries of the Rhine. Most samples are *U. crassus nanus*, however, one *U. tumidus* and one undetermined *Unio* shell are also used (Table 7.1).

7.4.2   Sampling and analysis of shells

Shells were sampled using a Merchantek Micromill microsampler. A detailed description of this method can be found in Versteegh et al. (2009; Chapter 4). Samples were subsequently analysed for stable oxygen and carbon isotopic compositions on a Finnigan Delta+ mass spectrometer with a GasBench-II. The long-term standard deviation of a routinely analysed

in-house $CaCO_3$ standard is < 0.1 ‰. This $CaCO_3$ standard is regularly calibrated to NBS 18, 19 and 20.

7.4.3   River data

Data on the present (1997-2007) $\delta^{18}O_w$ values of the river Rhine and Meuse, measured at Eijsden and Lobith (Figure 1.10), were obtained from the Centre for Isotope Research, University of Groningen. In order to reconstruct $\delta^{18}O_w$ values, an estimate of water temperature is needed. For the time interval 1908-1944, water temperatures were obtained from Rijkswaterstaat (Dutch Directorate for Public Works and Water Management; http://www.waterbase.nl/). This time interval was chosen, because of the limited influence of warming by industrial cooling waters, which increased water temperatures in both rivers by 3 °C after that time. For the Meuse temperatures were measured at the gauging station at Borgharen, for the Rhine at Lobith (Figure 4.2).

7.4.4   Calculation of reconstructed $\delta^{18}O_w$

For the calculations of reconstructed $\delta^{18}O_w$, the equations of Grossman and Ku (1986), Dettman et al. (1999) and Gonfiantini et al. (1995) are used as shown in chapter 3. The best indication for past water temperatures available, are the instrumental water temperature records measured before the profound warming by industrial cooling water (late Holocene long-term temperature differences are ≤ 0.2 °C from modern-day values). Therefore, in $\delta^{18}O_w$ reconstructions, the average weekly water temperature in the time interval 1908-1944 is taken. For the Spijkenisse shell we used Meuse water temperatures and for the other shells we used Rhine water temperatures. The calculated $\delta^{18}O_w$ profiles give us insight into past river dynamics, such as extreme seasonal droughts and meltwater pulses or their frequencies (for methodology see chapter 5). The reconstructed $\delta^{18}O_w$ record is compared with $\delta^{18}O_w$ records covering 1997-2007.

7.5   Results

As a first examination of the shell records, and comparison with modern-day data, we present the ranges of $\delta^{18}O_{ar}$ values per shell as a box-whisker diagram in figure 7.2 with, in the background, the predicted $\delta^{18}O_{ar}$ values (± 1 σ) for modern Meuse and Rhine shells (Versteegh et al., 2009; Chapter 4).

The one shell from the Meuse, the Spijkenisse shell (4839-4437 BP), can be clearly distinguished from the other shells both by its higher average (-6.5 ‰) and its smaller range in $\delta^{18}O_{ar}$ values. All other shells fall within the
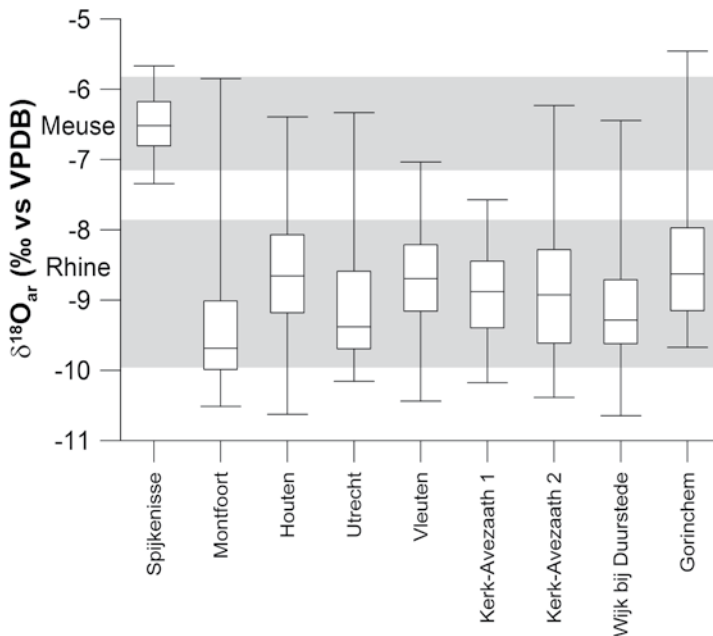
Figure 7.2: Box-and-whisker diagram showing the range of $\delta^{18}O_{ar}$ data for all shells. Grey areas indicate predicted modern values for both rivers according to chapter 3. The Spijkenisse shell clearly fits in the Meuse range; all other shells have mostly Rhine $\delta^{18}O_{ar}$ values. The Gorinchem shell grew in a mixture of Rhine and Meuse water. All specimens are *Unio crassus nanus*, except the Vleuten shell is an unknown *Unio* species and Kerk-Avezaath 1 is *Unio tumidus*.

range of the modern Rhine with average $\delta^{18}O_{ar}$ values from -9.4 ‰ to -8.4 ‰ and ranges from ~ -6.5 to ~ -11.0 ‰ (Versteegh et al., 2009; Chapter 4).

Secondly, the seasonal $\delta^{18}O_{ar}$ records of the shells are presented in figures 7.3a-i. All shells show the truncated sinusoidal pattern typical for seasonal growth. Sharp peaks represent winter growth cessations, whereas broad troughs represent fast growth during summer. Slow growth during spring and autumn causes the steep slopes of the peaks (Grossman and Ku, 1986; Dettman et al., 1999). This pattern is similar to that found in modern Unionidae from the Meuse and Rhine (Ricken et al., 2003; Verdegaal et al., 2005; Versteegh et al., 2009; Chapter 4 and 5; Figures 7.3a-i), and indicates that summer conditions are recorded in the shells.

Both the ranges and the seasonal patterns in $\delta^{18}O_{ar}$ values are very similar to those of modern-day shells (Versteegh et al., 2009; Chapters 4 and 5). Possible differences in seasonal patterns between these late Holocene shells and their recent equivalents are apparently too small to be readily detected in these $\delta^{18}O_{ar}$ records.
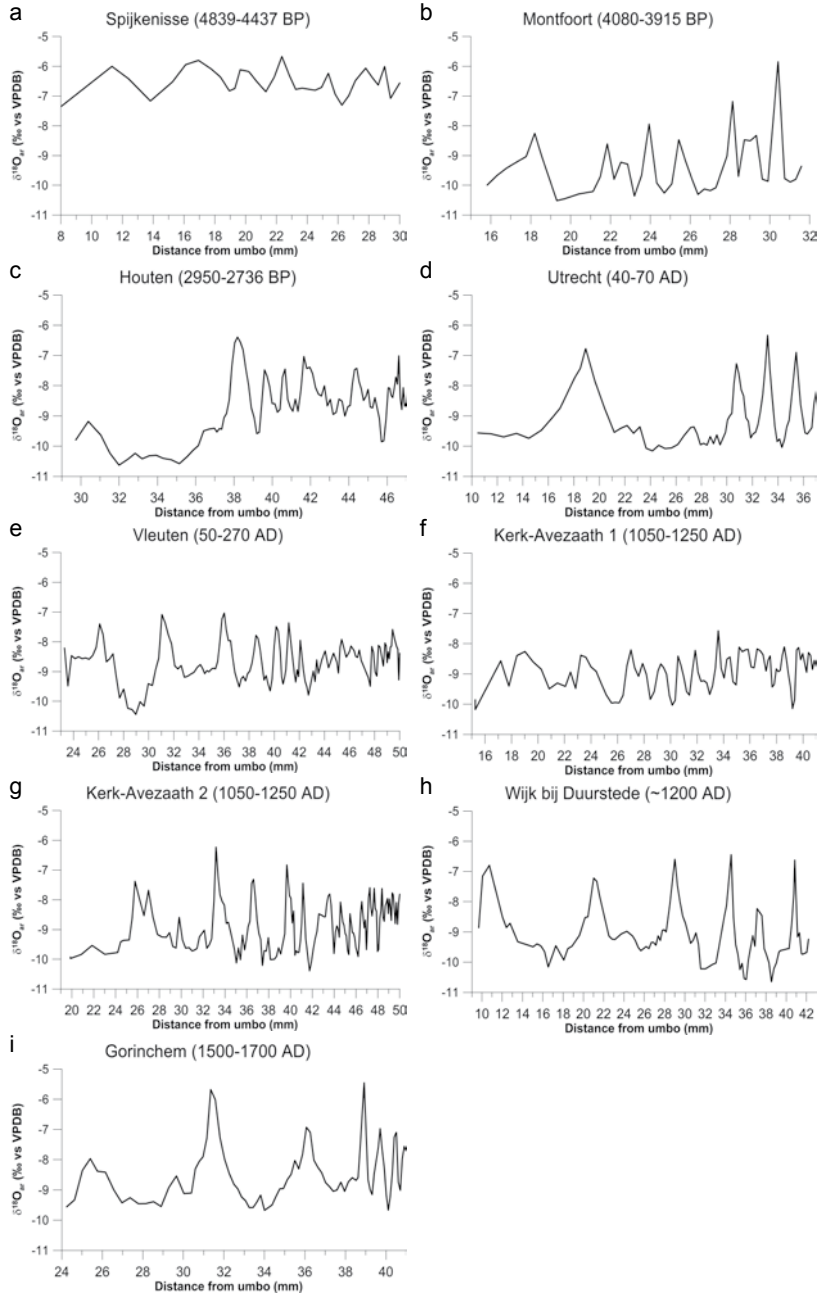
Figure 7.3a-i: $\delta^{18}O_{ar}$ records of the shells. All specimens show the truncated sinu-soidal pattern of seasonal growth with sharp upward pointing peaks representing winter growth cessations and broad troughs representing fast growth in summer. All specimens are *Unio crassus nanus*, except the Vleuten shell is an unknown *Unio* species and Kerk-Avezaath 1 is *Unio tumidus*.

7.6   Discussion

7.6.1   Influence of climate on unionid $\delta^{18}O_{ar}$

Variation in late Holocene summer temperatures and summer precipitation regimes may have influenced shell $\delta^{18}O_{ar}$ records from the different time intervals. With respect to the direct influence of temperature on $\delta^{18}O_{ar}$ values during aragonite precipitation, $\delta^{18}O_{ar}$ values should be lower during warmer time intervals than during cold intervals. However, the average summer temperature differences between cold and warm intervals during the late Holocene are around 0.4 °C, corresponding to very small differences in $\delta^{18}O_{ar}$ values, in the order of 0.1 ‰ (Grossman and Ku, 1986). In the rivers studied, both the intraseasonal temperature variation (average temperature warmest week - temperature of growth cessation) and the interannual temperature difference (warmest day cold summer - warmest day warm summer) potentially recorded by unionids lie around 6 °C. Therefore the effect of centennial to millennial scale temperature variability on $\delta^{18}O_{ar}$ in late Holocene bivalves is much smaller than the seasonal variability. Detecting any long-term temperature trends by means of $\delta^{18}O_{ar}$ composition of these shells will be very difficult, and only possible if many shells are measured.

Late Holocene climatic variations considerably influenced European hydrological regimes (Magny, 2004; Holzhauser et al., 2005). These hydrological changes, such as variations in precipitation regimes or the magnitude of Alpine snowmelt fluxes, are expected to be recognisable in unionid $\delta^{18}O_{ar}$ records (Ricken et al., 2003). At mid latitudes during summer there is a negative correlation between $\delta^{18}O_{w}$ values and the amount of precipitation (Dansgaard, 1964). This so-called amount effect influences river $\delta^{18}O_{w}$ values. Therefore, high discharge summers result in lower $\delta^{18}O_{w}$ values (in the order of 1‰) than low discharge summers (Chapter 5). Another factor that may have a large influence on (Rhine) river water is seasonal meltwater. Alpine meltwater pulses have relatively low $\delta^{18}O_{w}$ values (-12 to -17 ‰ (VSMOW); Mook, 2000), potentially lowering the overall Rhine $\delta^{18}O_{w}$ values up to 1 ‰ within a few days (Versteegh et al., 2009; Chapter 4). The above examples show that late Holocene changes in precipitation regime and seasonal meltwater discharge are likely to change $\delta^{18}O_{w}$ values by more than 1 ‰, which arguably has a much higher impact on shell $\delta^{18}O_{ar}$ values than the ~ 0.4 °C late Holocene long-term temperature variation.

Proxy records describing European precipitation regimes and river dynamics in relation to Holocene climate changes are: 1) relative water levels in
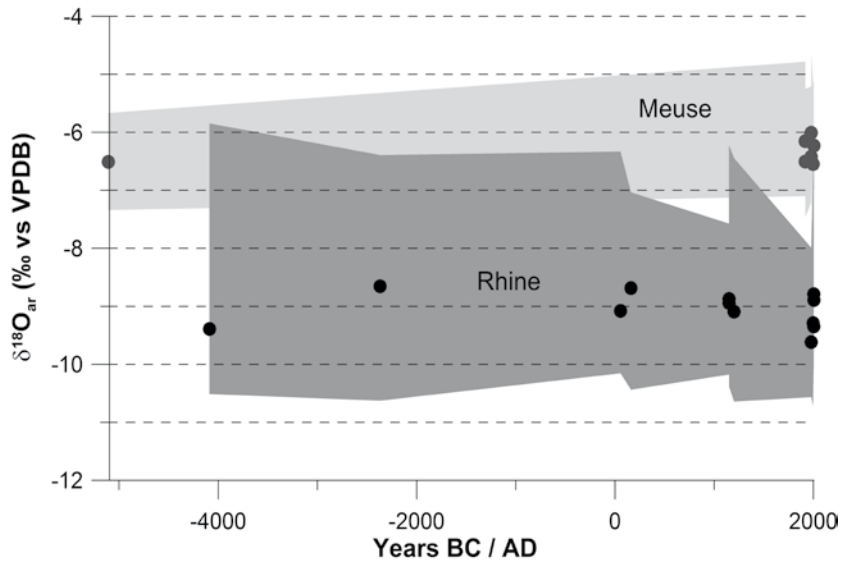
Figure 7.4: Time line indicating average $\delta^{18}O_{ar}$ values (black dots) and ranges (grey bands) for the shells presented here and several previously analysed modern shells (Versteegh et al., 2009; Chapter 4 and 5). There is no significant trend in either average or range of $\delta^{18}O_{ar}$ values.

lakes in the Jura region (France) and 2) fluctuations of glacier extension in the Alps (Holzhauser et al., 2005; Figure 7.1). These records indicate several episodes during which increased precipitation occurred. During these periods of increased precipitation, low $\delta^{18}O_w$ values must have prevailed due to the amount effect. Larger amounts of snow in the Alps may have caused frequent excursions to low $\delta^{18}O_w$ values in the Rhine, due to meltwater input in spring and summer. In contrast high $\delta^{18}O_w$ values must have prevailed during periods with less precipitation.

7.6.2 $\delta^{18}O_{ar}$ records

Average $\delta^{18}O_{ar}$ values and ranges for all shells are plotted along a time axis covering the entire late Holocene in figure 7.4. Previously published data on some recent shells (collected between 1918 and 2005) are shown as well (Versteegh et al., 2009; Chapter 4 and 5). The previously described oxygen isotopic difference between the Rhine and the Meuse (Versteegh et al., 2009; Chapter 3 and 4) is clearly visible in bulk shell $\delta^{18}O_{ar}$ values and appears to be constant throughout the late Holocene.

First of all, in the Meuse shell, the average and range of $\delta^{18}O_{ar}$ values are very similar between the Subboreal shell (Spijkenisse; 4839-4437 BP) and the recent specimens. It thus appears that river conditions in the Meuse

during this time interval were very similar to today. This is in agreement with our expectations, since the Subboreal is known as a relatively warm and dry episode, similar to our recent reference time interval (1997-2007).

Furthermore, the $\delta^{18}O_{ar}$ data of the Gorinchem (1500-1700 AD) shell are similar to those of the Rhine shells, but also overlap with Meuse values (Figure 7.2). This shell likely lived in a mixture of Meuse and Rhine waters, since the Meuse was connected to the Rhine system by the "Afgedamde Maas" (dammed Meuse) just upstream of Gorinchem during the time the shell grew (Berendsen and Stouthamer, 2001). Due to this mixing of waters it is not possible to draw any conclusions about river discharge or meltwater input from $\delta^{18}O_{ar}$ values of this shell, and we will not include this specimen in further discussion.

We established that the influence of temperature on the seasonal range of $\delta^{18}O_{ar}$ values is subordinate to that of $\delta^{18}O_{w}$. This means that minimum $\delta^{18}O_{ar}$ can be an indication for meltwater input and maximum $\delta^{18}O_{ar}$ can give insight in droughts. All Rhine shells in figure 7.4 have average, minimum and maximum $\delta^{18}O_{ar}$ values that fall within the range of recent specimens. There thus appear to be no large climate or palaeogeography related differences in meltwater amounts or droughts in comparison to the present day. A possible explanation for this observation can be that all specimens originate from relatively warm and dry intervals in the Holocene (Subboreal, RWP and MWP), which may have had very similar river conditions to the present day with respect to the amount of precipitation, discharge values and the influence of evapotranspiration.

Furthermore, it is likely that in comparison to interannual and intraseasonal variation in both temperature and $\delta^{18}O_{w}$, the centennial to millennial scale climate variations are too subtle to be readily recognised in these records. Interannual and intraseasonal variation in many environmental variables is large in the river systems studied. This introduces a significant amount of noise into our proxy records. Combined with the fact that these shells are relatively short-lived and only a small time window into a certain climate interval is opened, more specimens (> ~ 10) from a certain climatic interval need to be examined. This finding implies that these high-resolution/short time span records are not suitable for studying subtle centennial millennial scale climatic or palaeogeographic variations, but are very appropriate for examining higher frequency climatic variability, especially on decadal to subseasonal time scale.

159
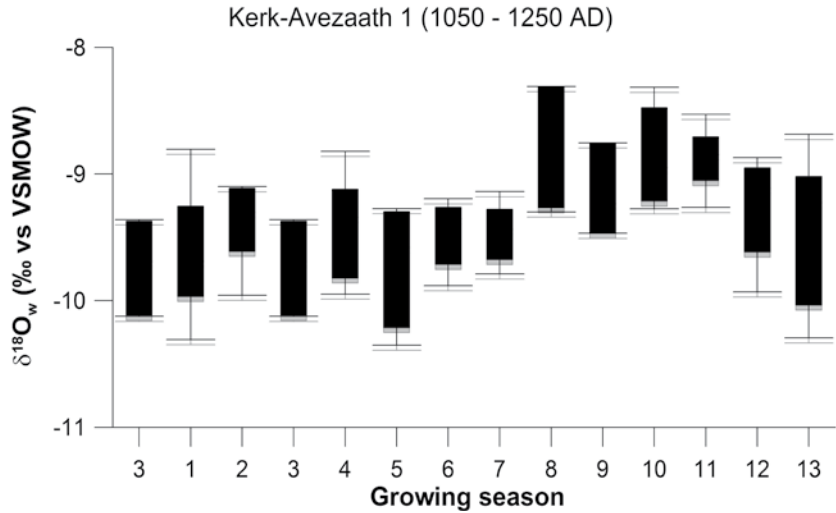
Figure 7.5: Comparison of reconstructed $\delta^{18}O_w$ values for one of the MWP shells (*Unio tumidus*) with average weekly water temperatures from the 1908-1944 time interval (grey) and 0.2 °C elevated temperatures (black). The two approaches yield similar results.

7.6.3 Reconstructed $\delta^{18}O_w$ values

We established that the $\delta^{18}O_{ar}$ records presented show no obvious variation or trends that might be related to Holocene climate or land use changes, and that these long-term trends are probably overshadowed by higher frequency climate variation. We now examine these records for decadal to seasonal scale variability and proceed by reconstructing $\delta^{18}O_w$ values and comparing these to modern day $\delta^{18}O_w$ data from the Rhine and Meuse.

For reconstruction of $\delta^{18}O_w$ values we calculated an average water temperature for every week of the year in the time interval 1908-1944. We assumed the shells started and ceased growing in the week that average water temperature was 13.5 °C (Chapter 3). $\delta^{18}O_{ar}$ samples were linearly interpolated between these two dates and reconstructed $\delta^{18}O_w$ values were calculated using equations 3.1 and 3.2. As expected, an approach using slightly elevated summer temperatures for a warmer phase like the MWP (+0.2 °C) or lower temperatures for the LIA (-0.2 °C; Guiot et al., 2005) yielded very similar results (Figure 7.5). In figures 7.6a-h different shades of grey indicate 2 %, 5 %, 25 %, 75 %, 95 %, and 98 % percentiles of $\delta^{18}O_w$ values from the 1997-2007 summer record for both rivers.
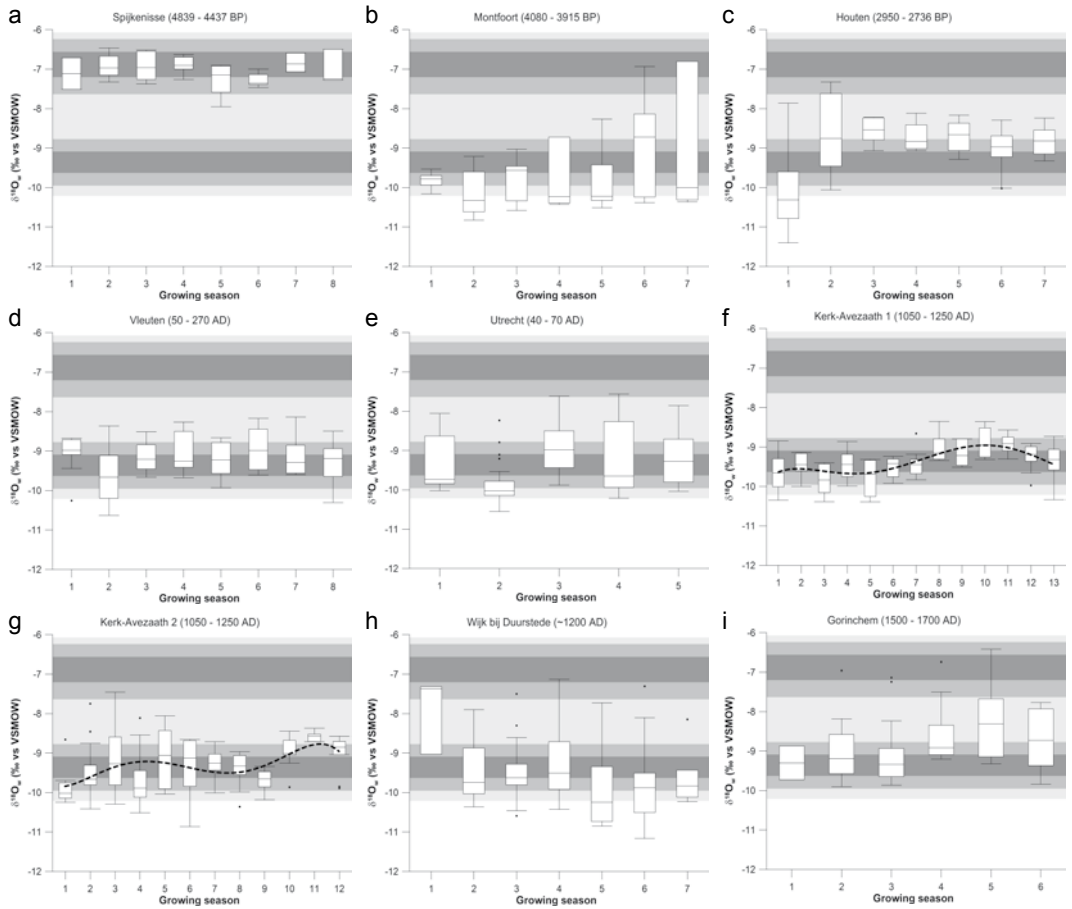
Figure 7.6a-h: Reconstructed $\delta^{18}O_w$ of the shells (using 1908-1944 weekly average temperatures). Grey areas indicate $\delta^{18}O_w$ values from the 1997-2007 summer record for both rivers. Dark grey indicates 50 % of the data, intermediate shading is the 90 % interval and lightest grey indicates 96 % of the data. The graphs drawn in darker grey indicate the average weekly $\delta^{18}O_w$ pattern over 1997-2007. Dashed lines in the Kerk-Avezaath shells indicate decadal-scale variability in $\delta^{18}O_w$ values. All specimens are *Unio crassus nanus*, except the Vleuten shell is an unknown *Unio* species and Kerk-Avezaath 1 is *Unio tumidus*.

7.6.4   Decadal-scale $\delta^{18}O_w$ variability

The reconstructed $\delta^{18}O_w$ records are presented as box-whisker diagrams in figures 7.6a-h. Similar to recent specimens, considerable interannual variation in average, minimum and maximum $\delta^{18}O_w$ values can be observed.

The two shells with the longest lifespan (Kerk-Avezaath 1 and 2; 1050-1250 AD; Figures 7.6f-g) appear to show decadal scale variability in reconstructed $\delta^{18}O_w$ values with a period of ~ 7-10 years. This possibly reflects decadal scale variations in precipitation regimes in the Rhine drainage ba-

161

sin. A likely candidate causing this type of variations in European climate records is the North Atlantic Oscillation (NAO).

The NAO is an important mode of variability influencing Western European precipitation regimes (Hurrell, 1995). It refers to the normalised difference in atmospheric pressure between the Arctic and subtropical Atlantic. Swings between one phase and another cause large changes in moisture transport towards the European continent, storm trajectories and European weather (Hurrell et al., 2003) and related river runoff (Kiely, 1999; Hanninen et al., 2000; Straile et al., 2003). The NAO has dominant periodicities around ~ 5-9 years, which are sometimes linked to external forcing mechanisms like solar and multi-annual tidal cycles (nodal and perigee period; Berger, 2008). It has previously been demonstrated that NAO-related climate variability can be recorded by marine (Schöne et al., 2004; Schöne et al., 2005a; Schöne et al., 2005b; Dunca et al., 2009; Wanamaker et al., 2009), as well as freshwater bivalves (Dunca et al., 2005). Unionids are also known to record similar time scale ENSO-related precipitation variability (Schöne et al., 2007). It thus does seem likely that the Kerk-Avezaath shells recorded $\delta^{18}O_w$ variations that are related to NAO variability during the MWP.

The question arises if similar decadal-scale patterns are visible in the shorter records of the other shells in this study. This cannot be determined conclusively, since these shells were too short-lived to capture a full wavelength of $\delta^{18}O_w$ variability. However, several specimens (e.g. Houten, Figure 7.6c; Wijk bij Duurstede, Figure 7.6h) do show trends that could be part of decadal scale oscillations as observed in the Kerk-Avezaath shells.

An alternative explanation could be that the NAO influence on climate behaved differently during the MWP than during the other time intervals sampled. Trouet et al. (2009) demonstrate that the NAO mode was persistently positive during the MWP, possibly caused by increased solar activity. Normally, the NAO has its most pronounced influence on European climate during winter, when the unionid shells do not grow. However, winter NAO is significantly correlated to the spring-summer atmospheric circulations during solar maximum years (Ogi et al., 2003), enabling the recording of this variability by unionid shells. As solar activity was at a maximum during the MWP (Jirikowic and Damon, 1994; Bard et al., 2000), this could be why these shells specifically exhibit NAO-like variability.

162

7.7   Conclusions

The application of unionid $\delta^{18}O_{ar}$ records as a proxy for late Holocene river dynamics and hydrological regimes in the Rhine and Meuse drainage basins yields promising results. The following conclusions are drawn:

All shells have average, minimum and maximum $\delta^{18}O_{ar}$ values that fall within the range of recent specimens. There appear to be no large differences in meltwater amounts or severity of droughts in comparison to the present day. River conditions during several warm and dry intervals in the Holocene probably were similar to those of the present day. Possible centennial to millennial scale climate variations between the time intervals studied, as well as the human influences like embankment of the rivers and land-use changes, are too subtle to be readily recognised in these records.

Two medieval shells show decadal-scale variation in reconstructed $\delta^{18}O_{w}$ values, with a period of ~ 7-10 years. These possibly reflect NAO variability, which is strongly linked to European spring-summer atmospheric circulations and related river runoff.

This is the first study applying unionid $\delta^{18}O_{ar}$ records for the reconstruction of past river dynamics in the Rhine and Meuse. These first results show the potential of this proxy, though more work is needed. River $\delta^{18}O_{w}$ values and water temperature can be influenced by local factors, such as habitat (e.g. riverbed, lake connected to the river) or water levels. On a regional scale climate variables can vary greatly between seasons and influence for example mixing proportions of different source waters or the influence of evapotranspiration on river $\delta^{18}O_{w}$ values. Combined with the fact that the species presented here attain a maximum age of ~ 15 years (Gittenberger et al., 1998; Versteegh et al., 2009; Chapter 4), many more individuals than presented here (> 10) need to be analysed to draw solid conclusions about river dynamics in a certain time interval. It appears that the high resolution/short time window archive of unionid $\delta^{18}O_{ar}$ values is not very suitable for detection of long-term climatic trends, but very useful for studying decadal to seasonal scale environmental variability.

The apparent detection of NAO-variability is particularly tantalising and calls for more research on late Holocene freshwater mussels, especially on species with a long lifespan like *Margaritifera margaritifera*.

Chapter 8

Synthesis

8.1   Objective and research questions

The overall objective of our research was to examine the potential of freshwater mussel shell chemistry as a proxy for past river conditions, in order to reconstruct late Holocene river dynamics in the Rhine-Meuse delta. This objective was addressed in three steps: (1) a monitoring experiment in which mussels were kept in cages in both rivers for a period of 1.5 years; (2) the analysis of shells from both rivers, collected during the 20th century; (3) the analysis of late Holocene shells from the Rhine-Meuse delta.

Key questions were:

1.   Are seasonally changing stable oxygen and carbon isotope ratios of ambient water recorded in growth increments of unionid freshwater mussels? Which ecological parameters influence the accuracy of bivalve shell $\delta^{18}O_{ar}$ and $\delta^{13}C_{ar}$ values as proxy systems in the Meuse and Rhine rivers? Are the differences in composition between the Meuse (rain-fed) and the Rhine (rain-fed/meltwater), as reflected in stable oxygen isotopic values of the water, recorded in unionid shells?

2.   Can we establish models for interannual and intraseasonal growth rates from stable oxygen and carbon isotope chemistry of river water and equivalent sclerochronological shell records?

3.   What is the empirical relation between measured $\delta^{18}O_w$ values and river discharge? Can we use this relation to reconstruct past $\delta^{18}O_w$ values and link these to measured river discharge values? Can extremely low and high discharge events be recognised in the reconstructed $\delta^{18}O_w$ and discharge records?

4.   What information can unionid $\delta^{18}O_{ar}$ records provide about past river development and the climate during the late Holocene? Can centennial to millennial scale late Holocene climatic variations be recognised in unionid $\delta^{18}O_{ar}$? What were the effects of late Holocene climate change on seasonal (summer) $\delta^{18}O_w$ values and related river conditions (i.e. Alpine meltwater input, Meuse summer droughts)?

8.2   Unionids as recorders of seasonal $\delta^{18}O_w$ and $\delta^{13}C_{DIC}$ values

Unionid species living in the Rhine and Meuse rivers, precipitate skeletal aragonite in oxygen isotopic equilibrium with ambient water. Seasonal patterns in shell $\delta^{18}O_{ar}$ values are a result of seasonal variation in both ambient water $\delta^{18}O_w$ values and temperature. Freshwater bivalve $\delta^{18}O_{ar}$ records can therefore serve as a proxy for past river $\delta^{18}O_w$ values, in relation to discharge seasonality and river dynamics.

Shells from the rivers Rhine and Meuse differ significantly in bulk $\delta^{18}O_{ar}$ values, accurately reflecting the difference of $\delta^{18}O_w$ values between the two rivers (rainwater/meltwater versus rainwater only). These bulk $\delta^{18}O_{ar}$ values can be applied to determine if an ancient river channel was fed by the Rhine, by the Meuse, or by both.

River $\delta^{13}C_{HCO3-}$ has a seasonal cycle with low values in winter and spring. Abruptly rising values in early summer are caused by preferential removal of ^{12}C from the DIC pool by phytoplankton photosynthesis. This seasonal $\delta^{13}C_{HCO3-}$ cycle is accurately recorded in the $\delta^{13}C_{ar}$ values of growth increments of unionid shells.

Freshwater bivalve $\delta^{13}C_{ar}$ records can potentially serve as a proxy for past primary productivity, although other parameters (e.g. input of metabolic carbon or CO_2 exchange with atmosphere) will probably affect $\delta^{13}C_{ar}$ as well.

8.3   Interannual and intraseasonal growth

Knowing that unionid bivalves faithfully record both $\delta^{18}O_w$ and $\delta^{13}C_{HCO3-}$, we can reconstruct interannual and intraseasonal growth. The seasonal $\delta^{18}O_{ar}$ records of the unionids we studied show a truncated sinusoidal pattern with narrow peaks and wide troughs, caused by a combination of temperature fractionation and winter growth cessation. This record can be applied to reconstruct accurate interannual growth rate variation. In the first 2 to 3 years of their life both *Unio pictorum* and *U. tumidus* grew relatively fast. In later years, growth slowed down considerably. Such an ontogenetic growth decrease is common in unionids, and has been observed in previous studies as well (Ravera and Sprocati, 1997; Christian et al., 2000; Anthony et al., 2001).

Based on a correlation of intraseasonal $\delta^{18}O$ and $\delta^{13}C$ variation in ambient water and shells, a growth model is constructed which indicates non-linear growth of these unionids. Onset and cessation of growth of unionid freshwater mussels are induced by water temperature, whereas intraseasonal growth rates are a result of primary productivity (food availability).

8.4   Linking $\delta^{18}O_w$ values to river discharge

If $\delta^{18}O_{ar}$ values are to be used as a proxy for past river discharge, we first need to characterise the relation between river discharge and $\delta^{18}O_w$ values. In the Meuse this is a logarithmic relationship, which allows reconstruction of past discharge from reconstructed $\delta^{18}O_w$ values. Low discharge episodes during summer are recorded in the shells. Summer high discharge events

cannot be reconstructed from shell $\delta^{18}O_{ar}$ records, because the predictive power of $\delta^{18}O_w$ values with respect to discharge is limited for the normal to high discharge situation due to the logarithmic nature of the relation between the two.

For the Rhine no significant relation between discharge and $\delta^{18}O_w$ values could be found. Quantitative reconstruction of past $\delta^{18}O_w$ values and discharge from unionid $\delta^{18}O_{ar}$ values is therefore not possible. However, extremely large Alpine meltwater pulses might be detected by their very low $\delta^{18}O_w$ values.

8.5   The Holocene

The final step towards reconstruction of past river dynamics using unionid shell chemistry as a proxy, is the actual analysis of late Holocene shells.

All shells have average, minimum and maximum $\delta^{18}O_{ar}$ values within the range of recent specimens. This suggests that meltwater amounts and severity of droughts during the climatic intervals studied (Subboreal, Roman Warm Period and Medieval Warm Period) were similar to the present day. It is likely that possible centennial to millennial scale climate variations between the time intervals studied are too subtle to readily be recognised in these records. Due to the considerable amount of noise in the $\delta^{18}O_{ar}$ records, introduced by large interannual and intraseasonal environmental variation in these rivers, these shells are more suitable for studying seasonal to decadal scale environmental variability.

Two medieval shells show decadal-scale variation in reconstructed $\delta^{18}O_w$ values, with a period of ~ 7-10 years. These possibly reflect NAO variability, which is strongly linked to European spring-summer atmospheric circulations and related river runoff.

In order to draw firm conclusions about late Holocene variability in river dynamics, a larger number of shells, comprising many seasons, need to be analysed. The apparent detection of NAO-variability is particularly tantalising and calls for more research on Medieval Warm Period freshwater mussels, especially on species with a long lifespan.

8.6   Final outcome and outlook

This study investigates unionid shell chemistry as a proxy for past river dynamics and is one of the first combining a monitoring experiment and analysis of recent specimens with their application on late Holocene material. We demonstrated that three species of *Unio* faithfully record their environment with respect to both stable oxygen and carbon isotopes, making

them a useful tool in palaeoclimate research.

The combination of different high-resolution chemical records within a single shell enabled us to construct preliminary models for interannual and intraseasonal growth.

The spatial and temporal heterogeneity of the river environments studied here introduces a considerable amount of noise to the background climate signal. This means that both local circumstances as well as significant intraseasonal environmental variation can obscure a lower frequency climate-related signal in these shells. In comparison to most freshwater systems, in the marine realm, both water temperature and $\delta^{18}O_w$ tend to be less variable within and between seasons. Therefore, sclerochemical records of freshwater shells are more complicated to interpret than their marine counterparts, hampering the straightforward interpretation of stable isotope records from subfossil Unionidae.

To minimise these problems, several directions of research can be pursued. First of all it is necessary to analyse a sufficient number of shells ($> \sim 10$) from a given climate interval, in order to capture the full range of interannual variability.

Furthermore, in order to better match certain parts of the shell with the corresponding time frame within the growing season, there is need for accurate intraseasonal and interannual growth models. Noteworthy work on these subjects has been done by Goodwin et al. (2003), De Ridder et al. (2004) and De Brauwere et al. (2008) and is still ongoing (Beelaerts et al., 2009). With respect to intraseasonal growth, Goodwin et al. (2009) achieved promising results with a numerical model based on predicted and measured $\delta^{18}O_{ar}$ values (MoGroFunGen).

Interannual growth is briefly addressed in chapter 4 (Versteegh et al., 2009). Growth increment size appears to decrease with shell length logarithmically as was previously described in *Unio mancus* and *Anodonta cygnea* (Ravera and Sprocati, 1997). In addition, differences in growth strategy have been found between species and between reservoirs (Christian et al., 2000). We have strong indications that growth strategies differ between time intervals en between reservoirs in the species studied here. More work is desirable on these subjects as well.

Reconstructions of past environmental variability might be greatly improved by using multiple proxies within one organism (Schöne and Surge, 2005; Schöne et al., 2006). For example, $\delta^{18}O$ values as well as certain trace element records might be influenced by (and serve as a proxy for) temperature. When these are also influenced by other factors, a temperature recon-

struction based on one proxy alone might be highly uncertain, whereas a reconstruction considering all proxies at once will have much smaller associated errors (Bauwens et al., 2009). Furthermore, another approach to determine past river discharge is by salinity reconstructions derived from $\delta^{18}O$, $\delta^{13}C$ and Ba/Ca records in estuarine bivalves (Gillikin et al., 2006a; Gillikin et al., 2006b). Combining these records with freshwater bivalve $\delta^{18}O_{ar}$ values can strengthen reconstructions of palaeo-discharge.

Providing the above suggestions are met to a sufficient degree, stable isotope records of archaeological shells can serve as a proxy for reconstructing past river dynamics and possible droughts and meltwater fluxes. These reconstructions are much needed for validation of models predicting the impact of climate change in the Rhine-Meuse delta (Cohen and Lodder, 2007; Ward, 2009).

8.7   Future research and recommendations

The results of this thesis are a major step forward in our understanding of the relation between freshwater bivalve chemistry and environmental variability. Besides the interesting results, there is of course always room for improvement. In addition, directions for future research have arisen, which could not be pursued within this project:

- As discussed above, using a multi-proxy approach and developing accurate intraseasonal and interannual growth models can significantly improve the accuracy of river dynamics reconstructions.
- The monitoring experiment showed that both $\delta^{18}O_w$ and $\delta^{13}C_{HCO3-}$ values are recorded in *Unio* shells. The ambient water $\delta^{13}C_{HCO3-}$ values however, exhibit significant leaps, suggesting that it is desirable to collect water samples at a higher temporal resolution. This will improve both our understanding of shell $\delta^{13}C_{ar}$ composition and the construction of intraseasonal growth models.
- During the monitoring experiment, most shells grew very little. This can be problematic for the subsequent comparison of shell and water records and the construction of growth models. Accomplishing a higher temporal resolution with respect to shell samples is mainly a question of attaining higher growth rates during a monitoring experiment. The use of juvenile specimens (rapid growth) and lower population densities (less competition) will likely help. In addition, it appears that unionids are highly sensitive to handling and transplantation. It is therefore desirable to perform future experiments in the same river as where the mussels were collected, and minimise the frequency and

duration of handling for measuring, tagging and staining.

- For a reliable reconstruction of past river discharges, floods and droughts, the influence of variability in local environmental conditions between individual shells collected needs to be minimised. Therefore a substantial number of summer seasons needs to be sampled, implying that a sufficiently large number of shells (> 10) from a given climatic interval is needed.

- Apart from Holocene unionids from the rivers Rhine and Meuse, museum collections also contain specimens from the Eemian (Wesselingh, pers. comm.). Stable isotope analyses on these shells can possibly shed light on relative contributions of different source waters and palaeogeography of northwestern European rivers during the previous interglacial.

- Trace element profiles of unionid freshwater mussels are known to exhibit seasonal patterns (Tynan et al., 2005; Kaandorp et al., 2006; Carroll and Romanek, 2008; Soldati et al., 2008). More work is needed to understand the mechanisms behind seasonal trace element variations, but they probably harbour useful environmental information. Laser Ablation Inductively Coupled Plasma Mass Spectrometry (LA-ICP-MS) is a promising technique to gain these trace element profiles at an extremely high resolution in little time (Toland et al., 2000). In cooperation with the Australian National University we applied this technique on the specimens presented in this study. Publications on this subject are in preparation.

- Within the CS-09 project three other subprojects collaborate towards better understanding of late Holocene precipitation regimes, river discharges and flood frequencies. These subprojects comprise a modelling study investigating the Meuse discharge (Ward et al., 2008; Ward, 2009), a study using chemistry of Sphagnum mosses as a proxy for precipitation (Brader et al., 2008) and a sedimentological and palynological study investigating palaeo river channels. The intended integration of results from these four subprojects will yield an informative picture of late Holocene precipitation and river discharges in the Meuse valley.

References

Aerts, J. C. J. H., H. Renssen, P. J. Ward, H. de Moel, E. Odada, L. M. Bouwer, H. Goosse, 2006. Sensitivity of global river discharges under Holocene and future climate conditions. Geophysical Research Letters, 33: 5.

Al-Aasm, I. S., J. D. Clarke, B. J. Fryer, 1998. Stable isotopes and heavy metal distribution in *Dreissena polymorpha* (Zebra Mussels) from western basin of Lake Erie, Canada. Environmental Geology, 33(2): 122-129.

Aldridge, D. C., 1999. The morphology, growth and reproduction of Unionidae (Bivalvia) in a Fenland waterway. Journal of Molluscan Studies, 65(1): 47-60.

Andral, B., J. Y. Stanisiere, D. Sauzade, E. Damier, H. Thébault, F. Galgani, P. Boissery, 2004. Monitoring chemical contamination levels in the Mediterranean based on the use of mussel caging. Marine Pollution Bulletin, 49(9-10): 704-712.

Anthony, J. L., D. H. Kesler, W. L. Downing, J. A. Downing, 2001. Length-specific growth rates in freshwater mussels (Bivalvia: Unionidae): extreme longevity or generalized growth cessation? Freshwater Biology, 46(10): 1349-1359.

Arnell, N. W., 1999. The effect of climate change on hydrological regimes in Europe: a continental perspective. Global Environmental Change, 9(1): 5-23.

Arter, H. E., 1989. Effect of eutrophication on species composition and growth of freshwater mussels (Mollusca, Unionidae) in Lake Hallwil (Aargau, Switzerland). Aquatic Sciences - Research Across Boundaries, 51(2): 87-99.

Aucour, A.-M., S. M. F. Sheppard, R. Savoye, 2003. $\delta^{13}C$ of fluvial mollusk shells (Rhône River): A proxy for dissolved inorganic carbon? Limnology and Oceanography, 48(6): 2186-2193.

Bard, E., G. Raisbeck, F. Yiou, J. Jouzel, 2000. Solar irradiance during the last 1200 years based on cosmogenic nuclides. Tellus B, 52(3): 985-992.

Bauer, G., 1988. Threats to the freshwater pearl mussel *Margaritifera margaritifera* L. in Central Europe. Biological Conservation, 45(4): 239-253.

Bauwens, M., H. Ohlsson, V. Beelaerts, K. Barbé, F. Dehairs, J. Schoukens, 2009. Non-linearities in proxy space: Three methods to deal with the non-linear behavior of proxies in calcareous marine skeletons. Geophysical Research Abstracts, 11. EGU2009-1460, EGU General Assembly 19-24 April 2009, Vienna, Austria.

Beelaerts, V., F. De Ridder, N. Schmitz, M. Bauwens, F. Dehairs, J. Schoukens, R. Pintelon, 2009. On the elimination of bias averaging-errors in proxy records. Mathematical Geosciences, 41(2): 129-144.

Berendsen, H. J. A., E. Stouthamer, 2001. Palaeogeographic development of the Rhine-Meuse delta, The Netherlands. Koninklijke Van Gorcum, Assen, 268 p.

173

Berger, W. H., 2008. Solar modulation of the North Atlantic Oscillation: Assisted by the tides? Quaternary International, 188(1): 24-30.

Bice, K. L. J., M. A. Arthur, L. J. Marincovich, 1996. Late Paleocene Arctic Ocean shallow-marine temperatures from mollusc stable isotopes. Paleoceanography, 11(3): 241-250.

Booij, M. J., 2002. Extreme daily precipitation in Western Europe with climate change at appropriate spatial scales, 69-85.

Brader, A. V., S. J. P. Bohncke, C. J. Beets, G. J. Reichart, 2008. Deducing climate signals from hydrogen isotopes in *Sphagnum*, NAC 9, 18-19 March 2009, Veldhoven, The Netherlands.

Bradley, R. S., M. K. Hughes, H. F. Diaz, 2003. Climate Change: Climate in medieval time. Science, 302(5644): 404-405. 10.1126/science.1090372

Brázdil, R., C. Pfister, H. Wanner, H. V. Storch, J. Luterbacher, 2005. Historical climatology in Europe – The state of the art. Climatic Change, 70(3): 363-430.

Brey, T., A. Mackensen, 1997. Stable isotopes prove shell growth bands in the Antarctic bivalve *Laternula elliptica* to be formed annually. Polar Biology, 17(5): 465-468.

Buhl, D., R. D. Neuser, D. K. Richter, D. Riedel, B. Roberts, H. Strauss, J. Veizer, 1991. Nature and nurture: Environmental isotope story of the River Rhine. Naturwissenschaften (Historical Archive), 78(8): 337-346.

Bürger, G., 2002. Selected precipitation scenarios across Europe. Journal of Hydrology, 262(1-4): 99-110.

Burlakova, L. E., A. Y. Karatayev, D. K. Padilla, 2000. The impact of *Dreissena polymorpha* (Pallas) invasion on unionid bivalves. International Review of Hydrobiology, 85(5-6): 529-541.

Carré, M., I. Bentaleb, D. Blamart, N. Ogle, F. Cardenas, S. Zevallos, R. M. Kalin, L. Ortlieb, M. Fontugne, 2005. Stable isotopes and sclerochronology of the bivalve *Mesodesma donacium*: Potential application to Peruvian paleoceanographic reconstructions. Palaeogeography, Palaeoclimatology, Palaeoecology, 228(1-2): 4-25.

Carroll, M., C. Romanek, 2008. Shell layer variation in trace element concentration for the freshwater bivalve *Elliptio complanata*. Geo-Marine Letters, 28(5): 369-381.

Chauvaud, L., A. Lorrain, R. Dunbar, Y.-M. Paulet, G. Thouzeau, F. Jean, J.-M. Guarini, D. Mucciarone, 2005. The shell of the Great Scallop *Pecten maximus* as a high-frequency archive of paleoenvironmental changes. Geochemistry Geophysics Geosystems, 6(8): 15.

Christian, A. D., C. L. Davidson, W. R. Posey II, P. J. Rust, J. L. Farris, J. L. Harris, G. L. Harp, 2000. Growth curves of four species of commercially valuable freshwater mussels (Bivalvia: Unionidae) in Arkansas. Journal of the Arkansas Academy of Science, 54: 41-50.

Christian, A. D., B. N. Smith, D. J. Berg, J. C. Smoot, R. H. Findlay, 2004. Trophic position and potential food sources of 2 species of unionid bivalves (Mollusca: Unionidae) in 2 small Ohio streams. Journal of the North American Benthological Society, 23(1): 101-113.

Clark, I. D., P. Fritz, 1997. Environmental isotopes in hydrogeology. Lewis Publishers, New York, 328 p.

Cohen, K. M., Q. J. Lodder, 2007. Paleogeografie en veiligheid tegen overstromen. Universiteit Utrecht & Rijkswaterstaat RIZA, Utrecht, ATB10050206/WRV/Van Essen ES/RWS/06/12-9.

Cook, E. R., J. Esper, R. D. D'Arrigo, 2004. Extra-tropical Northern Hemisphere land temperature variability over the past 1000 years. Quaternary Science Reviews, 23(20-22): 2063-2074.

Coplen, T. B., 1996. New guidelines for reporting stable hydrogen, carbon, and oxygen isotope-ratio data. Geochimica et Cosmochimica Acta, 60(17): 3359-3360.

Crowley, T. J., T. S. Lowery, 2000. How warm was the Medieval Warm Period? Ambio, 29(1): 51-54.

Dansgaard, W., 1964. Stable isotopes in precipitation. Tellus, 16(4): 336-368.

Davis, L. G., K. Muehlenbachs, 2001. A late Pleistocene to Holocene record of precipitation reflected in *Margaritifera falcata* shell $\delta^{18}O$ from three archaeological sites in the lower Salmon River Canyon, Idaho. Journal of Archaeological Science, 28(3): 291-303.

Day, R. W., M. C. Williams, G. P. Hawkes, 1995. A comparison of fluorochromes for marking abalone shells. Marine & Freshwater Research, 46(3): 599-605.

De Brauwere, A., F. De Ridder, R. Pintelon, J. Meersmans, J. Schoukens, F. Dehairs, 2008. Identification of a periodic time series from an environmental proxy record. Computers & Geosciences, 34(12): 1781-1790.

De Ridder, F., R. Pintelon, J. Schoukens, D. P. Gillikin, L. André, W. Baeyens, A. de Brauwere, F. Dehairs, 2004. Decoding nonlinear growth rates in biogenic environmental archives. Geochemistry Geophysics Geosystems, 5(12): 16.

De Wit, M., B. van den Hurk, P. Warmerdam, P. Torfs, E. Roulin, W. van Deursen, 2007. Impact of climate change on low-flows in the river Meuse. Climatic Change, 82(3): 351-372.

Dettman, D. L., K. C. Lohmann, 1993. Seasonal change in Paleogene surface water δ¹⁸O: Fresh-water bivalves of western North America, 374 p. In: Swart, P. K., K. C. Lohmann, J. McKenzie, S. Savin (eds.), Climate change in continental isotopic records. Volume 78. American Geophysical Union, Washington.

Dettman, D. L., A. K. Reische, K. C. Lohmann, 1999. Controls on the stable isotope composition of seasonal growth bands in aragonitic fresh-water bivalves (Unionidae). Geochimica et Cosmochimica Acta, 63(7-8): 1049-1057.

Diggins, T. P., K. M. Stewart, 2000. Evidence of large change in unionid mussel abundance from selective muskrat predation, as inferred by shell remains left on shore. International Review of Hydrobiology, 85(4): 505-520.

Dunca, E., B. R. Schöne, H. Mutvei, 2005. Freshwater bivalves tell of past climates: But how clearly do shells from polluted rivers speak? Palaeogeography, Palaeoclimatology, Palaeoecology, 228(1-2): 43-57.

Dunca, E., H. Mutvei, P. Göransson, C.-M. Mörth, B. Schöne, M. Whitehouse, M. Elfman, S. Baden, 2009. Using ocean quahog (*Arctica islandica*) shells to reconstruct palaeoenvironment in Öresund, Kattegat and Skagerrak, Sweden. International Journal of Earth Sciences, 98(1): 3-17.

Dutton, A. L., K. C. Lohmann, W. J. Zinsmeister, 2002. Stable isotope and minor element proxies for Eocene climate of Seymour Island, Antarctica. Paleoceanography, 17(2): 1016.

Eads, C. B., J. B. Layzer, 2002. How to pick your mussels out of a crowd: using fluorescence to mark juvenile freshwater mussels. Journal of the North American Benthological Society, 21(3): 476-486.

Esper, J., E. R. Cook, F. H. Schweingruber, 2002. Low-frequency signals in long tree-ring chronologies for reconstructing past temperature variability. Science, 295(5563): 2250-2253. 10.1126/science.1066208

Farquhar, G. D., J. R. Ehleringer, K. T. Hubick, 1989. Carbon isotope discrimination and photosynthesis. Annual Review of Plant Physiology and Plant Molecular Biology, 40(1): 503-537. 10.1146/annurev.pp.40.060189.002443

Fastovsky, D. E., M. A. Arthur, N. H. Strater, A. Foss, 1993. Freshwater bivalves (Unionidae), disequilibrium isotopic fractionation, and temperatures. Palaios, 8(6): 602-608.

Freitas, P. S., L. J. Clarke, H. Kennedy, C. A. Richardson, F. Abrantes, 2006. Environmental and biological controls on elemental (Mg/Ca, Sr/Ca and Mn/Ca) ratios in shells of the king scallop *Pecten maximus*. Geochimica et Cosmochimica Acta, 70(20): 5119-5133.

Friedman, E., B. Mower, 2004. Final report 2003 Kennebec River caged mussel study. Applied Biomonitoring, Kirkland, WA.

Frisia, S., A. Borsato, C. Spötl, I. M. Villa, F. Cucchi, 2005. Climate variability in the SE Alps of Italy over the past 17 000 years reconstructed from a stalagmite record. Boreas, 34(4): 445-455.

Fritz, P., S. Poplawski, 1974. ^{18}O and ^{13}C in the shells of freshwater molluscs and their environments. Earth and Planetary Science Letters, 24(1): 91-98.

Gajurel, A. P., C. France-Lanord, P. Huyghe, C. Guilmette, D. Gurung, 2006. C and O isotope compositions of modern fresh-water mollusc shells and river waters from the Himalaya and Ganga plain. Chemical Geology, 233(1-2): 156-183.

Geist, J., K. Auerswald, A. Boom, 2005. Stable carbon isotopes in freshwater mussel shells: Environmental record or marker for metabolic activity? Geochimica et Cosmochimica Acta, 69(14): 3545-3554.

Gillies, R. R., J. Brim Box, J. Symanzik, E. J. Rodemaker, 2003. Effects of urbanization on the aquatic fauna of the Line Creek watershed, Atlanta - A satellite perspective. Remote sensing of environment 86(3): 411-422.

Gillikin, D. P., F. Dehairs, W. Baeyens, J. Navez, A. Lorrain, L. Andre, 2005. Inter- and intra-annual variations of Pb/Ca ratios in clam shells (*Mercenaria mercenaria*): A record of anthropogenic lead pollution? Marine Pollution Bulletin, 50(12): 1530-1540.

Gillikin, D. P., A. Lorrain, S. Bouillon, P. Willenz, F. Dehairs, 2006a. Stable carbon isotopic composition of *Mytilus edulis* shells: relation to metabolism, salinity, $\delta^{13}C_{DIC}$ and phytoplankton. Organic Geochemistry, 37(10): 1371-1382.

Gillikin, D. P., F. Dehairs, A. Lorrain, D. Steenmans, W. Baeyens, L. Andre, 2006b. Barium uptake into the shells of the common mussel (*Mytilus edulis*) and the potential for estuarine paleo-chemistry reconstruction. Geochimica et Cosmochimica Acta, 70(2): 395-407.

Gillikin, D. P., K. A. Hutchinson, Y. Kumai, 2009. Ontogenic increase of metabolic carbon in freshwater mussel shells (*Pyganodon cataracta*). Journal of Geophysical Research, 114.

Gittenberger, E., A. W. Janssen, W. J. Kuijper, J. G. J. Kuiper, T. Meijer, G. van der Velde, J. N. de Vries, 1998. De Nederlandse zoetwatermollusken - Recente en fossiele weekdieren uit zoet en brak water. Nationaal Natuurhistorisch Museum Naturalis - KNNV Uitgeverij, Leiden, 2, 288 p.

Goewert, A., D. Surge, S. J. Carpenter, J. Downing, 2007. Oxygen and carbon isotope ratios of *Lampsilis cardium* (Unionidae) from two streams in agricultural watersheds of Iowa, USA. Palaeogeography, Palaeoclimatology, Palaeoecology, 252(3-4): 637-648.

Gonfiantini, R., W. Stichler, K. Rozanski, 1995. Standards and intercomparison materials distributed by the International Atomic Energy Agency for stable isotope measurements. I.A.E.A.

Goodwin, D. H., B. R. Schöne, D. L. Dettman, 2003. Resolution and fidelity of oxygen isotopes as paleotemperature proxies in bivalve mollusk shells: models and observations. Palaios, 18(2): 110-125.

Goodwin, D. H., P. Paul, C. L. Wissink, 2009. MoGroFunGen: A numerical model for reconstructing intra-annual growth rates of bivalve molluscs. Palaeogeography, Palaeoclimatology, Palaeoecology, 276(1-4): 47-55.

Goosse, H., H. Renssen, A. Timmermann, R. S. Bradley, 2005. Internal and forced climate variability during the last millennium: a model-data comparison using ensemble simulations. Quaternary Science Reviews, 24(12-13): 1345-1360.

Goosse, H., O. Arzel, J. Luterbacher, M. E. Mann, H. Renssen, N. Riedwyl, A. Timmermann, E. Xoplaki, H. Wanner, 2006. The origin of the European "Medieval Warm Period". Climate of the Past, 2(2): 99-113.

Gregory, J. M., J. F. B. Mitchell, A. J. Brady, 1997. Summer drought in northern midlatitudes in a time-dependent CO_2 climate experiment, 662-686.

Grossman, E. L., T.-L. Ku, 1986. Oxygen and carbon isotope fractionation in biogenic aragonite: Temperature effects. Chemical Geology: Isotope Geoscience section, 59: 59-74.

Guiot, J., A. Nicault, C. Rathgeber, J. L. Edouard, F. Guibal, G. Pichard, C. Till, 2005. Last-millennium summer-temperature variations in western Europe based on proxy data. The Holocene, 15(4): 489-500. 10.1191/0959683605hl-819rp

Gustafson, L., W. Showers, T. Kwak, J. Levine, M. Stoskopf, 2007. Temporal and spatial variability in stable isotope compositions of a freshwater mussel: implications for biomonitoring and ecological studies. Oecologia, 152(1): 140-150.

Haag, W. R., J. L. Staton, 2003. Variation in fecundity and other reproductive traits in freshwater mussels. Freshwater Biology, 48(12): 2118-2130.

Hanninen, J., I. Vuorinen, P. Hjelt, 2000. Climatic factors in the Atlantic control the oceanographic and ecological changes in the Baltic Sea. Limnology and Oceanography, 45(3): 703-710.

Hanson, J. M., W. C. Mackay, E. E. Prepas, 1989. Effect of size-selective predation by muskrats (*Ondatra zebithicus*) on a population of unionid clams (*Anodonta grandis simpsoniana*). Journal of Animal Ecology, 58(1): 15-28.

Hass, H. C., 1996. Northern Europe climate variations during late Holocene: evidence from marine Skagerrak. Palaeogeography, Palaeoclimatology, Palaeoecology, 123(1-4): 121-145.

Hellings, L., F. Dehairs, M. Tackx, E. Keppens, W. Baeyens, 1999. Origin and fate of organic carbon in the freshwater part of the Scheldt Estuary as traced by stable carbon isotope composition. Biogeochemistry, 47(2): 167-186.

Hickey, C. W., D. S. Roper, S. J. Buckland, 1995. Metal concentrations of resident and transplanted freshwater mussels *Hyridella menziesi* (Unionacea: Hyriidae) and sediments in the Waikato River, New Zealand. Science of The Total Environment, 175(3): 163-177.

Holzhauser, H., M. Magny, H. J. Zumbuuhl, 2005. Glacier and lake-level variations in west-central Europe over the last 3500 years. The Holocene, 15(6): 789-801. 10.1191/0959683605hl853ra

Howard, A. D., 1922. Experiments in the culture of fresh-water mussels. Bulletin of the Bureau of Fisheries, 38: 63-89.

Hudson, J. H., E. A. Shinn, R. B. Halley, B. Lidz, 1976. Sclerochronology: A tool for interpreting past environments. Geology, 4: 361-364.

Hurrell, J. W., 1995. Decadal trends in the North Atlantic Oscillation: Regional temperatures and precipitation. Science, 269(5224): 676-679.

Hurrell, J. W., Y. Kushnir, G. Ottersen, M. Visbeck, 2003. An overview of the North Atlantic Oscillation, 1-35 p, The North Atlantic Oscillation: Climatic significance and environmental impact. Volume 134. American Geophysical Union.

Hyötyläinen, T., A. Karels, A. Oikari, 2002. Assessment of bioavailability and effects of chemicals due to remediation actions with caging mussels (*Anodonta anatina*) at a creosote-contaminated lake sediment site. Water Research, 36(18): 4497-4504.

IPCC, 2007. Climate Change 2007: The physical science basis. Contribution of working group I to the fourth assessment - Report of the Intergovernmental Panel on Climate Change. Cambridge University Press, Cambridge, 996 p.

Jirikowic, J. L., P. E. Damon, 1994. The medieval solar activity maximum. Climatic Change, 26(2): 309-316.

Jokela, J., P. Mutikainen, 1995. Phenotypic plasticity and priority rules for energy allocation in a freshwater clam: a field experiment. Oecologia, 104(1): 122-132.

Jokela, J., 1996. Within-season reproductive and somatic energy allocation in a freshwater clam, *Anodonta piscinalis*. Oecologia, 105(2): 167-174.

Jones, D. S., 1980. Annual cycle of shell growth increment formation in two continental shelf bivalves and its paleoecologic significance. Paleobiology, 6(3): 331-340.

Jones, D. S., 1983. Sclerochronology: Reading the record of the molluscan shell. American Scientist, 71: 384-391.

Joordens, J. C. A., F. P. Wesselingh, J. de Vos, H. B. Vonhof, D. Kroon, 2009. Relevance of aquatic environments for hominins: a case study from Trinil (Java, Indonesia). Journal of Human Evolution, In Press, Corrected Proof. 10.1016/j.jhevol.2009.06.003

Kaandorp, R. J. G., H. B. Vonhof, C. Del Busto, F. P. Wesselingh, G. M. Ganssen, A. E. Marmol, L. Romero Pittman, J. E. van Hinte, 2003. Seasonal stable isotope variations of the modern Amazonian freshwater bivalve *Anodontites trapesialis*. Palaeogeography, Palaeoclimatology, Palaeoecology, 194(4): 339-354.

Kaandorp, R. J. G., H. B. Vonhof, F. P. Wesselingh, L. R. Pittman, D. Kroon, J. E. van Hinte, 2005. Seasonal Amazonian rainfall variation in the Miocene Climate Optimum. Palaeogeography, Palaeoclimatology, Palaeoecology, 221(1-2): 1-6.

Kaandorp, R. J. G., F. P. Wesselingh, H. B. Vonhof, 2006. Ecological implications from geochemical records of Miocene Western Amazonian bivalves. Journal of South American Earth Sciences, 21(1-2): 54-74.

Kabat, P., H. van Schaik, 2003. Climate changes the water rules: how water managers can cope with today's climate variability and tomorrow's climate change. Dialogue on Water and Climate, Liverpool, 105 p.

Kauss, P. B., Y. S. Hamdy, 1985. Biological monitoring of organochlorine contaminants in the St. Clair and Detroit rivers using introduced clams, *Elliptio complanatus*. Journal of Great Lakes Research, 11(3): 247-263.

Kauss, P. B., Y. S. Hamdy, 1991. Polycyclic aromatic hydrocarbons in surficial sediments and caged mussels of the St. Marys River, 1985. Hydrobiologia, 219(1): 37-62.

Kesler, D., J. Downing, 1997. Internal shell annuli yield inaccurate growth estimates in the freshwater mussels *Elliptio complanata* and *Lampsilis radiata*. Freshwater Biology, 37(2): 325-332.

Kesler, D. H., T. J. Newton, L. Green, 2007. Long-term monitoring of growth in the Eastern Elliptio, *Elliptio complanata* (Bivalvia: Unionidae), in Rhode Island: a transplant experiment. Journal of the North American Benthological Society, 26(1): 123-133.

Kiely, G., 1999. Climate change in Ireland from precipitation and streamflow observations. Advances in Water Resources, 23(2): 141-151.

Kim, S.-T., J. R. O'Neil, C. Hillaire-Marcel, A. Mucci, 2007. Oxygen isotope fractionation between synthetic aragonite and water: Influence of temperature and Mg^{2+} concentration. Geochimica et Cosmochimica Acta, 71(19): 4704-4715.

Klocker, C. A., D. L. Strayer, 2004. Interactions among an invasive crayfish (*Orconectes rusticus*), a native crayfish (*Orconectes limosus*), and native bivalves (Sphaeriidae and Unionidae). Northeastern Naturalist, 11(2): 167-178.

Koide, M., D. S. Lee, E. D. Goldberg, 1982. Metal and transuranic records in mussel shells, byssal threads and tissues. Estuarine, Coastal and Shelf Science, 15(6): 679-695.

Können, G. P., W. Fransen, 1996. De toestand van het klimaat in Nederland 1996. KNMI, De Bilt.

Kuijper, W. J., 1990. De mollusken van de holocene fluviatiele afzettingen bij Hekelingen (Spijkenisse, Zuid-Holland). Basteria, 54: 3-16.

Lamb, H. H., 1965. The early medieval warm epoch and its sequel. Palaeogeography, Palaeoclimatology, Palaeoecology, 1: 13-37.

Lemarié, D. P., D. R. Smith, R. F. Villella, D. A. Weller, 2000. Evaluation of tag types and adhesives for marking freshwater mussels (Mollusca: Unionidae). Journal of Shellfish Research, 19(1): 247-250.

Louwe Kooijmans, L. P., P. W. van den Broeke, H. Fokkens, A. van Gijn, 2005. Nederland in de prehistorie. Uitgeverij Bert Bakker, Amsterdam, 850 p.

Luterbacher, J., R. Rickli, E. Xoplaki, C. Tinguely, C. Beck, C. Pfister, H. Wanner, 2001. The late Maunder Minimum (1675–1715) - A key period for studying decadal scale climatic change in Europe. Climatic Change, 49(4): 441-462.

Luterbacher, J., D. Dietrich, E. Xoplaki, M. Grosjean, H. Wanner, 2004. European seasonal and annual temperature variability, trends, and extremes since 1500. Science, 303(5663): 1499-1503.

Magny, M., 2004. Holocene climate variability as reflected by mid-European lake-level fluctuations and its probable impact on prehistoric human settlements. Quaternary International, 113(1): 65-79.

Malley, D. F., A. R. Stewart, B. D. Hall, 1996. Uptake of methyl mercury by the floater mussel, *Pyganodon grandis* (Bivalvia, Unionidae), caged in a flooded wetland. Environmental Toxicology and Chemistry, 15(6): 928-936.

Mann, M. E., R. S. Bradley, M. K. Hughes, 1998. Global-scale temperature patterns and climate forcing over the past six centuries. Nature, 392(6678): 779-787.

Mann, M. E., R. S. Bradley, M. K. Hughes, 1999. Northern hemisphere temperatures during the past millennium: Inferences, uncertainties, and limitations. Geophysical Research Letters, 26(6): 759-762.

Mann, M. E., C. M. Ammann, R. S. Bradley, K. R. Briffa, T. J. Crowley, P. D. Jones, M. Oppenheimer, T. J. Osborn, J. T. Overpeck, S. Rutherford, K. E. Trenberth, T. M. L. Wigley, 2003. On past temperatures and anomalous late-20th century warmth. Eos Transactions AGU.

Martel, P., T. Kovacs, R. Voss, S. Megraw, 2003. Evaluation of caged freshwater mussels as an alternative method for environmental effects monitoring (EEM) studies. Environmental Pollution, 124(3): 471-483.

McConnaughey, T. A., J. Burdett, J. F. Whelan, C. K. Paull, 1997. Carbon isotopes in biological carbonates: Respiration and photosynthesis. Geochimica et Cosmochimica Acta, 61(3): 611-622.

McConnaughey, T. A., D. Gillikin, 2008. Carbon isotopes in mollusk shell carbonates. Geo-Marine Letters, 28(5): 287-299.

Mook, W. G., 1968. Geochemistry of the stable carbon and oxygen isotopes of natural waters in the Netherlands. PhD thesis, University of Groningen, Groningen, 157 p.

Mook, W. G., J. C. Vogel, 1968. Isotopic equilibrium between shells and their environment. Science, 159(3817): 874-875.

Mook, W. G., 2000. Introduction, theory, methods and reviews. I.A.E.A., 1, 280 p.

Morris, T. J., L. D. Corkum, 1999. Unionid growth patterns in rivers of differing riparian vegetation. Freshwater Biology, 42(1): 59-68.

Muncaster, B. W., P. D. N. Hebert, R. Lazar, 1990. Biological and physical factors affecting the body burden of organic contaminants in freshwater mussels. Archives of Environmental Contamination and Toxicology, 19(1): 25-34.

Negus, C. L., 1966. A quantitative study of growth and production of unionid mussels in the river Thames at Reading. Journal of Animal Ecology, 35(3): 513-532.

Nichols, S. J., D. Garling, 2000. Food-web dynamics and trophic-level interactions in a multispecies community of freshwater unionids. Canadian Journal of Zoology, 78(5): 871-882.

Norum, U., V. W.-M. Lai, W. R. Cullen, 2005. Trace element distribution during the reproductive cycle of female and male spiny and Pacific scallops, with implications for biomonitoring. Marine Pollution Bulletin, 50(2): 175-184.

Ogi, M., K. Yamazaki, Y. Tachibana, 2003. Solar cycle modulation of the seasonal linkage of the North Atlantic Oscillation (NAO). Geophysical Research Letters, 30.

Oudhof, J. W. M., J. Dijkstra, A. A. A. Verhoeven, 2000. 'Huis Malburg' van spoor tot spoor - Een middeleeuwse nederzetting in Kerk-Avezaath. NS Railinfrabeheer B.V., Utrecht, 368 p.

Parmalee, P. W., W. E. Klippel, 1974. Freshwater mussels as a prehistoric food resource. American Antiquity, 39(3): 421-434.

Parmet, B., M. Burgdorffer, 1995. Extreme discharges of the Meuse in the Netherlands: 1993, 1995 and 2100 - Operational forecasting and long term expectations. Physics and Chemistry of The Earth, 20(5-6): 485-489.

Peacock, E., T. R. James, 2002. A prehistoric unionid assemblage from the Big Black River drainage in Hinds County, Mississippi. Journal of the Mississippi Academy of Sciences, 47(2): 121-125.

Pfister, L., J. Kwadijk, A. Musy, A. Bronstert, L. Hoffmann, 2004. Climate change, land use change and runoff prediction in the Rhine-Meuse basins. River Research and Applications, 20(3): 229-241.

Plug, I., J. C. C. Pistorius, 1999. Animal remains from industrial Iron Age communities in Phalaborwa, South Africa. African Archaeological Review, 16(3): 155-184.

Raikow, D. F., S. K. Hamilton, 2001. Bivalve diets in a Midwestern U.S. stream: A stable isotope enrichment study. Limnology and Oceanography, 46(3): 514-522.

Raith, A., W. T. Perkins, N. J. G. Pearce, T. E. Jeffries, 1996. Environmental monitoring on shellfish using UV laser ablation ICP-MS. Fresenius' Journal of Analytical Chemistry (Historical Archive), 355(7 - 8): 789-792.

Ravera, O., A. R. Sprocati, 1997. Population dynamics, production, assimilation and respiration of two fresh water mussels: *Unio mancus*, Zhadin and *Anodonta cygnea* Lam. Memorie dell'Istituto Italiano di Idrobiologia, 56: 113-130.

Ravera, O., G. M. Beone, R. Cenci, P. Lodigiani, 2003. Metal concentrations in *Unio pictorum mancus* (Mollusca, Lamellibranchia) from of 12 Northern Italian lakes in relation to their trophic level. Journal of Limnology, 62(2): 121-138.

Ricciardi, A., R. J. Neves, J. B. Rasmussen, 1998. Impending extinctions of North American freshwater mussels (Unionoida) following the Zebra Mussel (*Dreissena polymorpha*) invasion. Journal of Animal Ecology, 67(4): 613-619.

Ricken, W., T. Steuber, H. Freitag, M. Hirschfeld, B. Niedenzu, 2003. Recent and historical discharge of a large European river system - oxygen isotopic composition of river water and skeletal aragonite of Unionidae in the Rhine. Palaeogeography, Palaeoclimatology, Palaeoecology, 193(1): 73-86.

Ricken, W., T. Steuber, H. Erlenkeuser, H. Freitag, M. Hirschfeld, H. U. Kasper, M. Spitzlei, U. Ulbricht, 2004. Discharge evolution of the Rhine river during the last 200 years. Geophysical Research Abstracts, 6(00490). EGU General Assembly 2004, 25-30 April 2004, Nice, France.

Rodrigues, D., P. I. Abell, S. Kröpelin, 2000. Seasonality in the early Holocene climate of Northwest Sudan: interpretation of *Etheria elliptica* shell isotopic data. Global and Planetary Change, 26(1-3): 181-187.

Romanek, C. S., E. L. Grossman, J. W. Morse, 1992. Carbon isotopic fractionation in synthetic aragonite and calcite: Effects of temperature and precipitation rate. Geochimica et Cosmochimica Acta, 56(1): 419-430.

Ross, K. A., J. P. Thorpe, T. A. Norton, A. R. Brand, 2001. An assessment of some methods for tagging the great scallop, *Pecten maximus*. Journal of the Marine Biological Association of the United Kingdom, 81(6): 975-977.

Russell-Smith, J., D. Lucas, M. Gapindi, B. Gunbunuka, N. Kapirigi, G. Namingum, K. Lucas, P. Giuliani, G. Chaloupka, 1997. Aboriginal resource utilization and fire management practice in Western Arnhem Land, monsoonal Northern Australia: Notes for prehistory, lessons for the future. Human Ecology, 25(2): 159-195.

Rutten, M., N. van de Giesen, M. Baptist, J. Icke, W. Uijttewaal, 2008. Seasonal forecast of cooling water problems in the River Rhine. Hydrological Processes, 22(7): 1037-1045.

Schloesser, D. W., E. C. Masteller, 1999. Mortality of unionid bivalves (Mollusca) associated with dreissenid mussels (*Dreissena polymorpha* and *D. bugensis*) in Presque Isle Bay, Lake Erie. Northeastern Naturalist, 6(4): 341-352.

Schöne, B. R., K. Tanabe, D. L. Dettman, S. Sato, 2003. Environmental controls on shell growth rates and δ^{18}O of the shallow-marine bivalve mollusk *Phacosoma japonicum* in Japan. Marine Biology, V142(3): 473-485.

Schöne, B. R., A. D. Freyre Castro, J. Fiebig, S. D. Houk, W. Oschmann, I. Kroncke, 2004. Sea surface water temperatures over the period 1884-1983 reconstructed from oxygen isotope ratios of a bivalve mollusk shell (*Arctica islandica*, southern North Sea). Palaeogeography, Palaeoclimatology, Palaeoecology, 212(3-4): 215-232.

Schöne, B. R., J. Fiebig, M. Pfeiffer, R. Gleβ, J. Hickson, A. L. A. Johnson, W. Dreyer, W. Oschmann, 2005a. Climate records from a bivalved Methuselah (*Arctica islandica*, Mollusca; Iceland). Palaeogeography, Palaeoclimatology, Palaeoecology, 228(1-2): 130-148.

Schöne, B. R., M. Pfeiffer, T. Pohlmann, F. Siegismund, 2005b. A seasonally resolved bottom-water temperature record for the period AD 1866-2002 based on shells of *Arctica islandica* (Mollusca, North Sea). International Journal of Climatology, 25(7): 947-962.

Schöne, B. R., D. Surge, 2005. Looking back over skeletal diaries - High-resolution environmental reconstructions from accretionary hard parts of aquatic organisms. Palaeogeography, Palaeoclimatology, Palaeoecology, 228(1-2): 1-3.

Schöne, B. R., D. L. Rodland, J. Fiebig, W. Oschmann, D. Goodwin, K. W. Flessa, D. Dettman, 2006. Reliability of multitaxon, multiproxy reconstructions of environmental conditions from accretionary biogenic skeletons. The Journal of Geology, 114(3): 267-285.

Schöne, B. R., N. Page, D. Rodland, J. Fiebig, S. Baier, S. Helama, W. Oschmann, 2007. ENSO-coupled precipitation records (1959-2004) based on shells of freshwater bivalve mollusks (*Margaritifera falcata*) from British Columbia. International Journal of Earth Sciences, 96(3): 525-540.

Shabalova, M. V., A. F. V. van Engelen, 2003. Evaluation of a reconstruction of winter and summer temperatures in the Low Countries, AD 764–1998. Climatic Change, 58(1): 219-242.

Soldati, A. L., D. E. Jacob, B. R. Schöne, M. M. Bianchi, A. Hajduk, 2008. Seasonal periodicity of growth and composition in valves of *Diplodon chilensis patagonicus* (d'Orbigny, 1835). Journal of Molluscan Studies, 75: 75-85. 10.1093/mollus/eyn044

Stirling, H. P., I. Okumus, 1995. Growth and production of mussels (*Mytilus edulis* L.) suspended at salmon cages and shellfish farms in two Scottish sea lochs. Aquaculture, 134(3-4): 193-210.

Straile, D., D. M. Livingstone, G. A. Weyhenmeyer, D. G. George, 2003. The response of freshwater ecosystems to climate variability associated with the North Atlantic Oscillation, 263-279 p. In: The North Atlantic Oscillation: Climatic significance and environmental impact, American Geophysical Union, Volume 134.

Surge, D., K. C. Lohmann, D. L. Dettman, 2001. Controls on isotopic chemistry of the American oyster, *Crassostrea virginica*: implications for growth patterns. Palaeogeography, Palaeoclimatology, Palaeoecology, 172(3-4): 283-296.

TAW, 1995. Druk op de dijken 1995 - De toestand van de rivierdijken tijdens het hoogwater van januari-februari 1995, Delft.

Thébault, J., L. Chauvaud, J. Clavier, J. Guarini, R. B. Dunbar, R. Fichez, D. A. Mucciarone, E. Morize, 2007. Reconstruction of seasonal temperature variability in the tropical Pacific Ocean from the shell of the scallop, *Comptopallium radula*. Geochimica et Cosmochimica Acta, 71(4): 918-928.

Toland, H., B. Perkins, N. Pearce, F. Keenan, M. J. Leng, 2000. A study of sclerochronology by laser ablation ICP-MS. Journal of Analytical Atomic Spectrometry, 15(9): 1143-1148.

Trouet, V., J. Esper, N. E. Graham, A. Baker, J. D. Scourse, D. C. Frank, 2009. Persistent positive North Atlantic Oscillation mode dominated the Medieval Climate Anomaly. Science, 324(5923): 78-80. 10.1126/science.1166349

Tu, M., 2006. Assessment of the effects of climate variability and land use change on the hydrology of the Meuse river basin. PhD thesis, VU University Amsterdam, Amsterdam, 191 p.

Tudorancea, C., 1972. Studies on Unionidae populations from the Crapina-Jijila complex of pools (Danube zone liable to inundation). Hydrobiologia, 39(4): 527-561.

Tynan, S., S. Eggins, L. Kinsley, S. A. Welch, D. Kirste, 2005. Mussel shells as environmental tracers: an example from the Loveday Basin, Regolith 2005 - Ten Years of CRC LEME, Adelaide/Canberra.

Valdovinos, C., P. Pedreros, 2007. Geographic variations in shell growth rates of the mussel *Diplodon chilensis* from temperate lakes of Chile: Implications for biodiversity conservation. Limnologica - Ecology and Management of Inland Waters, 37(1): 63-75.

Van der Kamp, J. S., 2007. Vroege wacht - LR31 Zandweg: archeologisch onderzoek van twee eerste-eeuwse houten wachttorens in Leidsche Rijn. Sectie Cultuurhistorie gemeente Utrecht, Utrecht.

Van Geel, B., J. Buurman, H. T. Waterbolk, 1996. Archaeological and palaeoecological indications of an abrupt climate change in The Netherlands, and evidence for climatological teleconnections around 2650 BP. Journal of Quaternary Science, 11(6): 451-460.

Van Vliet, M. T. H., J. J. G. Zwolsman, 2008. Impact of summer droughts on the water quality of the Meuse river. Journal of Hydrology, 353(1-2): 1-17.

Vaughn, C. C., C. C. Hakenkamp, 2001. The functional role of burrowing bivalves in freshwater ecosystems. Freshwater Biology, 46(11): 1431-1446.

Veinott, G. I., R. J. Cornett, 1998. Carbon isotopic disequilibrium in the shell of the freshwater mussel *Elliptio complanata*. Applied Geochemistry, 13(1): 49-57.

Verdegaal, S., S. R. Troelstra, C. K. J. Beets, H. B. Vonhof, 2005. Stable isotopic records in unionid shells as a paleoenvironmental tool. Netherlands Journal of Geosciences - Geologie en Mijnbouw, 84(4): 403-408.

Versteegh, E. A. A., S. R. Troelstra, H. B. Vonhof, D. Kroon, 2009. Oxygen isotopic composition of bivalve seasonal growth increments and ambient water in the rivers Rhine and Meuse. Palaios, 24(8): 497-504. 10.2110/palo.2008. p08-071r

Wanamaker, A., K. Kreutz, B. Schöne, K. Maasch, A. Pershing, H. Borns, D. Introne, S. Feindel, 2009. A late Holocene paleo-productivity record in the western Gulf of Maine, USA, inferred from growth histories of the long-lived ocean quahog (*Arctica islandica*). International Journal of Earth Sciences, 98(1): 19-29.

Ward, P., 2009. Simulating discharge and sediment yield characteristics in the Meuse basin during the late Holocene and 21st Century. PhD thesis, VU University Amsterdam, Amsterdam, 173 p.

Ward, P. J., H. Renssen, J. C. J. H. Aerts, R. T. van Balen, J. Vandenberghe, 2008. Strong increases in flood frequency and discharge of the River Meuse over the late Holocene: impacts of long-term anthropogenic land use change and climate variability. Hydrology and Earth System Sciences, 12(1): 159 -175.

Williams, J. D., M. L. Warren, K. S. Cummings, J. L. Harris, R. J. Neves, 1993. Conservation status of freshwater mussels of the United States and Canada. Fisheries, 18(9): 6-22.

Witbaard, R., M. I. Jenness, K. van der Borg, G. Ganssen, 1994. Verification of annual growth increments in *Arctica islandica* L. from the North Sea by means of oxygen and carbon isotopes. Netherlands Journal of Sea Research, 33(1): 91-101.

Wu, H., J. Guiot, S. Brewer, Z. Guo, 2007. Climatic changes in Eurasia and Africa at the last glacial maximum and mid-Holocene: reconstruction from pollen data using inverse vegetation modelling. Climate Dynamics, 29(2): 211-229.

Zahner-Meike, E., J. M. Hanson, 2001. Effect of muskrat predation on naiads, 163-184 p. In: Bauer, G., K. Wächtler (eds.), Ecology and Evolution of the Freshwater Mussels Unionoida. Volume 145. Springer, Berlin.

Zeebe, R. E., D. Wolf-Gladrow, 2001. CO_2 in seawater: equilibrium, kinetics, isotopes. Elsevier, Amsterdam, 65, 346 p.

Appendices

Appendix 1: Monitoring water isotope data

Location	Date	δ¹³C	δ¹⁸O
Grave	22/05/2006	-14.60	-7.07
Grave	22/05/2006	-14.71	-7.04
Grave	01/06/2006	-14.31	-7.32
Grave	01/06/2006	-15.84	-7.21
Grave	15/06/2006	-15.31	-7.23
Grave	15/06/2006	-14.88	-7.28
Grave	29/06/2006	-13.54	-6.94
Grave	29/06/2006	-13.89	-6.89
Lith	06/07/2006	-13.32	-6.89
Lith	06/07/2006	-13.38	-6.86
Lith	14/07/2006	-11.26	-6.41
Lith	14/07/2006	-11.13	-6.35
Lith	27/07/2006	-11.16	-6.52
Lith	27/07/2006	-9.24	-6.38
Lith	10/08/2006	-11.21	-6.58
Lith	10/08/2006	-11.22	-6.41
Lith	24/08/2006	-10.80	-6.65
Lith	24/08/2006	-10.86	-6.56
Lith	07/09/2006	-11.12	-7.14
Lith	07/09/2006	-11.19	-7.14
Lith	21/09/2006	-9.26	-6.80
Lith	21/09/2006	-12.42	-6.68
Lith	05/10/2006	-10.92	-6.76
Lith	05/10/2006	-10.17	-6.64
Lith	19/10/2006	-10.97	
Lith	19/10/2006	-11.16	
Lith	02/11/2006	-11.30	-6.66
Lith	02/11/2006	-10.31	-6.60
Lith	16/11/2006	-11.43	-7.23
Lith	16/11/2006	-12.03	-7.08
Lith	30/11/2006	-12.10	-8.07
Lith	30/11/2006	-12.27	-7.94
Lith	14/12/2006		-7.86
Lith	14/12/2006		-7.91
Lith	28/12/2006	-10.61	-7.81
Lith	28/12/2006		-8.14
Lith	11/01/2007	-11.40	-7.38
Lith	11/01/2007	-11.25	-7.57
Lith	25/01/2007	-11.51	-7.13
Lith	25/01/2007	-11.77	-6.81
Lith	09/02/2007	-11.97	-7.28

Location	Date	δ¹³C	δ¹⁸O
Lith	09/02/2007	-12.14	-7.41
Lith	22/02/2007	-12.04	-7.64
Lith	22/02/2007	-11.86	-7.64
Lith	08/03/2007	-12.45	-7.64
Lith	08/03/2007	-12.15	-7.50
Lith	22/03/2007	-11.31	-7.37
Lith	22/03/2007	-11.44	-7.41
Lith	05/04/2007	-10.98	-7.46
Lith	05/04/2007	-11.09	-7.40
Lith	19/04/2007	-11.05	-7.53
Lith	19/04/2007	-10.78	-7.45
Lith	03/05/2007	-10.48	-7.12
Lith	03/05/2007	-10.10	-7.05
Lith	17/05/2007	-10.90	-6.68
Lith	17/05/2007	-10.54	-6.81
Lith	31/05/2007	-11.42	-6.69
Lith	31/05/2007	-11.36	-6.69
Lith	13/06/2007	-11.18	-6.52
Lith	13/06/2007	-11.41	-6.57
Lith	27/06/2007	-12.16	-6.53
Lith	27/06/2007	-11.84	-6.48
Lith	12/07/2007	-13.96	
Lith	12/07/2007	-15.09	
Hagestein	15/12/2005	-11.14	-8.82
Hagestein	15/12/2005	-11.13	-8.41
Hagestein	15/12/2005		-8.34
Hagestein	13/01/2006	-10.61	-8.14
Hagestein	13/01/2006	-10.79	-8.09
Hagestein	13/01/2006	-13.93	-8.11
Hagestein	13/01/2006	-13.43	-8.09
Hagestein	26/01/2006	-11.31	-8.33
Hagestein	26/01/2006	-10.89	-8.38
Hagestein	09/02/2006	-12.79	-8.08
Hagestein	09/02/2006	-13.65	-8.07
Hagestein	09/02/2006	-11.25	-8.28
Hagestein	09/02/2006	-11.05	-8.33
Hagestein	23/02/2006	-11.58	-8.81
Hagestein	23/02/2006	-11.02	-8.70
Hagestein	23/02/2006	-10.77	-8.76
Hagestein	23/02/2006	-11.83	-8.77
Hagestein	09/03/2006	-10.95	-8.60

Location	Date	δ¹³C	δ¹⁸O
Hagestein	09/03/2006	-11.05	-8.55
Hagestein	09/03/2006	-11.00	-9.01
Hagestein	09/03/2006	-10.93	-8.92
Hagestein	23/03/2006	-11.03	-9.16
Hagestein	23/03/2006	-11.13	-9.12
Hagestein	23/03/2006	-12.25	-9.04
Hagestein	23/03/2006	-12.16	-9.09
Hagestein	06/04/2006	-11.23	-9.14
Hagestein	06/04/2006	-11.91	-8.95
Hagestein	06/04/2006	-11.28	-9.17
Hagestein	06/04/2006	-11.54	-9.14
Hagestein	20/04/2006	-13.53	-9.08
Hagestein	20/04/2006	-13.45	-9.05
Hagestein	04/05/2006	-12.46	-9.09
Hagestein	04/05/2006	-12.73	-9.00
Hagestein	18/05/2006	-12.20	-9.88
Hagestein	18/05/2006	-12.63	-9.94
Hagestein	01/06/2006	-13.15	-9.29
Hagestein	01/06/2006	-13.68	-9.35
Hagestein	15/06/2006	-13.21	-9.93
Hagestein	15/06/2006	-13.05	-10.04
Hagestein	29/06/2006		-9.85
Hagestein	29/06/2006		-9.80
Hagestein	14/07/2006	-9.01	-9.37
Hagestein	14/07/2006	-8.58	-9.36
Hagestein	27/07/2006	-9.30	-9.39
Hagestein	27/07/2006	-8.95	-9.44
Hagestein	10/08/2006	-10.69	-9.50
Hagestein	10/08/2006	-10.36	-9.54
Hagestein	24/08/2006	-9.97	-9.21
Hagestein	24/08/2006	-9.87	-9.26
Hagestein	07/09/2006	-10.40	-9.33
Hagestein	07/09/2006	-10.25	-9.40
Hagestein	21/09/2006	-10.31	-9.09
Hagestein	21/09/2006	-9.85	-9.08
Hagestein	05/10/2006	-9.31	-9.17
Hagestein	05/10/2006	-10.34	-9.31
Hagestein	19/10/2006	-12.13	
Hagestein	19/10/2006	-12.58	
Hagestein	02/11/2006	-8.40	-8.69
Hagestein	02/11/2006	-9.07	-8.86
Hagestein	16/11/2006	-10.78	-9.64
Hagestein	16/11/2006	-11.63	

Appendix 2: Monitoring shell isotope data

Location	Date	δ¹³C	δ¹⁸O
Hagestein	30/11/2006	-11.68	-9.30
Hagestein	30/11/2006	-11.88	-9.32
Hagestein	14/12/2006	-11.27	-9.85
Hagestein	14/12/2006	-11.30	-9.50
Hagestein	28/12/2006	-11.60	-9.65
Hagestein	28/12/2006	-12.03	-9.66
Hagestein	11/01/2007	-10.87	-8.17
Hagestein	11/01/2007	-10.89	-8.09
Hagestein	25/01/2007	-11.07	-7.89
Hagestein	25/01/2007	-10.87	
Hagestein	09/02/2007	-10.62	-8.30
Hagestein	09/02/2007	-10.70	-8.30
Hagestein	22/02/2007	-11.60	-8.38
Hagestein	22/02/2007	-12.10	-8.51
Hagestein	08/03/2007	-11.65	-8.39
Hagestein	08/03/2007	-12.34	-8.36
Hagestein	22/03/2007	-10.64	-8.57
Hagestein	22/03/2007	-11.31	-8.58
Hagestein	05/04/2007	-12.59	-8.71
Hagestein	05/04/2007	-12.44	-8.80
Hagestein	19/04/2007	-10.67	-9.01
Hagestein	19/04/2007	-10.73	-8.92
Hagestein	03/05/2007	-8.98	-8.69
Hagestein	03/05/2007	-8.95	-8.69
Hagestein	17/05/2007	-9.66	-8.64
Hagestein	17/05/2007	-9.78	-8.11
Hagestein	31/05/2007	-10.35	-8.41
Hagestein	31/05/2007	-10.56	-8.38
Hagestein	13/06/2007	-10.66	-8.87
Hagestein	13/06/2007	-11.01	-8.87
Hagestein	27/06/2007	-11.06	-8.54
Hagestein	27/06/2007	-11.56	-8.67

3110 *Unio tumidus*

Sample #	δ¹³C	δ¹⁸O	Distance from umbo (mm)
1	-9.95	-8.69	54.00
2	-10.31	-9.03	53.95
4	-12.47	-9.81	53.84
5	-12.49	-9.90	53.79
6	-12.66	-10.01	53.73
14	-11.13	-9.19	53.31
18	-10.52	-6.49	53.09
20	-10.01	-7.64	52.99
22	-11.15	-8.23	52.88
24	-13.73	-8.95	52.47
26	-11.63	-9.26	52.06
27	-11.80	-9.22	51.85
30	-12.51	-7.20	51.23
31	-13.60	-6.10	51.03
32	-13.12	-4.61	50.82

3114 *Unio pictorum*

Sample #	δ¹³C	δ¹⁸O	Distance from umbo (mm)
1	-9.72	-8.90	39.00
2	-9.74	-9.43	38.95
3	-12.26	-8.91	38.90
4	-12.43	-8.79	38.85
5	-12.92	-8.70	38.80
6	-13.04	-8.89	38.75
7	-13.59	-8.41	38.69
8	-12.96	-7.67	38.64
9	-12.11	-7.59	38.59
10	-12.80	-7.94	38.54
11	-13.37	-7.76	38.49
12	-11.40	-7.38	38.44
13	-10.27	-7.54	38.39
14	-11.42	-8.74	38.34
15	-10.78	-8.65	38.29
16	-10.02	-8.78	38.24
17	-10.31	-8.77	38.18
18	-10.10	-9.40	38.13
19	-11.62	-9.49	38.08
20	-11.75	-9.60	38.03

3114 *Unio pictorum*

Sample #	δ¹³C	δ¹⁸O	Distance from umbo (mm)
21	-12.54	-9.84	37.98
22	-12.76	-9.81	37.93
23	-12.71	-9.83	37.88
24	-12.55	-9.98	37.83
25	-13.35	-9.75	37.77
26	-14.02	-9.77	37.71
27	-14.02	-9.92	37.66
28	-13.69	-9.76	37.60
29	-13.57	-9.67	37.54
30	-13.79	-9.52	37.48
31	-12.52	-9.74	37.43
32	-12.72	-9.37	37.37
33	-13.50	-9.10	37.31
34	-14.18	-8.89	37.26
35	-13.76	-8.76	37.20
36	-13.98	-8.71	37.14
37	-13.45	-8.80	37.09
38	-13.42	-9.02	37.03
39	-13.60	-8.91	36.97
40	-13.07	-7.92	36.91
41	-12.72	-7.61	36.86
42	-11.85	-7.98	36.80
43	-11.14	-7.73	36.74
44	-11.11	-7.60	36.69
45	-10.94	-8.73	36.63
46	-11.13	-9.31	36.57

3115 *Unio pictorum*

sample #	δ¹³C	δ¹⁸O	Distance from umbo (mm)
1	-9.68	-8.32	50.00
2	-9.72	-7.97	49.91
3	-9.25	-8.97	49.83
4	-9.10	-9.36	49.74
5	-9.74	-9.14	49.66
6	-10.82	-8.30	49.57
7	-11.33	-7.70	49.48
8	-10.21	-7.23	49.40
9	-9.94	-7.96	49.31

3115 *Unio pictorum*

sample #	δ¹³C	δ¹⁸O	Distance from umbo (mm)
10	-9.86	-7.97	49.23
11	-10.01	-8.49	49.14
12	-10.30	-8.96	49.05
13	-9.97	-8.13	48.97
14	-10.20	-8.01	48.88
15	-10.85	-7.03	48.80
16	-11.12	-5.99	48.71
17	-11.82	-5.71	48.62
18	-12.84	-5.74	48.54
19	-13.98	-5.58	48.45
20	-12.95	-5.19	48.37
21	-10.37	-5.93	48.28
22	-9.91	-7.38	48.19
23	-10.18	-7.83	48.09
24	-9.22	-8.60	47.99
25	-10.19	-8.84	47.89
26	-10.12	-8.42	47.78
27	-10.16	-8.52	47.68
28	-10.04	-8.45	47.58
29	-9.75	-8.03	47.47
30	-9.92	-7.98	47.37
31	-10.08	-8.25	47.27
32	-10.18	-8.55	47.16
33	-10.21	-8.82	47.06
34	-10.19	-8.62	46.96
35	-11.19	-7.50	46.85
36	-11.59	-7.45	46.75
37	-11.59	-6.82	46.65
38	-11.00	-7.11	46.55
39	-11.49	-6.67	46.44
40	-12.00	-6.54	46.34
41	-11.83	-6.68	46.24
42	-11.03	-6.77	46.13
43	-10.36	-7.68	46.03

3117 *Unio pictorum*

Sample #	δ¹³C	δ¹⁸O	Distance from umbo (mm)
1	-9.87	-7.02	39.00
2	-10.17	-8.40	38.95
4	-10.38	-9.05	38.84

3117 *Unio pictorum*

Sample #	δ¹³C	δ¹⁸O	Distance from umbo (mm)
5	-10.52	-8.79	38.79
6	-10.46	-8.95	38.74
7	-10.54	-9.02	38.68
8	-10.77	-9.50	38.63
14	-12.34	-10.04	38.32
15	-12.79	-10.13	38.26
16	-12.83	-9.62	38.21
17	-13.04	-9.51	38.16
18	-13.02	-9.74	38.11
21	-12.46	-10.13	37.97
22	-12.18	-9.73	37.92
23	-12.22	-9.85	37.88
25	-12.62	-9.71	37.78
28	-13.25	-9.71	37.64
30	-13.46	-9.62	37.55
34	-13.27	-9.29	37.36
35	-13.09	-9.28	37.31
38	-13.15	-8.80	37.17
40	-13.36	-8.73	37.08
42	-13.18	-8.21	36.98
43	-13.05	-7.99	36.93
44	-13.10	-8.14	36.89
46	-13.18	-7.92	36.79
50	-12.03	-7.31	36.60
52	-9.97	-8.29	36.51
53	-10.84	-7.78	36.46
56	-10.46	-8.02	36.32
57	-10.78	-5.65	35.96
58	-10.84	-9.28	35.59
59	-11.18	-7.50	35.23
60	-10.27	-5.17	34.86
61	-10.72	-8.63	34.50
62	-10.86	-8.77	34.14
63	-11.38	-8.78	33.77
64	-11.96	-8.76	33.41
65	-12.25	-9.05	33.04
66	-12.03	-8.73	32.68
67	-11.55	-8.82	32.31
68	-12.22	-9.31	31.95
69	-12.14	-9.52	31.58
70	-12.64	-9.62	31.22

3117 *Unio pictorum*

Sample #	δ¹³C	δ¹⁸O	Distance from umbo (mm)
71	-12.04	-8.91	30.85
72	-11.95	-8.80	30.49
73	-12.47	-8.37	30.13
74	-12.55	-7.87	29.76
75	-12.48	-7.50	29.40
77	-12.62	-6.38	28.67
78	-12.90	-6.57	28.30
79	-13.67	-5.90	27.94
80	-13.32	-5.32	27.57
81	-11.09	-5.66	27.21
82	-10.79	-6.99	26.84
83	-11.17	-7.90	26.48
84	-10.87	-7.91	26.12
85	-10.81	-7.77	25.75
86	-10.64	-7.73	25.39
87	-10.42	-8.69	25.02
88	-10.83	-8.88	24.66
89	-11.08	-9.06	24.29
90	-11.17	-8.74	23.93
91	-11.36	-8.46	23.56
92	-10.55	-7.47	23.20
93	-9.97	-7.77	22.83
94	-10.11	-8.41	22.47
95	-10.29	-8.50	22.11
96	-10.20	-9.29	21.74
97	-10.21	-9.26	21.38
98	-10.38	-9.10	21.01
99	-10.80	-9.03	20.65
100	-11.30	-9.27	20.28
101	-11.13	-9.06	19.92
102	-11.07	-8.57	19.55
103	-12.03	-8.13	19.19
104	-12.19	-7.92	18.82
105	-12.19	-7.71	18.46
106	-13.18	-7.18	18.10
107	-12.23	-6.66	17.73
108	-11.04	-7.75	17.37
109	-10.80	-8.28	17.00

3119 Unio tumidus

Sample #	δ¹³C	δ¹⁸O	Distance from umbo (mm)
2	-10.23	-8.57	33.80
3	-10.26	-9.23	33.60
4	-12.33	-10.14	33.39
5	-13.08	-9.88	33.18
6	-11.59	-10.78	32.96
7	-11.67	-9.54	32.68
8	-12.04	-8.02	32.39
9	-10.93	-7.43	32.17

3129 Unio tumidus

Sample #	δ¹³C	δ¹⁸O	Distance from umbo (mm)
1	-10.43	-8.49	43.00
2	-10.65	-8.47	42.93
3	-10.26	-8.29	42.86
4	-9.31	-8.74	42.79
5	-9.98	-8.99	42.72
6	-10.27	-9.37	42.65
7	-10.01	-10.08	42.59
9	-10.13	-9.65	42.45
10	-10.13	-9.33	42.38
11	-10.66	-9.06	42.31
12	-9.79	-7.91	42.24
13	-11.21	-8.00	42.17
14	-11.65	-7.80	42.10
15	-11.11	-7.04	42.03
16	-10.66	-6.40	41.96
17	-10.22	-6.61	41.89
18	-9.58	-7.59	41.83
19	-9.62	-8.82	41.76
20	-10.26	-8.60	41.66
21	-10.19	-7.63	41.57
22	-10.36	-8.46	41.48

3135 Anodonta anatina

Sample #	δ¹³C	δ¹⁸O	Distance from umbo (mm)
1	-11.11	-9.16	26.00
2	-10.98	-9.48	25.10
3	-11.20	-9.53	23.46
4	-12.08	-9.32	21.77

3135 Anodonta anatina

Sample #	δ¹³C	δ¹⁸O	Distance from umbo (mm)
5	-11.54	-9.28	20.15

3149 Unio pictorum

Sample #	δ¹³C	δ¹⁸O	Distance from umbo (mm)
1	-12.07	-6.55	43.00
2	-13.34	-6.51	42.91
3	-8.03	-3.85	42.82
4	-9.50	-3.12	42.73
5	-8.63	-0.76	42.63
6	-7.89	-1.46	42.54
7	-7.70	-2.13	42.45
8	-8.13	-1.85	42.37
9	-8.99	-1.81	42.28
10	-7.98	-2.75	42.20
11	-7.67	-2.46	42.12
12	-9.15	-4.22	42.03
13	-9.40	-2.75	41.94
14	-8.85	-3.40	41.86

3153 Unio pictorum

Sample #	δ¹³C	δ¹⁸O	Distance from umbo (mm)
1	-11.24	-6.54	47
2	-12.2	-6.69	46.95
3	-12.29	-6.45	46.91
4	-10.3	-5.61	46.86
5	-10.46	-4.86	46.82
6	-10.04	-3.8	46.77
7	-9.7	-4.34	46.73
8	-8.29	-2.28	46.68
9	-7.58	-1.89	46.65
10	-7.62	-2.36	46.62
11	-7.68	-2.97	46.59
12	-8.81	-5.38	46.56
13	-7.79	-4.34	46.54
14	-9.66	-6.46	46.5
15	-7.59	-3.98	46.47
16	-7.73	-2.14	46.44
17	-8.72	-2.5	46.41
18	-9.51	-6.88	46.37

3153 Unio pictorum

Sample #	δ¹³C	δ¹⁸O	Distance from umbo (mm)
19	-9.52	-6	46.34

3170 Unio pictorum

Sample #	δ¹³C	δ¹⁸O	Distance from umbo (mm)
1	-9.57	-4.23	44.00
2	-9.28	-3.33	43.95
3	-8.88	-1.89	43.90
4	-8.19	-1.35	43.85
5	-8.03	-1.62	43.80
6	-7.32	-0.26	43.75
7	-7.41	-2.28	43.70
8	-7.77	-2.12	43.65
9	-8.69	-2.35	43.60
10	-8.35	-2.10	43.50
11	-7.28	-3.26	43.40
12	-5.85	-1.95	43.30
13	-7.65	-4.28	43.21
14	-8.79	-3.29	43.11
15	-8.67	-2.45	43.01
16	-8.00	-2.88	42.91
17	-7.61	-2.80	42.81
18	-9.46	-4.37	42.71
19	-9.38	-4.03	42.62
20	-8.85	-3.30	42.52
21	-8.20	-3.05	42.41
22	-7.94	-1.37	42.31
23	-9.40	-1.91	42.22
28	-9.02	-3.10	41.52
29	-9.21	-3.58	41.40
30	-7.92	-2.74	41.28
31	-8.47	-3.98	41.16
32	-9.22	-5.65	41.06
33	-8.00	-5.33	40.94
34	-7.02	-4.51	40.83
35	-8.11	-4.19	40.72
36	-7.32	-3.05	40.59
37	-7.61	-4.80	40.46
38	-7.42	-5.52	40.32
39	-7.54	-4.07	40.20
40	-8.08	-4.53	40.08

3170 *Unio pictorum*			
Sample #	$\delta^{13}C$	$\delta^{18}O$	Distance from umbo (mm)
41	-8.01	-5.17	39.97
42	-7.82	-5.69	39.81
43	-8.43	-6.51	39.66
44	-8.29	-6.45	39.50
45	-7.73	-6.05	39.35
46	-8.04	-6.13	39.20
47	-8.93	-7.11	39.05
48	-9.10	-7.19	38.89
49	-8.08	-6.41	38.73
50	-7.07	-6.06	38.57
51	-6.44	-5.36	38.41
52	-6.92	-3.02	38.25
53	-7.83	-3.78	38.10
54	-7.66	-4.44	37.94
55	-7.12	-4.59	37.77
56	-6.75	-3.58	37.62
57	-6.80	-3.24	37.46
58	-6.59	-2.24	37.30
59	-6.29	-2.95	37.15
60	-6.40	-4.07	37.00
61	-6.06	-4.68	36.87
62	-6.32	-5.19	36.72
63	-7.06	-4.90	36.58
64	-7.70	-5.26	36.45
65	-7.31	-4.09	36.31
66	-6.38	-2.03	36.18
67	-7.92	-2.45	36.02
68	-7.70	-2.77	35.87
69	-8.09	-3.69	35.71
70	-8.95	-4.39	35.55
71	-8.95	-4.84	35.39
72	-8.17	-5.11	35.24
73	-9.02	-5.24	35.09
74	-9.39	-5.69	34.93
75	-9.33	-6.34	34.73
76	-9.78	-6.49	34.51
77	-9.42	-6.57	34.29
78	-9.80	-6.43	34.08
79	-9.87	-6.34	33.87
80	-9.49	-5.84	33.66
81	-9.08	-5.99	33.44

3170 *Unio pictorum*			
Sample #	$\delta^{13}C$	$\delta^{18}O$	Distance from umbo (mm)
82	-9.57	-6.38	33.23
83	-9.62	-6.46	33.01
84	-10.27	-7.07	32.80
86	-9.48	-6.19	32.31
87	-9.69	-5.96	32.06
88	-9.79	-5.79	31.81
89	-9.66	-5.63	31.56
90	-10.24	-5.11	31.32
91	-9.52	-4.17	31.12
92	-8.70	-3.66	30.91
93	-8.23	-3.76	30.71
94	-8.58	-4.06	30.51
95	-8.96	-4.37	30.31
96	-8.31	-4.72	30.03
97	-7.84	-5.39	29.76
98	-8.19	-5.72	29.49
99	-8.41	-6.65	29.21
100	-9.15	-6.65	28.94
101	-9.09	-6.35	28.67
102	-10.07	-6.59	28.38
103	-10.41	-6.20	28.21
104	-8.67	-4.44	28.03
105	-7.50	-3.34	27.85
106	-7.18	-2.75	27.68
107	-6.82	-3.56	27.50
108	-6.50	-3.51	27.33
109	-6.84	-3.79	27.16
110	-7.05	-4.10	26.93
111	-7.53	-4.55	26.69
112	-7.46	-4.84	26.45
113	-7.59	-5.56	26.22
114	-7.85	-5.75	25.99
115	-8.16	-5.99	25.75
116	-8.12	-5.51	25.51
117	-7.61	-4.77	25.28
118	-7.02	-4.60	25.05
119	-6.92	-4.73	24.75
120	-7.40	-4.88	24.47
121	-7.10	-5.08	24.18
122	-6.58	-5.19	23.89
123	-6.94	-5.87	23.60

3170 *Unio pictorum*			
Sample #	$\delta^{13}C$	$\delta^{18}O$	Distance from umbo (mm)
124	-6.95	-6.08	23.22
125	-6.83	-5.87	22.84
126	-6.72	-5.82	22.45
127	-6.80	-5.80	22.06
128	-6.79	-6.31	21.68
129	-6.80	-6.42	21.37
130	-6.76	-6.48	21.06
131	-6.82	-6.70	20.76
132	-7.01	-6.49	20.45
133	-7.87	-7.01	20.14
134	-7.06	-6.12	19.82
135	-7.29	-5.04	19.51
136	-6.60	-4.40	19.20
137	-6.70	-4.69	18.97
138	-6.79	-4.93	18.73
139	-6.74	-4.45	18.49
140	-6.84	-4.65	18.26
141	-6.60	-4.70	18.02
142	-6.52	-4.80	17.79
143	-6.70	-5.34	17.54
144	-6.34	-4.85	17.30
145	-6.22	-4.43	17.06
146	-6.47	-4.27	16.82
147	-6.60	-3.98	16.57
148	-6.86	-4.74	16.25
149	-6.96	-5.21	15.93
150	-7.13	-5.33	15.61
151	-7.03	-5.26	15.30
152	-7.25	-5.58	14.98
153	-7.41	-5.83	14.66
154	-6.97	-5.73	14.34
155	-6.47	-5.85	13.82
156	-6.45	-5.57	13.28
157	-5.46	-7.90	12.76

3172 *Unio pictorum*			
Sample #	$\delta^{13}C$	$\delta^{18}O$	Distance from umbo (mm)
1	-11.37	-6.38	44.00
2	-12.04	-6.76	43.77
3	-12.30	-6.07	43.55

Appendix 3: Modern shell isotope data

3172 *Unio pictorum*

Sample #	δ¹³C	δ¹⁸O	Distance from umbo (mm)
4	-12.45	-6.66	43.33
5	-12.94	-6.53	43.09
6	-13.02	-6.40	42.87
7	-9.41	-4.28	42.64
8	-8.30	-2.59	42.55
9	-10.14	-2.84	42.46
10	-9.60	-1.97	42.37
11	-8.44	-1.23	42.28

Beegden 1918 *Unio tumidus*

Sample #	δ¹³C	δ¹⁸O	Distance from umbo (mm)
1	-10.90	-6.10	68.00
2	-10.93	-6.20	67.81
3	-10.41	-5.76	67.63
4	-9.92	-5.70	67.44
6	-10.07	-5.99	67.06
7	-10.25	-5.90	66.86
8	-10.18	-5.70	66.67
9	-10.53	-6.01	66.48
10	-10.52	-5.80	66.28
11	-9.84	-5.90	66.10
12	-10.17	-5.83	65.90
13	-10.25	-5.85	65.55
14	-10.58	-5.91	65.36
15	-10.37	-5.76	65.18
16	-10.21	-5.59	64.99
17	-11.38	-5.90	64.81
18	-11.05	-6.25	64.63
19	-10.50	-6.13	64.45
20	-10.78	-5.44	64.27
21	-11.33	-6.33	64.08
22	-10.46	-6.57	63.90
23	-10.40	-5.80	63.72
24	-11.76	-5.86	63.53
25	-11.81	-6.26	63.36
26	-10.91	-6.31	63.20
27	-10.75	-6.17	63.03
28	-10.63	-5.68	62.87
29	-11.16	-5.88	62.71
30	-11.12	-6.40	62.53
32	-9.82	-5.55	62.21
34	-10.35	-6.36	61.89
35	-9.98	-5.67	61.72
36	-10.38	-5.21	61.56
37	-11.48	-5.85	61.39
38	-11.91	-6.07	61.25
40	-11.48	-7.06	60.96
42	-10.15	-6.19	60.67
43	-10.50	-5.53	60.53
44	-10.89	-5.64	60.39

Beegden 1918 *Unio tumidus*

Sample #	δ¹³C	δ¹⁸O	Distance from umbo (mm)
45	-11.98	-6.11	60.25
46	-12.47	-6.31	60.10
48	-10.64	-5.93	59.82
49	-10.43	-6.21	59.68
50	-10.53	-6.31	59.54
51	-10.28	-5.63	59.39
52	-10.06	-4.78	59.25
53	-11.35	-5.63	59.12
54	-11.91	-6.03	58.98
56	-12.76	-6.33	58.69
58	-10.94	-6.76	58.40
59	-10.73	-6.32	58.27
60	-10.02	-5.99	58.12
62	-9.77	-4.97	57.84
63	-11.00	-5.62	57.69
64	-11.54	-6.04	57.57
65	-11.97	-6.30	57.45
66	-12.08	-6.49	57.33
68	-11.69	-6.61	57.09
69	-11.35	-6.31	56.96
70	-10.79	-6.15	56.83
72	-9.89	-5.92	56.58
74	-9.98	-5.29	56.33
75	-10.91	-5.59	56.21
76	-11.04	-5.97	56.06
77	-12.25	-6.63	55.91
78	-12.10	-6.40	55.76
79	-13.01	-6.68	55.61
80	-12.84	-6.83	55.47
81	-13.31	-7.00	55.31
82	-12.80	-6.84	55.17
83	-11.80	-6.86	55.02
84	-11.48	-6.96	54.88
85	-11.46	-7.04	54.73
86	-11.46	-6.89	54.59
87	-11.24	-6.79	54.43
88	-10.81	-6.48	54.29
90	-10.22	-5.72	53.99
91	-10.40	-6.03	53.85

Beegden 1918 *Unio tumidus*

Sample #	δ¹³C	δ¹⁸O	Distance from umbo (mm)
92	-10.73	-5.85	53.70
93	-11.89	-6.31	53.55
94	-11.26	-7.10	53.41
96	-11.01	-6.98	53.12
98	-10.06	-6.65	52.84
99	-11.39	-6.51	52.70
100	-11.07	-6.52	52.56
101	-11.18	-6.51	52.42
102	-11.32	-6.29	52.28
104	-11.15	-6.73	52.00
105	-11.44	-6.82	51.86
106	-10.24	-6.86	51.72
108	-8.51	-6.46	51.43
110	-10.36	-5.09	51.15
114	-12.24	-5.77	50.53
116	-12.21	-6.14	50.20
124	-11.77	-6.71	48.93
126	-10.26	-6.00	48.61
128	-10.08	-6.13	48.27
130	-10.12	-6.46	47.89
132	-9.36	-6.57	47.51
134	-9.01	-6.58	47.13
136	-9.08	-6.14	46.77
138	-9.40	-6.18	46.40
142	-8.84	-6.20	45.66
146	-9.38	-6.11	44.93
148	-10.20	-5.29	44.55

Bergen 1918 *Unio crassus nanus*

Sample #	δ¹³C	δ¹⁸O	Distance from umbo (mm)
1	-10.98	-6.32	34.00
2	-12.04	-6.70	33.63
3	-11.92	-6.77	33.24
4	-12.30	-6.60	32.85
5	-11.60	-6.59	32.48
6	-11.74	-6.44	32.11
7	-12.44	-6.88	31.77
8	-12.21	-6.60	31.42
9	-11.35	-5.62	31.07
10	-13.80	-7.33	30.71

Bergen 1918 *Unio crassus nanus*

Sample #	δ¹³C	δ¹⁸O	Distance from umbo (mm)
11	-12.41	-6.75	30.35
12	-10.94	-5.55	29.99
13	-13.60	-6.91	29.60
14	-12.73	-7.24	29.19
15	-12.38	-7.47	28.79
16	-11.98	-6.93	28.40
17	-11.05	-5.25	28.00
18	-11.86	-5.92	27.63
19	-11.97	-6.14	27.26
20	-12.24	-6.50	26.90
21	-11.19	-7.01	26.53
22	-11.54	-7.18	26.17
23	-11.43	-6.70	25.80
24	-11.58	-6.88	25.42
25	-12.41	-6.51	25.04
26	-12.32	-5.81	24.66
27	-12.04	-5.57	24.29
28	-12.19	-5.97	23.94
29	-12.62	-6.48	23.61
30	-11.81	-6.43	23.07
31	-11.48	-6.43	22.51
32	-11.40	-6.86	21.92
33	-11.20	-6.62	21.41
34	-12.28	-7.18	20.94
35	-12.19	-6.47	20.57
36	-14.25	-6.57	20.16
37	-11.48	-5.53	19.69
38	-11.36	-6.27	19.18
39	-10.93	-6.45	18.65
40	-10.40	-6.46	18.11
41	-10.17	-6.72	17.59
42	-9.91	-6.95	17.11
43	-10.01	-7.04	16.67
44	-11.36	-7.16	16.25
45	-11.20	-6.68	15.83
46	-12.38	-6.68	15.41
47	-13.56	-5.98	14.99
48	-11.13	-5.56	14.59
49	-11.87	-6.55	14.20
50	-10.39	-6.47	13.72
51	-9.74	-5.91	13.25

Bergen 1918 *Unio crassus nanus*

Sample #	δ¹³C	δ¹⁸O	Distance from umbo (mm)
52	-9.66	-6.63	12.78

Vierlingsbeek 1977 *Unio pictorum*

Sample #	δ¹³C	δ¹⁸O	Distance from umbo (mm)
1	-9.85	-6.46	52.00
2	-9.05	-6.07	51.84
3	-8.83	-6.21	51.69
4	-9.21	-6.51	51.54
5	-9.65	-6.47	51.38
6	-9.95	-6.53	51.23
7	-9.98	-5.89	51.07
8	-9.89	-6.16	50.92
9	-8.90	-5.76	50.77
10	-8.56	-6.08	50.61
11	-8.63	-6.10	50.46
12	-8.69	-5.81	50.30
13	-9.49	-5.86	50.14
14	-9.01	-5.92	49.98
15	-8.13	-6.55	49.82
16	-8.80	-6.54	49.69
17	-8.61	-6.93	49.55
18	-8.83	-6.95	49.41
19	-9.16	-6.75	49.27
20	-9.52	-6.78	49.12
21	-9.49	-6.46	48.99
22	-9.58	-6.09	48.85
23	-9.82	-5.84	48.70
24	-9.64	-5.38	48.56
25	-9.59	-5.97	48.42
26	-9.99	-6.16	48.28
27	-10.01	-6.12	48.13
28	-9.73	-6.24	47.99
29	-9.62	-6.41	47.85
30	-9.80	-6.58	47.71
31	-9.15	-6.59	47.57
32	-9.03	-6.74	47.43
33	-9.03	-6.71	47.28
34	-9.41	-6.52	47.14
35	-9.02	-6.17	47.00
36	-9.22	-6.28	46.85

Vierlingsbeek 1977 *Unio pictorum*			
Sample #	δ¹³C	δ¹⁸O	Distance from umbo (mm)
37	-10.61	-6.69	46.71
39	-9.87	-5.89	46.43
40	-9.29	-5.21	46.29
41	-8.98	-5.24	46.15
42	-8.69	-5.54	46.01
43	-8.93	-5.95	45.63
44	-8.57	-5.50	45.25
45	-9.05	-6.72	44.87
46	-9.34	-6.68	44.50
47	-10.13	-7.21	44.12
48	-9.98	-6.77	43.74
49	-9.81	-6.87	43.36
50	-9.60	-6.80	42.98
51	-9.49	-6.72	42.60
52	-9.45	-6.87	42.22
53	-9.58	-7.17	41.85
55	-9.76	-6.39	41.28
56	-9.51	-6.06	40.98
57	-9.56	-6.61	40.70
58	-10.07	-6.45	40.38
59	-10.01	-6.49	40.05
60	-10.28	-6.37	39.72
61	-9.73	-5.30	39.39
62	-9.79	-5.36	39.07
63	-10.01	-5.87	38.69
64	-10.19	-6.15	38.32
65	-10.24	-6.30	37.93
66	-10.19	-6.61	37.55
67	-10.11	-6.61	37.18
68	-10.07	-6.66	36.80
69	-10.07	-6.54	36.43
70	-9.80	-6.85	36.05
71	-9.67	-6.89	35.67
72	-9.86	-6.95	35.33
73	-10.07	-6.77	35.00
74	-10.40	-6.57	34.66
75	-9.86	-6.79	34.33
76	-9.83	-6.50	34.00
77	-9.54	-6.54	33.66
78	-9.43	-6.84	33.33
79	-9.36	-6.77	32.99

Vierlingsbeek 1977 *Unio pictorum*			
Sample #	δ¹³C	δ¹⁸O	Distance from umbo (mm)
80	-9.33	-6.78	32.55
81	-9.10	-6.90	32.11
82	-9.22	-7.05	31.66
83	-9.10	-6.99	31.21
84	-9.48	-7.00	30.78
85	-9.53	-6.79	30.33
86	-10.26	-6.70	29.89
87	-10.00	-6.23	29.44
88	-10.52	-5.87	29.00
89	-10.04	-5.81	28.55
90	-9.67	-5.82	28.11
91	-9.66	-5.96	27.90
92	-9.32	-6.22	27.70
93	-9.29	-6.26	27.49
94	-9.44	-6.36	27.29
95	-9.74	-6.26	27.08
96	-9.70	-6.15	26.88
97	-9.55	-6.16	26.67
98	-9.39	-6.15	26.46
99	-8.91	-6.51	26.26
100	-8.80	-6.56	25.85
101	-8.15	-6.76	25.44
102	-7.86	-6.61	25.03
103	-8.07	-6.78	24.62
104	-8.47	-6.90	24.21
105	-8.88	-7.04	23.81
106	-9.10	-7.14	23.39
107	-9.34	-7.00	22.99
108	-9.49	-6.94	22.49
109	-9.70	-6.86	21.99
110	-9.36	-6.77	21.49
111	-9.20	-6.87	20.98
112	-9.01	-6.88	20.48
113	-8.81	-6.74	20.03
114	-9.13	-6.34	19.58
115	-9.20	-6.12	19.13
116	-9.63	-6.07	18.68
117	-9.58	-6.08	18.23
118	-9.66	-6.27	17.76
119	-9.68	-6.47	17.30
120	-9.48	-6.68	16.82

Vierlingsbeek 1977 *Unio pictorum*			
Sample #	δ¹³C	δ¹⁸O	Distance from umbo (mm)
121	-9.49	-6.45	16.36
122	-9.52	-6.45	15.90
123	-9.15	-6.46	15.28
124	-8.81	-6.30	14.67
125	-9.00	-6.26	14.04

Waalwijk 1977 *Unio pictorum*			
Sample #	δ¹³C	δ¹⁸O	Distance from umbo (mm)
2	-10.34	-6.26	43.81
4	-10.75	-5.49	43.44
7	-7.97	-6.02	42.81
8	-7.35	-5.59	42.57
10	-7.11	-5.86	42.10
11	-6.77	-5.77	41.86
12	-6.83	-6.17	41.62
13	-6.70	-6.43	41.38
15	-7.86	-6.04	40.89
16	-8.66	-5.73	40.66
17	-9.27	-5.59	40.42
18	-9.90	-5.14	40.19
19	-9.41	-4.90	39.94
20	-9.31	-4.68	39.69
21	-9.21	-5.01	39.43
22	-9.31	-5.46	39.17
23	-9.39	-5.58	38.91
24	-9.19	-5.65	38.64
25	-9.03	-5.89	38.37
26	-8.97	-5.83	38.10
27	-8.90	-6.20	37.84
28	-8.86	-6.10	37.32
29	-8.88	-6.27	36.80
30	-9.15	-6.11	36.27
32	-8.44	-6.20	35.50
34	-8.50	-6.67	34.44
36	-8.29	-6.75	33.21
38	-8.65	-6.85	31.96
39	-8.68	-6.53	31.33
40	-8.78	-6.43	30.82
41	-8.90	-6.38	30.30
42	-8.56	-6.52	29.77

195

Waalwijk 1977 *Unio pictorum*

Sample #	δ¹³C	δ¹⁸O	Distance from umbo (mm)
43	-8.96	-6.44	29.25
44	-9.19	-6.66	28.24
45	-9.45	-6.78	27.37
46	-9.48	-6.51	26.72
47	-9.59	-6.32	26.06
48	-9.46	-6.31	25.40
49	-9.79	-6.58	24.74
50	-9.70	-6.51	24.09
51	-9.49	-6.55	23.44
52	-10.03	-6.04	21.42
53	-10.20	-6.17	20.72
54	-10.65	-5.70	20.04
55	-11.00	-5.34	19.36
56	-10.01	-5.23	18.66
57	-9.31	-5.37	18.08
58	-9.21	-5.68	17.48
59	-9.12	-5.70	16.88
60	-8.70	-6.40	16.29

Grevenbicht 1998 *Unio pictorum*

Sample #	δ¹³C	δ¹⁸O	Distance from umbo (mm)
2	-11.21	-5.84	41.92
3	-11.60	-6.07	41.76
4	-11.65	-5.60	41.59
5	-11.31	-6.25	41.42
6	-9.70	-5.66	41.24
7	-11.04	-6.80	41.08
8	-11.21	-6.73	40.90
10	-11.02	-7.09	40.55
13	-9.91	-8.15	40.03
14	-11.43	-7.15	39.86
16	-11.63	-7.39	39.48
17	-11.56	-7.38	39.27
18	-11.54	-7.28	39.07
19	-11.55	-7.66	38.87
20	-11.74	-7.40	38.61
21	-12.03	-7.45	38.36
22	-11.58	-7.54	38.12
23	-11.31	-7.44	37.92
24	-11.55	-7.34	37.72

Grevenbicht 1998 *Unio pictorum*

Sample #	δ¹³C	δ¹⁸O	Distance from umbo (mm)
26	-11.58	-7.32	37.34
27	-11.33	-7.93	37.17
30	-11.41	-7.81	36.66
32	-11.29	-7.28	36.32
34	-11.16	-6.94	35.97
35	-10.55	-6.68	35.81
37	-10.31	-6.80	35.41
40	-10.16	-6.61	34.76
41	-10.03	-6.76	34.55
42	-9.92	-6.81	34.33
43	-10.22	-6.86	34.10
44	-10.18	-6.76	33.88
47	-10.31	-7.01	33.19
48	-10.50	-7.14	32.95
51	-10.19	-6.43	32.23
52	-10.18	-6.66	31.98
54	-9.92	-6.14	31.50
56	-10.02	-5.76	31.02
58	-10.82	-5.57	30.64
61	-11.31	-5.34	30.08
63	-10.24	-5.14	29.71
67	-10.45	-5.97	28.95
68	-10.36	-6.02	28.75
70	-10.25	-6.57	28.37
71	-9.86	-6.52	28.11
72	-10.03	-6.91	27.87
76	-9.44	-6.24	26.86
78	-9.56	-6.19	26.36
80	-9.08	-6.23	25.87
82	-8.94	-6.09	25.36
83	-9.05	-5.77	25.02
86	-9.41	-5.92	23.99
89	-9.52	-6.00	22.96
91	-10.96	-6.29	22.29
93	-9.83	-5.70	20.90
94	-9.91	-5.58	20.21
95	-9.79	-5.66	19.52
97	-9.98	-6.02	18.72
98	-9.89	-6.10	18.32
99	-9.68	-6.46	17.92
100	-9.83	-6.33	17.52

Grevenbicht 1998 *Unio pictorum*

Sample #	δ¹³C	δ¹⁸O	Distance from umbo (mm)
101	-9.82	-6.51	17.12
102	-9.83	-6.12	15.52
103	-9.76	-5.41	15.03

Tuil 1998 *Unio tumidus*

Sample #	δ¹³C	δ¹⁸O	Distance from umbo (mm)
1	-7.88	-8.13	57.00
2	-8.17	-8.37	56.92
3	-9.20	-9.33	56.85
4	-9.71	-9.97	56.77
5	-9.36	-9.62	56.69
6	-8.74	-9.48	56.62
7	-8.53	-8.92	56.54
8	-8.53	-9.06	56.47
9	-8.81	-8.33	56.39
10	-8.59	-7.68	56.31
11	-8.83	-8.05	56.24
12	-8.89	-7.71	56.16
13	-8.77	-7.52	56.08
14	-8.62	-8.42	56.01
15	-8.66	-8.91	55.93
16	-9.22	-9.57	55.85
17	-9.72	-9.62	55.78
18	-10.16	-9.79	55.70
19	-9.55	-9.20	55.63
20	-9.59	-9.57	55.55
21	-9.16	-8.94	55.47
22	-9.21	-9.32	55.40
23	-8.68	-8.81	55.32
24	-8.88	-8.83	55.24
25	-9.53	-9.17	55.17
26	-9.40	-9.33	55.09
27	-9.76	-9.29	55.01
28	-9.39	-9.15	54.94
29	-9.54	-8.97	54.86
30	-8.95	-8.30	54.79
31	-9.22	-8.28	54.71
32	-9.44	-7.73	54.63
33	-9.09	-7.32	54.56
34	-7.76	-8.28	54.48

Tuil 1998 *Unio tumidus*			
Sample #	δ¹³C	δ¹⁸O	Distance from umbo (mm)
35	-9.41	-9.71	54.40
36	-9.79	-9.37	54.33
37	-10.44	-10.36	54.25
38	-10.18	-9.54	54.17
39	-10.53	-10.41	54.10
40	-10.17	-9.64	54.02
41	-10.29	-10.50	53.94
42	-9.51	-9.32	53.86
43	-8.17	-9.47	53.79
44	-9.59	-9.67	53.71
45	-9.40	-9.85	53.63
46	-9.58	-10.22	53.55
47	-9.86	-10.34	53.48
48	-9.77	-10.08	53.40
49	-9.68	-9.82	53.32
50	-9.55	-9.71	53.24
52	-9.25	-8.88	53.09
56	-8.93	-7.93	52.78
57	-8.28	-8.06	52.70
58	-8.28	-7.90	52.63
59	-8.27	-8.78	52.55
60	-9.18	-9.46	52.47
61	-9.41	-9.55	52.39
62	-10.57	-10.34	52.28
63	-10.59	-10.19	52.12
64	-10.86	-10.30	51.98
65	-10.38	-10.27	51.82
66	-10.10	-10.06	51.67
67	-10.14	-9.79	51.52
68	-9.97	-9.53	51.36
69	-9.94	-9.29	51.21
71	-9.10	-8.12	50.90
72	-9.08	-7.65	50.76
73	-8.26	-7.97	50.61
74	-8.25	-8.68	50.44
75	-8.52	-9.59	50.29
76	-8.79	-9.70	50.14
77	-8.84	-9.71	49.97
78	-8.90	-9.78	49.82
79	-8.99	-9.68	49.66
80	-9.25	-9.77	49.50

Tuil 1998 *Unio tumidus*			
Sample #	δ¹³C	δ¹⁸O	Distance from umbo (mm)
81	-9.08	-9.77	49.34
82	-9.00	-9.68	49.18
83	-9.16	-9.63	49.03
84	-9.51	-9.66	48.87
85	-9.50	-9.55	48.71
86	-9.46	-9.29	48.55
87	-9.58	-9.23	48.39
88	-9.52	-9.09	48.24
89	-9.52	-8.85	48.09
90	-9.34	-8.50	47.93
91	-9.48	-7.87	47.77
92	-8.97	-7.74	47.61
93	-8.77	-7.65	47.45
94	-8.05	-8.24	47.30
95	-8.29	-8.85	46.98
96	-8.47	-9.32	46.70
97	-8.77	-9.50	46.43
98	-8.68	-9.60	46.17
99	-8.28	-9.75	45.90
100	-8.15	-9.82	45.64
101	-8.21	-10.05	45.36
102	-8.64	-10.27	45.10
103	-8.82	-10.21	44.83
104	-8.54	-10.23	44.55
105	-9.13	-10.40	44.18
106	-9.37	-9.84	43.80
107	-9.83	-10.35	43.43
108	-9.93	-10.74	43.06
109	-9.84	-10.23	42.68
110	-9.45	-10.07	42.31
111	-8.85	-9.66	41.94
112	-8.88	-10.09	41.56
113	-8.99	-9.85	41.17
114	-8.98	-9.64	40.77
115	-8.52	-9.81	40.37
116	-8.77	-10.18	39.97
117	-8.88	-10.07	39.58
118	-8.68	-9.74	39.17
119	-8.58	-9.79	38.78
120	-8.45	-9.56	38.20
121	-8.60	-10.15	37.60

Tuil 1998 *Unio tumidus*			
Sample #	δ¹³C	δ¹⁸O	Distance from umbo (mm)
122	-8.60	-10.15	37.01
123	-8.69	-10.00	36.42
124	-8.55	-9.65	35.84
125	-8.36	-9.77	35.25
126	-8.72	-9.74	34.65
127	-9.29	-9.41	34.06
128	-10.10	-8.97	33.48
129	-11.13	-7.75	32.89
130	-10.26	-6.81	32.30
131	-8.84	-7.72	31.72

Herwijnen 2003 *Unio pictorum*			
Sample #	δ¹³C	δ¹⁸O	Distance from umbo (mm)
1	-12.27	-9.95	55.00
2	-13.01	-9.59	54.86
3	-13.20	-8.82	54.72
4	-12.76	-8.11	54.58
5	-10.78	-7.46	54.45
6	-8.94	-8.43	54.31
7	-9.40	-9.64	54.18
9	-11.25	-9.28	54.04
10	-11.98	-8.89	53.91
11	-12.08	-7.84	53.77
12	-10.25	-7.17	53.64
14	-11.27	-10.32	53.50
16	-11.38	-10.20	53.02
17	-11.86	-9.91	52.94
18	-11.66	-10.26	52.85
22	-10.74	-8.13	52.50
23	-9.17	-9.18	52.41
26	-12.10	-9.82	51.92
29	-13.16	-9.20	51.33
30	-12.02	-7.69	51.13
31	-9.39	-6.90	50.94
32	-8.77	-8.22	50.75
35	-11.08	-10.17	50.18
37	-11.60	-10.18	49.79
38	-13.08	-10.38	49.61
39	-13.12	-10.13	49.37
40	-15.43	-10.99	49.11

197

Herwijnen 2003 *Unio pictorum*

Sample #	δ¹³C	δ¹⁸O	Distance from umbo (mm)
42	-14.40	-10.43	48.59
44	-13.94	-10.61	48.07
45	-14.44	-10.52	47.74
47	-13.33	-9.75	46.95
48	-13.23	-9.66	46.57
49	-11.45	-8.47	46.20
50	-10.35	-8.94	45.80
51	-10.31	-9.82	45.42
53	-11.20	-9.33	44.77
54	-12.20	-9.30	44.44
57	-8.54	-8.36	43.47
59	-10.82	-10.21	42.81
60	-11.36	-10.41	42.50
62	-11.17	-9.95	41.53
63	-11.46	-9.59	41.04
64	-12.82	-9.92	40.58
65	-12.97	-9.86	40.25
66	-14.15	-9.75	39.95
67	-14.65	-9.30	39.61
68	-13.98	-9.01	39.03
69	-13.47	-8.33	38.40
70	-12.31	-7.44	37.78
71	-9.05	-7.46	37.15
73	-9.99	-9.87	35.66
74	-9.25	-9.05	34.89
75	-9.92	-9.29	34.09
76	-9.97	-9.63	33.30
77	-10.66	-9.33	32.51
78	-9.62	-8.72	31.73
79	-9.32	-8.56	31.16
80	-9.97	-9.13	30.59
81	-9.80	-8.68	30.01
82	-10.96	-9.72	29.28
83	-10.71	-9.44	28.55
84	-11.10	-9.41	27.82
85	-11.77	-9.30	27.10
87	-11.81	-8.34	25.34
88	-12.07	-8.52	24.47
89	-12.26	-7.73	23.33
92	-13.16	-8.46	21.57
95	-16.01	-7.87	20.77

Herwijnen 2003 *Unio pictorum*

Sample #	δ¹³C	δ¹⁸O	Distance from umbo (mm)
96	-10.78	-7.24	20.49
97	-9.56	-7.79	20.23
98	-9.90	-9.18	18.84
99	-9.26	-8.70	17.81
100	-9.43	-8.89	16.79
101	-9.39	-9.03	15.95
102	-9.49	-10.23	15.11
103	-9.48	-10.35	14.50
104	-8.86	-9.64	13.89
105	-8.97	-9.60	13.28
106	-8.53	-9.71	12.55
108	-8.48	-10.14	10.83
109	-8.48	-10.29	9.97
110	-8.61	-10.50	9.15
111	-8.89	-10.55	8.59
112	-9.15	-9.98	7.95
113	-8.98	-10.08	7.29
114	-9.09	-10.07	6.66
115	-9.34	-10.17	6.03
116	-8.90	-9.66	5.40
117	-8.96	-10.36	4.40
118	-8.85	-10.50	3.20
119	-8.55	-10.37	2.18
120	-8.09	-10.14	1.52
121	-8.16	-10.84	0.83
122	-8.37	-10.23	0.00

Hurwenen 2003 *Unio tumidus*

Sample #	δ¹³C	δ¹⁸O	Distance from umbo (mm)
2	-9.51	-9.30	67.66
4	-8.79	-8.22	67.57
8	-9.52	-9.32	67.32
10	-7.82	-8.64	67.19
12	-8.46	-8.54	67.04
14	-9.55	-9.39	66.89
16	-8.08	-8.37	66.74
17	-6.67	-8.02	66.66
18	-7.41	-8.63	66.57
19	-5.97	-7.88	66.50
20	-7.23	-9.18	66.40

Hurwenen 2003 *Unio tumidus*

Sample #	δ¹³C	δ¹⁸O	Distance from umbo (mm)
21	-7.11	-7.58	66.29
22	-7.40	-8.24	66.20
24	-7.58	-9.04	66.07
26	-8.18	-8.24	65.93
28	-7.78	-8.29	65.75
30	-9.11	-9.76	65.56
32	-9.16	-9.78	65.38
33	-9.02	-8.79	65.28
34	-9.49	-9.04	65.19
35	-8.02	-8.39	65.08
36	-8.34	-7.97	65.00
40	-8.14	-9.13	64.62
41	-8.79	-9.43	64.54
42	-10.11	-10.07	64.45
43	-10.08	-9.31	64.39
44	-10.70e	-9.30	64.33
46	-8.29	-8.13	64.22
47	-6.36	-7.77	64.17
48	-7.41	-9.07	64.11
49	-7.22	-8.89	64.05
50	-7.98	-9.24	64.00
51	-7.16	-8.23	63.95
52	-8.10	-8.91	63.89
53	-7.35	-7.25	63.83
54	-7.74	-7.43	63.77
55	-6.63	-7.36	63.71
56	-7.91	-9.04	63.66
57	-8.70	-9.21	63.61
58	-10.21	-10.09	63.55
60	-9.81	-9.97	63.43
62	-8.13	-9.71	63.31
63	-6.73	-8.77	63.26
64	-7.98	-8.09	63.20
65	-8.03	-6.32	63.12
66	-7.72	-6.33	63.03
67	-6.43	-6.74	62.93
69	-7.65	-8.39	62.73
70	-9.43	-9.40	62.64
71	-8.65	-8.91	62.53
72	-10.15	-9.92	62.43
73	-9.34	-9.39	62.34

Hurwenen 2003 *Unio tumidus*

Sample #	δ¹³C	δ¹⁸O	Distance from umbo (mm)
74	-9.19	-9.90	62.24
75	-8.03	-9.14	62.11
76	-9.04	-9.51	61.96
77	-7.95	-8.27	61.80
78	-8.80	-8.22	61.65
79	-7.87	-7.16	61.48
80	-8.27	-7.25	61.34
82	-7.79	-7.98	61.03
83	-7.44	-7.91	60.87
84	-8.61	-8.81	60.70
85	-8.60	-8.59	60.55
86	-9.68	-9.35	60.39
87	-9.25	-8.97	60.23
88	-10.20	-9.68	60.07
89	-9.57	-9.39	60.00
90	-11.12	-9.72	59.93
91	-11.08	-9.03	59.84
92	-10.88	-9.24	59.77
93	-9.13	-8.70	59.70
94	-10.00	-9.02	59.62
95	-8.37	-8.47	59.55
96	-9.13	-9.07	59.47
97	-8.34	-8.78	59.39
98	-9.36	-9.02	59.32
99	-8.43	-8.35	59.24
100	-9.45	-8.80	59.17
101	-9.20	-8.46	59.02
102	-10.14	-9.04	58.86
103	-9.24	-8.28	58.70
104	-9.62	-8.40	58.54
105	-9.26	-7.49	58.38
106	-10.03	-7.74	58.23
107	-8.24	-6.74	58.06
108	-8.57	-7.00	57.90
110	-7.75	-6.62	57.60
111	-6.76	-6.83	57.43
112	-7.47	-7.50	57.25
113	-7.08	-6.92	57.09
114	-7.76	-7.98	56.92
116	-7.57	-8.24	56.58
118	-8.03	-8.84	56.24
120	-8.26	-9.45	55.91
122	-8.87	-9.81	55.57
124	-9.01	-9.80	55.23
126	-8.93	-9.59	54.90
127	-8.35	-9.17	54.73
128	-9.02	-9.81	54.56
130	-9.04	-9.64	54.22
132	-9.29	-9.56	53.89
134	-9.56	-9.42	53.55
136	-9.73	-9.66	53.13
138	-10.61	-9.74	52.44
139	-9.67	-8.91	52.10
140	-9.68	-9.43	51.77
142	-10.11	-9.61	51.09
143	-9.89	-8.87	50.75
144	-10.29	-9.35	50.41
146	-9.82	-9.07	49.73
147	-9.57	-8.45	49.39
148	-11.27	-9.03	49.05
150	-11.33	-9.01	48.48
151	-10.57	-8.56	48.19
152	-10.43	-8.08	47.90
153	-9.50	-7.22	47.61
154	-10.17	-7.34	47.32
156	-8.89	-6.50	46.75
158	-8.26	-6.75	46.15
159	-7.76	-6.91	45.83
160	-8.06	-7.55	45.51
162	-8.10	-8.00	44.87
163	-7.91	-8.06	44.55
164	-8.61	-8.41	44.23
165	-8.23	-8.15	43.92
166	-8.53	-8.68	43.60
168	-8.36	-8.73	42.96
170	-8.63	-8.84	42.32
172	-8.23	-9.02	41.67
173	-7.55	-9.92	41.33
174	-8.12	-9.14	40.99
176	-7.98	-9.13	40.32
177	-7.32	-9.10	39.99
178	-8.17	-9.33	39.65
179	-7.94	-9.34	39.32
180	-8.61	-9.68	38.98
182	-8.71	-9.67	38.36
183	-8.18	-9.46	38.05
184	-8.60	-9.85	37.73
185	-8.19	-9.61	37.42
186	-8.35	-9.53	37.11
188	-8.43	-9.78	36.48
190	-8.69	-9.79	35.85
192	-8.94	-9.90	35.22
194	-8.86	-9.80	34.59
195	-8.56	-8.76	34.28
196	-8.74	-9.68	34.09
197	-8.21	-9.23	33.90
198	-8.53	-9.50	33.71
199	-8.07	-9.09	33.33
200	-8.45	-9.50	33.14
201	-8.06	-9.29	32.95
202	-8.56	-9.65	32.76
204	-8.82	-9.84	32.37
205	-8.03	-9.25	32.18
206	-8.77	-9.54	31.99
208	-8.90	-9.78	31.61
210	-8.95	-9.62	31.23
211	-8.15	-9.19	31.04
213	-8.23	-9.15	30.65
214	-9.36	-9.66	30.47
216	-9.15	-9.43	30.09
217	-7.83	-8.95	29.90
219	-7.84	-8.82	29.04
220	-8.69	-9.10	28.61
222	-8.91	-9.35	27.76
224	-8.76	-9.45	26.92
226	-8.64	-9.24	25.98
229	-8.39	-8.98	24.46
230	-8.62	-9.25	23.95
232	-8.72	-9.26	22.99
233	-8.68	-8.83	22.51
236	-10.01	-8.35	18.86
238	-10.66	-7.53	16.72

Hagestein 2005 *Unio tumidus*					Hagestein 2005 *Unio tumidus*					Kerkdriel 2005 *Unio pictorum*			
Sample #	$\delta^{13}C$	$\delta^{18}O$	Distance from umbo (mm)		Sample #	$\delta^{13}C$	$\delta^{18}O$	Distance from umbo (mm)		Sample #	$\delta^{13}C$	$\delta^{18}O$	Distance from umbo (mm)
1	-11.09	-8.16	62.00		49	-11.16	-8.53	55.57		1	-10.58	-6.18	50.00
2	-11.20	-7.80	61.90		50	-12.01	-8.91	55.44		2	-10.52	-5.86	49.68
3	-10.98	-6.99	61.80		51	-12.28	-8.82	55.29		3	-11.06	-5.91	49.35
6	-12.02	-8.87	61.48		52	-12.25	-8.84	55.16		5	-10.31	-6.09	48.70
7	-11.17	-8.43	61.37		53	-11.99	-8.69	55.03		6	-10.84	-6.21	48.38
8	-11.30	-8.27	61.27		54	-13.42	-9.05	54.89		7	-11.31	-6.14	48.06
9	-11.53	-7.37	61.16		56	-13.61	-9.17	54.62		8	-12.13	-5.84	47.73
10	-11.17	-7.67	61.06		57	-12.77	-8.65	54.49		9	-11.49	-5.78	47.42
12	-11.22	-8.49	60.85		60	-12.89	-8.89	54.07		10	-11.08	-6.29	47.09
13	-10.52	-8.11	60.75		61	-12.16	-7.94	53.93		11	-11.86	-6.33	46.78
14	-10.86	-8.63	60.64		62	-13.35	-7.63	53.80		12	-12.49	-6.12	46.47
15	-10.78	-8.76	60.54		65	-11.15	-8.65	53.38		13	-12.57	-6.05	46.15
16	-10.67	-7.99	60.43		67	-10.82	-8.97	52.91		14	-12.16	-6.06	45.84
17	-10.85	-8.95	60.29		68	-12.46	-9.68	52.58		15	-12.26	-5.58	45.52
18	-10.58	-9.14	60.14		69	-12.35	-9.44	52.22		16	-10.94	-6.11	45.20
20	-12.05	-8.08	59.84		70	-11.94	-9.32	51.85		17	-11.15	-6.49	44.91
21	-11.36	-8.97	59.69		71	-11.14	-9.39	51.48		18	-11.86	-6.57	44.61
22	-10.78	-8.81	59.54		75	-11.73	-9.39	50.01		19	-12.26	-6.34	44.31
23	-10.91	-8.37	59.40		76	-12.12	-9.70	49.65		21	-11.51	-6.25	43.72
24	-10.86	-8.53	59.25		77	-12.14	-9.87	49.28		23	-12.82	-6.06	43.13
25	-11.40	-9.20	59.11		78	-11.73	-9.84	48.92		25	-12.19	-6.13	42.54
26	-11.61	-9.42	58.95		80	-11.34	-9.97	48.18		27	-12.78	-6.04	41.95
27	-11.40	-9.23	58.81		81	-11.95	-9.97	47.82		29	-11.95	-6.51	41.32
28	-10.60	-8.54	58.66		82	-11.59	-9.97	47.46		30	-11.57	-6.48	41.00
29	-10.69	-8.53	58.51		84	-11.57	-10.19	46.64		31	-11.89	-6.58	40.67
30	-10.75	-8.19	58.36		85	-12.17	-10.08	46.22		33	-14.00	-5.82	40.04
31	-11.03	-8.21	58.21		87	-13.17	-9.59	45.40		34	-12.04	-5.84	39.72
32	-10.68	-8.01	58.06		89	-13.29	-9.23	44.60		37	-12.27	-6.18	38.77
34	-10.76	-8.90	57.77		90	-13.99	-8.91	44.20		39	-12.58	-6.43	38.14
36	-12.82	-9.84	57.47		91	-12.70	-9.18	43.80		40	-12.02	-5.77	37.81
37	-13.11	-9.82	57.32		93	-14.30	-8.90	42.98		41	-10.07	-6.41	37.50
38	-13.52	-9.85	57.18		95	-14.75	-8.29	42.14		43	-13.05	-6.63	36.66
39	-13.46	-9.89	57.03		96	-13.40	-8.42	41.71		44	-12.56	-6.59	36.24
40	-13.35	-9.73	56.88		98	-11.26	-7.83	40.86		45	-12.90	-6.63	35.82
41	-13.14	-9.79	56.74		99	-9.93	-7.94	40.38		47	-13.20	-6.05	34.98
42	-13.32	-9.49	56.60		102	-9.64	-8.71	38.93		48	-13.69	-5.47	34.56
43	-12.88	-9.37	56.44		105	-10.51	-9.13	37.14		49	-12.31	-5.13	34.15
44	-12.29	-9.27	56.30		106	-10.39	-9.45	36.54		50	-12.43	-5.50	33.73
45	-11.66	-8.87	56.16		110	-10.18	-9.69	34.14		51	-12.29	-5.98	33.32
46	-10.86	-8.23	56.01							53	-13.21	-6.18	32.49
48	-10.68	-7.68	55.71							54	-13.34	-6.07	32.08

Kerkdriel 2005 *Unio pictorum*

Sample #	δ¹³C	δ¹⁸O	Distance from umbo (mm)
55	-14.21	-6.19	31.67
56	-13.56	-6.13	31.25
57	-13.22	-5.45	30.84
58	-11.24	-5.43	30.42
59	-9.44	-5.97	29.98
60	-8.44	-6.65	29.54
61	-9.06	-6.75	29.11
63	-9.89	-7.16	28.25
64	-9.93	-7.16	27.82
65	-10.69	-7.18	27.37
66	-11.74	-7.35	26.94
67	-13.18	-6.96	26.46
69	-13.39	-6.26	25.51
71	-13.30	-5.40	24.53
72	-11.84	-5.44	24.04
73	-10.51	-5.64	23.71
74	-9.27	-6.24	23.38
75	-8.65	-6.93	23.05
76	-8.18	-7.12	22.35
77	-7.81	-7.07	21.65
78	-7.54	-7.01	20.95

Lith 2005 *Unio tumidus*

Sample #	δ¹³C	δ¹⁸O	Distance from umbo (mm)
1	-10.11	-5.77	53.00
2	-10.54	-6.17	52.85
3	-10.55	-5.94	52.70
4	-10.04	-5.74	52.55
5	-9.96	-6.00	52.40
6	-10.51	-5.89	52.30
7	-10.02	-5.90	52.19
8	-9.92	-6.02	52.03
9	-10.56	-5.79	51.86
10	-9.83	-7.58	51.70
11	-10.65	-6.13	51.53
12	-11.09	-6.03	51.37
13	-11.90	-6.75	51.20
14	-13.08	-6.98	51.04
15	-11.00	-6.52	50.88
16	-10.83	-6.26	50.71

Lith 2005 *Unio tumidus*

Sample #	δ¹³C	δ¹⁸O	Distance from umbo (mm)
17	-10.67	-5.37	50.55
18	-9.94	-5.66	50.38
19	-9.85	-5.81	50.22
20	-11.00	-6.08	50.06
21	-11.31	-5.44	49.90
22	-10.67	-5.35	49.73
23	-10.57	-6.38	49.57
24	-11.06	-6.91	49.42
25	-10.58	-6.97	49.25
26	-10.30	-6.59	49.08
27	-11.80	-5.87	48.93
28	-11.02	-5.39	48.76
29	-9.48	-5.88	48.60
30	-10.98	-7.28	48.38
31	-11.63	-7.24	48.17
32	-11.94	-7.30	47.96
33	-12.03	-7.21	47.74
34	-12.56	-7.23	47.53
35	-12.43	-7.06	47.32
37	-13.57	-6.81	46.89
38	-13.22	-6.58	46.68
39	-12.94	-6.49	46.47
40	-12.57	-5.93	46.25
41	-12.47	-5.65	46.04
42	-11.47	-5.46	45.83
43	-11.04	-5.63	45.62
44	-10.60	-5.44	45.42
46	-11.81	-5.63	45.12
47	-10.49	-5.75	44.98
48	-10.74	-5.71	44.82
49	-12.21	-6.11	44.68
50	-12.34	-5.96	44.53
51	-12.06	-5.82	44.28
52	-11.34	-5.91	44.04
53	-11.21	-6.14	43.79
54	-11.16	-6.19	43.54
55	-11.87	-6.26	43.29
56	-12.07	-6.31	43.05
57	-11.58	-5.88	42.80
58	-11.74	-5.88	42.55
59	-11.95	-6.13	42.31

Lith 2005 *Unio tumidus*

Sample #	δ¹³C	δ¹⁸O	Distance from umbo (mm)
60	-12.27	-6.24	42.07
61	-12.46	-5.97	41.81
62	-13.80	-5.80	41.57
63	-14.34	-5.80	41.33
64	-14.46	-5.82	41.09
65	-14.12	-5.26	40.85
66	-12.52	-4.75	40.61
67	-11.67	-4.47	40.37
68	-11.50	-4.75	40.13
69	-11.79	-5.12	39.89
71	-10.98	-5.98	38.94
72	-11.08	-6.00	38.77
73	-10.82	-6.31	38.61
74	-10.51	-6.26	38.40
75	-11.19	-6.59	38.18
77	-9.51	-6.37	37.55
78	-10.85	-6.67	37.13
79	-10.82	-6.64	36.70
80	-10.74	-6.59	36.28
81	-10.77	-6.69	35.86
82	-10.79	-6.66	35.20
83	-10.67	-6.65	34.54
84	-10.82	-6.66	33.88
85	-10.92	-6.87	33.22
86	-11.30	-7.03	32.56
87	-11.46	-6.89	31.69
88	-11.49	-6.94	30.82

Appendix 4: Archaeological shell isotope data

Spijkenisse *Unio crassus nanus*

Sample #	$\delta^{13}C$	$\delta^{18}O$	Distance from umbo (mm)
1	-7.95	-6.56	30.00
3	-8.52	-7.07	29.40
4	-8.23	-6.00	29.02
5	-8.81	-6.63	28.60
6	-8.62	-6.36	28.19
7	-8.28	-6.06	27.79
8	-8.88	-6.48	27.12
9	-9.74	-6.99	26.68
10	-9.24	-7.30	26.24
11	-9.57	-6.94	25.81
12	-8.65	-6.24	25.36
13	-8.91	-6.71	24.92
14	-9.56	-6.80	24.50
16	-9.61	-6.73	23.66
17	-9.20	-6.77	23.25
18	-8.80	-6.29	22.83
19	-9.07	-5.67	22.34
20	-9.99	-6.36	21.86
21	-10.60	-6.85	21.31
22	-9.45	-6.53	20.75
23	-8.82	-6.18	20.20
24	-9.15	-6.11	19.64
25	-9.79	-6.74	19.29
26	-9.87	-6.82	18.94
27	-9.22	-6.36	18.35
28	-9.01	-6.09	17.77
29	-8.85	-5.80	16.93
30	-9.21	-5.94	16.10
31	-9.79	-6.52	15.24
32	-10.25	-7.17	13.81
33	-10.03	-6.42	12.39
34	-9.69	-6.00	11.31
38	-9.90	-7.34	8.02

Montfoort *Unio crassus nanus*

Sample #	$\delta^{13}C$	$\delta^{18}O$	Distance from umbo (mm)
13	-12.44	-9.36	31.58

Montfoort *Unio crassus nanus*

Sample #	$\delta^{13}C$	$\delta^{18}O$	Distance from umbo (mm)
15	-13.62	-9.80	31.30
17	-12.33	-9.89	31.02
19	-13.67	-9.77	30.74
23	-7.57	-5.85	30.41
29	-12.41	-9.86	29.91
31	-12.51	-9.79	29.62
33	-13.36	-8.32	29.32
35	-10.92	-8.50	29.02
37	-9.44	-8.47	28.72
39	-11.21	-9.70	28.42
41	-10.94	-7.18	28.13
43	-11.04	-9.01	27.85
47	-12.34	-10.08	27.29
49	-12.63	-10.18	27.01
51	-12.01	-10.12	26.71
53	-12.39	-10.31	26.39
55	-12.86	-9.75	26.07
57	-13.39	-9.15	25.75
59	-13.05	-8.47	25.43
61	-12.48	-9.95	25.08
63	-11.67	-10.26	24.70
65	-11.59	-9.92	24.32
67	-11.62	-7.94	23.94
69	-12.09	-9.67	23.56
71	-10.64	-10.36	23.20
73	-12.05	-9.29	22.86
75	-11.27	-9.22	22.52
77	-10.85	-9.80	22.18
79	-10.84	-8.61	21.84
81	-10.82	-9.71	21.49
83	-10.45	-10.21	21.13
87	-10.21	-10.29	20.41
91	-8.46	-10.46	19.68
95	-11.37	-10.51	19.31
97	-12.26	-9.06	18.57
99	-10.79	-8.26	18.20
101	-9.22	-9.03	17.77
103	-8.43	-9.22	17.28

Montfoort *Unio crassus nanus*

Sample #	$\delta^{13}C$	$\delta^{18}O$	Distance from umbo (mm)
105	-8.32	-9.42	16.79
107	-8.11	-9.67	16.30
109	-7.90	-9.99	15.82

Houten *Unio crassus nanus*

Sample #	$\delta^{13}C$	$\delta^{18}O$	Distance from umbo (mm)
1	-10.23	-8.58	47.00
2	-10.10	-8.68	46.92
3	-9.78	-8.07	46.84
4	-10.06	-8.78	46.76
5	-9.12	-8.37	46.68
6	-8.72	-7.01	46.61
7	-9.68	-7.95	46.53
8	-9.98	-7.71	46.45
9	-10.93	-8.09	46.37
10	-10.61	-8.39	46.29
11	-9.55	-8.31	46.21
12	-9.21	-8.09	46.14
13	-8.97	-8.07	46.06
14	-9.75	-9.13	45.94
15	-10.59	-9.82	45.82
16	-10.22	-9.85	45.70
17	-9.96	-9.08	45.59
18	-9.90	-8.73	45.47
19	-9.93	-8.39	45.36
20	-10.23	-8.73	45.24
21	-10.01	-8.70	45.12
22	-9.73	-8.12	45.00
23	-9.79	-8.36	44.88
24	-9.79	-8.49	44.77
25	-9.81	-8.10	44.65
26	-9.87	-7.86	44.53
27	-9.97	-7.42	44.41
28	-10.21	-7.47	44.30
29	-10.22	-7.94	44.18
30	-10.93	-8.65	44.07
31	-11.31	-8.69	43.95
32	-11.18	-9.00	43.79
33	-10.71	-8.51	43.64
34	-10.79	-8.44	43.48

Houten *Unio crassus nanus*			
Sample #	δ¹³C	δ¹⁸O	Distance from umbo (mm)
35	-11.25	-8.88	43.34
36	-11.07	-8.95	43.18
37	-10.21	-8.45	43.02
38	-10.82	-8.67	42.87
39	-10.01	-8.00	42.72
40	-10.03	-8.34	42.56
41	-10.72	-8.28	42.42
42	-10.14	-8.07	42.26
43	-9.75	-7.60	42.11
44	-10.05	-7.39	41.96
45	-10.42	-7.43	41.80
46	-10.27	-7.03	41.65
47	-11.18	-8.14	41.49
48	-11.70	-8.85	41.34
49	-11.59	-8.44	41.20
50	-11.98	-8.84	41.07
51	-10.29	-8.70	40.94
52	-10.42	-8.45	40.80
53	-9.88	-7.45	40.67
54	-9.49	-7.71	40.53
55	-10.54	-8.79	40.40
56	-11.17	-8.88	40.27
57	-10.86	-8.60	40.13
58	-10.01	-8.59	39.99
59	-10.16	-8.03	39.86
60	-10.48	-7.68	39.72
61	-10.32	-7.48	39.59
62	-10.83	-8.56	39.45
63	-11.55	-9.54	39.32
64	-12.26	-9.58	39.19
65	-11.96	-9.05	39.05
66	-12.32	-8.73	38.90
67	-11.77	-7.98	38.76
68	-11.00	-7.44	38.62
69	-10.98	-6.81	38.47
70	-10.86	-6.55	38.32
71	-10.22	-6.39	38.18
72	-9.69	-6.58	38.03
73	-9.92	-7.34	37.89
74	-11.09	-8.48	37.75
75	-10.86	-8.92	37.61

Houten *Unio crassus nanus*			
Sample #	δ¹³C	δ¹⁸O	Distance from umbo (mm)
76	-10.26	-9.05	37.48
77	-9.72	-9.44	37.35
78	-9.55	-9.42	37.23
79	-9.46	-9.53	37.11
80	-9.56	-9.41	36.98
81	-9.40	-9.43	36.70
82	-9.01	-9.49	36.41
83	-9.33	-9.98	36.13
84	-9.36	-10.14	35.85
85	-9.33	-10.33	35.57
86	-9.25	-10.58	35.14
87	-9.14	-10.45	34.72
88	-9.03	-10.40	34.30
89	-8.86	-10.30	33.93
90	-9.13	-10.32	33.57
91	-9.33	-10.41	33.20
92	-9.25	-10.24	32.83
93	-9.43	-10.43	32.46
94	-9.38	-10.63	31.99
95	-9.30	-10.24	31.52
96	-9.39	-9.64	31.04
97	-9.23	-9.18	30.39
98	-9.47	-9.79	29.73

Utrecht *Unio crassus nanus*			
Sample #	δ¹³C	δ¹⁸O	Distance from umbo (mm)
1	-10.25	-8.19	37.00
2	-11.17	-8.59	36.83
3	-11.06	-9.39	36.65
5	-9.83	-9.59	36.30
6	-11.12	-9.56	36.12
8	-12.18	-8.63	35.77
10	-11.29	-6.90	35.42
12	-12.02	-8.39	35.06
13	-12.43	-9.14	34.87
14	-13.31	-9.36	34.68
15	-12.07	-9.78	34.50
16	-12.11	-10.04	34.31
17	-12.27	-9.76	34.12
18	-12.00	-9.85	33.93

Utrecht *Unio crassus nanus*			
Sample #	δ¹³C	δ¹⁸O	Distance from umbo (mm)
19	-11.52	-9.33	33.75
20	-11.29	-8.42	33.56
21	-10.96	-7.48	33.37
22	-9.99	-6.33	33.18
23	-11.34	-7.39	33.00
24	-12.31	-8.28	32.81
25	-12.51	-8.86	32.61
26	-12.04	-9.28	32.43
27	-11.03	-9.54	32.24
28	-10.53	-9.59	32.05
29	-10.60	-9.72	31.86
30	-10.94	-9.18	31.68
31	-11.50	-9.06	31.49
32	-11.07	-8.33	31.30
33	-10.70	-8.14	31.11
34	-11.22	-7.60	30.93
35	-10.64	-7.27	30.74
36	-11.38	-7.92	30.55
37	-10.84	-8.91	30.38
38	-10.28	-9.00	30.21
39	-9.96	-9.13	30.05
40	-9.64	-9.55	29.88
41	-9.71	-9.71	29.71
42	-10.27	-9.95	29.46
43	-10.06	-9.63	29.20
44	-10.05	-9.91	28.94
45	-10.44	-9.68	28.69
46	-10.32	-9.96	28.43
47	-10.15	-9.91	28.18
48	-10.21	-9.95	27.92
49	-9.79	-9.60	27.67
50	-9.11	-9.36	27.41
51	-8.93	-9.38	27.15
52	-8.94	-9.64	26.65
53	-9.18	-9.94	26.15
54	-9.12	-10.06	25.65
55	-9.50	-10.08	25.14
56	-9.36	-9.97	24.65
57	-9.48	-10.16	24.16
58	-9.18	-10.07	23.67
59	-8.96	-9.36	23.17

Utrecht *Unio crassus nanus*			
Sample #	δ¹³C	δ¹⁸O	Distance from umbo (mm)
60	-9.47	-9.57	22.68
61	-9.40	-9.31	22.17
62	-9.67	-9.41	21.67
63	-9.94	-9.54	21.16
64	-10.69	-8.75	20.41
65	-11.65	-7.87	19.67
66	-10.57	-6.77	18.92
67	-9.88	-7.43	18.50
68	-9.88	-7.73	18.07
70	-9.68	-8.74	16.91
71	-9.48	-9.12	16.18
72	-9.37	-9.48	15.44
73	-8.79	-9.74	14.47
74	-8.66	-9.58	13.50
75	-8.74	-9.69	12.49
76	-9.31	-9.59	11.48
77	-9.71	-9.56	10.48

Vleuten *Unio sp.*			
Sample #	δ¹³C	δ¹⁸O	Distance from umbo (mm)
1	-9.73	-8.38	50.00
2	-8.48	-9.28	49.92
3	-9.52	-8.25	49.85
4	-9.27	-8.17	49.76
5	-9.37	-7.92	49.60
7	-9.83	-7.58	49.43
8	-9.66	-8.14	49.34
9	-9.45	-8.18	49.25
10	-9.09	-8.57	49.17
11	-8.96	-8.33	49.08
12	-8.93	-8.70	49.00
13	-9.57	-8.13	48.91
14	-9.62	-8.04	48.82
15	-9.50	-8.81	48.69
17	-10.51	-8.18	48.43
18	-10.18	-8.12	48.30
19	-9.86	-9.15	48.17
20	-9.71	-9.02	48.04
21	-10.56	-8.35	47.90
22	-10.43	-8.16	47.77

Vleuten *Unio sp.*			
Sample #	δ¹³C	δ¹⁸O	Distance from umbo (mm)
23	-9.84	-9.49	47.64
24	-9.20	-9.21	47.50
28	-9.63	-8.62	46.92
29	-9.41	-8.27	46.78
30	-9.38	-8.52	46.64
31	-9.25	-8.49	46.49
32	-8.91	-8.30	46.37
34	-10.30	-8.14	46.11
35	-10.05	-8.33	45.99
37	-10.01	-8.51	45.74
40	-10.02	-7.92	45.37
41	-10.87	-8.20	45.24
42	-11.62	-9.05	45.12
43	-9.04	-8.67	44.98
45	-9.34	-8.38	44.72
47	-9.96	-8.72	44.45
48	-10.26	-8.87	44.32
50	-9.62	-8.31	44.05
52	-9.88	-8.61	43.78
54	-9.32	-9.06	43.52
55	-9.15	-8.61	43.38
56	-9.18	-9.33	43.25
57	-9.19	-8.98	43.12
60	-10.71	-9.79	42.72
61	-9.75	-9.50	42.59
62	-9.48	-9.32	42.46
63	-10.52	-8.96	42.33
65	-10.95	-7.95	42.07
66	-12.08	-9.17	41.94
67	-10.16	-8.93	41.82
68	-9.62	-9.35	41.71
69	-10.17	-9.08	41.60
73	-10.68	-7.36	41.15
75	-12.40	-8.95	40.92
76	-11.29	-9.21	40.81
77	-9.72	-9.41	40.70
78	-9.53	-9.18	40.59
79	-9.99	-8.32	40.48
80	-11.02	-7.63	40.32
81	-10.89	-7.49	40.16
82	-10.81	-8.14	39.99

Vleuten *Unio sp.*			
Sample #	δ¹³C	δ¹⁸O	Distance from umbo (mm)
83	-11.70	-9.24	39.83
84	-11.90	-9.65	39.67
85	-11.39	-9.42	39.51
86	-11.04	-9.13	39.35
87	-10.71	-9.28	39.19
88	-10.61	-8.75	39.03
89	-10.23	-8.24	38.86
90	-10.20	-7.89	38.70
91	-10.43	-7.78	38.54
92	-10.63	-8.32	38.38
93	-10.25	-8.72	38.22
94	-10.03	-8.99	38.05
95	-9.70	-9.07	37.88
96	-9.29	-9.31	37.71
97	-9.28	-9.16	37.54
98	-9.41	-9.24	37.37
99	-9.45	-9.51	37.20
100	-9.58	-9.27	37.03
101	-10.13	-9.02	36.86
102	-10.88	-8.52	36.69
103	-11.04	-7.96	36.52
104	-11.19	-7.96	36.34
105	-11.62	-7.58	36.17
106	-11.02	-7.03	36.01
107	-10.10	-7.23	35.84
108	-10.17	-8.02	35.66
109	-10.73	-8.66	35.49
110	-11.02	-8.91	35.32
111	-11.08	-8.89	35.15
112	-11.19	-8.92	34.97
113	-11.42	-9.01	34.80
114	-11.57	-8.97	34.63
115	-11.17	-9.07	34.45
116	-10.77	-8.89	34.28
117	-9.21	-8.76	34.11
118	-8.56	-8.86	33.85
119	-8.90	-9.03	33.60
120	-9.31	-9.09	33.34
121	-9.79	-9.16	33.09
122	-10.04	-9.19	32.84
123	-10.30	-8.80	32.58

Sample #	δ¹³C	δ¹⁸O	Distance from umbo (mm)

Vleuten *Unio sp.*

Sample #	$\delta^{13}C$	$\delta^{18}O$	Distance from umbo (mm)
124	-10.19	-8.91	32.32
125	-10.79	-8.81	32.07
126	-11.27	-8.06	31.81
127	-11.75	-7.77	31.56
128	-11.95	-7.36	31.31
129	-9.88	-7.08	31.05
130	-10.68	-8.55	30.80
131	-10.47	-8.95	30.54
132	-9.43	-9.46	30.28
133	-9.55	-9.41	29.96
134	-10.07	-10.16	29.63
135	-9.97	-10.01	29.30
136	-10.32	-10.44	28.97
137	-10.08	-10.27	28.65
138	-9.98	-10.23	28.33
139	-10.03	-9.59	28.00
140	-9.56	-9.88	27.67
141	-9.17	-9.17	27.41
142	-8.71	-8.40	27.15
143	-9.85	-8.57	26.88
144	-10.54	-8.67	26.62
145	-10.48	-7.75	26.35
146	-9.10	-7.40	26.09
147	-8.50	-8.19	25.81
148	-8.19	-8.46	25.53
149	-8.32	-8.58	25.25
150	-8.28	-8.54	24.97
151	-8.29	-8.56	24.69
152	-8.36	-8.50	24.40
153	-8.26	-8.56	24.12
154	-8.06	-8.46	23.84
155	-8.25	-9.48	23.56
156	-7.74	-8.21	23.28

Kerk-Avezaath 1 *Unio crassus nanus*

Sample #	$\delta^{13}C$	$\delta^{18}O$	Distance from umbo (mm)
1	-9.77	-8.77	41.00
2	-9.19	-8.55	40.86
3	-10.27	-8.85	40.71
4	-10.31	-8.39	40.57

Kerk-Avezaath 1 *Unio crassus nanus*

Sample #	$\delta^{13}C$	$\delta^{18}O$	Distance from umbo (mm)
5	-9.60	-8.29	40.42
6	-8.83	-8.94	40.27
7	-9.87	-8.64	40.13
8	-9.93	-8.32	39.97
9	-9.28	-8.53	39.82
10	-9.76	-8.13	39.67
11	-9.96	-8.21	39.51
12	-11.25	-9.85	39.36
13	-11.43	-10.14	39.20
14	-10.97	-9.42	39.05
15	-11.54	-9.01	38.90
16	-11.03	-8.52	38.75
17	-10.05	-8.11	38.59
18	-9.43	-8.39	38.43
19	-9.62	-8.88	38.28
20	-10.20	-8.92	38.13
21	-9.83	-8.83	37.98
22	-10.12	-9.34	37.82
23	-10.78	-9.43	37.67
24	-10.73	-8.40	37.51
25	-9.69	-8.55	37.36
26	-9.77	-8.90	37.21
27	-10.14	-8.36	36.98
28	-10.71	-8.23	36.76
29	-9.80	-8.17	36.53
30	-9.89	-8.80	36.31
31	-9.91	-8.77	36.08
32	-10.27	-8.18	35.86
33	-9.70	-8.20	35.64
34	-9.32	-8.26	35.41
35	-9.22	-8.11	35.18
36	-9.83	-9.36	34.95
37	-10.02	-9.26	34.72
38	-10.91	-8.44	34.49
39	-9.13	-8.51	34.25
40	-9.25	-9.13	34.04
41	-9.74	-8.81	33.82
42	-9.86	-7.57	33.60
43	-9.50	-8.80	33.39
44	-10.56	-9.40	33.17
45	-10.27	-9.68	32.95

Kerk-Avezaath 1 *Unio crassus nanus*

Sample #	$\delta^{13}C$	$\delta^{18}O$	Distance from umbo (mm)
46	-9.60	-9.29	32.73
47	-10.50	-9.22	32.52
48	-11.54	-9.24	32.29
49	-11.77	-8.95	32.08
50	-10.87	-8.22	31.86
51	-10.12	-8.93	31.64
52	-10.67	-9.70	31.43
53	-11.66	-9.58	31.20
54	-11.01	-9.08	30.99
55	-10.48	-8.70	30.78
56	-9.67	-8.41	30.56
57	-9.79	-9.87	30.34
58	-10.03	-10.03	30.13
59	-10.30	-9.71	29.91
60	-10.43	-9.00	29.70
61	-10.30	-8.80	29.48
62	-10.27	-8.67	29.27
63	-10.07	-8.90	29.05
64	-9.98	-9.58	28.77
65	-11.18	-9.84	28.47
66	-11.80	-9.01	28.18
67	-12.01	-8.65	27.88
68	-12.80	-9.08	27.59
69	-12.09	-8.80	27.29
70	-11.24	-8.20	27.00
71	-10.57	-8.73	26.71
72	-11.50	-9.70	26.42
73	-12.29	-9.96	26.12
74	-12.84	-9.94	25.83
75	-12.64	-9.96	25.54
76	-12.04	-9.70	25.15
77	-11.23	-9.32	24.77
78	-11.29	-8.91	24.38
79	-11.94	-8.77	23.99
80	-11.15	-8.44	23.60
81	-10.17	-8.38	23.23
82	-10.68	-9.48	22.84
83	-10.84	-8.94	22.45
84	-10.75	-9.41	22.06
85	-11.34	-9.30	21.45
86	-11.65	-9.49	20.84

Kerk-Avezaath 1 *Unio crassus nanus*

Sample #	δ¹³C	δ¹⁸O	Distance from umbo (mm)
87	-11.45	-8.84	20.23
88	-11.23	-8.60	19.62
89	-10.51	-8.26	19.01
90	-10.40	-8.39	18.40
91	-10.35	-9.40	17.79
92	-7.63	-8.57	17.18
93	-9.29	-10.18	15.26
94	-9.00	-9.86	15.26

Kerk-Avezaath 2 *Unio tumidus*

Sample #	δ¹³C	δ¹⁸O	Distance from umbo (mm)
1	-9.31	-7.81	50.00
2	-9.74	-8.11	49.90
3	-9.58	-8.82	49.80
4	-9.49	-8.09	49.70
5	-10.16	-8.80	49.60
6	-10.44	-8.26	49.49
7	-10.97	-7.84	49.41
8	-9.86	-7.77	49.32
9	-10.16	-8.69	49.23
10	-10.94	-8.23	49.14
11	-10.83	-7.97	49.05
12	-10.35	-8.46	48.96
13	-9.98	-7.96	48.87
14	-10.44	-8.10	48.78
15	-10.69	-8.18	48.68
16	-10.88	-8.72	48.58
17	-10.41	-8.60	48.48
18	-10.17	-7.62	48.38
19	-10.35	-8.37	48.27
20	-11.11	-8.63	48.18
21	-11.45	-9.66	48.07
22	-11.26	-9.73	47.97
23	-10.14	-8.39	47.87
24	-10.45	-8.28	47.77
25	-9.98	-7.62	47.67
26	-10.16	-8.28	47.56
27	-10.93	-8.54	47.46
28	-11.57	-8.23	47.36
29	-11.21	-7.59	47.26

Kerk-Avezaath 2 *Unio tumidus*

Sample #	δ¹³C	δ¹⁸O	Distance from umbo (mm)
30	-11.13	-7.92	47.16
31	-11.38	-8.76	47.05
32	-11.34	-9.67	46.95
33	-10.49	-8.68	46.85
34	-10.48	-8.94	46.74
35	-10.26	-8.51	46.64
36	-10.19	-8.06	46.53
37	-10.34	-8.48	46.42
38	-11.03	-9.34	46.31
39	-11.85	-9.90	46.20
40	-11.82	-9.75	46.09
41	-11.50	-9.60	45.98
42	-11.65	-9.27	45.88
43	-11.80	-9.11	45.77
44	-11.72	-9.10	45.66
45	-11.78	-8.76	45.55
46	-11.35	-8.47	45.45
47	-11.46	-9.84	45.34
48	-11.10	-9.70	45.23
49	-10.86	-9.20	45.12
50	-10.91	-9.13	45.01
51	-10.89	-8.85	44.90
52	-11.05	-8.75	44.79
53	-11.42	-8.42	44.69
54	-10.78	-8.08	44.58
55	-11.17	-9.25	44.47
56	-10.84	-8.97	44.36
57	-10.83	-8.87	44.25
58	-11.75	-9.08	44.12
59	-12.03	-9.80	43.98
60	-12.21	-8.96	43.86
61	-11.85	-8.17	43.72
62	-12.03	-7.81	43.59
63	-10.87	-7.87	43.45
64	-12.68	-8.13	43.32
65	-13.05	-8.57	43.19
66	-12.84	-8.57	43.05
67	-12.20	-8.53	42.93
69	-12.75	-8.47	42.60
70	-12.01	-9.05	42.43
71	-11.89	-9.31	42.26

Kerk-Avezaath 2 *Unio tumidus*

Sample #	δ¹³C	δ¹⁸O	Distance from umbo (mm)
72	-11.94	-9.66	42.08
73	-12.54	-10.09	41.92
74	-11.91	-10.39	41.75
75	-11.87	-9.86	41.57
76	-11.70	-9.30	41.40
77	-12.17	-8.35	41.27
78	-11.57	-7.44	41.15
79	-10.75	-8.79	41.03
80	-11.39	-9.39	40.91
81	-12.49	-9.76	40.78
82	-12.01	-9.77	40.66
83	-11.53	-9.71	40.53
84	-11.34	-9.86	40.41
85	-10.68	-8.37	40.29
86	-11.67	-8.77	40.16
87	-11.77	-7.95	40.04
88	-11.58	-7.86	39.91
89	-11.16	-7.35	39.79
90	-10.33	-6.83	39.67
91	-11.42	-9.14	39.48
92	-11.73	-9.48	39.29
93	-11.93	-9.82	39.10
94	-11.86	-9.61	38.92
95	-12.20	-9.90	38.73
96	-12.56	-9.99	38.54
98	-11.67	-10.01	38.17
99	-10.95	-9.27	37.98
100	-11.23	-9.72	37.79
101	-11.40	-9.71	37.60
102	-11.43	-10.20	37.44
103	-11.59	-9.33	37.27
104	-11.60	-9.13	37.11
105	-12.21	-8.70	36.95
106	-11.99	-7.89	36.78
107	-11.51	-7.31	36.62
108	-10.42	-7.44	36.45
109	-10.56	-8.72	36.29
110	-10.96	-8.91	36.13
111	-11.14	-9.37	35.96
112	-10.22	-9.68	35.80
113	-9.63	-9.19	35.61

Kerk-Avezaath 2 *Unio tumidus*

Sample #	δ¹³C	δ¹⁸O	Distance from umbo (mm)
114	-10.17	-10.01	35.43
115	-10.00	-9.62	35.24
116	-10.41	-10.12	35.06
117	-10.64	-9.66	34.87
119	-11.37	-9.06	34.50
120	-10.75	-8.75	34.31
121	-11.10	-8.79	34.13
122	-11.40	-8.17	33.94
123	-11.52	-8.05	33.75
124	-12.62	-7.84	33.56
125	-12.56	-7.20	33.38
126	-10.51	-6.23	33.19
127	-9.96	-8.03	33.01
128	-9.96	-9.31	32.79
129	-10.61	-9.51	32.57
130	-10.70	-9.63	32.35
131	-9.86	-9.02	32.12
133	-9.23	-9.24	31.68
134	-9.34	-9.63	31.45
135	-9.36	-9.69	31.23
136	-9.17	-9.72	31.01
137	-8.61	-9.60	30.71
138	-8.42	-9.62	30.41
139	-8.11	-9.35	30.12
140	-7.48	-8.59	29.82
141	-8.35	-9.62	29.53
142	-8.53	-9.57	29.23
143	-8.14	-9.10	28.94
144	-8.35	-9.26	28.65
145	-8.48	-9.25	28.24
146	-8.74	-9.16	27.83
147	-9.79	-8.58	27.42
148	-9.97	-7.68	27.01
149	-10.22	-8.53	26.60
150	-10.63	-7.97	26.19
151	-10.49	-7.38	25.78
152	-9.67	-8.61	25.52
153	-8.36	-9.35	25.25
155	-8.12	-9.36	24.73
156	-7.81	-9.41	24.46
157	-7.24	-9.77	24.20

Kerk-Avezaath 2 *Unio tumidus*

Sample #	δ¹³C	δ¹⁸O	Distance from umbo (mm)
158	-6.78	-9.83	23.02
159	-6.68	-9.53	21.85
160	-6.57	-9.84	20.85
161	-6.53	-9.97	19.86
162	-6.44	-9.93	19.86

Wijk bij Duurstede *Unio crassus nanus*

Sample #	δ¹³C	δ¹⁸O	Distance from umbo (mm)
3	-13.34	-9.24	42.19
5	-13.61	-9.67	42.02
10	-13.86	-9.74	41.58
11	-13.93	-9.71	41.49
13	-12.31	-9.03	41.30
15	-12.93	-9.16	41.11
18	-10.56	-6.62	40.84
19	-12.49	-7.73	40.74
21	-13.80	-8.76	40.52
23	-14.45	-9.55	40.27
24	-14.45	-9.55	40.15
30	-13.87	-9.62	39.39
31	-13.60	-9.67	39.27
33	-13.73	-10.02	39.02
35	-14.21	-10.21	38.78
37	-14.63	-10.64	38.54
39	-13.97	-10.02	38.29
41	-14.00	-9.76	38.05
43	-14.64	-9.55	37.82
45	-12.81	-8.46	37.59
49	-12.85	-8.23	37.13
51	-13.24	-9.47	36.90
53	-13.11	-9.12	36.69
57	-13.58	-9.92	36.27
59	-13.42	-10.57	36.06
61	-12.95	-10.54	35.85
63	-11.88	-10.04	35.64
65	-12.22	-10.24	35.43
67	-13.13	-9.73	35.22
69	-13.12	-9.42	35.01
71	-14.34	-8.50	34.80
73	-10.62	-6.44	34.57

Wijk bij Duurstede *Unio crassus nanus*

Sample #	δ¹³C	δ¹⁸O	Distance from umbo (mm)
77	-12.52	-8.13	34.11
79	-13.46	-8.49	33.88
83	-12.55	-9.52	33.35
85	-12.05	-10.03	33.07
87	-11.90	-10.06	32.79
93	-12.50	-10.22	32.02
97	-12.00	-10.22	31.56
99	-11.70	-9.40	31.33
101	-11.80	-9.03	31.09
103	-12.07	-9.27	30.83
105	-12.64	-9.37	30.57
109	-13.68	-8.71	30.05
111	-12.50	-8.47	29.79
113	-15.31	-8.02	29.53
115	-13.93	-7.47	29.27
117	-10.49	-6.60	29.01
121	-11.11	-8.08	28.53
125	-12.23	-9.00	28.15
127	-11.49	-8.93	27.97
129	-10.54	-8.95	27.78
131	-10.92	-9.28	27.58
133	-11.19	-9.13	27.36
135	-11.21	-9.44	27.14
137	-11.50	-9.34	26.92
139	-10.93	-9.35	26.70
141	-11.12	-9.55	26.46
143	-11.24	-9.48	26.19
145	-11.33	-9.55	25.93
147	-12.01	-9.62	25.66
149	-11.89	-9.51	25.40
151	-11.31	-9.29	25.13
153	-11.10	-9.13	24.85
157	-9.36	-8.98	24.29
161	-8.16	-9.07	23.72
165	-8.22	-9.25	23.12
167	-8.53	-9.24	22.82
169	-9.10	-9.14	22.52
175	-9.54	-7.84	21.62
177	-12.08	-7.33	21.32
179	-10.01	-7.22	21.02
183	-9.55	-8.50	20.45

Wijk bij Duurstede *Unio crassus nanus*

Sample #	δ¹³C	δ¹⁸O	Distance from umbo (mm)
185	-9.30	-8.52	20.17
189	-11.48	-9.12	19.61
193	-7.60	-9.47	18.87
195	-7.48	-9.55	18.47
197	-7.54	-9.93	18.07
201	-7.61	-9.45	17.28
205	-7.33	-10.16	16.54
207	-7.72	-9.65	16.17
209	-7.54	-9.46	15.80
211	-7.10	-9.39	15.43
213	-7.05	-9.49	15.05
221	-7.14	-9.32	13.53
225	-7.13	-8.72	12.78
227	-7.40	-8.85	12.40
229	-7.38	-8.51	12.02
237	-10.66	-6.79	10.73
241	-10.84	-7.15	10.06
243	-11.02	-8.86	9.68

Gorinchem *Unio crassus nanus*

Sample #	δ¹³C	δ¹⁸O	Distance from umbo (mm)
1	-8.61	-7.72	41.00
2	-8.70	-7.56	40.90
3	-8.87	-7.97	40.80
4	-8.47	-9.01	40.70
5	-8.53	-8.75	40.61
6	-8.49	-7.10	40.51
7	-9.63	-7.25	40.41
8	-10.57	-8.46	40.31
9	-10.64	-9.23	40.21
10	-9.99	-9.67	40.11
11	-8.93	-9.16	40.01
12	-8.54	-8.25	39.91
13	-9.02	-7.66	39.81
14	-9.20	-6.97	39.71
15	-10.82	-7.60	39.62
16	-10.59	-8.03	39.52
17	-10.65	-8.46	39.42
18	-9.55	-9.15	39.32
19	-8.83	-9.00	39.22

Gorinchem *Unio crassus nanus*

Sample #	δ¹³C	δ¹⁸O	Distance from umbo (mm)
20	-8.85	-8.67	39.11
21	-9.01	-7.13	39.02
22	-9.38	-5.46	38.92
23	-9.75	-6.60	38.82
24	-10.34	-7.66	38.72
25	-10.63	-8.59	38.62
26	-10.55	-8.68	38.52
27	-10.20	-8.59	38.34
28	-10.28	-8.73	38.14
29	-10.50	-9.05	37.96
30	-10.33	-8.74	37.77
31	-10.49	-9.00	37.58
32	-10.27	-9.04	37.39
33	-10.20	-8.88	37.20
34	-10.02	-8.76	37.02
35	-9.55	-8.43	36.82
36	-9.74	-8.25	36.63
37	-9.95	-8.02	36.44
38	-9.56	-7.09	36.26
39	-9.22	-6.93	36.07
40	-9.29	-7.82	35.88
41	-9.40	-8.30	35.69
42	-9.05	-8.03	35.51
43	-9.14	-8.48	35.32
44	-9.20	-8.66	35.13
45	-9.30	-8.95	34.94
46	-8.79	-8.96	34.76
47	-8.09	-9.22	34.56
48	-8.34	-9.50	34.38
49	-8.44	-9.67	34.00
50	-8.45	-9.17	33.82
51	-8.35	-9.40	33.62
52	-8.36	-9.58	33.44
53	-8.39	-9.58	33.25
54	-8.38	-9.35	33.06
55	-8.32	-9.23	32.87
56	-8.39	-8.96	32.69
57	-8.85	-8.81	32.49
58	-9.20	-8.46	32.27
59	-9.63	-7.99	32.03
60	-9.53	-7.28	31.81

Gorinchem *Unio crassus nanus*

Sample #	δ¹³C	δ¹⁸O	Distance from umbo (mm)
61	-9.45	-6.02	31.58
62	-8.39	-5.68	31.35
63	-8.43	-7.28	31.16
64	-8.60	-7.90	30.97
65	-8.64	-8.06	30.78
66	-8.06	-8.30	30.59
67	-7.99	-9.10	30.40
68	-7.81	-9.12	30.03
69	-8.29	-8.54	29.65
70	-8.41	-8.93	29.28
71	-8.83	-9.55	28.90
72	-9.20	-9.39	28.53
73	-9.66	-9.45	28.15
74	-10.01	-9.46	27.78
75	-9.77	-9.26	27.37
76	-9.81	-9.42	26.97
77	-9.97	-8.99	26.56
78	-8.75	-8.41	26.15
79	-8.75	-8.38	25.76
80	-10.26	-7.97	25.40
81	-11.41	-8.35	25.02
82	-10.93	-9.33	24.63
83	-10.08	-9.55	24.24